Biochemical Characterization of Drug Metabolizing Alkyl Thiol Methyltransferase 1A and 1B

Drake Anthony Russell

A dissertation

submitted in partial fulfillment of the

requirements for the degree of

Doctor of Philosophy

University of Washington

2023

Reading Committee:

Rheem A. Totah, Chair

Abhinav Nath

Miklos Guttman

Program Authorized to Offer Degree:

Medicinal Chemistry

University of Washington

Abstract

Biochemical Characterization of Drug Metabolizing Alkyl Thiol Methyltransferase 1A and 1B

Drake Anthony Russell

Chair of the Supervisory Committee:

Rheem A. Totah

Department of Medicinal Chemistry

In humans, *S*-methylation of aromatic and alkyl thiols is catalyzed by thiopurine methyltransferase (TPMT), and a putative enzyme(s) thought to be responsible for alkyl thiol methyltransferase (TMT) activity. In this work, we identified METTL7A along with METTL7B as the enzymes responsible for TMT activity and renamed them thiol methyltransferase 1A and 1B (TMT1A and TMT1B), respectively. TMT1A and TMT1B exhibited many characteristics ascribed to historic TMT activity, including similar molecular weight, microsomal association, and broad substrate specificity for several alkyl thiol containing drugs, including spironolactone, captopril, and mertansine. Interestingly, TMT1A but not TMT1B is potently inhibited by a historic probe inhibitor of TMT activity, 2,3-dichloro-α-methylbenzylamine (DCMB). Utilizing

DCMB to probe microsomal TMT activity suggests that TMT1A, not TMT1B, is responsible for most alkyl thiol methylation activity. To explain the difference in DCMB susceptibility, we compared the sequences of TMT1A and TMT1B and used homology models to identify key residues in the binding site. We then used site-directed-mutagenesis, to pinpoint a key tyrosine residue at position 47 (Tyr-47) in the binding site of TMT1A that was critical for DMCB inhibition. Mutating Tyr-47 to the corresponding Ser-47 in TMT1B abolished DCMB inhibition and confirmed the importance of Tyr-47 for DCMB binding and inhibition. Finally, we identified hydrogen sulfide (H_2S) as a potential endogenous substrate of TMT1A and TMT1B and showed that the metabolite methyl sulfide (MeSH), similar to H_2S, can efficiently adduct and sulfmethylate protein cysteines. To determine the physiological relevance of sulfmethylation, we developed a novel proteomics method to detect potential proteins adducted by MeSH. This protein adductomics method may help elucidate the endogenous role of MeSH in signaling and cell homeostasis.

TABLE OF CONTENTS

LIST OF FIGURES

LIST OF TABLES

LIST OF SUPPLEMENTARY TABLES

ACKNOWLEDGEMENTS

The first acknowledgment must go to Dr. Rheem Totah, my advisor throughout my graduate studies. You introduced me to medicinal chemistry as an undergraduate and then showed me how to be a scientist as a graduate student. The opportunity to participate in scientific research is a gift, and for this, I am truly grateful. You gave me room to explore my own ideas and scientific passions, but all the way kept me moving in the right direction.

Next, I would like to thank my colleagues and friends in the Totah lab who helped me accomplish this work. Dr. Ben Maldonato, you paved the way. If you had not discovered TMT1B, none of this would have been possible. On top of that, you were my graduate mentor, you introduced me to bench science and showed me the ropes. The environment that you fostered in the Totah lab during my time as an undergraduate researcher had a huge impact on my desire to enroll as a graduate student. Taeyoon Jung, the conversations we had about TMT1A and TMT1B helped guide my analysis of the homology models of TMT1A and TMT1B, and your computational work improved my confidence that we were on to something. Dr. Yuanyuan Shi, without your expert knowledge of proteomics, the quantitative proteomics in Chapter 2 would not have been possible. Additionally, you introduced me to proteomics and taught me how to run digestions and analyze proteomic data. The things that you taught me during your post-doc work helped me develop the Chapter 4 project. Marvin Chau, without your hard work optimizing the knockdown of TMT1A and TMT1B in HepG2 cells, that experiment would not have been nearly as successful. Also, the effort you put into developing the tissue culture capabilities in our new lab space was also invaluable. To the undergraduate researchers who helped me with various protein production work, you have my sincerest appreciation. A special thank you to Ian Levasseur and Carson Stafford. During those long days of sitting around watching liquid fall

through a gravity column, you helped break up the monotony. Jade Yang, it's been just a pleasure to work with you. Thanks for being willing to accommodate my ideas at the last minute. Your flexibility during the work we did together gave me the chance to try out some new things that eventually precipitated the idea to isolate TMT1 spheroplasts, something that I think will be an important tool for future work with these enzymes. Dr. Max Zeigler, the occasional climbing outing with you has been nice, we need to go climb together more. And last but not least, Alex Wiley, you started the trend of talking out the science, this made all of us Totah lab graduate students better scientists and better friends. I sincerely valued your scientific input and friendship throughout my graduate studies. To all the other Totah lab members that I crossed paths with, you all are in my thoughts as well. I am proud to be one of the many former and current members of the Totah lab.

I also thank my committee members, Dr. Allan Rettie, Dr. Abhi Nath, Dr. Mike Guttman, and Dr. Champak Chatterjee. You gave such great input over the years. Many of the questions or comments that you made during committee meetings had large impacts on the experiments I tried and the way I thought about each project. The committee meetings were imposing to prepare for but very enjoyable. How often do you get to hold a bunch of expert scientists hostage to brainstorm science with you? I would especially like to thank Dr. Nath and Dr. Guttman for reading my thesis and for their participation in certain aspects of these projects. Dr. Nath helped with much of the work in Chapter 3, and Dr. Guttman helped develop the adductomics methodologies in Chapter 4.

The Department of Medicinal Chemistry is filled with great people who have positively influenced my graduate studies. Dale Whittington, you were always there to help solve my mass spec problems and offer sage advice. I also would like to thank the administrative staff,

especially Sarah and Helen. To all the unnamed people, your participation in the culture and the science of this department has made this an enjoyable experience. The Medicinal Chemistry Department is a special place.

My parents, Matthew and Cindy Russell, have always promoted out of box thinking, and the pursuit of knowledge. Looking back, I think it was inevitable that I would become a scientist. Thank you both for your love and support. Finally, I would like to thank my wife, Georgiana, you married me knowing that I am a scientist. You were supportive the whole way through and put some things on hold to help me get through this. You listened to all of my talks, knowing very little about biology or biochemistry, and paid enough attention to explain my work to friends and family. You also ensured I had fun outside of the lab, which probably helped keep me sane throughout the years. My success as a scientist is very much our success. Thank you!

DEDICATION

To Georgiana, Matthew, Cindy, Blaisien, Larkin, and Trevan, the journey continues.

Thank you for all your love and support!

Chapter 1. **Introduction**

Methyltransferases represent a group of enzymes that catalyze the transfer of a methyl group from a small molecule cofactor donor to an acceptor substrate (Figure 1.1). Most methyltransferases utilize the cofactor *S*-adenosyl-L-methionine (SAM) as the methyl donor. In humans, SAM is the second most common co-factor following ATP, but other less common methyl donors such as betaine, methylcobalamin (Me-B_{12}), methyl tetrahydrofolate, and *S*-methylmethionine have been reported [1-3]. The basic SAM-dependent methyl transfer reaction is through an S_N2 attack of a nucleophile (carbon, oxygen, nitrogen, sulfur or selenium) of the acceptor on an activated methyl group to generate methylated derivatives of proteins, lipids, polysaccharides, nucleic acids, and various small molecules (Figure 1.2). The second product is *S*-adenosyl-L-homocysteine which serves as a competitive inhibitor for SAM dependent enzymes (Figure 1.3). Methyl conjugation is an important metabolic pathway for many drugs, xenobiotic compounds, environmental toxins, as well as endogenous neurotransmitters and hormones. Methylation on DNA/RNA nucleic acids and protein amino acids often alters gene transcription and protein expression and function.

SAM-dependent methyltransferases are an example of convergent evolution, a series of enzymes with very different overall structures but with similar properties in the active site, which facilitates catalysis of a methyl transfer [4, 5]. There are five structurally distinct families of SAM-dependent methyltransferases adopting different structures but with similar functions [5]. The *N*-methylation of pyridine, documented in the late 19th century, was the first described methyl conjugation reaction. [6, 7]. Since then, over 160 methyltransferases with confirmed methyltransferase activity have been discovered; a list of human methyltransferases is curated and annotated online from peer-reviewed sources by The Universal Protein Resource (UniProt,

Search: (ec:2.1.1.-) AND (reviewed:true) AND (organism_id:9606)). Of all the confirmed methyltransferases, roughly 50% are protein methyltransferases, 35% are RNA methyltransferases, 13% are small molecule methyltransferases, and 2% methylate DNA (https://www.uniprot.org/). Protein, DNA, and RNA methyltransferases have been recently reviewed elsewhere [8-10]. This thesis will focus on small molecule methyl transferases.

Small molecule methyltransferases, while only account for ~13% of the overall methyltransferases encoded in the human genome, participate in a wide array of endogenous and xenobiotic methylation reactions that are pharmacologically important (Figure 1.2). *N*-methylation reactions play an important role in the metabolic activation or deactivation of both endogenous neurotransmitters and drug molecules that contain amine functional groups. For example, nicotinamide *N*-methyltransferase (NNMT) methylates nicotinamide (vitamin B_3) to form 1-methylnicotinamide (1-MNAM), which affects cellular metabolism [11]. Histamine *N*-methyltransferase (HNMT) plays a central role in terminating the neurotransmitter signaling action of histamine [12]. Phenylethanolamine *N*-methyltransferase (PNMT) not only methylates norepinephrine to epinephrine but also methylates various catecholamines, including *p*-tyramine, and *p*-octopamine [13]. Indolethylamine *N*-methyltransferase (INMT) generates the highly hallucinogenic compound *N*,*N*-dimethyltryptamine (DMT) from endogenous tryptamine and plays a role in the biotransformation of sulfur and selenium-containing compounds [14, 15]. Catechol *O*-methyltransferase (COMT) methylates various neurotransmitters, including dopamine and epinephrine. In addition, COMT has several other important *in vivo* functions including the biosynthesis of melanin [16, 17] and other physiological compounds, such as catechol estrogens and ascorbic acid [18]. Finally, arsenic III *As*-methyltransferase (AS3MT), is

predominantly responsible for the metabolism and detoxification of arsenic, a lethal environmental toxin [19].

Unlike the previously introduced small molecule methyltransferases, no endogenous substrates have been robustly identified for *S*-methyltransferases. In humans, two enzymes exist: the well characterized cytosolic enzyme thiopurine methyltransferase (TPMT), and thiol alkyl methyltransferase (TMT), until very recently an unknown microsomal enzyme which is now understood to be a family of two enzymes, TMT1A and TMT1B [20]. The primary role of *S*-methyltransferases resides in the detoxification of xenobiotics [21]. *S*-methylation is an important pathway in the biotransformation of many sulfhydryl drugs, such as the antihypertensive agent captopril, thienopyridine platelet inhibitors clopidogrel and prasugrel, and the thiopurine antileukemic and immunosuppressive compounds mercaptopurine (6-MP), thioguanine (TG), and azathioprine [22].

In this work, the alkyl thiol *S*-methyltransferase 1A (TMT1A) is identified as the main enzyme responsible for the methylation of exogenous alkyl thiol containing small molecules (Chapter 2). This work summarizes the biochemical characterization and modeling of TMT1A, leading to the identification of unique residues in the active site TMT1A that promote its binding interactions with aromatic inhibitor 2,3-dichloro-α-methylbenzylamine (DCMB), a molecule that does not inhibit TMT1B, a close homolog of TMT1A (Chapter 3). Finally, there is evidence in the literature that TMT can methylate hydrogen sulfide (H_2S), which may be the first example of an endogenous substrate for thiol *S*-methyltransferase. TMT1B can methylate H_2S [23], and preliminary work in our lab suggests that TMT1A can also potentially catalyze this reaction. This work will introduce a novel approach to probe the relationship between the endogenous *S*-methylation of H_2S and H_2S-mediated signaling (Chapter 4). The following section in this

introductory chapter will describe the conserved structure of methyltransferases. Following this, select small molecule methyltransferases, relevant to this thesis work, will be reviewed. This chapter will then conclude with a short introduction to TMT1A and TMT1B.

1.1 Structure of Methyltransferases

The first solved crystal structure of a methyltransferase was for the bacterial M.H*ha*I DNA methyltransferase in 1993 [24]. Since then, a variety of structural motifs have been reported for SAM dependent methyltransferases. In 2003, Schubert *et al.* demonstrated that most SAM dependent methyltransferases conform to one of five distinct structural classes [5]. Class I methyltransferases have the most diverse substrate preference including small molecule *N*-, *O*-, and *S*-methyltransferases as well as many DNA, RNA, and protein methyltransferases conforming to the class I structural motif. For humans, there are a handful of protein-methyltransferases that methylate histone-lysines and are categorized as class V methyltransferases, and a few RNA methyltransferases that are categorized as class IV methyltransferases. Generally, class II through V methyltransferases are not as common as class I methyltransferases, and though they are biochemically interesting [5, 25, 26], they are beyond the scope of this work.

Class I methyltransferases have a highly conserved Rossman-fold-like 7-stranded β-sheet tertiary structure of unidirectional β-strands each flanked by alpha helices with a final strand, β-strand 7, oriented in the opposite direction of strands 1-6 (6↑, 7↓, 5↑, 4↑, 1↑, 2↑, 3↑: Figure 1.4, [5]). In addition to the core Rossman-fold-like 7-stranded β-sheet, there are two other conserved class I methyltransferase structural features: the first is a nucleotide binding motif, GXGXG or truncated variations, that follows the first β-strand, and the second is an acidic residue at the end of the second β-strand. The acidic residue, either a glutamic or aspartic acid, forms hydrogen

bonds with both hydroxyls of the SAM ribose and, together with the GXGXG nucleotide binding motif, helps stabilize SAM in the active site. Mutating the acidic residue to an aliphatic residue, such as alanine, ablates methyltransferase activity [23, 27].

All SAM-dependent small molecule methyltransferases are class I methyltransferases and exhibit the Rossman-fold-like 7-stranded β-sheet tertiary structure, except for thiopurine methyltransferase (TPMT). TPMT, which will be introduced in a later section, differs slightly and includes two additional strands between β-strands 2 and 3 that form an atypical antiparallel extension of the 7-stranded β-sheet (6↑, 7↓, 5↑, 4↑, 1↑, 2a↑, 3↑, 2c↓, 2b↑). The sequences for several small molecule methyltransferase's class I nucleotide GXGXG binding motif and acidic residue following their respective second β-strand are displayed in Table 1.1.

The SAM-dependent methyl transfer reaction occurs via an S_N2 nucleophilic substitution mechanism, where the substrate's nucleophilic methyl acceptor atom is positioned linear with the methyl carbon and sulfonium atoms of SAM approximately 3 and 4 Å away, respectively [26, 28]. This geometric arrangement is necessary for the methyl transfer reaction to occur [28]. While the overall reaction is simple, methyltransferases employ different catalytic mechanisms to facilitate the methyl transfer and select for substrate and nucleophilic heteroatom. The small molecule methyltransferase COMT utilizes a metal ion to coordinate and facilitate the deprotonation of substrates in the active site. Other methyltransferases utilize catalytic side chains in their active site to coordinate substrate binding and deprotonation to transfer the methyl group [26], and yet others, like AS3MT, utilize substrate and intramolecular cysteine bonding interactions to achieve a methyl transfer [29-33].

1.2 SMALL MOLECULE METHYLTRANSFERASES

1.2.1 *Introduction*

In the following sections, three select small molecule methyltransferases will be discussed in detail. The small molecule methyltransferases AS3MT, TPMT, and TMT were chosen because of their relationship to TMT1A and TMT1B and will be mentioned in later chapters. The enzyme AS3MT has a unique catalytic mechanism that includes cysteine residues in its active site that participate in the methyl transfer reaction. As discussed in Chapter 3, there are two cysteine residues in the active site of both TMT1A and TMT1B which could perhaps participate in methyl transfer reactions similar to AS3MT cysteine residues. Historically, TPMT was the only thiol *S*-methyltransferase that was identified and characterized, while TMT was a term used to describe an activity attributed to a putative microsomal enzyme with a unique substrate specificity compared to TPMT. A brief description of AS3MT, TPMT limited to their reaction mechanism and substrate specificity, and the historic TMT activity is presented below.

1.2.2 *Arsenite As-methyltransferase*

Arsenic III methyltransferase (AS3MT), is named after the oxidation state of its metalloid substrate As^{3+} oxidation state. AS3MT methylates arsenite (As^{III}) and monomethylarsenous acid (MMA^{III}). The final metabolic product of AS3MT-catalyzed arsenic methylation is the least toxic endogenously produced arsenic species dimethylarsinate (DMA^{V}) [34]. The earliest proposed pathway for arsenic metabolism consists of two AS3MT-catalyzed methyl additions transforming As^{III} to DMA^{V} (Figure 1.5) [35]. This scheme does not explain how arsenic is reduced from monomethylarsonate (MMA^{V}) to MMA^{III}, a necessary step for AS3MT to catalyze a second methyl transfer. Two candidate mammalian reductases have been identified, purine

nucleotide phosphatase and glutathione *S*-transferase (GST) [36, 37]. These enzymes can reduce arsenate (As^{V}) to As^{III}, and MMA^{V} to MMA^{III}, respectively, but early AS3MT studies indicated that AS3MT is itself involved in the reduction of MMA^{V} [38].

AS3MT belongs to the Class I small molecule methyltransferases with a typical 7-stranded-β-sheet tertiary structure, a conserved class I nucleotide binding motif following the first β-strand, and an acidic residue at the terminus of the second β-strand (Table 1.1). AS3MT is a cytosolic protein 375 amino acids long with a molecular weight of ~42 kDa purified from the soluble fraction of tissue homogenates [39]. To date, the molecular structure of human AS3MT has not been solved yet, but mutagenesis and *in vitro* mechanistic studies have identified specific residues in AS3MT's active site that are important for activity. AS3MT has 14 cysteine residues distributed across its sequence [32]. Two of these cysteines are vital for activity. Mutating either cysteine 156 or cysteine 206 to a serine destroys AS3MT's ability to methylate arsenic [33].

AS3MT is only active in the presence of a reducing thiol, such as glutathione (GSH), in the reaction mixture [38, 40]. Hayakawa *et al.*, 2005, suggested a metabolic scheme for inorganic methylation via arsenic-GSH complexes where GSH reacts with As^{III} forming arsenic triglutathione [30]. In their scheme, arsenic triglutathione undergoes two rounds of AS3MT-catalyzed methylation without requiring reduction between the first and second methyl transfer, this differs from other methyltransferase reactions because the methyl acceptor participates in the reaction as an electrophile rather than a nucleophile (Figure 1.6.A and 1.6.B). Cysteine residues 156 and 206 are vital for the activity of human AS3MT [33]. Mutating either of these residues to a serine completely ablates the function of AS3MT. Song *et al.* proposed an alternative scheme where GSH regenerates active AS3MT by reducing an intramolecular disulfide bond between Cys-156 and Cys-206 following the first methyl transfer (Figure 1.6.C) [31]. As^{III} forms a

covalent bond with one of the AS3MT cysteines facilitating the first methyl transfer, after which MMA^{III} is released by an intramolecular disulfide formed between Cys-156 and Cys-206. MMA^{III} can undergo a second methyl transfer to become dimethylarsenous acid (DMA^{III}) by the same mechanism once GSH regenerates active AS3MT. The enzyme system that reduces intramolecular disulfide bonds, consisting of thioredoxin and thioredoxin reductase, has been demonstrated to activate AS3MT and endogenously could function in the same way as GSH does in the Song *et al.* proposed reaction [40]. In both proposed reaction mechanisms, the end product of AS3MT-catalyzed methyl transfer is DMA^{III}, which is eventually oxidized to DMA^{V} and excreted in urine [41].

1.2.3 *Thiopurine S-methyltransferase*

Thiopurine methyltransferase (TPMT) is one of three enzymes involved in thiol *S*-methylation in humans. For many years after *S*-methyltransferase activity was first discovered, TPMT was the only thiol methyltransferase with a characterized gene and protein. Prior to the discovery that the alkyl thiol methyltransferase 1 family (TMT1), consisting of TMT1A and TMT1B, is responsible for microsomal alkyl thiol methyltransferase activity [20, 23], TPMT was distinguished from alkyl thiol methyltransferase activity (TMT activity) by its subcellular distribution and substrate specificity. TPMT is a cytosolic enzyme that preferentially catalyzes the *S*-methylation of exogenous thiopurines, thiopyrimidines, and thiophenols [42, 43]. TPMT plays a major role in the metabolism of the immunosuppressive and antileukemic agents azathioprine, 6-mercaptopurine (6-MP), and thioguanine (TG). To date, no endogenous substrate for TPMT has been identified and no endogenous activity has been reported. The level of TPMT activity in human tissue is controlled by several genetic polymorphisms, and inherited variations effect TPMT activity and are important factors in the individual differences in thiopurine drug

toxicity and therapeutic efficacy [44-46]. TPMT genetic polymorphisms are a well-validated example of the clinical importance of pharmacogenetics and the importance of pharmacogenomics research [47].

The structure of TPMT, truncated at the amino terminus, complexed with SAH has been solved (Protein Data Bank ID 2H11), and subsequently used in a molecular dynamics study of TPMT complexed with 6-MP [48]. The crystal structure of the murine ortholog of TPMT has also been used to study the properties of the active site of the enzyme. Two arginine residues participate in the methyl transfer reaction by deprotonating the substrate [49]. The tertiary structure of TPMT differs slightly from the classic 7-stranded β-sheet class I methyltransferase structure. There are two additional strands between β-strands 2 and 3 that form an atypical antiparallel extension of the canonical 7-stranded β-sheet (6↑, 7↓, 5↑, 4↑, 1↑, 2↑, 3↑, 2c↓, 2b↑). TPMT has an atypical nucleotide binding motif, with only a single conserved glycine residue, but TPMT does maintain a conserved acidic residue immediately following β-strand two, consistent with other small molecule methyltransferase (Table 1.1).

The frequency distribution of TPMT activity in a population of 300 adults was reported to be trimodal with a low activity group, an intermediate activity group, and a high activity group. Variation in human TPMT activity was largely attributed to inheritance and is regulated by the gene *TPMT* [50]. Characterization of *TPMT* led to the identification of two point mutations associated with low TPMT activity, a G460A substitution in exon 7 (Ala154Thr) and an A719G substitution in exon 10 (Tyr240Cys). Since the discovery of the low activity *TPMT* variants, several more variants have been identified and reported (Figure 1.7). These include *TPMT*3A,* which contains both the Ala154Thr and Tyr240Cys substitutions, *TPMT*3B,* which only has Ala154Thr, and *TPMT*3C,* which has the Tyr240Cys [51].

TPMT's most well-known substrates are 6-thiopurines and their nucleoside and nucleotide derivatives (Figure 1.8). Both 6-MP and TG are known substrates with K_m values of 383 and 557 μM, respectively, V_{max} values of 897 and 1080 nmol h^{-1} mg $protein^{-1}$, respectively and V_{max}/K_m values of 2.34 and 1.94, respectively [52]. The thiopurines 6-MP and TG have surprisingly high K_m values, given that TPMT's role in thiopurine metabolism. Thiophenol compounds are also substrates of TPMT, and methyltransferase researchers have suggested that TPMT be referred to as aryl thiol methyltransferase because of the affinity that TPMT has for thiophenols. The thiophenol K_m values are 0.8 μM for 2-bromothiophenol, and 7.8 μM for thiosalicylic acid [43, 53]. Recently, TPMT, alongside thiol ether methyltransferase (TEMT), has been implicated in hydrogen selenide and selenyl-sulfide methylation [54-56].

Methylmercaptopurine inhibits TPMT activity in the human kidney with a K_i of 0.56 mM. The COMT inhibitors tropolone and 3,4-dimethoxy-5-hydroxybenzoic acid inhibit TPMT activity with IC_{50} values of 1 and 0.02 mM, respectively [42, 53]. Benzoic acid derivatives inhibit TPMT, the most clinically relevant being the aspirin metabolite salicylic acid with an IC_{50} value of 0.28 mM; following therapeutic doses of aspirin, salicylic acid circulates at concentrations capable of inhibiting TPMT [53].

Because of the role of TPMT in the metabolism of several highly toxic compounds, clinicians are cautious when dosing individuals with thiopurines that are TPMT substrates. The U.S. Food and Drug Administration (FDA) has clear dosing instructions based on patient metabolizer status of toxic thiopurines. For example, the FDA-approved azathioprine (IMURAN®) drug label clearly states that death has been reported in patients lacking TPMT activity and receiving azathioprine. It is important to genotype individuals for low or absent TPMT variants to determine appropriate dose of azathioprine [57, 58]. The Clinical Pharmacogenetics

Implementation Consortium (CPIC), an international consortium of volunteers interested in facilitating the use of pharmacogenetic tests for patient care, advocate for genetic testing prior to starting patients on azathioprine, 6-MP, or TG [59]. CPIC classifies *TPMT** allele variants into two tiers, with tier one consisting of *TPMT*1, *2, *3A, *3B,* and *3C* (Figure 1.7); and tier two consisting of recently identified *TPMT*11, *29,* and *42*. Tier one alleles are considered the minimum set for testing, and tier two alleles are optional for an extended panel. See Couchana *et al.* for a detailed analysis of pharmacogenetic testing [60]. As thiol-containing xenobiotics arise as therapeutic drugs, environmental contaminants, or because of the intermediary metabolism of xenobiotics, if a thiol compound has an aromatic or heterocyclic structure, these compounds could serve as potential substrates for TPMT *S*-methylation.

1.2.4 *Alkyl thiol S-methyltransferase*

Alkyl *S*-methylation activity has been known since the late 1970s, and the thiol methylation in various tissues has been well described, but the enzymes responsible for TMT activity have only recently been identified [20, 23, 61]. Historically, TMT has been distinguished from TPMT by substrate specificity and subcellular location. TPMT is cytosolic and will methylate thiopurines and some thiophenol compounds, as mentioned above, while TMT is microsomal and will methylate alkyl thiols and small gaseous sulfides such as hydrogen sulfide (H_2S) (Figure 1.9) [42, 62, 63]. However, there is literature evidence where TPMT and TMT are reported to methylate thiophenol compounds, suggesting potential overlap in substrate specificity [53, 64]. In this section, for TMT studies published prior to the discovery of TMT1A and TMT1B, TMT will be described as “TMT activity”.

In 1979 Weisiger and Jakoby partially purified the enzyme responsible for TMT activity from rat liver and estimated the molecular weight to be 28 kDa [64]. TMT activity was SAM-

dependent. Based on structure-activity relationship (SAR) studies, the SAM/SAH carboxyl and adenosyl N6-amine are vital for binding (Figure 1.10, [65]). In humans, TMT activity is mostly associated with the liver as is the case for many xenobiotic and drug-metabolizing enzymes, but TMT activity is also high in gastrointestinal tissue and detectable in most other tissues, including blood (Supplementary Table 1.2, [62, 66]).

TMT activity in red blood cells (RBC) from individual subjects displays 5-fold variability. There is a significant aggregation of RBC TMT activities among genetically related individuals, and the heritability of TMT activity in RBC is 0.98 [67]. Human RBC and liver microsomal TMT have similar biochemical properties [68-70]. TMT activity, characterized using microsomal and RBC membranes, preferentially catalyzes the *S*-methylation of alkyl thiols or gaseous sulfides such as H_2S, and the drugs 7α-thiospironolactone (TSL), ziprasidone, captopril, and the active metabolites of prasugrel and clopidogrel [68, 71-73].

Microsomal TMT activity is significantly inhibited by 2,3-dichloro-α-methylbenzylamine (DCMB), a small molecule originally designed to inhibit PNMT and selectively reduce epinephrine formation *in vivo* [74]. While TPMT is inhibited by negatively charged small aromatic compounds, TMT is inhibited by neutral or positively charged small aromatic compounds. Structure-activity analysis of arylalkylamine inhibition of microsomal TMT determined that neutral or positively charged aromatic small molecules are excellent inhibitors of TMT [70]. Human erythrocyte TMT is also inhibited by cysteine thiol alkylating agents such as *N*-ethylmaleimide and ethacrynic acid and the inhibition was not reversible by dialysis, suggesting that free thiol cysteine residues are necessary for TMT activity [61].

The TMT inhibitor DCMB does not inhibit TPMT and has been used as a specific inhibitor to distinguish TMT activity from TPMT [20, 72, 73, 75, 76]. In one rare example of *N*-methylation

activity in liver microsomes, coincubation with DCMB inhibited the *N*-methylation of an imidazole ring nitrogen. The authors of this study concluded that, because DCMB inhibited this *N*-methylation reaction in liver microsomes and because TMT is the only known small molecule methyltransferase inhibited by DCMB in the microsomal fraction, TMT could be responsible for this *N*-methylation [76]. It is possible that TMT is responsible for this biotransformation, but it is also possible that there is another unknown methyltransferase in liver microsomes that is also inhibited by DCMB and can *N*-methylate an imidazole ring nitrogen.

The only known endogenous substrate of TMT to date is H_2S [63]. Early TMT researchers were interested in TMT's role in the detoxification of exogenous small molecule alkyl thiols and gaseous sulfides. TMT activity levels are highest in organs that are expected to be exposed to xenobiotics and microflora-derived H_2S, which supports the detoxification role of TMT for alkyl thiols and gaseous sulfides [62]. H_2S is an endogenously produced signaling gasotransmitter involved in many physiological functions that lead to cytoprotection, cardioprotection, regulation of synaptic transmission, and protection from oxidative stress [77-79]. Methylsulfide (MeSH) is an endogenous circulating metabolite of H_2S catalyzed by TMT [23, 80]. Low micromolar levels of H_2S and MeSH have been measured in human blood [81]. Conversely, H_2S is also a toxic gas that can be inhaled from the environment. High levels of exposure to H_2S cause mucous membrane irritation, nausea, vomiting, keratoconjunctivitis, corneal ulceration and irreversible corneal scarring, cardiopulmonary arrest, unconsciousness, and death [82, 83]. The mono and di-methylated metabolites of H_2S are less toxic than H_2S, and for this reason, the methylation of H_2S could potentially be a route of detoxification [82, 83]. It is also possible that H_2S methylation is an important part of H_2S-mediated signaling. More research is necessary to

understand the relationship between TMT-catalyzed methylation of H_2S, gaseous signaling, and detoxication.

S-Methylation of thiol-containing small molecules is another potential TMT-mediated detoxication pathway. *S*-methylation prevents reactive thiols from covalently interacting with and altering vital biomolecules, potentially changing the reactivity of alkyl thiol-containing drugs and other exogenous small molecules. While not many drugs contain a thiol moiety, most of those drugs that do, undergo thiol methylation as a biotransformation pathway, with sometimes unpredictable consequences. For example, clopidogrel and prasugrel are thienopyridine prodrugs that are activated by ring opening to expose a reactive thiol that forms a disulfide bond with and irreversibly inhibits their target receptor, $P2Y_{12}$, a transmembrane receptor that controls platelet aggregation. TMT-catalyzed *S*-methylation of the reactive thiol results in the inactivation of these drugs' active metabolites due to their inability to covalently bind to their receptor [84]. The *S*-methyl metabolite of the mineralocorticoid receptor antagonist spironolactone, 7α-thiomethylspironolactone (TMSL), is the major circulating metabolite and is responsible for most of the drug's activity *in vivo* [85]. The methylation of thiol-containing histone deacetylase inhibitors (HDACs) has been associated with cancer resistance [86]. Finally, ziprasidone, an antipsychotic medication, undergoes a unique glutathione-catalyzed ring opening, revealing a reactive free thiol that is subsequently methylated by TMT and eliminated as a major metabolite [71].

1.2.5 *Thiol methyltransferase family 1 (TMT1)*

TMT1A and TMT1B are both 244 residues long and have a molecular weight of 28.3 and 27.8 kDa, respectively. TMT1A and TMT1B were previously referred to as methyltransferase-like 7A and 7B (METTL7A, and METTL7B, respectively) before they were renamed in early

2023 [20]. The methyltransferase-like (METTL) label is given to genes and their protein sequences with uncharacterized function but qualities consistent with a SAM-binding methyltransferase (Supplementary Table 1.2, [87, 88]). The function for most METTL proteins has been identified, and they have been renamed with names more representative of their function. TMT1A and TMT1B share 76% sequence homology, and each share greater than 70% sequence identity with many of their mammalian isoforms (Figure 1.11 and 1.12). Most mammals express both a TMT1A and a TMT1B, some have multiple TMT1A isoforms. Mouse has three TMT1A isoforms, TMT1A1, TMT1A2, and TMT1A3 [89].

TMT1A and TMT1B are members of class I small molecule methyltransferases with a typical 7-stranded-β-sheet tertiary structure, a conserved class I nucleotide binding motif after the first β-strand, and an acidic residue at the end of the second β-strand (Table 1.1). The acidic residue of TMT1B has been confirmed to be important for SAM binding and activity [23]. TMT1A and TMT1B each contain a 28-residue hydrophobic signaling sequence at the *N*-terminus, which targets lipid droplets and is thought to form a hairpin loop and embed in the phospholipid monolayer surrounding lipid droplets [90, 91]. TMT1A, TMT1B, and membrane-bound catechol *O*-methyltransferase (MB-COMT) are the only membrane-bound small molecule methyltransferases known to date, and there are only two other METTL proteins that are membrane-associated (Supplementary Table 1.2). Scoring small molecule methyltransferases' sequences using the Kyte and Doolittle hydropathy score, only TMT1A, TMT1B, and MB-COMT have hydrophobic *N*-termini (Figure 1.13) [92]. Maldonato *et al.* discovered that coincubation of TMT1B with the lipid 1,2-dimyristoyl-*sn*-glycero-3-PG (DMPG) significantly improved enzyme activity, which also proved to be true for TMT1A [20, 23].

TMT1A and TMT1B are both highly expressed in liver (Supplementary Table 1.1). The endogenous function of TMT1A and TMT1B has not been established, yet their dysregulation is reportedly involved in several disease pathologies. Both TMT1A and TMT1B have been demonstrated to confer resistance to cancer by methylating and inactivating thiol containing histone deacetylase inhibitors [86]. In various cancers, TMT1A is significantly downregulated. In one large-cohort multi-cancer, multi-omic study, higher TMT1A was shown to have the most favorable survival across cancers compared to other methyltransferases [93]. TMT1B, however, is significantly upregulated across most cancers [93, 94]. TMT1B has been shown to regulate the epithelial-mesenchymal transition of thyroid cancer cells in the presence of TGF-β, is thought to be an important regulator of cancer immunosuppression, and is shown in multiple cell lines to promote G1 to S phase transition in cancer cells [95-98]. TMT1B overexpression is attributed to proliferation and tumorigenesis, which suggests an oncogenic role in cancer progression. Conversely, the consistent lower expression of TMT1A across cancers would suggest more of a tumor-suppressor role.

1.3 Hypothesis and Specific Aims

The overarching goal of this work is to biochemically characterize the enzyme thiol methyltransferase 1A, formally known as methyltransferase-like 7A (METTL7A), and to identify key components important for its structure and function.

Two main hypotheses are set forth as follows.

1. The enzyme formerly known as METTL7A (now TMT1A), is responsible for the majority of alkyl thiol methyltransferase activity in liver.
2. There are key differences in the substrate binding site residues between TMT1A and TMT1B that enable DCMB inhibition of TMT1A but not TMT1B.

Chapter 2 describes the biochemical characterization of TMT1A and shows that TMT1A is mostly responsible for TMT activity in human liver. We purified TMT1A and used mass spectrometric- and luminescence-based activity assays to determine its substrate specificity and kinetic parameters. The overexpression of TMT1A and TMT1B in cells is used to corroborate the biochemical characterization of recombinant TMT1A. Finally, we correlate TMT activity with TMT1A and TMT1B protein levels determined by mass spectral analysis in human liver microsomes.

In Chapter 3, we identify key residues that are important for DCMB binding to TMT1A and use plasmids that introduce various mutations and overexpress mutant TMT in cells to confirm their importance for DCMB inhibition. We then report a novel method to express and isolate TMT1A in bacterial spheroplasts and utilize them to identify the structure activity relationship of DCMB congeners and their ability to inhibit TMT1A.

Chapter 4 tackles the development of a novel adductomics technique to identify methyl sulfide adducts to protein cysteines. There is evidence that methyl sulfide can adduct cysteines but the data is equivocal. We utilize this adductomics method to demonstrate that methyl sulfide adduction is chemically feasible.

Chapter 5 summarizes the thesis's work and proposes future work that can increase our understanding of the physiological role of TMT1 family in drug metabolism and endogenous signaling.

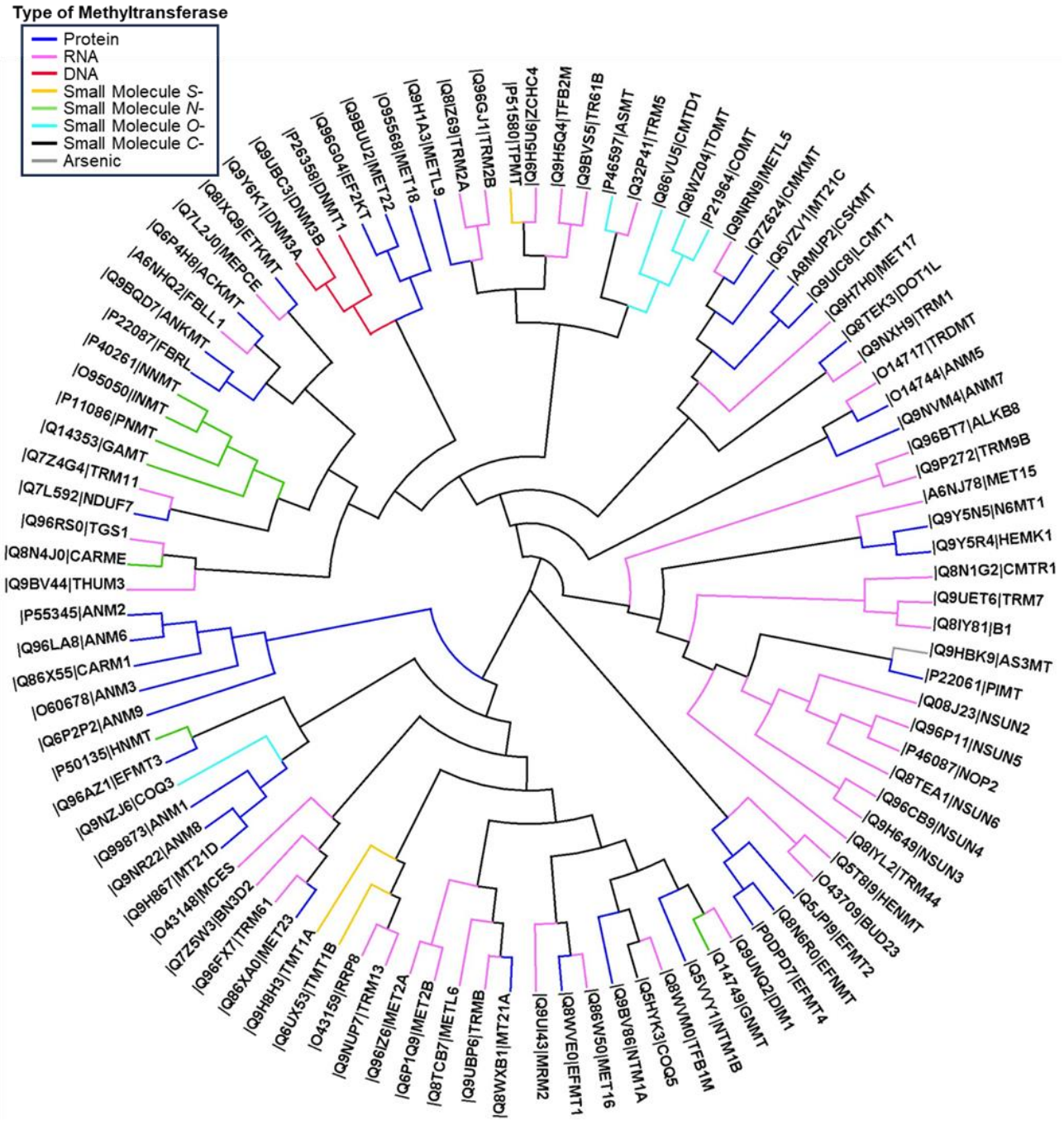

Figure 1.1. Cladogram of human class I methyltransferases

The tree was produced with sequence alignment scores from Clustal Omega multiple sequence alignment tool accessed at https://www.uniprot.org/align [99]. The number of nodes between any two proteins gives rank order sequence similarity. The methyltransferase type is designated by the color of edge leading to each label. The cladogram tree was edited with Dendroscope [100].

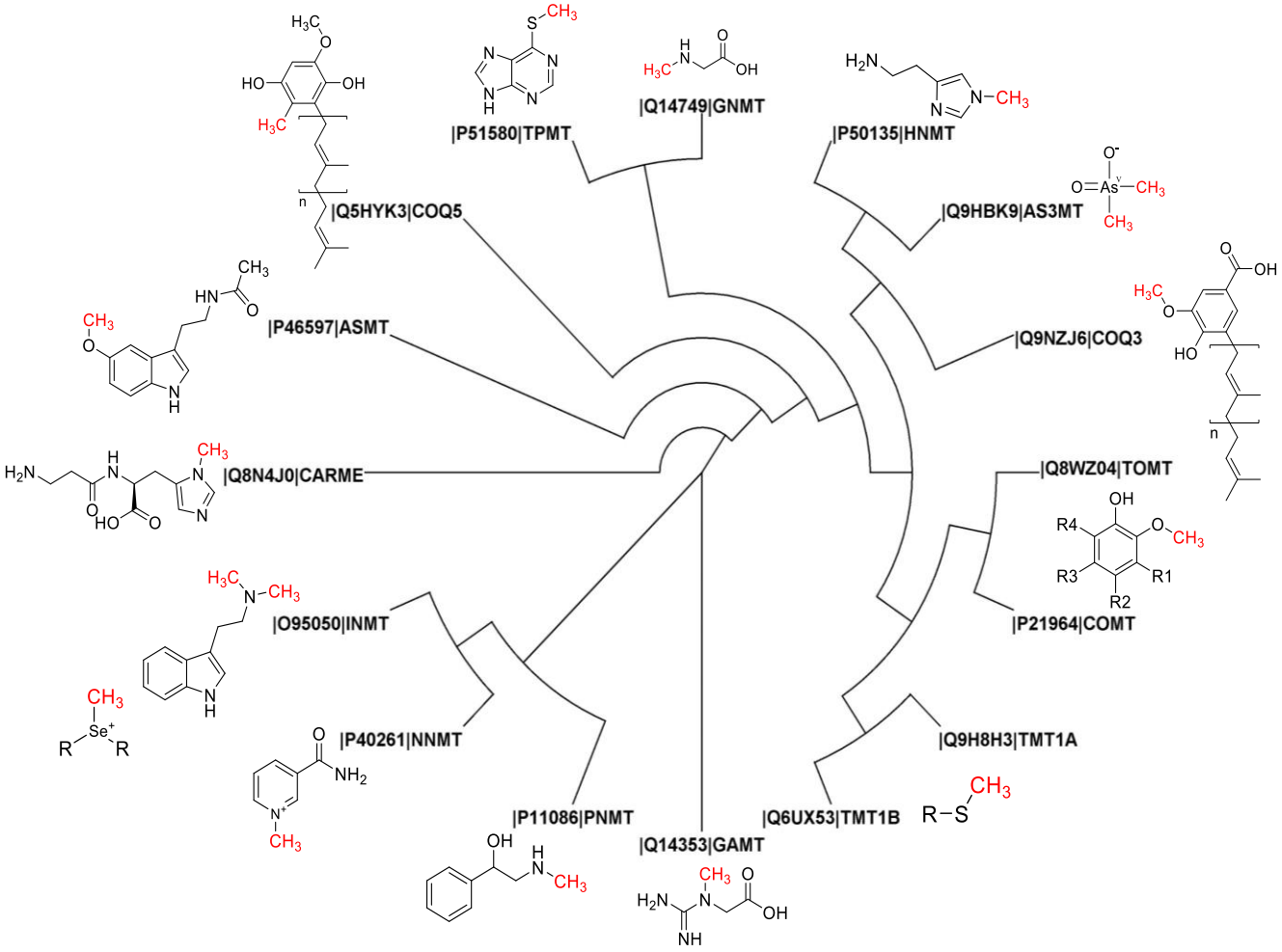

Figure 1.2. Cladogram of human class I small molecule methyltransferases

The tree was produced with sequence alignment scores from Clustal Omega multiple sequence alignment tool accessed at https://www.uniprot.org/align [99]. Nodal distance from any two proteins gives rank order sequence similarity. The structure of a characteristic methylated substrate is adjacent to each methyltransferase's label. The cladogram tree was edited with Dendroscope [100].

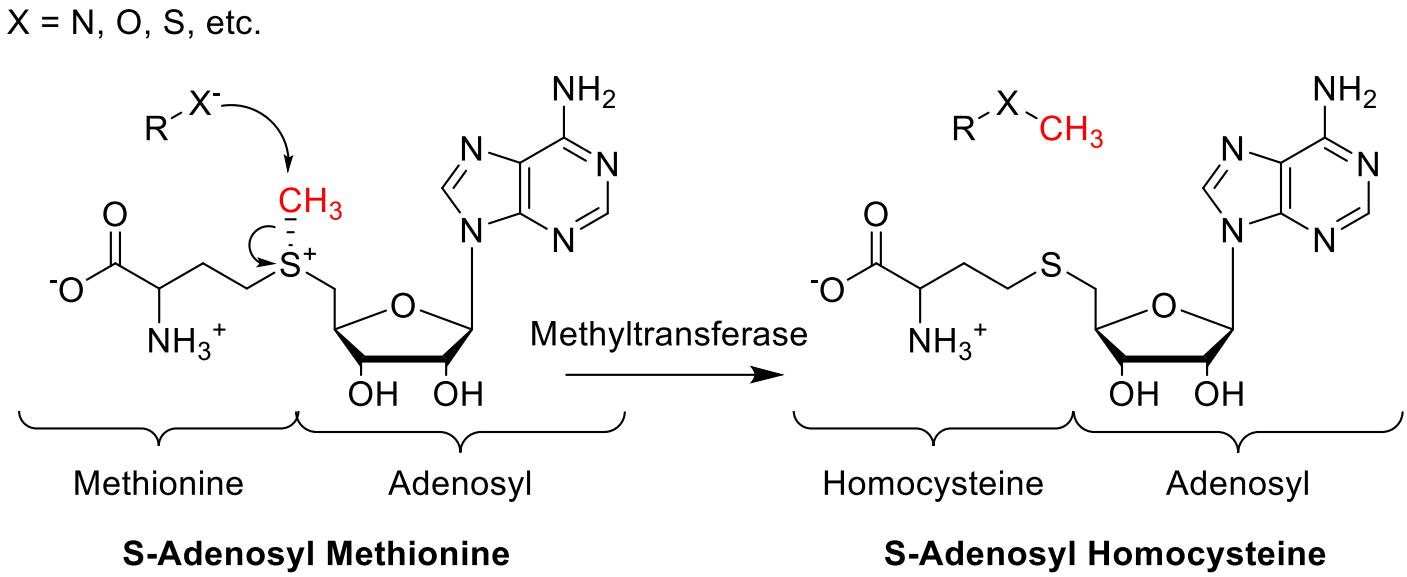

Figure 1.3. General SAM-dependent methyltransferase reaction mechanism

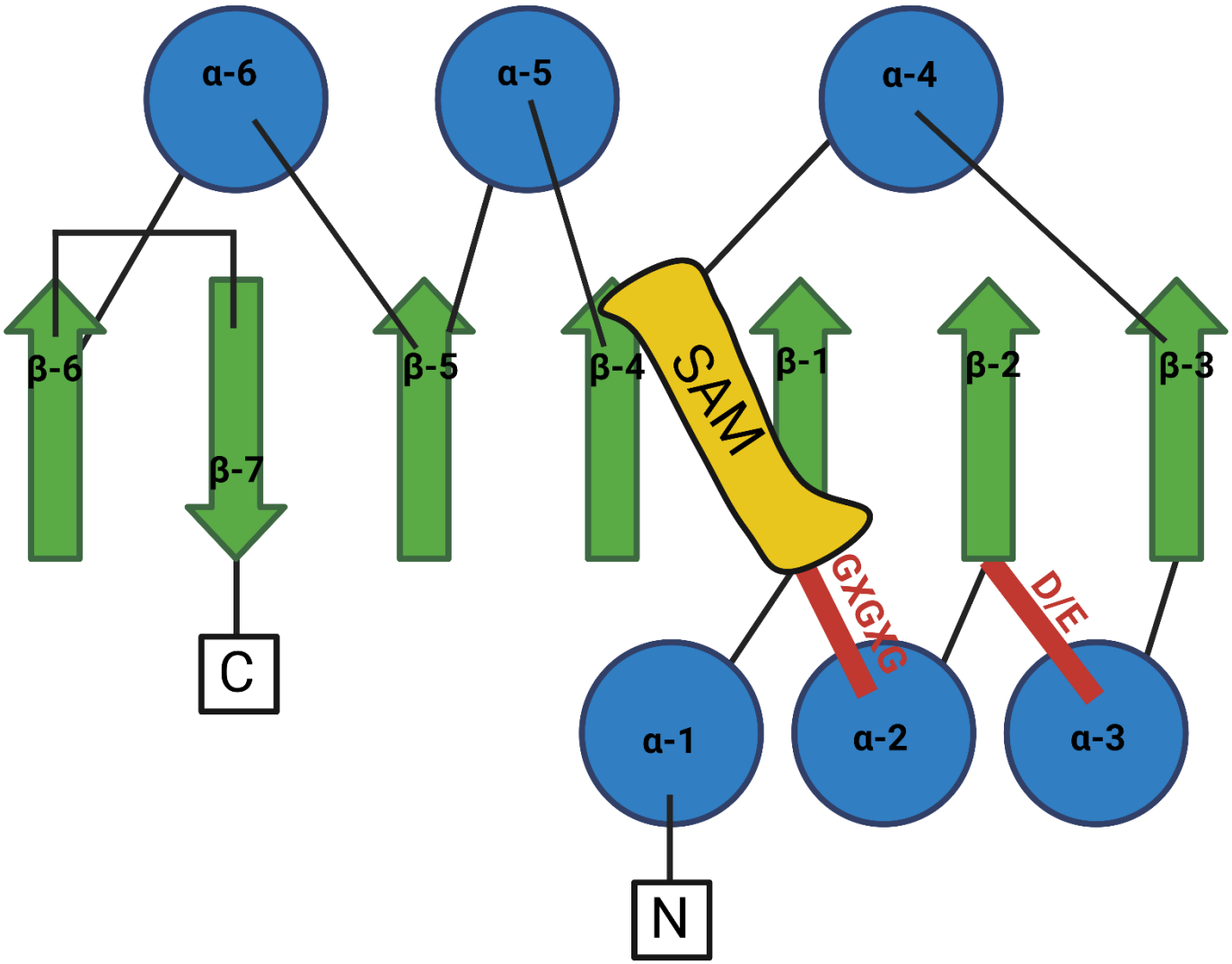

Figure 1.4. Cartoon representation of Class I methyltransferases

As described by Schubert *et al.* adapted from Russell *et al.* using BioRender [5, 20]. α-Helices (blue) are labeled α-1 through α-6, beta-sheets (green) are labeled β-1 through β-7. The SAM binding site is marked in yellow, and the GXGXG sequence and acidic residue are labeled and marked in red.

Table 1.1. Residues for class I methyltransferase binding motifs

Nucleotide binding motif and acidic residue (both in red) and local sequence (black) tabulated for several small molecule methyltransferases.

Methyltransferase	Nucleotide binding motif	Acidic Residue
AS3MT	N(75)-DLGSGSGRD-C(85)	N(99)-GIDMT-C(105)
COMT	N(113)-ELGAYCGYS-C(123)	N(137)-TIEIN-C(143)
HNMT	N(57)-SIGGGAGEI-C(67)	N(86)-VVEPS-C(92)
INMT/TEMT	N(59)-IDIGSGPTI-C(69)	N(82)-LSDFT-C(88)
NNMT	N(59)-IDIGSGPTI-C(69)	N(82)-VTDYS-C(88)
PNMT	N(75)-IDIGSGPTV-C(85)	N(98)-MTDFL-C(104)
TMT1A	N(75)-EVGCGTGAN-C(85)	N(95)-CIDPN-C(101)
TMT1B	N(75)-ELGCGTGAN-C(85)	N(95)-CLDPN-C(101)
TPMT	N(66)-FPLCGKAVE-C(76)	N(87)-GVEIS-C(93)

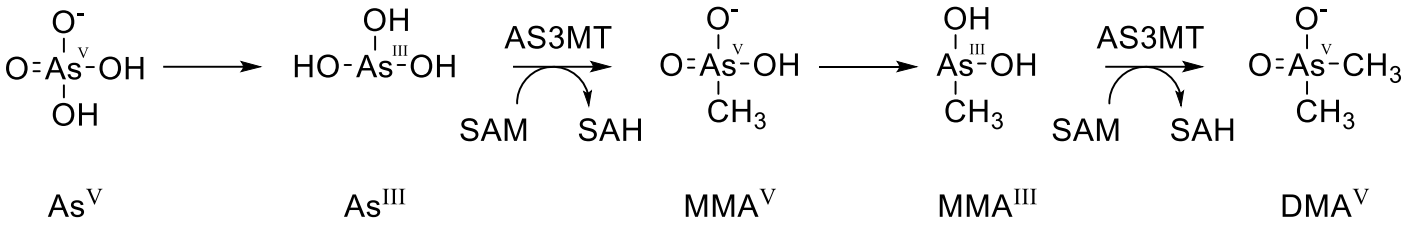

Figure 1.5. The general scheme originally proposed for the methylation of arsenic by AS3MT

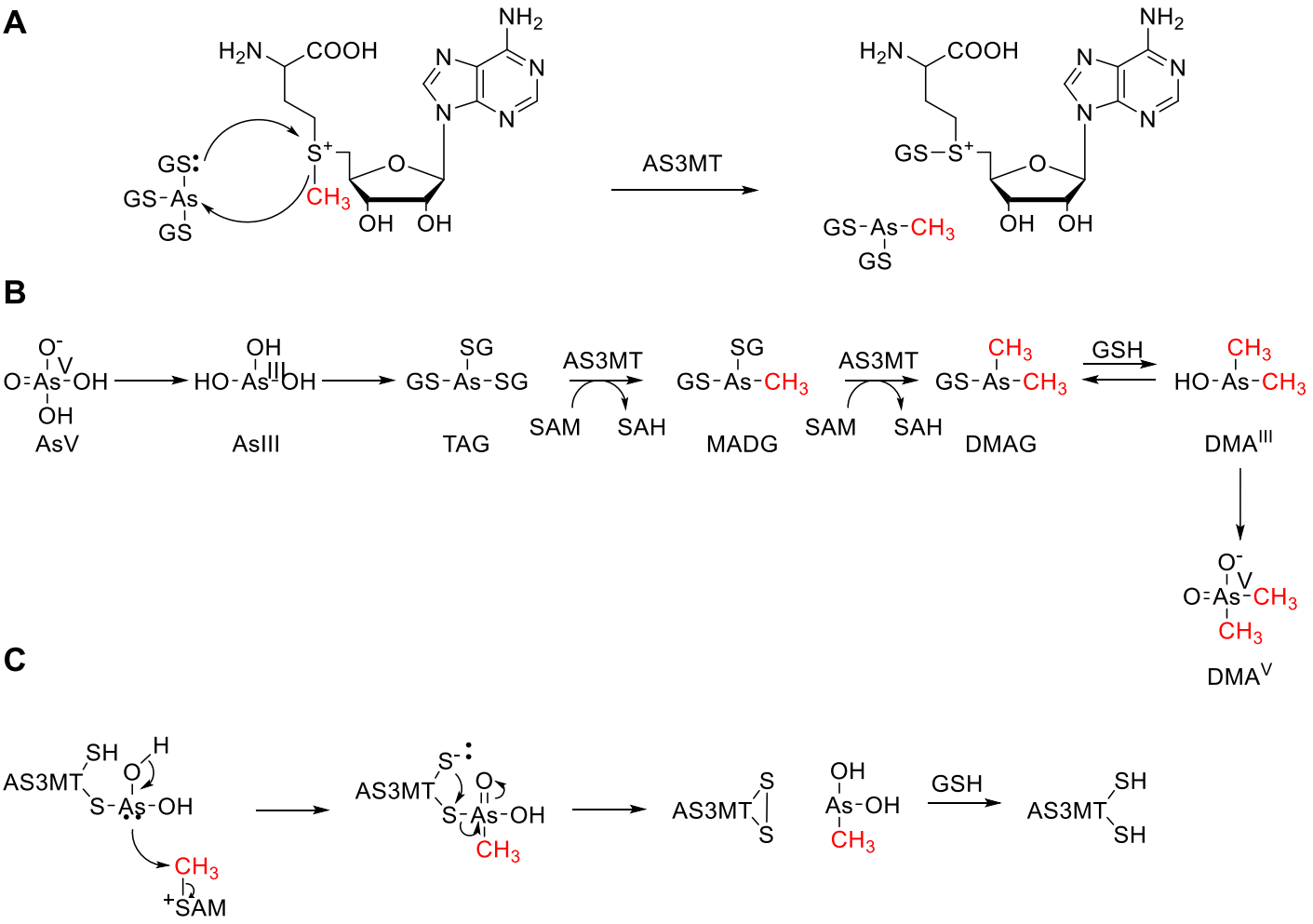

Figure 1.6. Proposed reaction mechanisms for AS3MT-catalyzed methylation of arsenic

Reaction mechanism (A) and scheme (B) for AS3MT-catalyzed methylation of arsenic proposed by Hayakawa *et al.* Reaction mechanism and scheme (C) proposed by Song *et al.*, for a GSH-mediated regeneration of AS3MT between AS3MT-catalyzed arsenic methylation steps.

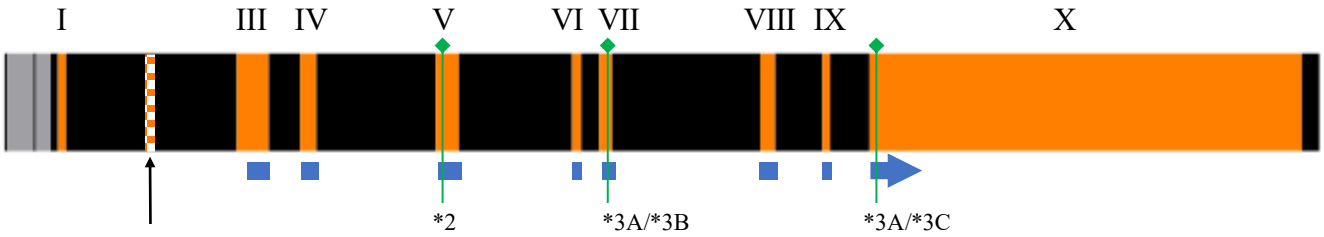

Exon II — identified by Szumlanski *et al.*, 1996. The sequence is no longer considered an exon in the current Ensembl TPMT gene annotation ENST00000309983.5. Exon numbers are kept the same to avoid confusion.

Allele	Base Change	Residue Change
*1	WT	WT
*2	G>C	A80P
*3A	G>A|A>G	A154T|Y240C
*3B	G>A	A154T
*3C	A>G	Y240C

Figure 1.7. Annotated TPMT gene

TPMT gene with introns (black) at 1/3 their length relative to exons (orange). An adjacent gene's exon (grey). The translated region of exons III-X is marked by the light blue elements below each exon. TPMT variants *2, *3A, *3B, and *3C are labeled and marked by green lines attached to diamond markers. The table summarizes the nucleotide base change and the residue change associated with each variant.

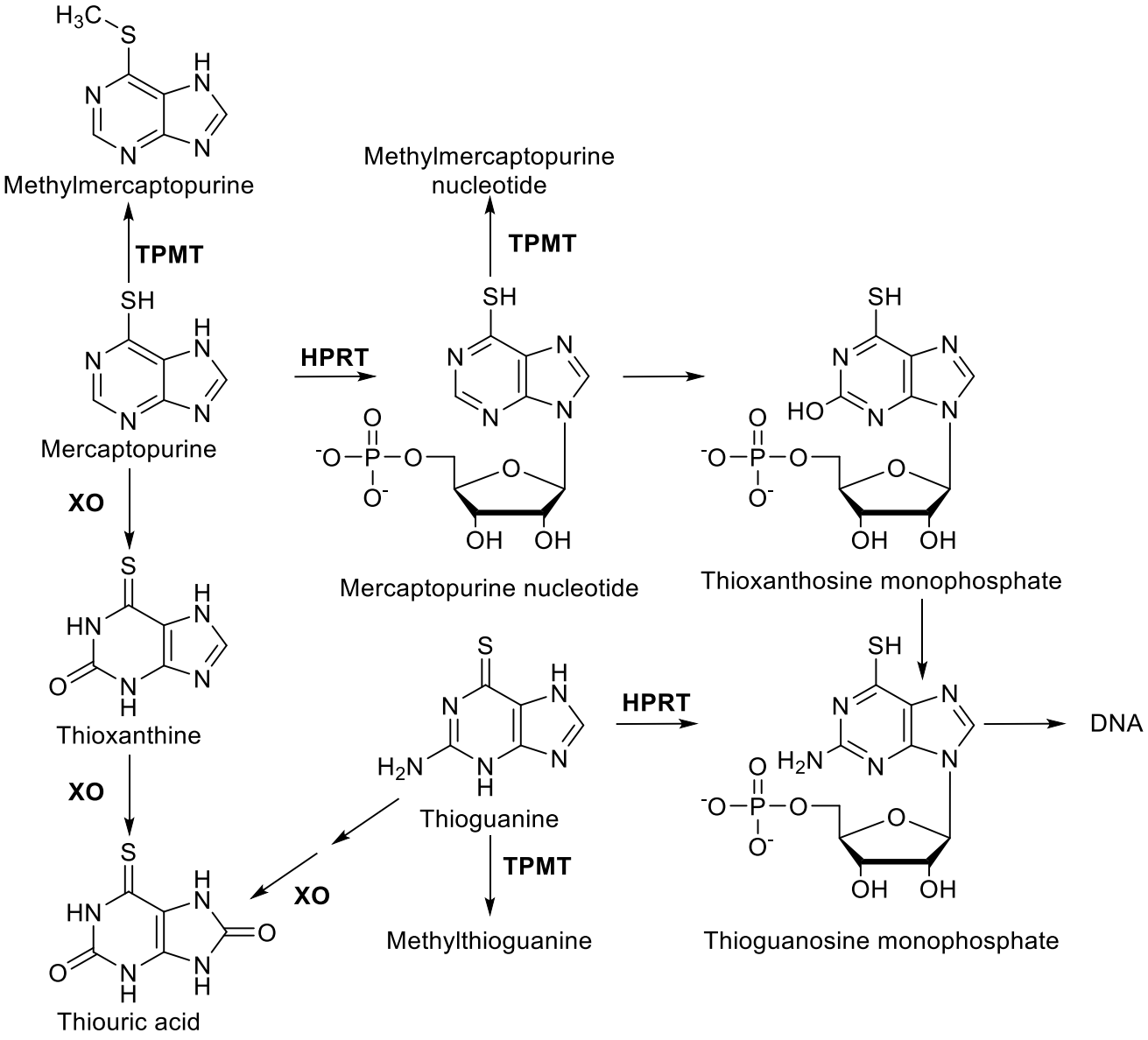

Figure 1.8. Metabolism scheme for TPMT thiopurine substrates

TPMT-mediated metabolism of the thiopurine drugs 6-MP and TG.

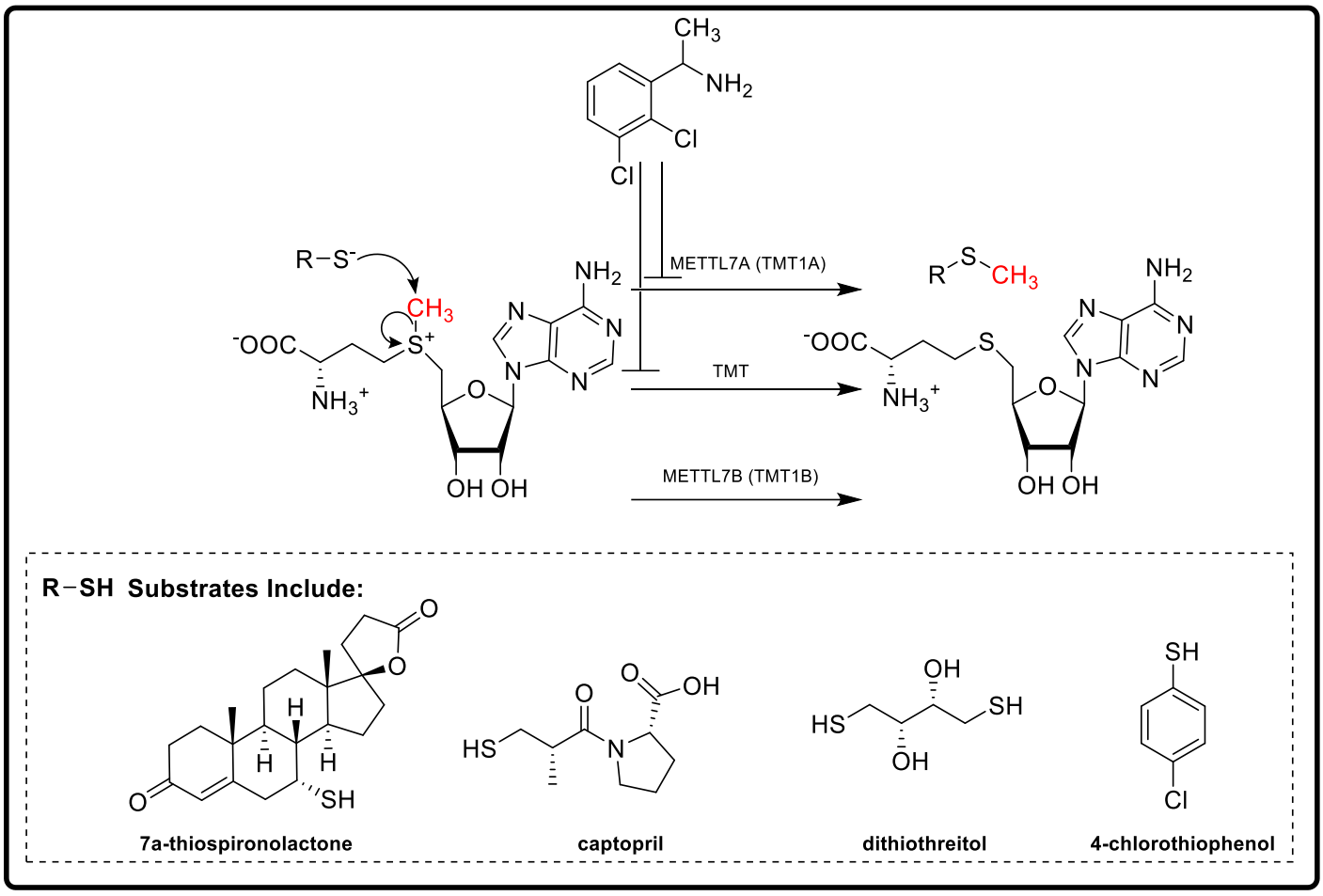

Figure 1.9. Graphical overview of TMT activity

An overview of TMT activity and the enzymes, TMT1A and TMT1B, that are responsible for it. Relevant substrates and the inhibitor DCMB are also presented.

Figure 1.9 reproduced in part, with permissions from Russell, D.A., et al., METTL7A (TMT1A) and METTL7B (TMT1B) Are Responsible for Alkyl. Drug Metab Dispos, 2023. 51(8): p. 1024-1034. DOI: 10.1124/dmd.123.001268

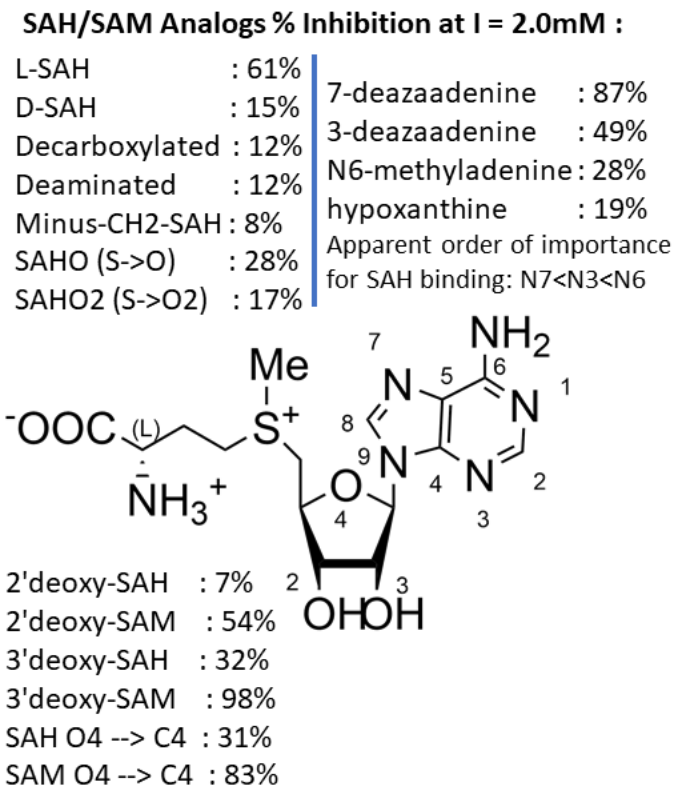

Figure 1.10. Structure activity relationship of SAM and SAH analogs binding TMT [65]

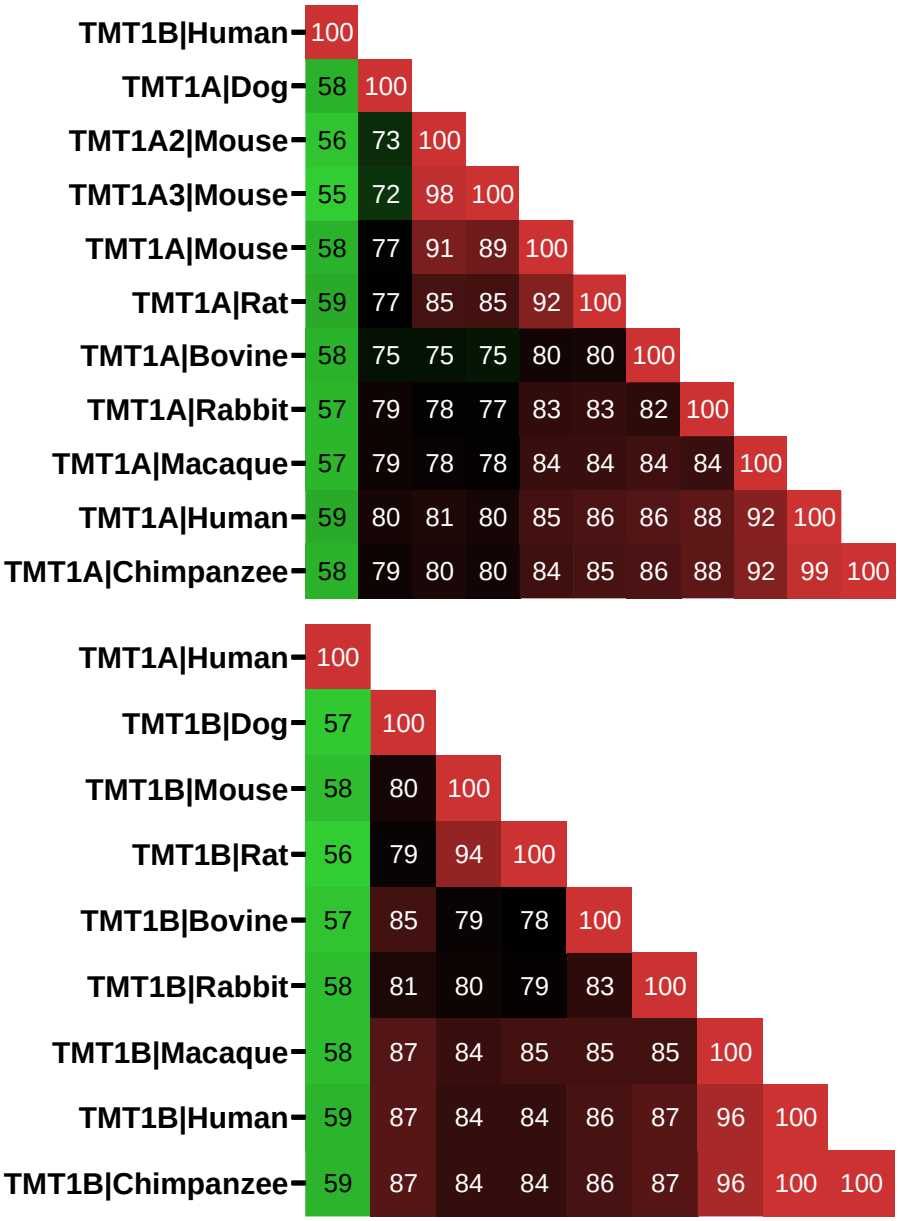

Figure 1.11. Percent identity matrix of select mammalian TMT1A and TMT1B proteins

Percent identity matrix of select mammalian TMT1A (A) and TMT1B (B) proteins calculated with Clustal Omega multiple sequence alignment tool accessed at https://www.uniprot.org/align [99]. Each cell label is the percent (%) of identical residues between two aligned TMT1 sequences.

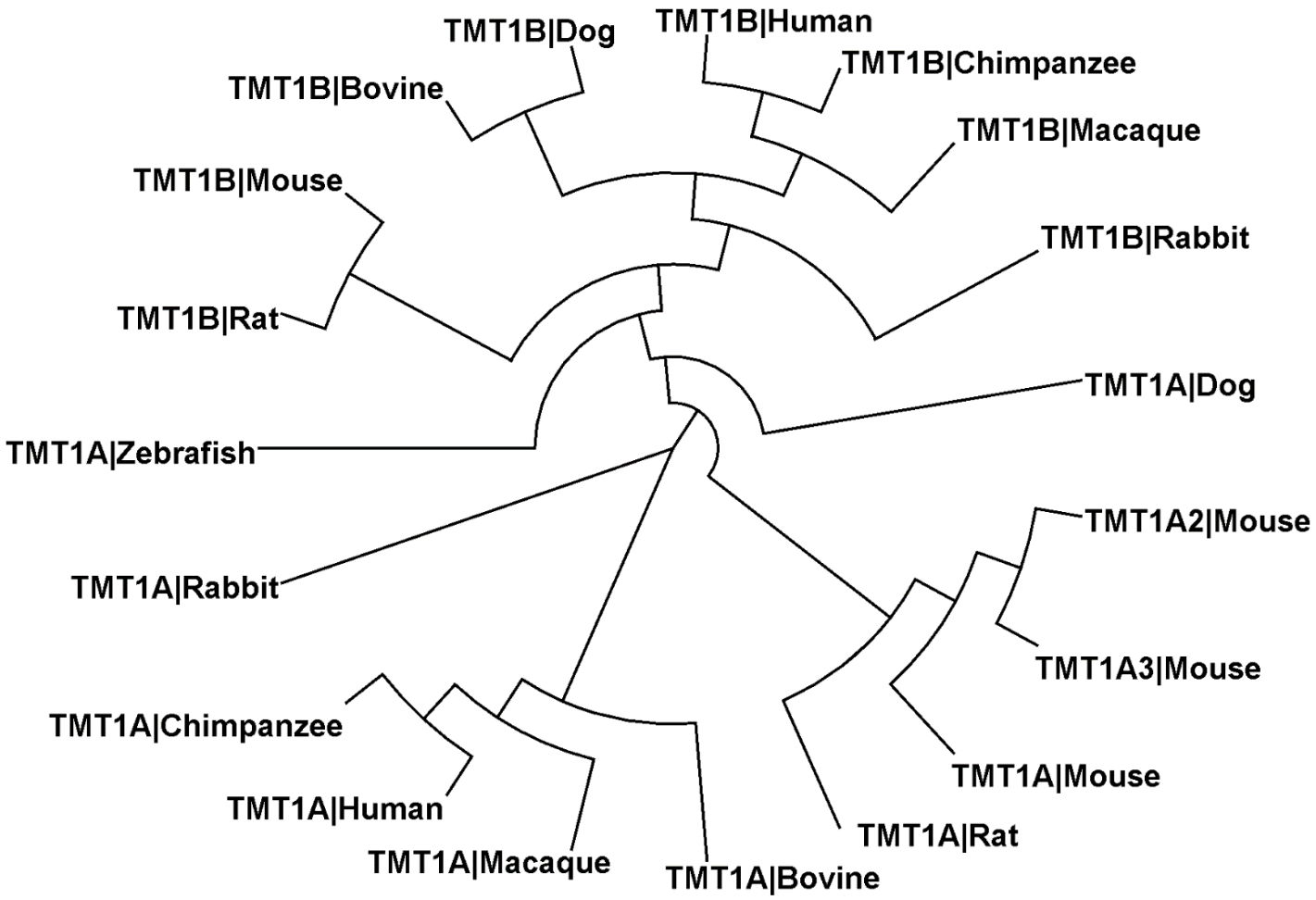

Figure 1.12. Cladogram of select mammalian and zebrafish TMT1 proteins

Proximity is correlated with sequence identity. The more similar two protein sequences are, the closer they will be to each other on the tree. The tree was produced with sequence alignment scores from Clustal Omega multiple sequence alignment tool accessed at https://www.uniprot.org/align [99]. The cladogram tree was edited with Dendroscope [100].

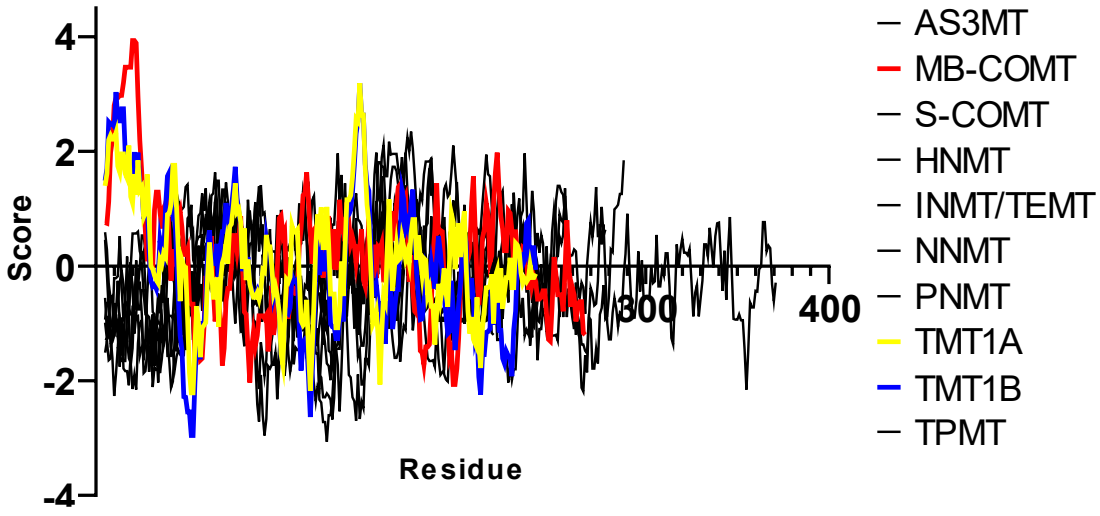

Figure 1.13. Hydrophobicity of TMT1A and TMT1B compared to other small molecule methyltransferases

Hydropathy score, using the Kyte and Doolittle scoring function, for each small molecule methyltransferase's protein sequence. The plot shows that TMT1A, TMT1B, and MB-COMT uniquely have hydrophobic *N*-termini.

.

1.4 REFERENCES

1. Garrow, T.A., *Purification, kinetic properties, and cDNA cloning of mammalian betaine-homocysteine methyltransferase.* J Biol Chem, 1996. **271**(37): p. 22831-8.

2. Ragsdale, S.W., *Catalysis of methyl group transfers involving tetrahydrofolate and B(12).* Vitam Horm, 2008. **79**: p. 293-324.

3. Szegedi, S.S., et al., *Betaine-homocysteine S-methyltransferase-2 is an S-methylmethionine-homocysteine methyltransferase.* J Biol Chem, 2008. **283**(14): p. 8939-45.

4. Schluckebier, G., et al., *Universal Catalytic Domain Structure of AdoMet-dependent Methyltransferases.* Journal of Molecular Biology, 1995. **247**(1): p. 16-20.

5. Schubert, H.L., R.M. Blumenthal, and X. Cheng, *Many paths to methyltransfer: a chronicle of convergence.* Trends in Biochemical Sciences, 2003. **28**(6): p. 329-335.

6. Weinshilboum, R.M., D.M. Otterness, and C.L. Szumlanski, *Methylation pharmacogenetics: catechol O-methyltransferase, thiopurine methyltransferase, and histamine N-methyltransferase.* Annu Rev Pharmacol Toxicol, 1999. **39**(1): p. 19-52.

7. His, W., *Ueber das stoffwechselproduct des pyridins.* Archiv für experimentelle Pathologie und Pharmakologie, 1887. **22**: p. 253-260.

8. Dhayalan, A. and A. Jeltsch, *Special Issue "Structure, Activity, and Function of Protein Methyltransferases".* Life (Basel), 2022. **12**(3).

9. Mattei, A.L., N. Bailly, and A. Meissner, *DNA methylation: a historical perspective.* Trends Genet, 2022. **38**(7): p. 676-707.

10. Boulias, K. and E.L. Greer, *Biological roles of adenine methylation in RNA.* Nat Rev Genet, 2023. **24**(3): p. 143-160.

11. Pissios, P., *Nicotinamide N-Methyltransferase: More Than a Vitamin B3 Clearance Enzyme.* Trends Endocrinol Metab, 2017. **28**(5): p. 340-353.

12. Rafalowska, U., J. Waskiewicz, and J. Albrecht, *Is neurotransmitter histamine predominantly inactivated in astrocytes?* Neurosci Lett, 1987. **80**(1): p. 106-10.

13. Evinger, M., et al., *A single transmitter regulates gene expression through two separate mechanisms: cholinergic regulation of phenylethanolamine N- methyltransferase mRNA*

via nicotinic and muscarinic pathways. The Journal of Neuroscience, 1994. **14**(4): p. 2106-2116.

14. Thompson, M.A., et al., *Human indolethylamine N-methyltransferase: cDNA cloning and expression, gene cloning, and chromosomal localization.* Genomics, 1999. **61**(3): p. 285-97.

15. Chu, U., et al., *Methylation of Thiols and Thioethers by Human Indolethylamine-N Methyl Transferase.* The FASEB Journal, 2015. **29**(S1): p. 1022.7.

16. Pavel, S., *Dynamics of Melanogenesis Intermediates.* Journal of Investigative Dermatology, 1993. **100**(2, Supplement): p. S162-S165.

17. Smit, N.P.M., et al., *Catechol-O-methyltransferase as a target for melanoma destruction?* Biochemical Pharmacology, 1994. **48**(4): p. 743-752.

18. Kaakkola, S., A. Gordin, and P.T. Männistö, *General properties and clinical possibilities of new selective inhibitors of catechol O-methyltransferase.* General Pharmacology: The Vascular System, 1994. **25**(5): p. 813-824.

19. Drobná, Z., et al., *Interindividual variation in the metabolism of arsenic in cultured primary human hepatocytes.* Toxicol Appl Pharmacol, 2004. **201**(2): p. 166-77.

20. Russell, D.A., et al., *METTL7A (TMT1A) and METTL7B (TMT1B) Are Responsible for Alkyl.* Drug Metab Dispos, 2023. **51**(8): p. 1024-1034.

21. Mulder, G.J. *Conjugation reactions in drug metabolism : an integrated approach : substrates, co-substrates, enzymes and their interactions in vivo and in vitro*. 1990.

22. Weinshilboum, R., *Pharmacogenetics of methylation: Relationship to drug metabolism.* Clinical Biochemistry, 1988. **21**(4): p. 201-210.

23. Maldonato, B.J., D.A. Russell, and R.A. Totah, *Human METTL7B is an alkyl thiol methyltransferase that metabolizes hydrogen sulfide and captopril.* Sci Rep, 2021. **11**(1): p. 4857.

24. Cheng, X., et al., *Crystal structure of the Hhal DNA methyltransferase complexed with S-adenosyl-l-methionine.* Cell, 1993. **74**(2): p. 299-307.

25. Sun, Q., M. Huang, and Y. Wei, *Diversity of the reaction mechanisms of SAM-dependent enzymes.* Acta Pharm Sin B, 2021. **11**(3): p. 632-650.

26. Abdelraheem, E., et al., *Methyltransferases: Functions and Applications.* ChemBioChem, 2022. **23**(18): p. e202200212.

27. Gopinath, A., et al., *The conserved aspartate in motif III of b family AdoMet-dependent DNA methyltransferase is important for methylation.* J Biosci, 2020. **45**.

28. Liscombe, D.K., G.V. Louie, and J.P. Noel, *Architectures, mechanisms and molecular evolution of natural product methyltransferases.* Nat Prod Rep, 2012. **29**(10): p. 1238-50.

29. Packianathan, C., P. Kandavelu, and B.P. Rosen, *The Structure of an As(III) S-Adenosylmethionine Methyltransferase with 3-Coordinately Bound As(III) Depicts the First Step in Catalysis.* Biochemistry, 2018. **57**(28): p. 4083-4092.

30. Hayakawa, T., et al., *A new metabolic pathway of arsenite: arsenic-glutathione complexes are substrates for human arsenic methyltransferase Cyt19.* Arch Toxicol, 2005. **79**(4): p. 183-91.

31. Song, X., et al., *New insights into the mechanism of arsenite methylation with the recombinant human arsenic (+3) methyltransferase (hAS3MT).* Biochimie, 2010. **92**(10): p. 1397-406.

32. Song, X., et al., *Functional and structural evaluation of cysteine residues in the human arsenic (+3 oxidation state) methyltransferase (hAS3MT).* Biochimie, 2011. **93**(2): p. 369-75.

33. Song, X., et al., *Structure-function roles of four cysteine residues in the human arsenic (+3 oxidation state) methyltransferase (hAS3MT) by site-directed mutagenesis.* Chem Biol Interact, 2009. **179**(2-3): p. 321-8.

34. Styblo, M., et al., *Comparative toxicity of trivalent and pentavalent inorganic and methylated arsenicals in rat and human cells.* Arch Toxicol, 2000. **74**(6): p. 289-99.

35. Healy, S.M., et al., *Diversity of inorganic arsenite biotransformation.* Biol Trace Elem Res, 1999. **68**(3): p. 249-66.

36. Gregus, Z. and B. Németi, *Purine nucleoside phosphorylase as a cytosolic arsenate reductase.* Toxicol Sci, 2002. **70**(1): p. 13-9.

37. Schmuck, E.M., et al., *Characterization of the monomethylarsonate reductase and dehydroascorbate reductase activities of Omega class glutathione transferase variants: implications for arsenic metabolism and the age-at-onset of Alzheimer's and Parkinson's diseases.* Pharmacogenet Genomics, 2005. **15**(7): p. 493-501.

38. Waters, S.B., et al., *Endogenous reductants support the catalytic function of recombinant rat cyt19, an arsenic methyltransferase.* Chem Res Toxicol, 2004. **17**(3): p. 404-9.

39. Zakharyan, R.A., et al., *Enzymatic methylation of arsenic compounds. VII. Monomethylarsonous acid (MMAIII) is the substrate for MMA methyltransferase of rabbit liver and human hepatocytes.* Toxicol Appl Pharmacol, 1999. **158**(1): p. 9-15.

40. Thomas, D.J., S.B. Waters, and M. Styblo, *Elucidating the pathway for arsenic methylation.* Toxicol Appl Pharmacol, 2004. **198**(3): p. 319-26.

41. Drobna, Z., M. Styblo, and D.J. Thomas, *An Overview of Arsenic Metabolism and Toxicity.* Curr Protoc Toxicol, 2009. **42**(431): p. 4.31.1-4.31.6.

42. Woodson, L.C. and R.M. Weinshilboum, *Human kidney thiopurine methyltransferase purification and biochemical properties.* Biochemical Pharmacology, 1983. **32**(5): p. 819-826.

43. Ames, M.M., et al., *Thiopurine methyltransferase: structure-activity relationships for benzoic acid inhibitors and thiophenol substrates.* Journal of medicinal chemistry, 1986. **29**(3): p. 354-358.

44. Lennard, L. and J.S. Lilleyman, *Variable mercaptopurine metabolism and treatment outcome in childhood lymphoblastic leukemia.* Journal of Clinical Oncology, 1989. **7**(12): p. 1816-1823.

45. Lennard, L., J.A. Van Loon, and R.M. Weinshilboum, *Pharmacogenetics of acute azathioprine toxicity: Relationship to thiopurine methyltransferase genetic polymorphism.* Clinical Pharmacology & Therapeutics, 1989. **46**(2): p. 149-154.

46. Lennard, L., et al., *Genetic variation in response to 6-mercaptopurine for childhood acute lymphoblastic leukaemia.* The Lancet, 1990. **336**(8709): p. 225-229.

47. Wang, L. and R. Weinshilboum, *Thiopurine S-methyltransferase pharmacogenetics: insights, challenges and future directions.* Oncogene, 2006. **25**(11): p. 1629-1638.

48. Mokmak, W., S. Tongsima, and E. Jenwitheesuk, *Molecular dynamics simulation of a human thiopurine S-methyltransferase complexed with 6-mercaptopurine model.* Bioinformation, 2009. **4**(2): p. 59-62.

49. Peng, Y., et al., *Structural Basis of Substrate Recognition in Thiopurine S-Methyltransferase.* Biochemistry, 2008. **47**(23): p. 6216-6225.

50. Weinshilboum, R.M. and S.L. Sladek, *Mercaptopurine pharmacogenetics: monogenic inheritance of erythrocyte thiopurine methyltransferase activity.* Am J Hum Genet, 1980. **32**(5): p. 651-62.

51. Otterness, D., et al., *Human thiopurine methyltransferase pharmacogenetics: Gene sequence polymorphisms.* Clinical Pharmacology & Therapeutics, 1997. **62**(1): p. 60-73.

52. Deininger, M., et al., *Purine substrates for human thiopurine methyltransferase.* Biochem Pharmacol, 1994. **48**(11): p. 2135-8.

53. Woodson, L.C., et al., *Thiopurine methyltransferase. Aromatic thiol substrates and inhibition by benzoic acid derivatives.* Molecular Pharmacology, 1983. **24**(3): p. 471-478.

54. Ranjard, L., S. Nazaret, and B. Cournoyer, *Freshwater bacteria can methylate selenium through the thiopurine methyltransferase pathway.* Appl Environ Microbiol, 2003. **69**(7): p. 3784-90.

55. Urbančič, D., et al., *Methylation of selenocysteine catalysed by thiopurine S-methyltransferase.* Biochim Biophys Acta Gen Subj, 2019. **1863**(1): p. 182-190.

56. Fukumoto, Y., et al., *Production of a Urinary Selenium Metabolite, Trimethylselenonium, by Thiopurine.* Chem Res Toxicol, 2020. **33**(9): p. 2467-2474.

57. Schutz, E., et al., *Azathioprine-induced myelosuppression in thiopurine methyltransferase deficient heart transplant recipient.* Lancet, 1993. **341**(8842): p. 436.

58. FDA, *IMURAN (azathioprine)*. 2011, Prometheus Laboratories Inc.

59. Relling, M.V., et al., *Clinical Pharmacogenetics Implementation Consortium guidelines for thiopurine methyltransferase genotype and thiopurine dosing.* Clin Pharmacol Ther, 2011. **89**(3): p. 387-91.

60. Chouchana, L., et al., *Interindividual variability in TPMT enzyme activity: 10 years of experience with thiopurine pharmacogenetics and therapeutic drug monitoring.* Pharmacogenomics, 2014. **15**(6): p. 745-57.

61. Weinshilboum, R.M., S. Sladek, and S. Klumpp, *Human erythrocyte thiol methyltransferase: radiochemical microassay and biochemical properties.* Clin Chim Acta, 1979. **97**(1): p. 59-71.

62. Weisiger, R.A., & Jakoby, W.B, *S-Methylation: Thiol S-Methyltransferase*, in *Enzymatic Basis of Detoxication Volume 2*, W.B. Jakoby, Editor. 1980, Academic Press: New York, NY. p. 131-140.

63. Weisiger, R.A. and W.B. Jakoby, *Thiol S-methyltransferase.* Methods Enzymol, 1981. **77**: p. 257-62.

64. Weisiger, R.A. and W.B. Jakoby, *Thiol S-methyltransferase from rat liver.* Arch Biochem Biophys, 1979. **196**(2): p. 631-7.

65. Borchardt, R.T. and C.F. Cheng, *Purification and characterization of rat liver microsomal thiol methyltransferase.* Biochim Biophys Acta, 1978. **522**(2): p. 340-53.

66. Pacifici, G.M., et al., *Thiol methyltransferase in humans: development and tissue distribution.* Dev Pharmacol Ther, 1991. **17**(1-2): p. 8-15.

67. Keith, R.A., et al., *Thiol methylation pharmacogenetics: Heritability of human erythrocyte thiol methyltransferase activity.* Clinical Pharmacology & Therapeutics, 1983. **34**(4): p. 521-528.

68. Keith, R.A., et al., *Human erythrocyte membrane thiol methyltransferase. S-methylation of captopril, N-acetylcysteine, and 7 alpha-thio-spirolactone.* Drug Metabolism and Disposition, 1984. **12**(6): p. 717-724.

69. Kerremans, A., H. Christensen, and R. Weinshilboum. *Thiol methyltransferase (TMT) activity in human renal cortex microsomes*. in *Federation Proceedings*. 1984.

70. Glauser, T.A., A.L. Kerremans, and R.M. Weinshilboum, *Human hepatic microsomal thiol methyltransferase. Assay conditions, biochemical properties, and correlation studies.* Drug Metab Dispos, 1992. **20**(2): p. 247-55.

71. Obach, R.S., C. Prakash, and A.M. Kamel, *Reduction and methylation of ziprasidone by glutathione, aldehyde oxidase, and thiol S-methyltransferase in humans: an in vitro study.* Xenobiotica, 2012. **42**(11): p. 1049-57.

72. Kazui, M., et al., *Hepatic microsomal thiol methyltransferase is involved in stereoselective methylation of pharmacologically active metabolite of prasugrel.* Drug Metab Dispos, 2014. **42**(7): p. 1138-45.

73. Liu, C., et al., *Human Liver Cytochrome P450 Enzymes and Microsomal Thiol Methyltransferase Are Involved in the Stereoselective Formation and Methylation of the Pharmacologically Active Metabolite of Clopidogrel.* Drug Metab Dispos, 2015. **43**(10): p. 1632-41.

74. Fuller, R.W., et al., *Inhibition of phenylethanolamine N-methyltransferase by benzylamines. 2. In vitro and in vivo studies with 2,3-dichloro- -methylbenzylamine.* J Med Chem, 1973. **16**(2): p. 106-9.

75. Glauser, T.A., et al., *Human liver microsomal thiol methyltransferase: inhibition by arylalkylamines.* Xenobiotica, 1993. **23**(6): p. 657-69.

76. Maw, H.H., et al., *-Methylation of BI 187004 by Thiol.* Drug Metab Dispos, 2018. **46**(6): p. 770-778.

77. Kimura, H., *Production and physiological effects of hydrogen sulfide.* Antioxid Redox Signal, 2014. **20**(5): p. 783-93.

78. Shen, Y., et al., *The Cardioprotective Effects of Hydrogen Sulfide in Heart Diseases: From Molecular Mechanisms to Therapeutic Potential.* Oxid Med Cell Longev, 2015. **2015**: p. 925167.

79. Xiao, Q., et al., *The biologic effect of hydrogen sulfide and its function in various diseases.* Medicine (Baltimore), 2018. **97**(44): p. e13065.

80. Weisiger, R.A., L.M. Pinkus, and W.B. Jakoby, *Thiol S-methyltransferase: suggested role in detoxication of intestinal hydrogen sulfide.* Biochem Pharmacol, 1980. **29**(20): p. 2885-7.

81. Zeigler, M.B., et al., *Plasma hydrogen sulfide, nitric oxide, and thiocyanate levels are lower during pregnancy compared to postpartum in a cohort of women from the Pacific northwest of the United States.* Life Sci, 2023. **322**: p. 121625.

82. Ljunggren, G. and B.O. Norberg, *On the Effect and Toxicity of Dimethyl Sulfide, Dimethyl Disulfide and Methyl Mercaptan.* Acta Physiologica Scandinavica, 1943. **5**(2-3): p. 248-255.

83. Tansy, M.F., et al., *Acute and subchronic toxicity studies of rats exposed to vapors of methyl mercaptan and other reduced-sulfur compounds.* J Toxicol Environ Health, 1981. **8**(1-2): p. 71-88.

84. Savi, P., et al., *The active metabolite of Clopidogrel disrupts P2Y12 receptor oligomers and partitions them out of lipid rafts.* Proc Natl Acad Sci U S A, 2006. **103**(29): p. 11069-74.

85. Overdiek, H.W. and F.W. Merkus, *The metabolism and biopharmaceutics of spironolactone in man.* Rev Drug Metab Drug Interact, 1987. **5**(4): p. 273-302.

86. Robey, R.W., et al., *The methyltransferases METTL7A and METTL7B confer resistance to thiol-based histone deacetylase inhibitors.* bioRxiv, 2023: p. 2022.10.07.511310.

87. Petrossian, T.C. and S.G. Clarke, *Uncovering the human methyltransferasome.* Mol Cell Proteomics, 2011. **10**(1): p. M110.000976.

88. Qi, Y.N., et al., *Methyltransferase-like proteins in cancer biology and potential therapeutic targeting.* J Hematol Oncol, 2023. **16**(1): p. 89.

89. Blake, J.A., et al., *Mouse Genome Database (MGD): Knowledgebase for mouse-human comparative biology.* Nucleic Acids Res, 2021. **49**(D1): p. D981-D987.

90. Zehmer, J.K., et al., *Identification of a novel N-terminal hydrophobic sequence that targets proteins to lipid droplets.* J Cell Sci, 2008. **121**(11): p. 1852-60.

91. Turró, S., et al., *Identification and characterization of associated with lipid droplet protein 1: A novel membrane-associated protein that resides on hepatic lipid droplets.* Traffic, 2006. **7**(9): p. 1254-69.

92. Kyte, J. and R.F. Doolittle, *A simple method for displaying the hydropathic character of a protein.* J Mol Biol, 1982. **157**(1): p. 105-32.

93. Campeanu, I.J., et al., *Multi-omics integration of methyltransferase-like protein family reveals clinical outcomes and functional signatures in human cancer.* Sci Rep, 2021. **11**(1): p. 14784.

94. Jiang, Z., et al., *METTL7B is a novel prognostic biomarker of lower-grade glioma based on pan-cancer analysis.* Cancer Cell Int, 2021. **21**(1): p. 383.

95. Liu, D., et al., *METTL7B Is Required for Cancer Cell Proliferation and Tumorigenesis in Non-Small Cell Lung Cancer.* Front Pharmacol, 2020. **11**: p. 178.

96. Li, W., et al., *Downregulation of METTL7B Inhibits Proliferation of Human Clear Cell Renal Cancer Cells.* Front Oncol, 2021. **11**: p. 634542.

97. Ye, D., et al., *METTL7B promotes migration and invasion in thyroid cancer through epithelial-mesenchymal transition.* J Mol Endocrinol, 2019. **63**(1): p. 51-61.

98. Xiong, Y., et al., *High Level of METTL7B Indicates Poor Prognosis of Patients and Is Related to Immunity in Glioma.* Front Oncol, 2021. **11**: p. 650534.

99. Sievers, F. and D.G. Higgins, *Clustal Omega for making accurate alignments of many protein sequences.* Protein Sci, 2018. **27**(1): p. 135-145.

100. Huson, D.H. and C. Scornavacca, *Dendroscope 3: an interactive tool for rooted phylogenetic trees and networks.* Syst Biol, 2012. **61**(6): p. 1061-7.

Chapter 2. **METTL7A (TMT1A) and METTL7B (TMT1B) are Responsible for Alkyl *S*-Thiol Methyl Transferase Activity in Liver**

Reproduced in part, with permissions from Russell, D.A., *et al.*, METTL7A (TMT1A) and METTL7B (TMT1B) Are Responsible for Alkyl. Drug Metab Dispos, 2023. 51(8): p. 1024-1034. DOI: 10.1124/dmd.123.001268

Note: In the original publication, we chose to change the name of METTL7A and METTL7B to TMT1A and TMT1B in the discussion because it was at that time in the publication the reader would be convinced that the change in names was appropriate. This stylistic choice was maintained in this chapter even though the enzymes have already been introduced as TMT1A and TMT1B in Chapter 1. The renaming of METTL7A and METTL7B to TMT1A and TMT1B was initiated by the Human Genome Organization (HUGO) Gene Nomenclature Committee (HGNC) after they read a preprint of the Russell *et al.* 2023 paper uploaded to bioRxiv. The HGNC concluded that there is precedent to rename these enzymes because "TMT was previously used as the abbreviation for this (non-purified) enzymatic activity, and TMT gives about 10 relevant PubMed hits, and all other small molecule Class I methyltransferases carry names reflecting their substrates (COMT, PEMT, NNMT, GNMT, TPMT, etc)".

2.1 INTRODUCTION

In humans, two distinct enzyme systems are associated with *S*-methyltransferase activity, thiopurine methyltransferase (TPMT) and a putative thiol methyltransferase (TMT) [1, 2]. TPMT is a well-characterized cytosolic enzyme, while putative TMT, or TMT activity, is used in the literature to describe one, or more, heretofore unidentified microsomal enzymes capable of thiol methylation, but the exact gene and protein remain uncharacterized. Both TPMT and TMT transfer a methyl group from the cofactor *S*-adenosyl-L-methionine (SAM) to a thiol group. Thiols are reactive nucleophiles capable of altering the oxidation potential of essential biomolecules by forming covalent bonds.

TPMT is a well-characterized methyltransferase that specifically methylates exogenous thiopurines [3], but to date, no endogenous substrate has been identified. TPMT substrates such as 6-mercaptopurine and azathioprine belong to a class of immunosuppressive chemotherapeutic

drugs with a narrow therapeutic index, and *S*-methylation is an inactivation and detoxification pathway. Genetic polymorphisms in TPMT, that result in decreased methylation activity, often lead to toxicity during treatment with these drugs [3, 4]. Weinshilboum and Sladek identified the enzyme responsible for TPMT activity in 1980 [5], and many studies detailing the biochemical and structural characterization of TPMT have since followed. Today, patients are routinely screened for TPMT polymorphisms prior to thiopurine drug therapy [6].

In contrast, the enzyme(s) responsible for TMT activity were not known and as a result, historically, the microsomal fractions of various tissue homogenates were used to characterize TMT activity. Past research established that the enzyme(s) responsible for TMT activity do not share substrates with TPMT but are responsible for the SAM-dependent *S*-methylation of exogenous alkyl and phenolic thiol-containing compounds. Endogenous thiols such as glutathione and cysteine are not substrates for TMT [7].

Many drugs characterized as substrates for this putative TMT require their thiol functional group for activity, and methylation potentially alters their pharmacology. Potential substrates include 7α-thiospironolactone (TSL), mertansine, the active metabolites of prasugrel and clopidogrel, ziprasidone, and captopril [8-13]. In most cases, it is difficult to determine *a priori* how methylation changes the activity of a particular drug. For example, the *S*-methyl metabolite of spironolactone, 7α-thiomethylspironolactone (TMSL), is the major circulating metabolite that is responsible for most of spironolactone's activity *in vivo* [14]. Mertansine, a potent microtubule inhibitor that is conjugated to antibodies through a disulfide bond, contains a free thiol upon reduction and release from the attached antibody [15]. Interestingly, one report suggested that *S*-methylation of mertansine’s free thiol alters its interaction with microtubules by increasing mertansine's effect on the dynamic instability of microtubules and promoting their aggregation; a

mechanism of action that is quite distinct from the parent free thiol which inhibits microtubule polymerization [16]. Clopidogrel and prasugrel are thienopyridine pro-drugs that require activation via cytochrome P450-mediated ring opening to expose a reactive thiol that forms a disulfide bond with, and irreversibly inhibits, P_2Y_{12}, a transmembrane receptor that controls platelet aggregation [17]. *S*-methylation of the reactive thiol results in the inactivation of these agents due to their inability to covalently bind to their receptor [17]. A better characterization of the enzyme(s) responsible for TMT activity could provide clinicians and drug developers alike, much needed insight when faced with a compound with an alkyl thiol.

Recently, we identified methyltransferase-like protein 7B (METTL7B) as an enzyme capable of catalyzing SAM-dependent methylation of alkyl thiols [18]. METTL7B is a 28 kDa microsomal protein with similar tissue distribution and substrate specificity to the putative TMT [19]. Although there is no specific inhibitor for the enzyme(s) responsible for TMT activity, 2,3-dichloro-α-methylbenzylamine (DCMB) potently inhibits TMT but not TPMT activity in liver microsomes [20, 21]. Interestingly, despite possessing several attributes that are characteristic of an enzyme responsible for TMT activity, METTL7B is not inhibited by DCMB even at high concentrations suggesting that additional enzymes also account for microsomal TMT activity.

The gene "*putative methyltransferase-like protein 7A* (*METTL7A*)" codes for the protein METTL7A in the same family as METTL7B [19]. METTL7A is proposed to be a membrane-associated methyltransferase and shares 75% sequence homology with METTL7B, but biochemical characterization that defines METTL7A's function is scant. In this chapter, we report that METTL7A, like METTL7B, is a SAM dependent *S*-methyltransferase with many similarities to the historic TMT, including potent inhibition by DCMB. Using multiple approaches including quantitative proteomics, single donor human liver microsomes (HLM), and

gene modulation experiments in HepG2 and HeLa cells, we determine that TMT activity is strongly associated with METTL7A protein levels. Furthermore, the purification of a novel His-GST-tagged recombinant protein and extensive biochemical characterization established that METTL7A methylates a wide variety of thiol-containing substrates, including TSL, dithiothreitol (DTT), 4-chlorothiophenol, and mertansine.

2.2 Materials and Methods

2.2.1 *Materials*

Activity assay substrates, reagents, cofactor, inhibitor, and internal standards:

Phenylethanolamine, dopamine, 6-mercaptopurine, cysteine, 4-chlorothiophenol, and L-penicillamine were obtained from Sigma Aldrich (St. Louis, MO); mertansine and 1,2-Dimyristoyl-sn-glycero-3-PG (DMPG) were obtained from Cayman Chemicals (Ann Arbor, Mi); 7α-thiospironolactone was produced in-house from spironolactone using a previously published method [22]; spironolactone, reduced glutathione, captopril, and DL-1,4-dithiothreitol were obtained from Fisher Scientific (Hampton, NH); *S*-methyl mertansine, D3-6-methylmercaptopurine, and 7α-thiomethylspironolactone-d7 were obtained from Toronto Research Chemicals (Toronto, ON, Canada); *S*-adenosyl-L-methionine was obtained from New England Biolabs (Ipswich, MA); and 2,3-dichloro-alpha-methylbenzylamine was sourced from Enamine (Monmouth Jct., NJ). Reagents and materials for *E. coli* culture, protein purification, and activity assay experiments: ampicillin sodium salt, isopropyl-β-D-thiogalactopyranoside, yeast extract, tryptone, NaCl, KH_2PO_4, K_2HPO_4, Thermo Scientific™ Halt™ Protease Inhibitor Cocktail, glycerol, CHAPS, white 96-well microplate, Nunc™ 96-Well Polypropylene Storage Microplates, Nunc™ 96-Well Slit-Cap Mats, and ultra-15 10 K molecular weight cut off centrifugal filter units were obtained from Fisher Scientific (Hampton, NH); His60 Ni Superflow

Resin from Takara (Mountain View, CA); 5mL GSTrap Fast Flow column from Cytiva (Marlborough, MA); deoxyribonuclease I, lysozyme, and imidazole were obtained from Sigma Aldrich (St. Louis, MO); and MTase-Glo™ Methyltransferase Assay Kit was obtained from Promega (Madison, WI). All primers that are described for the sequencing or production of the N-GST METTL7A plasmid were obtained from Integrated DNA Technologies (San Diego, Ca). Reagents and materials for activity assay cleanup and downstream LC/MS analysis: acetonitrile (LC/MS grade), formic acid (LC/MS grade), acetic acid (LC/MS grade), Optima water, barium hydroxide, and zinc sulfate were obtained from Fisher Scientific (Hampton, NH); maleimide was obtained from Sigma Aldrich (St. Louis, MO). Reagents and materials for SDS-page and western blot analysis: NuPAGE™ MOPS SDS Running Buffer (20X), PageRuler Plus Prestained Protein Ladder (10 to 250 kDa), GelCode™ Blue Safe Protein Stain, iBlot™ Nitrocellulose Transfer Stacks, and METTL7B Rabbit anti-Human Polyclonal antibody were sourced from Fisher Scientific (Hampton, NH); Polyclonal Rabbit anti-Human METTL7A Antibody was obtained from LifeSpan BioSciences (Seattle, WA); DYKDDDDK (Anti-FLAG) Tag Rabbit monoclonal antibody, ß-actin rabbit monoclonal antibody, and GST-Tag rabbit monoclonal antibody were obtained from Cell Signaling (Danvers, MA); IRDye 680RD Goat anti-Rabbit secondary antibody was obtained from LiCor (Lincoln, NE); and Rabbit Polyclonal Anti-METTL7A Antibody was obtained from Origene (Rockville, MD). Reagents and materials for cell culture and gene modulation: Eagle's Minimum Essential Medium, Gibco™ Opti-MEM™, Gibco™ Penicillin-Streptomycin, Corning™ Falcon™ Polystyrene 12-well and 6-well Microplates, Gibco™ Trypsin-EDTA (0.25%), Cytiva HyClone™ Fetal Bovine Serum, Invitrogen™ Lipofectamine™ 3000 & P3000 Transfection Reagents, and cell culture treated T75 plates were obtained from Fisher Scientific (Hampton, NH); Empty-, METTL7A-, and METTL7B-pCMV6

expression vectors were sourced from Origene (Rockville, MD); Dulbecco′s Phosphate Buffered Saline, METTL7A-specific siRNA, METTL7B-specific siRNA, and scramble non-specific negative control siRNA were obtained from Sigma Aldrich (St. Louis, MO). Reagents for gene expression analysis: Invitrogen™ MagMAX™ Total RNA Isolation Kit, Applied Biosystems™ High-Capacity RNA-to-cDNA™ Kit, Applied Biosystems™ TaqMan™ Fast Advanced Master Mix, and RT-PCR primers specific for METTL7A, METTL7B and GUSB were obtained from Fisher Scientific (Hampton, NH).

2.2.2 *METTL7A expression and purification*

Recombinant wild-type METTL7A (N-GST-METTL7A) was cloned in *E. coli* using a unique expression plasmid that was created in-house. The expression plasmid backbone (pET21-10XHis-GST-HRV-dL5) was a gift from Marcel Bruchez (Addgene plasmid # 73214; http://n2t.net/addgene:73214; RRID: Addgene_73214). An open reading frame sequence that codes for METTL7A (Uniprot: Q9H8H3) was synthesized by BlueHeronBio (Bothell, WA) and inserted into the plasmid using BamHI and EcoRI restriction sites and general molecular biology techniques. The forward primer for insertion of the METTL7A sequence is as follows: 5′ CTAGCTAGGGATCCGCTCCGGCACCGGCTCCGGCACCGGCACCGATGGAGTTGACT ATCTTCATCTTGCGCCTG 3′. The reverse primer for insertion of the METTL7A sequence was 5′ CTAGCTAGGAATTCTTATTAACGCGTTTTGACCGCGTA 3'. All plasmid inserts were validated by sequencing through Eurofins Genomics (Louisville, KY) and the sequencing histograms were analyzed using FinchTV software. The forward sequencing primer was 5′ GGGCTGGCAAGCCACGTTTGGTG 3′, and the reverse sequencing primer was 5′ CGTACCACTTCCACAAGTAAGTA 3′. The final expression plasmids positioned an *N*-

terminal His-GST affinity tag onto the wild-type METTL7A protein sequence separated by a 10-residue poly-alanine-proline (AP)5 linker.

Expression plasmids were propagated using heat-shocked Stellar cells (Takara, Mountain View, CA, Ref: 636763, Lot: 2106487A). Competent LOBSTR-BL21(DE3) *E. coli* (Kerafast, Winston-Salem, NC, Ref: EC1002) transformed via heat shock with plasmids validated by sequencing. *E. coli* cells were cultured in an orbital shaker at 250 rpm, 37 °C, and in the presence of 100 µg/mL ampicillin.

To express recombinant protein in LOBSTR-BL21(DE3) cells, overnight cultures were added to ampicillin-containing TB expression media at a ratio of 1:100. METTL7A production was initiated via the addition of isopropyl β-D-1-thiogalactopyranoside (IPTG) to a final concentration of 1 mM. The temperature was reduced to 15 °C, and the cells were grown for an additional 24 h. Cells were harvested via centrifugation at 2500 RCF for 30 min, and the resulting pellets were stored at − 80 °C until future processing.

Frozen cell pellets were thawed on ice in a 4 °C cold cabinet overnight prior to resuspension in lysis buffer (50 mM KPi pH 7.0, 20% glycerol, 150 mM NaCl, 10 mM CHAPS, EDTA-free Halt Protease Inhibitor Cocktail) supplemented with 100 µg/mL lysozyme (Sigma Aldrich, St. Louis, MO, Ref: L-6876, Lot: 65H7025). The lysate was placed on a rocker at 4 °C until it became extremely viscous, then 100 µg/mL DNA Nuclease I (Sigma Aldrich, St. Louis, MO, Ref: DN25-100MG, Lot: SLCB6648) was added and the lysate was placed on a rocker at 4 °C until it was no longer viscous. The lysate was then centrifuged at 48,000 x g for 30 min at 4 °C, and the resulting supernatant was retained for subsequent purification steps.

The purification was performed using a vertical column hand-packed with 4 mL of His60 Ni Superflow Resin, followed by GST column purification using the ÄKTA start

chromatography system (GE Healthcare, Chicago, IL). Cell lysate supernatant was added to the column containing nickel resin and it was recirculated across the column by a peristaltic pump overnight at 0.5 ml/min. The column was washed with 50 column volumes of His60 Ni purification buffer (50 mM KPi pH 7.0, 20% glycerol, 10 mM CHAPS, 300 mM NaCl) containing 50 mM imidazole. The protein was eluted from the column with 10 column volumes of His60 Ni purification buffer containing 300 mM imidazole.

The His60 Ni column eluent was directly applied to a pre-conditioned GSTrapFF column at a flow rate of 1 mL/min and recirculated for 4 h. The column was then washed with GSTrapFF purification buffer (50 mM KPi pH 7.0, 20% glycerol, 10 mM CHAPS, 150 mM NaCl) until the absorbance at 280 nm decreased to baseline. The recombinant protein was eluted from the column using purification buffer, which contained 10 mM reduced glutathione and was adjusted to pH 8.0. The eluent was concentrated using MilliporeSigma™ Amicon™ Ultra-15 10 K molecular weight cut-off centrifugal filter units and the final protein concentration was determined by A280 measurement. Purified protein stocks were aliquoted and stored at − 80 °C for future use.

2.2.3 *Protein purity analysis*

All SDS-PAGE Coomassie stained or western blot analysis were conducted with Invitrogen™ NuPAGE™ 4 to 12%, Bis-Tris, 1.0 mm, Mini Protein Gels in the XCell SureLock Mini-Cell Electrophoresis system using PageRuler Plus Prestained Protein Ladder as a molecular weight marker. Gels were run at room temperature and a constant 200 V. Total protein purity was determined with GelCode™ Blue Stain Reagent, a colloidal Coomassie dye. For western blot analysis, proteins were transferred to nitrocellulose membranes using the iBlot™ Gel Transfer Device. Primary antibody incubations were conducted overnight at 4 °C at a 1:500 dilution with

rabbit anti-METTL7A (LifeSpan BioSciences, Seattle WA, Ref: LS-C82875, Lot: 178089), anti-METTL7B (Invitrogen, Carlsbad, CA, Ref: PA5-58478, Lot: XC3518324A), or anti-GST (Cell Signaling, Danvers, MA, #2625S, Lot:8) primary antibodies. The secondary incubation was performed at room temperature for 1 h with IRDye 680RD goat anti-rabbit secondary antibody at a 1:10,000 dilution (LiCor, Lincoln, NE, Ref: 926-68071, Lot: D11102-15). Western blots and Coomassie-stained gels were visualized with an Odyssey gel scanner and blot images were analyzed using Image Studio Version 4.0 software.

2.2.4 *In vitro 7a-thiospironolactone and captopril methylation using recombinant METTL7A and METTL7B*

For methyl transferase activity assays, aliquots of purified recombinant METTL7A or METTL7B were diluted with reaction buffer (50 mM KPi pH 7.0, 20% glycerol, 150 mM NaCl, 10 mM CHAPS) to 0.2 mg/mL. The diluted protein was then combined with two parts reaction buffer containing 9 mg/mL DMPG. A fraction of diluted protein was boiled for 10 min while the remaining active protein was incubated on ice for 30 min to equilibrate with DMPG.

For the TSL methylation assay, TSL was dissolved in acetonitrile and then deposited in the appropriate wells of a 96-well reaction plate. The plate was dried under a vacuum for 10 min to remove the organic solvent. The diluted recombinant protein was then added to the plate and placed on a shaker at room temperature and 625 RPM for 5 min. DCMB, dissolved in water, was added to wells requiring DCMB and an equal volume of water was added to the remaining wells as a vehicle control. The reaction was initiated by adding SAM at a final concentration of 100 µM. The final TSL concentration was 50 µM, the final DCMB concentration was 100 µM, and the final protein concentration was 0.07 mg/mL. The plate was again placed on a plate shaker, sealed with a silicon plate mat, and then incubated at 37 °C for 30 min. For IC_{50} determination, METTL7A was incubated with 50 µM TSL, DCMB was added at 0.001, 0.01, 0.1, 0.5, 1.0, 10,

50, and 100 µM final concentration. *In vitro* assays were performed as micro-assays to conserve protein and final reaction volumes were 30 µL unless otherwise specified.

After 30 min, the reaction was quenched with 5 × the reaction volume with ice-cold ethyl acetate containing 5 µM 7α-thiomethylspironolactone-d7 deuterated internal standard (TMSL-D7). During the quench step, each sample was mixed with ethyl acetate by gentle pipetting up and down. The plate was then immediately frozen at -80 °C for 12 min. After 12 min, the aqueous layer was frozen, and the liquid organic top layer was transferred to a new plate. The transferred samples were dried with gentle heat and nitrogen gas flow (Biotage, Charlotte, NC) followed by reconstitution with 50:50 MeCN:H_2O containing 0.2% acetic acid. Samples were analyzed with a Waters Xevo TQS mass spectrometer paired with a Waters Acquity LC using a 2.1 × 50 mm Waters 1.7 µm C18 column and 0.2% acetic acid in water and 0.2% acetic acid in MeCN as solvents A and B respectively. Elution of TMSL and TMSL-D7 was achieved with an isocratic gradient held at a 50:50 ratio of solvent A to solvent B. Flow rate was constant at 0.4 mL/min. The transitions used to monitor for methyl metabolite 7α-thiomethylspironolactone (TMSL) and IS TMSL-D7 were 389.223>341.308 and 396>347.05, respectively, and TSL methylation was reported as the peak area ratio (PAR) of TMSL / TMSL-D7.

For captopril methylation assay, captopril dissolved in water, was added to 96-well plate wells containing diluted (active or boiled) protein, prepared with DMPG as described above. A no enzyme control incubation was prepared by replacing the protein-containing portion of the components with reaction buffer. DCMB dissolved in water, or water as a vehicle control, was added to the appropriate wells. The final protein concentration was 0.07 mg/mL; for wells including DCMB, the final DCMB concentration was 100 µM. The final captopril concentration was 5 mM. The plate was placed on a shaker for 2 min at 625 RPM at room temperature and the

reaction was initiated by the addition of SAM to a final concentration of 100 µM. After initiating the reaction, the plate was mixed on the shaker, sealed with a silicon plate mat, and incubated at 37 °C for 25 min. The reaction was quenched by adding 15% zinc sulfate (w/v) at 1/8th the reaction volume. The quenched solution was incubated on ice for 10 minutes before a solution of saturated barium hydroxide, containing the d3-*S*-methyl captopril internal standard, was added at a 1:1 v/v with zinc sulfate. The plate was mixed at 625 RPM for 2 min and then incubated on ice for another 10 min. The 96-well plate was centrifuged at 4,500 × g for 15 min to pellet all precipitated proteins and salts. The supernatant was transferred to a new 96-well plate and NaOH was added a final concentration of 125 mM. Finally, maleimide was added to the reaction to a final concentration of 500 mM. Maleimide reacts with unmethylated captopril to remove excess captopril and avoids complications in mass spec analysis. The plate was sealed with a silicon plate mat, wrapped in foil, and incubated at room temperature for 1 hour. The plate was centrifuged again to precipitate any salts that formed during the alkylation reaction, the supernatant was transferred to a new 96-well plate, and was analyzed by LC-MS/MS. LC-MS/MS conditions for monitoring captopril methylation were similar to those described previously by Maldonato *et al.* [18]. Captopril methylation was reported as the peak area ratio of Me-captopril / D3-Me-captopril subtracted from the average peak area ratio determined for the no-enzyme control group (the background).

2.2.5 *In vitro Michaelis Menten kinetics using recombinant METTL7A and METTL7B*

Purified N-GST-METTL7A, or N-GST-METTL7B, were diluted into a DMPG-containing buffer, and TSL was deposited into the wells of a 96-well plate as described above.

For single time point experiments with increasing concentrations of SAM, TSL was added to a final concentration of 250 µM, and SAM was added at 1, 5, 10, 25, 50, 100, 250, and 1000 µM to initiate the reaction.

For the SAH and SAM single time point activity assay matrix, TSL was added to a final concentration of 250 µM, SAH was added at 0, 5, 10, 50, and 100 µM, and SAM was added at 1, 5, 10, 25, 50, 100, 250, and 1000 µM to initiate the reaction.

For the TSL single time point activity assay with increasing concentrations of TSL, TSL was added to a final concentration of 1, 5, 10, 25, 50, 100, 250, and 1000 µM. SAM was added to a final concentration of 100 µM to initiate the reaction.

All reactions were incubated for 30 min at 37 °C before quenching with ethyl acetate containing TMSL-D7. The reactions were quenched, processed, and analyzed similar to the procedure described above.

2.2.6 *Substrate screening*

Potential substrates were screened for methylation using the Promega MTase-Glo™ Methyltransferase Assay Kit. Purified N-GST-METTL7A was diluted into a DMPG-containing buffer similar to the procedure described above. The substrate screening assay was performed in a 96-well plate at a final protein concentration of 0.07 mg/mL. Each probe substrate (1 mM final concentration) was added to the diluted enzyme. Samples were pre-equilibrated with shaking at 625 RPM for 5 min at room temp, and the reactions were initiated by adding SAM (100 µM). The plate was sealed with a silicon plate mat and incubated at 37 °C for 1 h. Enzymatic activity was quenched by adding DCMB to a final concentration of 100 µM. A volume of 20 µL from each well in the enzyme reaction plate was transferred to a new well in a white-walled 96-well flat bottom plate and then the plate was processed according to the manufacturer's protocol.

Luminescence was recorded from each well using a Synergy HTX Multi-Mode Reader (BioTek, Winooski, VT). All compounds were tested in triplicate with boiled and active N-GST-METTL7A, and relative turnover was determined by subtracting the response of boiled N-GST-METTL7A from active N-GST-METTL7A for each compound. The resulting difference for a no substrate control was then subtracted from all the active minus boiled differences that were determined for each compound using the following equation (X is relative luminescence units RLU):

$$(\bar{X}(active, substrate) - \bar{X}(boiled, substrate)) - (\bar{X}(active, no\ substrate) - \bar{X}(boiled, no\ substrate))$$

We noticed a significantly high background signal when using the Promega MTase-Glo™ Methyltransferase Assay Kit which is likely due to the presence of a thiol compound in the developing kit that is readily methylated by METTL7A or METTL7B. It is necessary to be cautious in designing controls, quenching the reactions, and interpreting data when using this kit to screen for thiol methyl transferase activity.

2.2.7 *Silencing METTL7A and METTL7B genes in HepG2 cells*

HepG2 cells (ATCC, Manassas VA, Ref: HB-8065) were cultured in Eagle's minimum essential media (EMEM) with 10% fetal bovine serum, 0.1% v/v penicillin-streptomycin and seeded into 12-well tissue culture plates at 200K cells/well (n=3). Cells were reverse transfected with Lipofectamine 3000 and siRNA following the manufacturer's protocol for gene knockdown. The final concentration of small interfering RNA (siRNA) per treatment was 10 nM, and the final concentration of lipofectamine 3000 reagent was 2 µL/mL. Cells were reverse transfected with siRNA targeting *METTL7A*, *METTL7B*, *METTL7A* and *METTL7B* (combo), or scramble non-specific siRNA (Sigma Aldrich St. Louis, MO, Ref: METTL7A/EHU153411,

METTL7/EHU008171, Scramble/SIC001). Cells were incubated with siRNA for 48 hours, washed with warm DPBS, and treated with serum-free EMEM containing TMT substrates (125 µM TSL or 500 µM captopril) in the presence or absence of 20 µM DCMB. Cells were incubated with TMT substrates for 24 hours after which the media was collected and analyzed for methylated metabolites by LC-MS/MS. The LC-MS/MS analysis of captopril and TSL were conducted as described above. The results were normalized to the media collected from negative control scramble siRNA-treated cells. The knockdown efficiency analysis was conducted as described by Maldonato *et al.*, 2021 using proprietary TaqMan FAM reporter primers for *METTL7A*, *METTL7B*, and the housekeeping gene *GUSB*.

2.2.8 *Overexpression of METTL7A and METTL7B in HeLa cells*

HeLa cells (ATCC, Manassas VA, Ref: CCL-2™) were cultured in EMEM with 10% fetal bovine serum, 0.1% v/v penicillin-streptomycin and seeded into 6-well tissue culture plates at 500K cells/well (n=3). The cells were reverse transfected using Lipofectamine 3000 and P3000 reagent along with different pCMV expression vectors following the manufacturer's protocol. The final concentration of pCMV plasmid expression vector per treatment was 1250 ng/mL, the final concentration of Lipofectamine 3000 reagent was 1.5 µL/mL, and the final concentration of P3000 reagent was 1 µL/mL. Cells were incubated with media containing Lipofectamine reagents and either a METTL7A (Origene, Rockville MD, Ref: RC202601), METTL7B (Origene, Rockville MD, Ref: RC203838), or empty control (Origene, Rockville MD, Ref: PS100001) expression vector for 36 h. After 36 h, the cell media was removed, the cells washed with warm DPBS, and the media replaced with serum-free EMEM containing 125 µM TSL ±20 µM DCMB. Cells were incubated with TMT substrate for 24 h before the media was collected and analyzed for methylated metabolites by LC-MS/MS as described above.

Protein overexpression was confirmed by western blot analysis. After incubation with the expression vector for 36 hours, cells were harvested by scraping each well with 1 mL of DPBS. Cells were then transferred to a 1.5 mL Eppendorf tube and pelleted by centrifuging for 5 min at 750 × g, 4 °C. The DPBS was removed and the cells from each treatment were lysed in 150 µL of RIPA buffer containing 1X halt protease inhibitor cocktail. The lysis was performed by resuspending cells in lysis buffer and pipetting up and down 20 times. The cell lysates were analyzed for protein concentration using the BCA method. 5.5 µg of protein from each cell lysate was loaded onto a protein SDS-PAGE gel. Protein separation by gel-electrophoresis, and subsequent western blot analysis, were performed as described above. The primary antibody incubation lasted overnight with anti-β-actin (Cell Signaling, Danvers MA, Ref: 4970S, Lot: 18) and anti-FLAG-Tag (Cell Signaling, Danvers MA, Ref: 14793S, Lot: 5) primary antibodies. Each antibody was diluted at 1:500.

2.2.9 *Identification of METTL7A and METTL7B in human liver microsomes*

Pooled human liver microsomes (50-donors, 16 female and 34 male Fisher Scientific, Hampton NH, Ref: HMMCPL, Lot: PL050F-B,) and pooled liver cytosol (50-donor human 16 female and 34 male) Fisher Scientific, Hampton NH, Ref: HMMCPL, Lot: PL028-J, were protein normalized, and 40 µg of protein from each subcellular fraction was loaded onto a NuPAGE™ 4 to 12%, Bis-Tris protein gel. Protein separation by gel-electrophoresis, and subsequent western blot analysis were performed as described above. Two western blots were developed, one stained with an anti-METTL7B (Invitrogen, Carlsbad, CA, Ref: PA5-58478, Lot: XC3518324A) and the other with anti-METTL7A primary antibody (Origene, Rockville MD, Ref: TA346478, Lot: Qa2850). The antibodies were diluted 1:1000 and 1:300, respectively.

2.2.10 *Analysis of DCMB inhibition of TMT activity in liver sub-cellular fractions*

Fifty-donor pooled HLM and human liver cytosol were diluted to 1 mg/mL in KPi reaction buffer (50 mM KPi pH 7.0, 20% glycerol, 150 mM NaCl, 10 mM CHAPS). Captopril was added to a final concentration of 5 mM, DCMB was added to a final concentration of 100 µM, and SAM was added to a final concentration of 100 µM to initiate the reaction. The mixtures were incubated for 45 min at 37 ºC. Following incubations, all samples were processed and then analyzed by LC-MS/MS, using the same sample prep and LC-MS/MS method as described above in **section 2.2.4**.

2.2.11 *Quantification of METTL7A and METTL7B protein levels in individual donor human liver microsomes*

Microsomes were prepared by thawing individual donor liver samples (10 female and 9 male, Supplementary Table 2.1) on ice in homogenization buffer (50 mM KPi pH 7.4, 250 mM sucrose, 1 mM EDTA, and 1X Halt protease inhibitor cocktail). The thawed tissue was transferred to a sterile petri dish on ice and a razor blade was used to remove fibrotic tissue. Next, the tissues samples were placed in a 55 mL Dounce homogenizer and homogenized using 4-6 passes with a powered Teflon pestle. The homogenate was transferred to a centrifuge tube and centrifuged at 8,000 × g for 30 min at 4 °C to pellet all intact cells, nuclei, and mitochondria. The supernatant was then transferred to a fresh tube and centrifuged it at 100,000 × g for 60 minutes at 4 °C. The supernatant containing cytosolic fraction was removed and the pellet containing the microsomal fraction was resuspended in 2 mL of homogenization buffer via Dounce homogenization and then aliquoted and stored at -80 °C until future use.

For the quantitative proteomic analysis of METTL7A and METTL7B protein levels in individual donor HLMs, the protein samples were normalized to 2 mg/mL with homogenization buffer. HLM samples 30 µL of 2 mg/mL were combined with an equal volume of ammonium

bicarbonate 100 mM and 10 µL of DTT (250 mM). The samples were then incubated at 37 °C for 30 min. The samples were allowed to cool back to room temperature followed by the addition of 10 µL of iodoacetamide (IAA: 500 mM iodoacetamide in 50 mM ammonium bicarbonate) to each sample. Each sample was then vortexed and incubated for 30 min at room temperature in the dark. 1 mL of crash solution (methanol:chloroform:water, 5:1:4) was added to the samples and centrifuged for 5 min at 16,000 × g and 4 °C. A protein pellet appeared as a disc suspended between the immiscible methanol/water and chloroform layers. Both layers were carefully aspirated and then the protein was allowed to air dry for 10 min. Methanol (0.5 mL) was added to the pellet. Samples were centrifuged for 5 min at 8,000 × g and 4 °C, the methanol was aspirated, and the pellet was allowed to air dry for 30 min followed by the addition of 20 µL of trypsin, dissolved in 50 mM ammonium bicarbonate at 1:80 trypsin:protein ratio (w/w). The protein pellet was digested by the trypsin for 16 h while incubating at 37 °C and shaking at 300 rpm. After digestion, 20 µL of LC/MS buffer (80% acetonitrile, with 0.5% formic acid that contains the relative heavy peptides) was added to each sample. The samples where then centrifuged for 10 min at 4,000 x g and 4 °C. The supernatant was transferred and analyzed by LC-MS/MS.

A UPLC-MS/MS (SCIEX Triple Quadrupole 6500 system (Framingham, WA) coupled to an ACQUITY UPLC system (Waters Technologies, Milford, MA) was utilized for proteomic analysis and 5 µl of each sample was injected onto the column (ACQUITY UPLC CSH 1.7 µm, C18; 100x2.1 mm, Waters, Milford, MA). A gradient method (0.3 mL/min) with mobile phase A consisting of 0.1% formic acid in water and mobile phase B consisting of 0.1% formic acid in acetonitrile was used for peptide separation.

Two surrogate peptides obtained from Thermo Fisher Scientific (Waltham, MA) were chosen separately for METTL7A and METTL7B. The relevant transitions for each peptide are shown in supplementary table 2.2. Analyst 1.6 software (Sciex, USA) was used for peak integration and data analysis. Peakview 2.0 was applied for checking the quality of peaks and initial method development. Chromatographic integration and peak area analysis were performed by using Skyline 20.0.1.31 (University of Washington, Seattle, WA).

2.2.12 *Determination of thiol methylation activity across HLMs from individual donors*

Individual liver donor microsomes diluted to 0.25 mg/mL in KPi reaction buffer (50 mM KPi pH 7.0, 20% glycerol, 150 mM NaCl, 10 mM CHAPS) were incubated with 250 µM TSL and 100 µM SAM for 30 min at 37 °C. For the small cohort of individual donor HLMs that were incubated ±DCMB, the final TSL, DCMB, and SAM concentrations were all 100 µM. The reaction quench and downstream determination of TSL methylation was performed by LC-MS/MS as described above.

2.2.13 *Determination of thiol methylation activity in human blood*

Washed red blood cells were diluted into KPi reaction buffer (50 mM KPi, ph 7.4, 10% glycerol). The ratio of red blood cells to KPi reaction buffer was 1:5, respectively. 140 µL of diluted blood was transferred to 1 mL cluster tubes. A fraction of the diluted blood was reserved for boil control. The boil control samples were heated in boiling water for 5 min. To each cluster tube, either TSL or 6-mercaptopurine was added (6-MP). DCMB dissolved in water was added to the relevant sample tubes or the same volume of water for vehicle control. The reaction was initiated by the addition of SAM, samples not receiving SAM got the same volume of water as a vehicle control. The final substrate concentration was 100 µM, and the final SAM concentration was 1 mM. The cluster tubes were vortexed, and the samples were incubated for 45 min at 37 °C.

After incubation, the reaction was quenched by adding 75 µL of each sample to 75 µL of acetonitrile containing 20 µM IS and 1% formic acid. The IS for TSL treated samples was TMSL-D7 and the IS for 6-MP treated samples was D3-6-methylmercaptopurine (D3-6-MMP). To each sample, 30 µL of 15% $ZnSO_4$ was added. Samples were incubated on ice for 10 min. Then, 30 µL of barium hydroxide was added to each sample and incubated on ice for an additional 10 min. The samples were then centrifuged at 16,000 × g for 15 min to precipitate proteins and salts. The supernatant was transferred to a clean 96-well plate and analyzed by mass spec.

The TSL treated samples were analyzed with a Waters TQS mass spectrometer paired with a Waters ACQUITY LC using a 2.1 × 50-mm Waters CORTECS UPLC 1.6 µm C18 column and 1% acetic acid in water and 1% acetic acid in acetonitrile as solvents A and B, respectively. Consistent elution of TMSL and TMSL-D7 was achieved with an isocratic gradient held at 50:50 ratio of solvent A to solvent B. Flow rate was constant 0.5 mL/min. The mass transitions used to monitor for methyl metabolite 7a-thiomethylspironolactone (TMSL) and IS TMSL-D7 were 389.223 > 341.308 and 396.61 > 347.05 , respectively. TSL methylation was reported as the peak area ratio (PAR) of TMSL/TMSL-D7.

The 6-MP treated samples were analyzed with a Waters TQS mass spectrometer paired with a Waters ACQUITY LC using a 2.1 × 50-mm Waters CORTECS UPLC 1.6 µm C18 column and 1% acetic acid in water and 1% acetic acid in acetonitrile as solvents A and B, respectively. The elution of 6-methylmercaptopurine and D3-6-MMP was achieved by using the following gradient: The ratio of solvent A to solvent B was held at 95:5 from 0 to 1 min, then transitioned to 5:95 from 1 to 3 min with a gradient curve of 7, from 3 min to 3.5 min the solvent ratio

remained at 95:5, and finally, the column was re-equilibrated with a solvent ratio of 95:5 solvent A to solvent B from 3.5 min to 5 min. The flow rate was held at 0.35 mL/min.

The mass transitions used to monitor for methyl metabolite 6-MMP and IS D3-6-MMP were 167.18 > 124.99 and 170.22 > 125.02 , respectively. 6-MMP methylation was reported as the peak area ratio (PAR) of 6-MMP/D3-6-MMP.

2.2.14 *Data analysis*

Unless noted otherwise, all experiments were conducted in triplicates and all data is reported as the mean ± standard deviation. Statistical significance was determined by a two-tailed unpaired student t-test with a threshold P value of 0.05. Kinetic parameter K_m (for TSL and SAM), K_i (for SAH), and IC_{50} (for DCMB) values were calculated using GraphPad Prism, version 9.4.1 for Windows (GraphPad Software, La Jolla, CA). A two-tailed Spearman's non-parametric correlation was computed to assess the relationship between two variables with a threshold P value of 0.05.

2.3 RESULTS

2.3.1 *Sequence similarity and structural homology between METTL7A and METTL7B*

Both METTL7A and METTL7B are 244 residues long and have a molecular weight of 28 kDa, similar to prior literature reporting TMT activity [7]. Both isoforms share 76% sequence homology and 60% sequence identity as determined by BLAST analysis [23] (Supplementary fig. 2.1). Homology models of METTL7A and METTL7B, produced by AlphaFold [24, 25], indicate high structural similarity (Figure 2.1).

2.3.2 *Expression and purification of His-GST-METTL7A*

Consistent with the previous expression of METTL7B [18], we inserted the METTL7A gene sequence into a pET21 expression plasmid and expressed the protein in *E. coli*. The pET21 expression vector adds a unique tag to the *N*-terminus of the inserted ORF, a 10X histidine-tag (His) followed by a glutathione-*S*-transferase (GST) tag (Figure 2.2). The *N*-terminal GST tag is essential to solubilize METTL7A from the bacterial membrane. The recombinant protein 10XHis-GST-METTL7A (N-GST-METTL7A) has a molecular weight of 57.6 kDa. We confirmed the successful purification of N-GST-METTL7A with a visible protein band at ~58 kDa by SDS-PAGE Coomassie stain (Figure 2.2). A band at ~58 kDa is also visible on a western blot using an anti-METTL7A and anti-GST-antibody; no band is visible using an anti-METTL7B-antibody (Figure 2.2). The purity of recombinant METTL7A was comparable to the purity we previously achieved for recombinant METTL7B. The lower molecular weight bands that were identified as a non-functional GST tag portion of N-GST-METTL7B also co-purified with N-GST-METTL7A. We suspect that the HRV-(AP)5 linker-sequence between GST and METTL7A or 7B introduced a feature that leads to the formation of this *N*-terminal tag portion of this protein construct during the process of bacterial protein expression. There is no concern that the non-specific proteins observed in the purified protein eluent are involved in TMT activity as we have demonstrated with a non-functional D98A mutant METTL7B that there is no TMT activity in purification eluent or bacterial lysate without a functional, expressed thiol methyltransferase [18].

2.3.3 *Validation of N-GST-METTL7A S-methyltransferase activity*

Purified N-GST-METTL7A methylated captopril and TSL (Figure 2.3) in a time- and protein-dependent fashion. Like N-GST-METTL7B, purified N-GST-METTL7A required

preincubation with dimyristoyl-sn-glycero-3-PG (DMPG) liposomes for activity (Supplementary fig. 2.2).

2.3.4 *Inhibition of METTL7A by DCMB*

DCMB potently inhibits N-GST-METTL7A but not N-GST-METTL7B (Figure 2.3). An IC_{50} of 1.2 ±0.4 μM was determined for DCMB and METTL7A, using TSL as a reporter substrate (Figure 2.3). There is virtually no 7α-thiomethylspironolactone (TMSL) observed in the inactivated boil controls (Supplementary fig. 2.3), and because of this, we deemed TSL a suitable probe substrate for further METTL7 characterization experiments.

2.3.5 *Competitive inhibition of N-GST-METTL7A by S-adenosyl-homocysteine*

We determined the K_m for the methyl donating cofactor SAM by measuring the formation of TMSL by LC-MS/MS (Figure 2.4). The SAM activity curve followed Michaelis-Menten kinetics with a K_m for SAM at 53.7 ±14.1 μM. Analysis of the METTL7A homology model generated by AlphaFold indicated that this protein is a class I small molecule methyltransferase (Supplementary fig. 2.4). Class I methyltransferases have a conserved binding site with a high affinity for SAM and the demethylated cofactor *S*-Adenosyl-homocysteine (SAH) [26]. As expected with a class I small molecule methyltransferase, SAH inhibited TSL methylation in a concentration-dependent manner and exhibited a competitive mechanism of inhibition with respect to SAM (Figure 2.4), with a K_i of 53.9 ±27.8 μM. This value is similar to the K_i that we previously determined for METTL7B [18]. We measured all kinetic parameters under linear conditions for incubation time and protein concentration (Supplementary fig 2.5). For SAM and SAH kinetic analysis, a saturating amount of TSL was used in these assays to guarantee the condition of no substrate depletion.

2.3.6 *Kinetic analysis of N-GST-METTL7A and N-GST METTL7B S-methylation of TSL*

We determined the K_m value for TSL by measuring the formation of TMSL for both N-GST-METTL7A and N-GST-METTL7B by LC-MS/MS (Figure 2.4). The TSL activity curves for each enzyme followed Michaelis-Menten kinetics. The K_m values for TSL methylation by METTL7A and METTL7B were 39.4 ±18.3 and 32.5 ±3.8 µM, respectively. The K_m for TSL methylation by recombinant METTL7B by LC-MS/MS, was similar to what we have previously reported for METTL7B [18].

2.3.7 *Substrate specificity of N-GST-METTL7A*

Substrates for class I small molecule methyltransferases were screened for N-GST-METTL7A methylation with the Promega MTaseGlo kit. In previous screens with this kit, METTL7B activity was normalized to dopamine, a compound that showed no activity. Normalization was necessary because METTL7B produced a high response in the kit in absence of a substrate compared to a boiled enzyme control. METTL7A, incubated without a substrate, also demonstrated a high response compared to the boiled enzyme. Adding DCMB, as a quench step, at the end of incubation significantly reduced the baseline signal (Supplementary fig. 2.6). This observation indicates that METTL7A and METTL7B catalyze the methylation of a compound in the reagents supplied with the kit. As such, it became standard practice to include DCMB in the quench step to prevent further METTL7A activity during downstream signal development steps.

Potential substrates were screened at concentrations at least three times higher than their literature reported K_m values to ensure the detection of methylated metabolites [7, 13, 27-31]. METTL7A preferentially methylated exogenous thiol-containing compounds and did not methylate the endogenous thiols tested; cysteine and glutathione (Figure 2.5). METTL7A did not

methylate compounds that are known *O*- and *N*- methyltransferase substrates. Mertansine, a thiol-containing microtubule inhibitor, was significantly methylated. We also tested *S*-methyl mertansine as a negative control, and the response was close to baseline. We assume that mertansine can only be methylated on its thiol moiety. Since *S*-methyl mertansine has no available site for further methylation, we used *S*-methyl mertansine activity level as a non-substrate baseline control for screening other potential substrates with the Promega MTaseGlo assay.

2.3.8 *Modulating METTL7A and METTL7B gene expression in HepG2 cells and its effect on thiol methylation activity*

HepG2 cells were treated with scrambled negative control small interfering RNA (siRNA), METTL7A-specific siRNA, METTL7B-specific siRNA, or a combination of both. METTL7A-specific siRNA exclusively reduced METTL7A gene expression by 90%, whereas METTL7B-specific siRNA reduced the expression of METTL7B and METTL7A by 90% and 30%, respectively. The non-specific reduction in METTL7A gene expression using a METTL7B-specific siRNA is likely caused by the siRNA design. The METTL7B-specific siRNA shares 60% sequence identity with a METTL7A coding mRNA segment, potentially inducing modest suppression (Supplementary fig. 2.7). The combined treatment of METTL7A- and METTL7B-specific siRNA reduced the expression of both genes by 90% (Figure 2.6).

After incubation with siRNA for 48 h, cell media was replaced with media containing either TSL or captopril. The methylated metabolites for each compound were measured in the culture media by LC-MS/MS. We observed the largest decrease in TSL and captopril methylation in the combined siRNA-treated cell media compared to cells treated with control siRNA. The smallest decrease was observed in METTL7B-specific siRNA-treated cell media (Figure 2.6).

2.3.9 *Modulating METTL7A and METTL7B protein levels in HeLa cells and its effect on thiol methylation activity*

HeLa cells were incubated with pCMV expression vectors encoding FLAG-tagged METTL7A, FLAG-tagged METTL7B, or an empty insert to act as a negative control. Protein expression of METTL7A or METTL7B was determined in cell lysate by protein normalized anti-FLAG western blotting. An anti-β-actin antibody was included as a co-stain for loading control. FLAG-tagged METTL7A and METTL7B are visible at the correct molecular weights, only in lysates of cells incubated with the appropriate expression vector (Figure 2.7). No FLAG-tagged protein is visible in the empty control vector-treated cells. Cells expressing FLAG-tagged METTL7A or FLAG-tagged METTL7B had significantly increased TSL methylation compared with empty vector control-treated cells, determined by LC-MS/MS (Figure 2.7). With the addition of DCMB, only METTL7A overexpressing cells showed a significant reduction in TSL methylation compared to cells not treated with DCMB.

2.3.10 *Subcellular localization of METTL7A and METTL7B in human liver*

Using 50-donor pooled HLMs, we observed bands at the molecular weight of 28 kDa in anti-METTL7A and anti-METTL7B stained western blots (Figure 2.8). We observed similar bands in the pooled liver cytosolic fraction, albeit at much lower intensities.

We determined TMT activity in the 50-donor pooled microsomal or cytosolic fractions, that were protein-normalized to 1 mg/mL, by measuring captopril methylation via LC-MS/MS analysis (Figure 2.8). HLMs contained the highest TMT activity, while lowest TMT activity was observed in liver cytosol, which had 30% TMT activity compared to HLMs.

We determined the effect of DCMB on TMT activity in pooled HLMs and cytosol by adding saturating concentrations of DCMB during captopril methylation assays (Figure 2.8). There was

≥70% reduction in TMT activity in HLMs and liver cytosol when incubated with DCMB. In a similar inhibition experiment, we screened individual-donor HLMs for TMT activity ±DCMB using TSL instead of captopril as the probe substrate (Figure 2.8). Saturating concentrations of DCMB, added during TSL methylation assays, reduced each individual-donor HLM's TMT activity by >80%.

2.3.11 *Quantifying of METTL7A and METTL7B protein levels in HLMs and correlation with S-methylation activity*

We quantified METTL7A and METTL7B protein levels in 19 adult single-donor HLMs by LC-MS/MS quantitative proteomics (Figure 2.9). METTL7A protein levels are, on average, 3-fold higher than METTL7B levels. We also determined TSL methylation activity in the same donor HLMs (Figure 2.9). There was an 8-fold difference in activity among the total donors.

We computed a non-parametric Spearman's correlation to assess the relationship between METTL7A and METTL7B protein levels. The Spearman correlation coefficient was 0.89, and the P-value was < 0.0001 (Figure 2.9). This indicates a positive correlation between METTL7A and METTL7B. We also calculated a Spearman correlation coefficient to assess the relationship between relative TSL methylation activity and the combined protein levels of METTL7A and METTL7B. The Spearman correlation coefficient for this analysis was 0.87, and the P-value was < 0.0001 (Figure 2.9). This indicates a positive correlation between METTL7A and METTL7B protein levels and relative TMT activity across individual HLMs.

2.3.12 *Thiol methyltransferase activity in human red blood cells.*

We identified alkyl thiol methyltransferase activity and thiopurine methyltransferase activity in blood. The alkyl thiol methyltransferase activity was a magnitude higher than the thiopurine activity based on the PARs (Figure 2.10). The final internal standard concentrations were similar,

allowing for a direct comparison of the peak areas if both ionization efficiency is equal. Alkyl thiol methyltransferase activity was inhibited by DCMB while thiopurine methyltransferase activity was not.

2.4 DISCUSSION

The key finding in this investigation is that METTL7A is a thiol methyltransferase and along with METTL7B, both enzymes account for most of *S*-thiol methylation activity in HLMs. We will refer to METTL7A and METTL7B as TMT1A and TMT1B, respectively, for the rest of the discussion and use *TMT1A* (https://www.ncbi.nlm.nih.gov/gene/25840) and *TMT1B* (https://www.ncbi.nlm.nih.gov/gene/196410) when referring to the genes as agreed upon with the HUGO Gene Nomenclature Committee (See note at the beginning of Chapter 2). TMT1A can selectively methylate exogenous alkyl and phenolic thiols, and is inhibited by DCMB, the historic TMT inhibitor with an IC_{50} of 1.2 µM which is within the range of the previously determined IC_{50} of 0.45 µM for TMT activity in HLMs [21]. Although TMT1B is a thiol methyltransferase, it cannot entirely account for TMT activity because DCMB has no effect on its activity. TMT1A shares 60% sequence identity with TMT1B and has a similar substrate specificity, yet only TMT1A is potently inhibited by DCMB. The structural features in TMT1A that confer DCMB selectivity compared to TMT1B will be discussed in Chapter 3.

Recombinant TMT1A transfers a methyl group to several exogenous thiol-containing compounds, including DTT, mertansine, captopril, and 6-chlorothiophenol in a general methyltransferase substrate screening assay (Figure 2.5). Similar to prior reports for TMT activity, TMT1A did not methylate endogenous thiols including cysteine and glutathione or other small molecules specific for *N*- and *O*-methyl transferases [7] although other endogenous thiols may be substrates.

TMT1A behaves like a class I small molecule methyltransferase determined by a series of kinetic experiments. TMT1A utilizes SAM as the methyl donor and methylates TSL following classic Michaelis-Menten kinetics (Figure 2.4). It is competitively inhibited by SAH, as evidenced by higher SAM concentrations overcoming SAH inhibition. The Michaelis-Menten constant (K_m) for SAM and TSL are 53.7 µM and 39.4 µM, respectively; within the range of the values 43 µM and 27 µM previously reported in the literature [13, 32]. In addition, we compared the kinetic curves of TSL methylation by TMT1A and TMT1B and established that both recombinant enzymes have similar K_m values for TSL. The K_m value for TMT1B mediated methylation of TSL, reported by LC-MS/MS, was 32.5 µM, similar to the value determined in our previous study, which instead utilized the Promega MTase-Glo™ Methyltransferase assay to report on the methylation of TSL.

TMT1A and *TMT1B* gene silencing experiments in HepG2 cells caused a significant decrease in *S*-methylation activity, while overexpression of *TMT1A* and *TMT1B* in HeLa cells significantly increased TMT activity. Only HeLa cells overexpressing TMT1A had reduced TMT activity following DCMB addition confirming that the TMT1A's specificity for exogenous alkyl and phenolic thiols is not influenced by the *in vitro* expression or incubation systems that were utilized in these studies.

TMT activity is described in the literature as most abundant in liver microsomes [28, 33, 34], and an RNA sequencing analysis reported that like TMT, *TMT1A*, and *TMT1B* expression levels are highest in the human liver [35] compared to other tissues. By western blot analysis, we determined that TMT1A and TMT1B are present in human liver and are associated with the microsomal fraction. We also confirmed that TMT activity is highest in the microsomal fraction and lowest in the cytosol consistent with previous reports [2, 7, 36, 37].

Saturating concentrations of DCMB added to a TMT activity assay performed in HLMs, results in ≥70% decrease in TMT activity towards captopril methylation and >80% decrease in activity towards TSL methylation. Since TMT1A is potently inhibited by DCMB while TMT1B is not, TMT1A is responsible for most of TMT activity in HLMs while the remaining activity with saturating concentrations of DCMB can be attributed to TMT1B. Finally, we measured the protein levels of TMT1A and TMT1B by quantitative proteomics. TMT1A protein levels are, on average, 3-fold greater than TMT1B but the two proteins are highly correlated. TMT activity was determined for each donor and correlated well with the sum of TMT1A and TMT1B protein levels, as observed in Figure 2.9.

The high TMT1A and TMT1B protein levels in the liver compared to other tissue and their association with the endoplasmic reticulum parallel other drug-metabolizing enzymes like cytochrome P450s. Other class I small molecule methyltransferases such as catechol *O*-methyltransferase (COMT), phenylethanolamine *N*-methyltransferase (PNMT), and nicotinamide *N*-methyltransferase (NNMT) have very limited examples of exogenous substrates but clear examples of endogenous substrates—dopamine, noradrenaline, and nicotinamide, respectively [38-40]. In this regard, it is reasonable to consider TMT1A and TMT1B as drug metabolizing enzymes, with a potential endogenous role, such as the methylation of hydrogen sulfide or other endogenous thiol containing biomolecules. We have previously reported that TMT1B methylates hydrogen sulfide [18], and preliminary data from our lab suggests that TMT1A also methylates hydrogen sulfide (data not shown). The methylation of hydrogen sulfide to methyl sulfide by TMT1A and TMT1B and the potential role MeSH has in modifying cysteines is discussed in Chapter 4.

At least five different methyltransferase activities have been identified in blood. Indolethanolamine N-methyltransferase (INMT), COMT, histamine N-methyltransferase, TPMT, and TMT activity have all been measured in red blood cells [5, 32, 41, 42]. TMT1A and COMT have been identified in red blood cells by proteomic analysis, and alkyl thiol methyltransferase activity in red blood cells is inhibited by DCMB [43]. This suggests that alkyl thiol methyltransferase activity in blood can be attributed to TMT1A activity. Thiopurine methyltransferase activity was also identified in red blood cells, and it was not inhibited by DCMB, consistent with what has been reported previously [21].

While the endogenous function of TMT1A and TMT1B remains unknown, their dysregulation is continually reported in different diseases, especially cancer. In one large-cohort multi-cancer, multi-omics study, higher *TMT1A* expression was determined to have the most favorable survival across cancers compared to other METTLs [44]. In contrast, *TMT1B* is significantly upregulated in most cancers [45]. TMT1B regulates the epithelial-mesenchymal transition of thyroid cancer cells in the presence of TGF-β, an important regulator of cancer immunosuppression [46-48]; and in multiple cell lines, TMT1B promotes G1 to S phase transition in cancer cells [49, 50]. Overexpression of *TMT1B* is attributed to proliferation and tumorigenesis, which suggests an oncogenic role in cancer progression. Conversely, the consistent lower expression of *TMT1A* across cancers would suggest a tumor-suppressing role. Although the nature of TMT1A and TMT1B's involvement in cancers is not well understood, the high level of dysregulation of *TMT1A* and *TMT1B* might impact the metabolism of thiol-containing chemotherapeutics by cancer cells.

Our results are inconsistent with one report suggesting that TMT1A and TMT1B are capable of RNA methylation [51] but align with the recent data that TMT1A and TMT1B are involved in

the S-methylation of histone deacetylase inhibitor romidepsin [52]. While we cannot rule out that TMT1A or TMT1B may have RNA methylating functions and further work is needed to confirm this, the microsomal association of these enzymes strongly suggests a role in small-molecule methyl transfer.

In summary, our findings are consistent with the hypothesis that TMT1A and TMT1B account for the majority of microsomal TMT. Future work will focus on identifying endogenous thiol-containing substrates for TMT1A and TMT1B and examining their role in tumorigenesis.

2.5 Conclusion

The alkyl thiol methyltransferase 1 family of enzymes consists of TMT1A and TMT1B. These enzymes account for the majority of microsomal TMT activity. We also presented preliminary evidence that at least TMT1A is involved in red blood cell TMT activity as well. These enzymes methylate a broad range of thiol containing drugs. Thiol methylation significantly alters the pharmacology of the substrate drug, positioning TMT1A and TMT1B as important drug metabolizing enzymes. TMT1A and TMT1B are also involved in different cancers and clearly have some endogenous signaling role but their endogenous substrate is still unknown. Future work will focus on identifying endogenous thiol-containing substrates for TMT1A and TMT1B and examining their role in tumorigenesis.

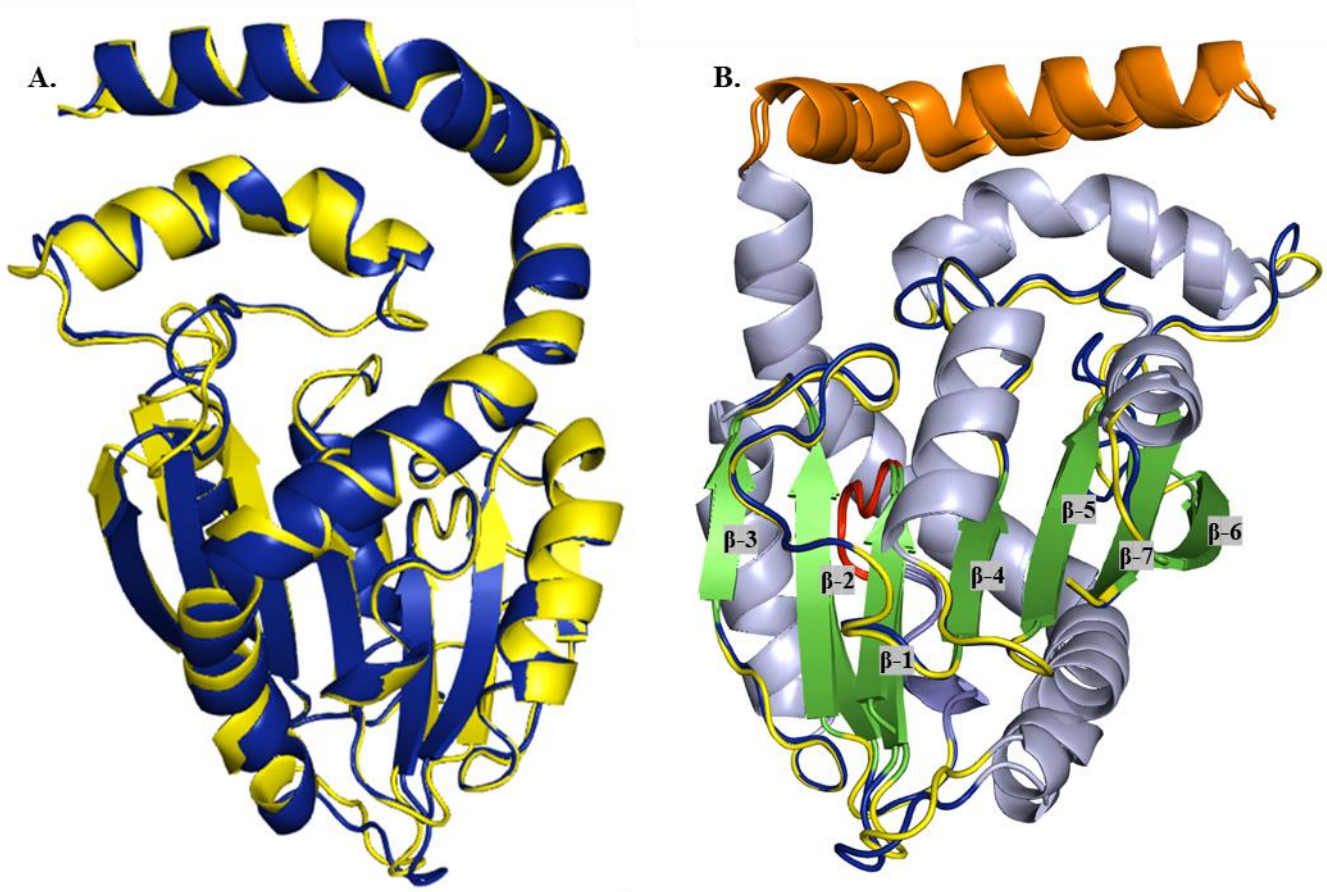

Figure 2.1. Annotated homology models of METTL7A (TMT1A) and METTL7B (TMT1B)

AlphaFold homology models of METTL7A (TMT1A) (yellow) and METTL7B (TMT1B) (blue) aligned with Pymol alignment function (A). AlphaFold homology models of METTL7A (TMT1A) (yellow) and METTL7B (TMT1B) (blue) aligned and oriented to visualize secondary structural features (B), with hydrophobic *N*-terminus in orange, GXGXG sequence, red, beta sheets, green and labeled β-1 through β-7 by order along the sequence, and alpha helices colored light blue.

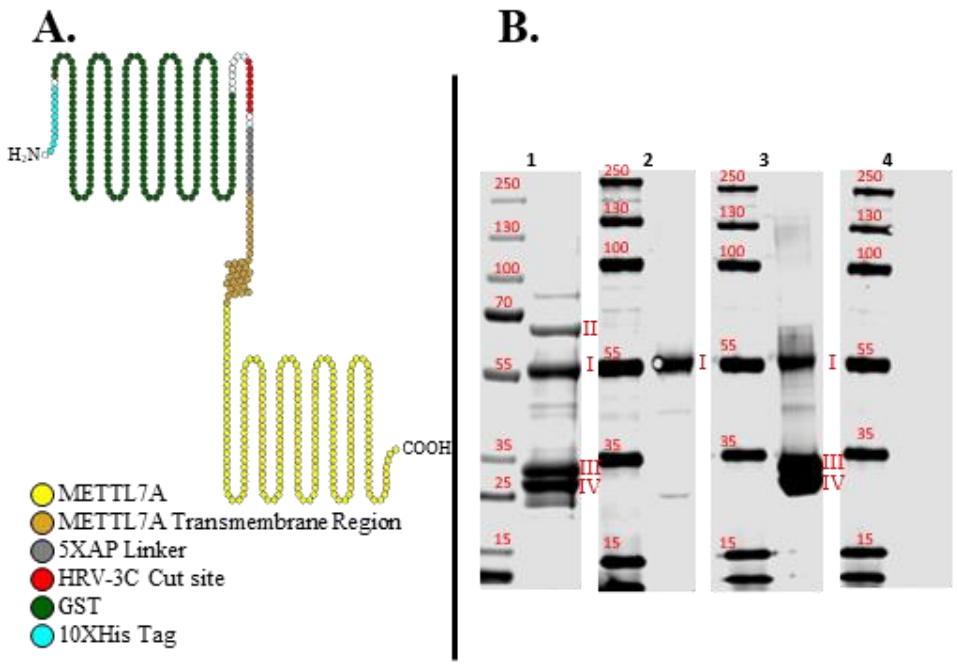

Figure 2.2. Cartoon of N-GST-METTL7A and SDS-PAGE analysis of purified protein

Cartoon representation of *N*-GST-METTL7A (*N*-GST-TMT1A) with features highlighted and identified in the legend (A) Figure produced with Protter [53]. SDS-PAGE Coomassie stain (B.1), anti-METTL7A (anti-TMT1A) western blot (B.2), anti-GST western blot (B.3), and anti-METTL7B (anti-TMT1B) western blot (B.4) of purified *N*-GST-METTL7A (*N*-GST-TMT1A). Labeled bands are *N*-GST-METTL7A (*N*-GST-TMT1A) (I), a contaminant chaperone protein (II), and GST devoid of METTL7A (TMT1A) (III, IV).

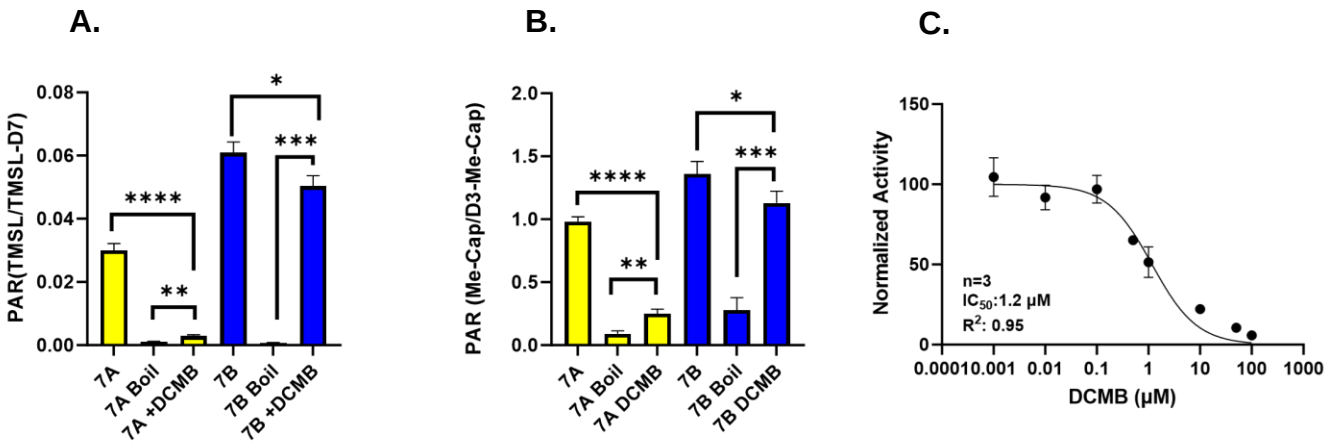

Figure 2.3. Methylation activity of METTL7A and METTL7B compared and DCMB IC_{50}

Methylation of TSL by purified recombinant *N*-GST-METTL7A (*N*-GST-TMT1A) and *N*-GST-METTL7B (*N*-GST-TMT1B) ±DCMB (A) or captopril (B). IC_{50} for the inhibition of purified recombinant *N*-GST-METTL7A (*N*-GST-TMT1A) by DCMB was determined by single time-point activity assays with increasing concentrations of DCMB (C). Data (n=3) are reported as the mean ±S.D. ****$P < 0.0001$. ***$P < 0.001$. **$P < 0.01$.

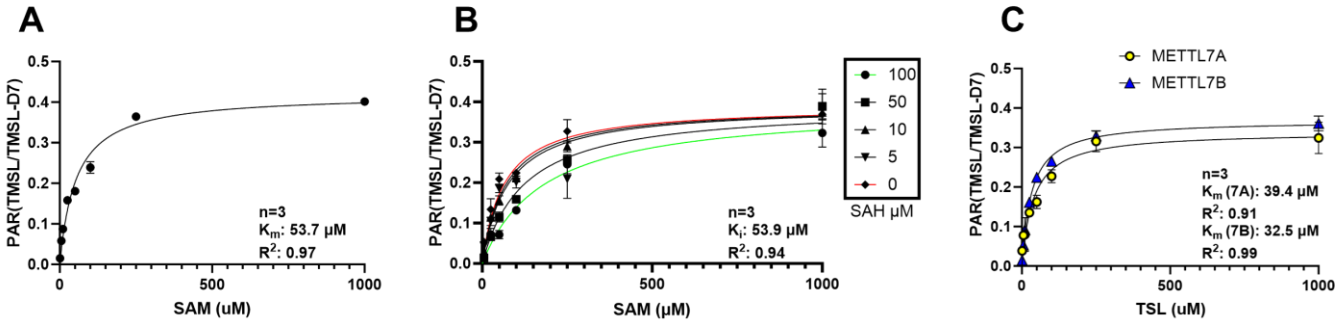

Figure 2.4. Kinetic analysis of N-GST-METTL7A

TSL methylation by N-GST-METTL7A (*N*-GST-TMT1A) at various concentrations of SAM in absence (A) or presence of increasing concentrations of SAH (B); and single time-point kinetics profiles of N-GST-METTL7A (*N*-GST-TMT1A) or N-GST-METTL7B (*N*-GST-TMT1B) with increasing concentrations of TSL (C). Data (n=3) are reported as the mean ±S.D.

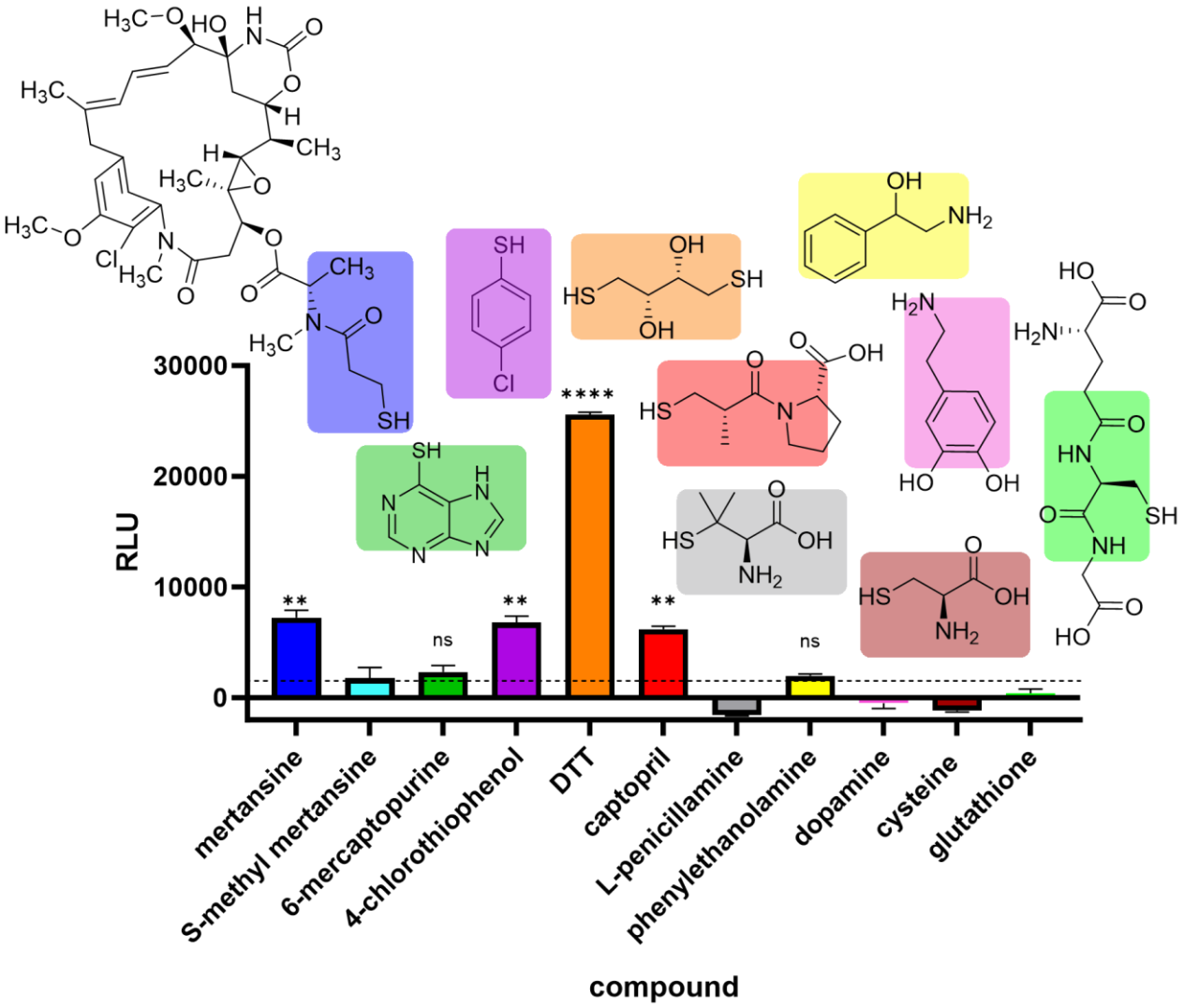

Figure 2.5. METTL7A substrate screen

Semi-quantitative screening of select small molecule methyltransferase probe substrates. Known methyltransferase probe substrates were incubated at saturating concentrations for 1 h with *N*-GST-METTL7A (*N*-GST-TMT1A). Formation of SAH (indication of methyl transfer) was converted/directly linked to luminescence and measured via the Promega MTaseGlo kit. Enzyme activity was determined after normalizing to compound-specific and general assay background signal. All data (n=3) are presented as the mean ±S.D. Significance was determined using unpaired two-tailed t-test comparing the baseline subtracted response of each compound with that of S-methyl mertansine as a baseline (dotted line). ****P < 0.0001. ***P < 0.001. **P < 0.01.

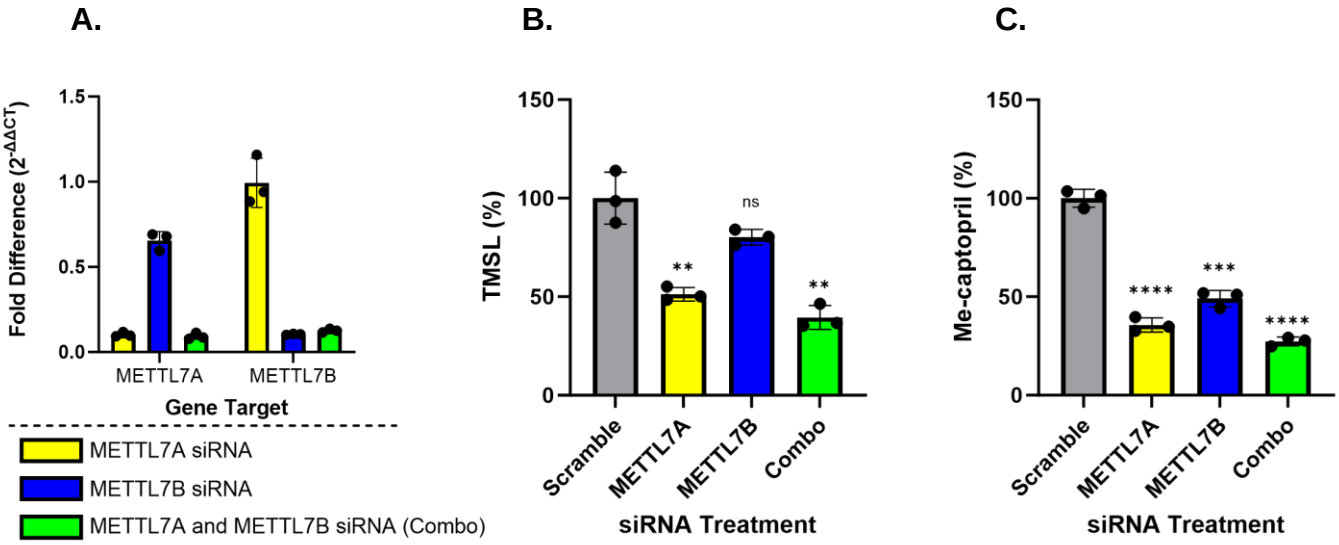

Figure 2.6. Knockdown of *METTL7A* and *METTL7B* in HepG2 and impact on TMT activity

Knockdown of *METTL7A* (*TMT1A*) and *METTL7B* (*TMT1B*) in HepG2 cells. RT-PCR data measuring fold difference of *METTL7A* (*TMT1A*) or *METTL7B* (*TMT1B*) expression following 48-hour siRNA treatment with *METTL7A* (*TMT1A*)- and/or *METTL7B* (*TMT1B*)-targeting siRNA (A). Percent TMSL (B) and S-methyl captopril (C) formed in cell media. All data (n=3) are presented as the mean ±S.D. Significance was determined using an unpaired two-tailed t-test. ****$P < 0.0001$. ***$P < 0.001$. **$P < 0.01$.

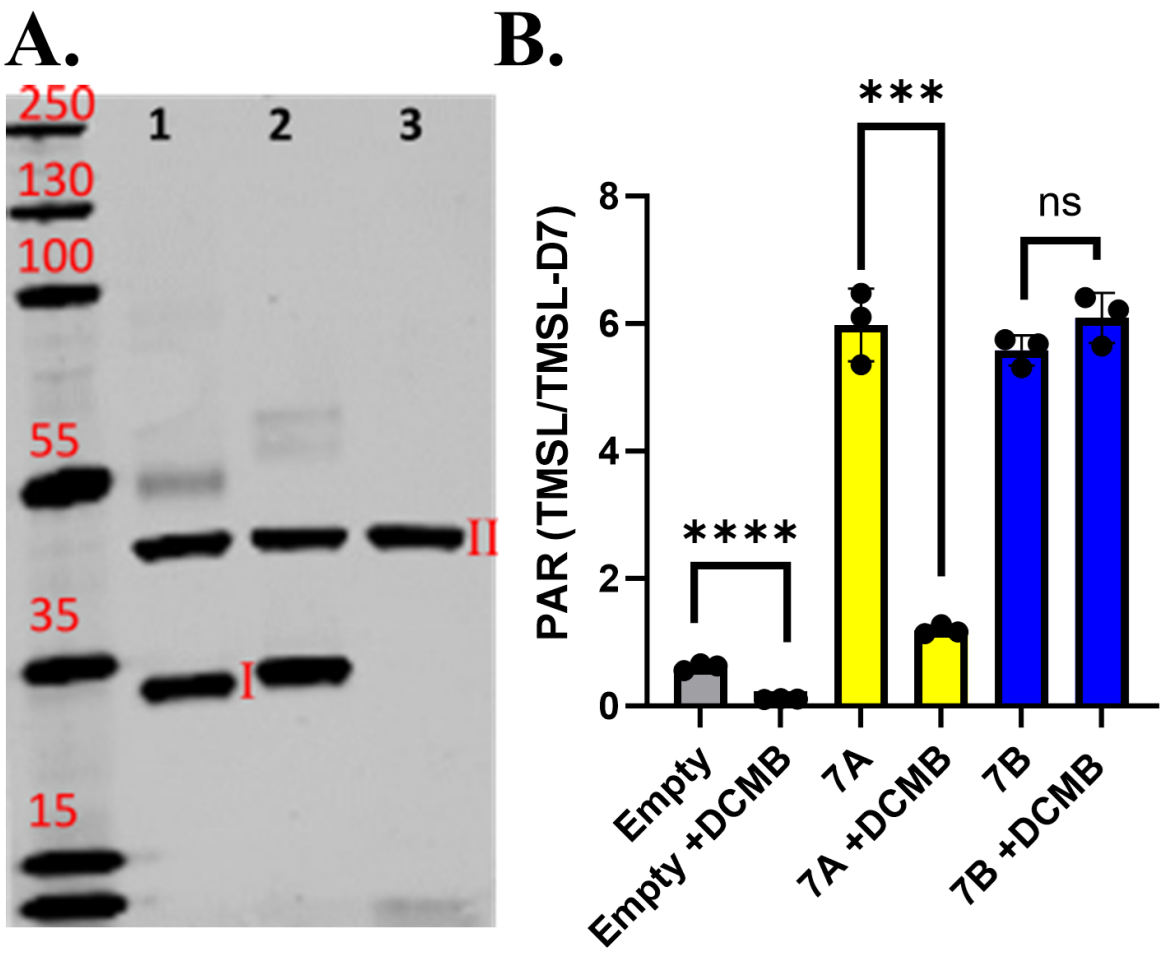

Figure 2.7. Overexpression of METTL7A and METTL7B in HeLa cells and impact on activity

Overexpression of METTL7A (TMT1A) and METTL7B (TMT1B) in HeLa cells. Anti-flag and anti-β-actin western blot verify the overexpression of flag-tagged proteins in METTL7A (TMT1A) (A.1) and METTL7B (TMT1B) (A.2) which show a band at I, compared to cells treated with empty vector control (A.3.). Labeled bands are flag-tagged METTL7A (TMT1A) and flag-tagged METTL7B (TMT1B) (I), and β-actin (II). Formation of TMSL in HeLa cells overexpressing METTL7A (TMT1A) or METTL7B (TMT1B) following a 24-hour incubation with TSL ±DCMB (B). All data (n=3) are presented as the mean ±S.D. Significance was determined using unpaired two-tailed t-test. ****$P < 0.0001$. ***$P < 0.001$. **$P < 0.01$.

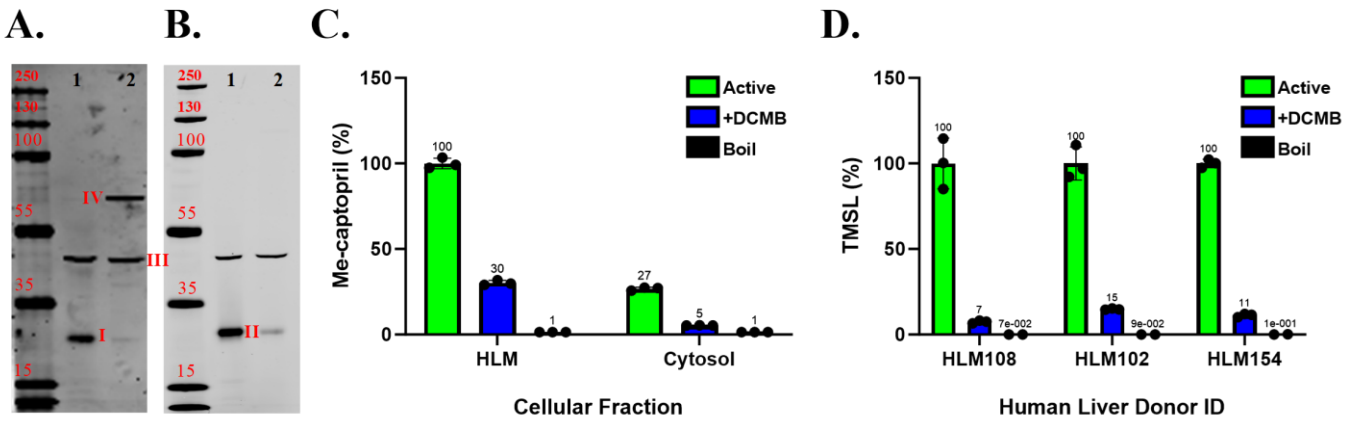

Figure 2.8. Subcellular localization of METTL7A and METTL7B in human liver

Anti-METTL7A (anti-TMT1A) (A) and anti-METTL7B (anti-TMT1B) (B) western blots of human liver microsomes (1) and cytosol (2). Labeled bands are METTL7A (TMT1A) (I), METTL7B (TMT1B) (II), and β-actin (III), the band at IV is an unknown protein that reacts with anti-METTL7A (anti-TMT1A) antibody in the cytosolic fraction. Relative formation of S-methyl-captopril in pooled human liver microsomes and cytosol ±DCMB (C) Relative formation of TMSL in individual liver donor microsomes ±DCMB (D). All treatments performed in triplicate (n=3) except for the boil controls in panel D which were performed in duplicate (n=2). All data are presented as the mean ±S.D.

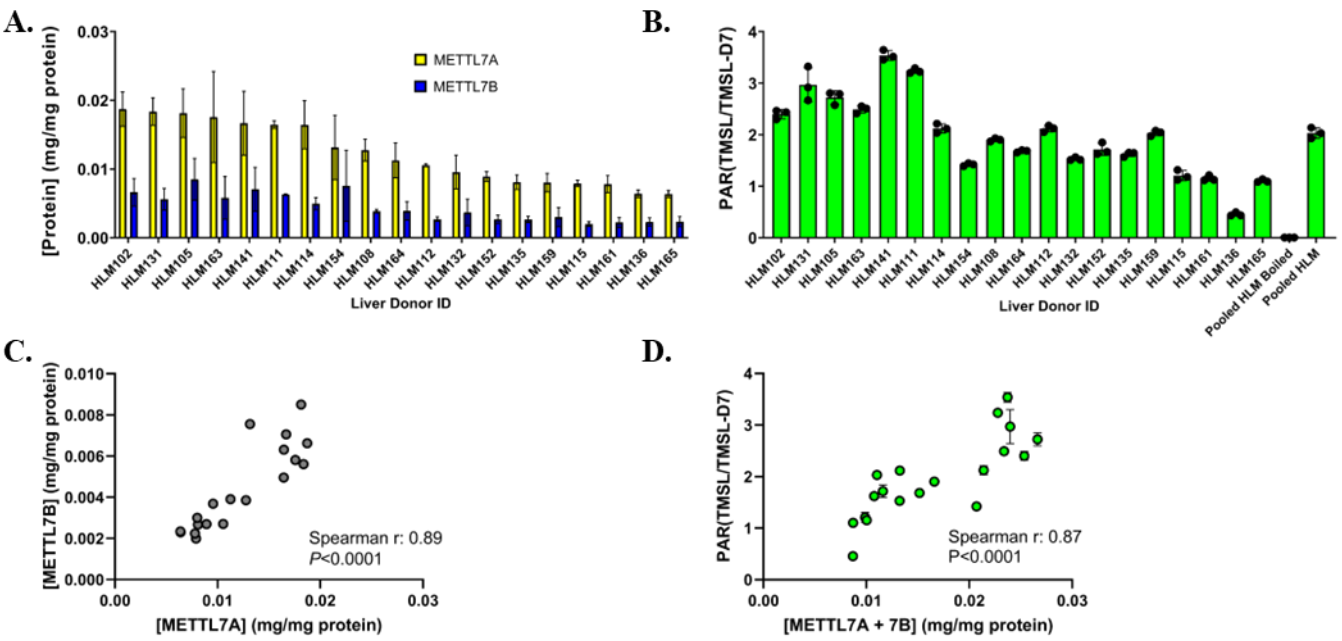

Figure 2.9. Correlation of TMT activity with METTL7A and METTL7B protein levels in liver

METTL7A (TMT1A) and METTL7B (TMT1B) protein levels measured in individual donor HLMs using quantitative proteomics; protein levels of METTL7A (TMT1A) and METTL7B (TMT1B) are reported normalized to total protein per digestion. (A). Methyltransferase activity, reported as PAR, of single-donor HLMs incubated with TSL, and SAM (B) compared with commercially available 50-donor pooled HLMs. METTL7A (TMT1A) and METTL7B (TMT1B) protein correlation (C). TMT activity correlated with METTL7A (TMT1A) and METTL7B (TMT1B) protein levels (D). Data are presented as the mean ±S.D.

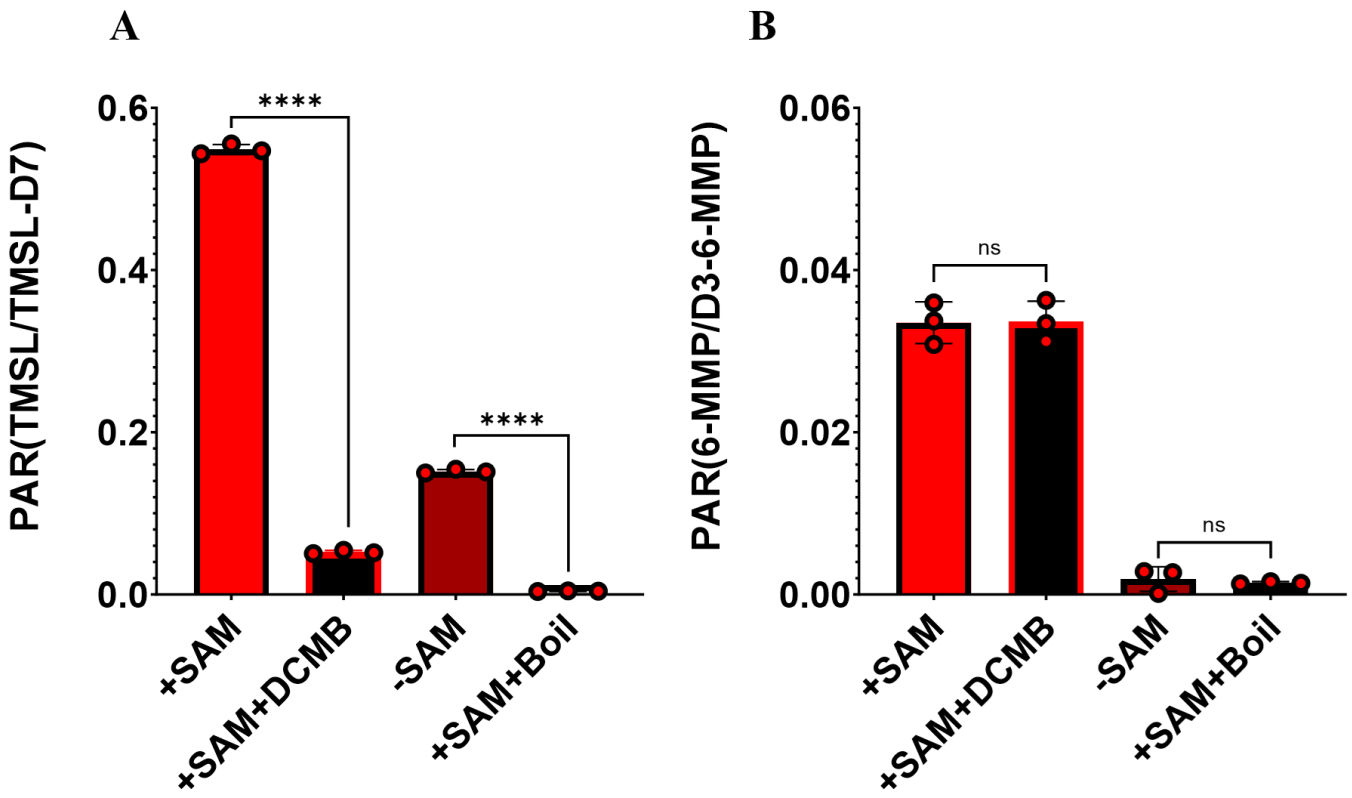

Figure 2.10. TMT and TPMT activity in blood

Methyltransferase activity in blood ±DCMB. (A) Alkyl thiol methyltransferase (TMT) activity reported as TSL methylation. (B) Thiopurine methyltransferase activity reported as 6-MP methylation. All data (n=3) are presented as the mean ±S.D. Significance was determined using unpaired two-tailed t-test. ****$P < 0.0001$. ***$P < 0.001$. **$P < 0.01$.

2.6 REFERENCES

1. Yates, C.R., et al., *Molecular diagnosis of thiopurine S-methyltransferase deficiency: genetic basis for azathioprine and mercaptopurine intolerance.* Ann Intern Med, 1997. **126**(8): p. 608-14.

2. Bremer, J. and D.M. Greenberg, *Enzymic methylation of foreign sulfhydryl compounds.* Biochimica et Biophysica Acta, 1961. **46**(2): p. 217-224.

3. Krynetski, E. and W.E. Evans, *Drug methylation in cancer therapy: lessons from the TPMT polymorphism.* Oncogene, 2003. **22**(47): p. 7403-13.

4. Wusk, B., et al., *Thiopurine S-methyltransferase polymorphisms: efficient screening method for patients considering taking thiopurine drugs.* Eur J Clin Pharmacol, 2004. **60**(1): p. 5-10.

5. Weinshilboum, R.M. and S.L. Sladek, *Mercaptopurine pharmacogenetics: monogenic inheritance of erythrocyte thiopurine methyltransferase activity.* Am J Hum Genet, 1980. **32**(5): p. 651-62.

6. Lennard, L., *Implementation of TPMT testing.* Br J Clin Pharmacol, 2014. **77**(4): p. 704-14.

7. Weisiger, R.A. and W.B. Jakoby, *Thiol S-methyltransferase from rat liver.* Arch Biochem Biophys, 1979. **196**(2): p. 631-7.

8. Obach, R.S., C. Prakash, and A.M. Kamel, *Reduction and methylation of ziprasidone by glutathione, aldehyde oxidase, and thiol S-methyltransferase in humans: an in vitro study.* Xenobiotica, 2012. **42**(11): p. 1049-57.

9. Kazui, M., et al., *Hepatic microsomal thiol methyltransferase is involved in stereoselective methylation of pharmacologically active metabolite of prasugrel.* Drug Metab Dispos, 2014. **42**(7): p. 1138-45.

10. Liu, C., et al., *Human Liver Cytochrome P450 Enzymes and Microsomal Thiol Methyltransferase Are Involved in the Stereoselective Formation and Methylation of the Pharmacologically Active Metabolite of Clopidogrel.* Drug Metab Dispos, 2015. **43**(10): p. 1632-41.

11. Taplin, S., et al., *Hepatotoxicity with antibody maytansinoid conjugates: A review of preclinical and clinical findings.* J Appl Toxicol, 2018. **38**(5): p. 600-615.

12. Erickson, H.K., et al., *Tumor Delivery and In Vivo Processing of Disulfide-Linked and Thioether-Linked Antibody−Maytansinoid Conjugates.* Bioconjugate Chemistry, 2010. **21**(1): p. 84-92.

13. Keith, R.A., et al., *Human erythrocyte membrane thiol methyltransferase. S-methylation of captopril, N-acetylcysteine, and 7 alpha-thio-spirolactone.* Drug Metab Dispos, 1984. **12**(6): p. 717-24.

14. Overdiek, H.W. and F.W. Merkus, *The metabolism and biopharmaceutics of spironolactone in man.* Rev Drug Metab Drug Interact, 1987. **5**(4): p. 273-302.

15. Bargh, J.D., et al., *Cleavable linkers in antibody-drug conjugates.* Chem Soc Rev, 2019. **48**(16): p. 4361-4374.

16. Lopus, M., et al., *Maytansine and cellular metabolites of antibody-maytansinoid conjugates strongly suppress microtubule dynamics by binding to microtubules.* Mol Cancer Ther, 2010. **9**(10): p. 2689-99.

17. Savi, P., et al., *The active metabolite of Clopidogrel disrupts P2Y12 receptor oligomers and partitions them out of lipid rafts.* Proc Natl Acad Sci U S A, 2006. **103**(29): p. 11069-74.

18. Maldonato, B.J., D.A. Russell, and R.A. Totah, *Human METTL7B is an alkyl thiol methyltransferase that metabolizes hydrogen sulfide and captopril.* Scientific Reports, 2021. **11**(1): p. 4857.

19. Zehmer, J.K., et al., *Identification of a novel N-terminal hydrophobic sequence that targets proteins to lipid droplets.* J Cell Sci, 2008. **121**(11): p. 1852-60.

20. Maw, H.H., et al., *N-Methylation of BI 187004 by Thiol S-Methyltransferase.* Drug Metab Dispos, 2018. **46**(6): p. 770-778.

21. Glauser, T.A., et al., *Human liver microsomal thiol methyltransferase: inhibition by arylalkylamines.* Xenobiotica, 1993. **23**(6): p. 657-69.

22. Agusti, G., et al., *A safe and practical method for the preparation of 7α-thioether and thioester derivatives of spironolactone.* Steroids, 2013. **78**(1): p. 102-7.

23. Altschul, S.F., et al., *Basic local alignment search tool.* J Mol Biol, 1990. **215**(3): p. 403-10.

24. Jumper, J., et al., *Highly accurate protein structure prediction with AlphaFold.* Nature, 2021. **596**(7873): p. 583-589.

25. Varadi, M., et al., *AlphaFold Protein Structure Database: massively expanding the structural coverage of protein-sequence space with high-accuracy models.* Nucleic Acids Res, 2022. **50**(D1): p. D439-d444.

26. Schubert, H.L., R.M. Blumenthal, and X. Cheng, *Many paths to methyltransfer: a chronicle of convergence.* Trends Biochem Sci, 2003. **28**(6): p. 329-35.

27. Rivett, A.J. and J.A. Roth, *Kinetic studies on the O-methylation of dopamine by human brain membrane-bound catechol O-methyltransferase.* Biochemistry, 1982. **21**(8): p. 1740-2.

28. Drummer, O.H., P. Miach, and B. Jarrott, *S-methylation of captopril. Demonstration of captopril thiol methyltransferase activity in human erythrocytes and enzyme distribution in rat tissues.* Biochem Pharmacol, 1983. **32**(10): p. 1557-62.

29. Hiemke, C. and R. Ghraf, *Distribution and properties of thiol S-methyltransferase in rat brain.* J Neurochem, 1983. **40**(2): p. 592-4.

30. Keith, R.A., et al., *S-Methylation of D- and L-penicillamine by human erythrocyte membrane thiol methyltransferase.* Drug Metab Dispos, 1985. **13**(6): p. 669-76.

31. Grunewald, G.L., et al., *Conformational and steric aspects of phenylethanolamine and phenylethylamine analogues as substrates or inhibitors of phenylethanolamine N-methyltransferase.* Mol Pharmacol, 1989. **35**(1): p. 93-7.

32. Weinshilboum, R.M., S. Sladek, and S. Klumpp, *Human erythrocyte thiol methyltransferase: radiochemical microassay and biochemical properties.* Clin Chim Acta, 1979. **97**(1): p. 59-71.

33. Weisiger, R.A. and W.B. Jakoby, *S-methylation: thiol S-methyltransferase.* Enzymatic basis of detoxication, 1980. **1**: p. 131-40.

34. Weisiger, R.A., L.M. Pinkus, and W.B. Jakoby, *Thiol S-methyltransferase: suggested role in detoxication of intestinal hydrogen sulfide.* Biochem Pharmacol, 1980. **29**(20): p. 2885-7.

35. Karlsson, M., et al., *A single–cell type transcriptomics map of human tissues.* Science Advances, 2021. **7**(31): p. eabh2169.

36. Pacifici, G.M., et al., *Thiol methyltransferase in humans: development and tissue distribution.* Dev Pharmacol Ther, 1991. **17**(1-2): p. 8-15.

37. Borchardt, R.T. and C.F. Cheng, *Purification and characterization of rat liver microsomal thiol methyltransferase.* Biochim Biophys Acta, 1978. **522**(2): p. 340-53.

38. Aksoy, S., C.L. Szumlanski, and R.M. Weinshilboum, *Human liver nicotinamide N-methyltransferase. cDNA cloning, expression, and biochemical characterization.* J Biol Chem, 1994. **269**(20): p. 14835-40.

39. Drinkwater, N., et al., *Molecular recognition of physiological substrate noradrenaline by the adrenaline-synthesizing enzyme PNMT and factors influencing its methyltransferase activity.* Biochem J, 2009. **422**(3): p. 463-71.

40. Júlio-Costa, A., et al., *Count on dopamine: influences of COMT polymorphisms on numerical cognition.* Front Psychol, 2013. **4**: p. 531.

41. AXELROD, J. and C.K. COHN, *METHYLTRANSFERASE ENZYMES IN RED BLOOD CELLS.* Journal of Pharmacology and Experimental Therapeutics, 1971. **176**(3): p. 650-654.

42. Wyatt, R.J., J.M. Saavedra, and J. Axelrod, *A dimethyltryptamine-forming enzyme in human blood.* Am J Psychiatry, 1973. **130**(7): p. 754-60.

43. Bryk, A.H. and J.R. Wiśniewski, *Quantitative Analysis of Human Red Blood Cell Proteome.* J Proteome Res, 2017. **16**(8): p. 2752-2761.

44. Campeanu, I.J., et al., *Multi-omics integration of methyltransferase-like protein family reveals clinical outcomes and functional signatures in human cancer.* Scientific Reports, 2021. **11**(1): p. 14784.

45. Jiang, Z., et al., *METTL7B is a novel prognostic biomarker of lower-grade glioma based on pan-cancer analysis.* Cancer Cell International, 2021. **21**(1): p. 383.

46. Chen, X., et al., *Characterization of METTL7B to Evaluate TME and Predict Prognosis by Integrative Analysis of Multi-Omics Data in Glioma.* Front Mol Biosci, 2021. **8**: p. 727481.

47. Xiong, Y., et al., *High Level of METTL7B Indicates Poor Prognosis of Patients and Is Related to Immunity in Glioma.* Front Oncol, 2021. **11**: p. 650534.

48. Ye, D., et al., *METTL7B promotes migration and invasion in thyroid cancer through epithelial-mesenchymal transition.* J Mol Endocrinol, 2019. **63**(1): p. 51-61.

49. Liu, D., et al., *METTL7B Is Required for Cancer Cell Proliferation and Tumorigenesis in Non-Small Cell Lung Cancer.* Front Pharmacol, 2020. **11**: p. 178.

50. Li, W., et al., *Downregulation of METTL7B Inhibits Proliferation of Human Clear Cell Renal Cancer Cells In Vivo and In Vitro.* Front Oncol, 2021. **11**: p. 634542.

51. Wang, Z., et al., *Induction of m(6)A methylation in adipocyte exosomal LncRNAs mediates myeloma drug resistance.* J Exp Clin Cancer Res, 2022. **41**(1): p. 4.

52. Robey, R.W., et al., *The methyltransferases METTL7A and METTL7B confer resistance to thiol-based histone deacetylase inhibitors.* bioRxiv, 2023: p. 2022.10.07.511310.

53. Omasits, U., et al., *Protter: interactive protein feature visualization and integration with experimental proteomic data.* Bioinformatics, 2014. **30**(6): p. 884-6.

Chapter 3. **Functional characterization of TMT1A and TMT1B**

3.1 INTRODUCTION

In Chapter 2, we discussed the characterization of TMT1A, one of three human thiol *S*-methyltransferases alongside TMT1B and TPMT [1, 2]. We demonstrated that TMT1A and TMT1B are both responsible for alkyl thiol methylation, but only TMT1A is inhibited by the small molecule methyltransferase inhibitor 2,3-dichloro-α-methylbenzylamine (DCMB). Since almost all alkyl thiol methyltransferase activity in blood and microsomes is inhibited by DCMB, we hypothesized that TMT1A is responsible for most of this activity [1, 3]. It was surprising that TMT1A and TMT1B, two enzymes that are 76% homologous and nearly 60% identical across their sequences, would have such a significant difference in susceptibility to inhibition to a small molecule like DCMB. To better understand the active site structure and function of these enzymes and explain this difference in inhibition, we sought to identify differences in the active sites of TMT1A and TMT1B that would explain the difference in susceptibility to DCMB and eventually guide us to develop specific inhibitors for each isoform.

Methyltransferases employ different catalytic mechanisms to facilitate the methyl transfer and select for substrate and nucleophilic heteroatom. The small molecule methyltransferase catechol *O*-methyltransferase (COMT) utilizes a metal ion to coordinate and facilitate deprotonation of substrates in the active site [4]. Other methyltransferases have catalytic sidechains in their active site to coordinate substrate binding and deprotonation for methyl transfer [5], and others, like arsenic III methyltransferase (AS3MT), utilize substrate and intramolecular cysteine bonding interactions to catalyze the methyl transfer [6-10].

While small molecule methyltransferases employ different catalytic mechanisms to facilitate methyl transfer, the binding interactions with the cofactor *S*-adenosyl-L-methionine (SAM) are

highly conserved with near-identical structural and sequence homology in the SAM binding region (Chapter 1, **section 1.1**, Figure 1.4, [11]). TMT1A and TMT1B have yet to be crystallized, so we used AlphaFold-generated models®, for our structural modeling [12]. We compared TMT1A and TMT1B with other methyltransferase structures to identify potential key residues involved in TMT1A- and TMT1B-SAM binding interactions. We pinpointed where and in which orientation SAM potentially binds to TMT1A and TMT1B by aligning TMT1A and TMT1B homology models with a crystal structure of COMT and then utilized docking analysis to identify a region where substrates can bind close to SAM's labile methyl group. We identified conserved cysteine residues, in the regions suspected to be TMT1A and TMT1B substrate binding sites, that may participate in thiol methyl transfer reactions similar to the cysteine residues in AS3MT. We also discovered several residues that are different in the TMT1A and TMT1B substrate binding sites. There are unique hydrophobic residues in TMT1A's substrate binding sites that we hypothesized could form π-π stacking interactions with DCMB that would not be possible in TMT1B. We mutated each unique residue in TMT1A's substrate binding site to the corresponding TMT1B residue and identified the residues that are vital for DCMB binding and inhibition of TMT1A.

We then developed a novel recombinant protein expression and isolation method that significantly increased the yield of recombinant TMT1 produced from bacteria. Taking inspiration from a technique that has been used to generate active recombinant cytochrome P450s, another membrane-associate and major drug-metabolizing family of enzymes [13], we cultured TMT1A-expressing bacteria, isolated bacterial spheroplasts that contained large quantities of active TMT1A and verified that TMT1A spheroplasts closely approximate the biochemical characteristics of purified recombinant TMT1A. With these TMT1A-containing

spheroplasts, we screened compounds for TMT1A inhibition and identified several novel inhibitors of TMT1A. We also purified recombinant TPMT and completed our analysis of thiol methyltransferases by demonstrating that TPMT and TMT1 have separate and distinct substrate specificities. TPMT methylates aromatic thiols such as thiopurines, and the TMT1 family methylates alkyl thiols exclusively.

The work discussed in this chapter significantly improves our understanding of the structure and function of the TMT1 family. This work will help us to eventually produce specific probe inhibitors for TMT1A and TMT1B, which will be invaluable tools to identify the relative contribution of TMT1A and TMT1B to drug metabolism as well as determine their endogenous function.

3.2 Materials and Methods

3.2.1 *Materials*

Activity assay substrates, reagents, cofactor, inhibitors, and internal standards: 1,2-Dimyristoyl-sn-glycero-3-PG (DMPG) was obtained from Cayman Chemicals (Ann Arbor, Mi); 7α-thiospironolactone was produced in-house from spironolactone using a previously published method [14]; spironolactone, reduced glutathione, *S*-methyl glutathione, 4-Nitrobenzenethiol (4-NBT), 6-Mercaptopurine (6-MP), Ibuprofen, 2,4-Dichloro-6-methylbenzylamine (DC6MB), Caffeine, 2-amino-1-phenylethanol (2-APE), 1-(2,4-dichlorophenyl)ethylamine (2,4-DCMB), DCMB 2,3-dichloro-α-methylbenzylamine (DCMB), and DL-1,4-dithiothreitol were obtained from Fisher Scientific (Hampton, NH); 7α-thiomethylspironolactone-d7 was obtained from Toronto Research Chemicals (Toronto, ON, Canada); *S*-adenosyl-L-methionine was obtained from New England Biolabs (Ipswich, MA). Reagents and materials for *E. coli* culture, protein purification, and activity assay experiments, and mutagenesis: Q5 Site-Directed Mutagenesis Kit

was from New England Biolabs (Ipswich, MA); ampicillin sodium salt, isopropyl-β-D-thiogalactopyranoside, yeast extract, tryptone, NaCl, KH_2PO_4, K_2HPO_4, Thermo Scientific™ Halt™ Protease Inhibitor Cocktail, glycerol, CHAPS, white 96-well microplate, Nunc™ 96-Well Polypropylene Storage Microplates, Nunc™ 96-Well Slit-Cap Mats, Corning 96-Well (Non-Binding, Flat-Bottom, Half-Area Microplate, Bottom: Flat, Black, Clear Bottom) microplates, and ultra-15 10 K molecular weight cut off centrifugal filter units were obtained from Fisher Scientific (Hampton, NH); His60 Ni Superflow Resin from Takara (Mountain View, CA); deoxyribonuclease I, lysozyme, and imidazole were obtained from Sigma Aldrich (St. Louis, MO); All primers were obtained from Integrated DNA Technologies (San Diego, Ca). Open reading frames for TPMT, TMT1A-FLAG, and TMT1A-GFP were purchased from Twist Bioscience (San Fransico, CA) Reagents and materials for activity assay cleanup and downstream LC/MS analysis: acetonitrile (LC/MS grade), acetic acid (LC/MS grade), and Optima water were obtained from Fisher Scientific (Hampton, NH). Reagents and materials for SDS-page and western blot analysis: NuPAGE™ MOPS SDS Running Buffer (20X), PageRuler Plus Prestained Protein Ladder (10 to 250 kDa), GelCode™ Blue Safe Protein Stain, and iBlot™ Nitrocellulose Transfer Stacks were sourced from Fisher Scientific (Hampton, NH); DYKDDDDK (Anti-FLAG) Tag Rabbit monoclonal antibody, β-actin rabbit monoclonal antibody was obtained from Cell Signaling (Danvers, MA); IRDye 680RD Goat anti-Rabbit secondary antibody was obtained from LiCor (Lincoln, NE); TPMT rabbit polyclonal antibody was purchased from ProteinTech (Rosement, IL). Reagents and materials for cell culture and gene modulation: Eagle's Minimum Essential Medium, Gibco™ Opti-MEM™, Gibco™ Penicillin-Streptomycin, Corning™ Falcon™ Polystyrene 12-well and 6-well Microplates, Gibco™ Trypsin-EDTA (0.25%), Cytiva HyClone™ Fetal Bovine Serum, Invitrogen™

Lipofectamine™ 3000 & P3000 Transfection Reagents, 12-well cell culture plates, and cell culture treated T75 plates were obtained from Fisher Scientific (Hampton, NH); Empty-, METTL7A-, and METTL7B-pCMV6 expression vectors were sourced from Origene (Rockville, MD); Dulbecco′s Phosphate Buffered Saline (PBS) was obtained from Sigma Aldrich (St. Louis, MO).

3.2.2 *Kinetic parameters of the in vitro inhibition of purified recombinant TMT1A*

For single time point inhibition, aliquots of purified recombinant N-GST-TMT1A (See Chapter 2 **section 2.3.6**) were diluted with reaction buffer (50 mM KPi pH 7.0, 20% glycerol, 150 mM NaCl, 10 mM CHAPS) to 0.2 mg/mL. The diluted protein was then combined with two parts reaction buffer containing 9 mg/mL DMPG. A fraction of diluted protein was boiled for 10 min while the other portion of active protein was incubated on ice for 30 min to equilibrate with DMPG.

For single time point inhibition with variable substrate, TSL was dissolved in acetonitrile and then deposited in the appropriate wells of a 96-well reaction plate. The plate was dried under vacuum for 10 min to remove the organic solvent. The diluted recombinant protein was then added to the plate and placed on a shaker at room temperature and 625 RPM for 5 min. DCMB, dissolved in water, was added to wells requiring DCMB, and an equal volume of water was added to the remaining wells as a vehicle control. The reaction was initiated by adding SAM at a final concentration of 100 µM. The final TSL concentrations were 5, 25, 50, and 100 µM, the final DCMB concentrations were 0, 0.5, 1, 10, and 50 µM, and the final protein concentration was 0.07 mg/mL. Sample replicates for all combinations of TSL and DCMB concentrations were generated to produce a 4 (TSL) × 5 (DCMB) substrate/inhibitor matrix. The plate was then sealed with a silicon plate mat, and incubated at 37 °C for 30 min.

For single time point inhibition with variable cofactor, TSL was dissolved in acetonitrile and then pipetted in the appropriate wells of a 96-well reaction plate. The plate was dried under vacuum for 10 min to remove the organic solvent. The diluted recombinant protein prepared that same as above was then added to the plate and placed on a shaker at room temperature and 625 RPM for 5 min. DCMB, dissolved in water, was added to wells requiring DCMB, and an equal volume of water was added to the remaining wells as a vehicle control. The reactions were initiated by adding SAM at a final concentration of 5, 50, 100, 250, and 1000 µM. The final TSL concentration was 250 µM, the final DCMB concentrations were 0, 0.5, 1, 10, and 50 µM, and the final protein concentration was 0.07 mg/mL. Sample replicates for all combinations of concentrations of SAM and DCMB were generated to produce a 5 (SAM) × 5 (DCMB) inhibition matrix. This assay was performed as a microassay to conserve protein, and the final reaction volume was 30 µL. The plate was sealed with a silicon plate mat, and incubated at 37 °C for 30 min.

For both the variable substrate and variable cofactor experiments, following the 30 min incubation at 37 °C, the reaction was quenched with 5× the reaction volume with ice-cold ethyl acetate containing 5 µM 7α-thiomethylspironolactone-d7 deuterated internal standard (TMSL-D7). During the quench step, each sample was mixed with ethyl acetate by gentle pipetting up and down. The plate was then immediately frozen at -80 °C for 12 min. After 12 min, the aqueous layer was frozen, and the liquid organic top layer was transferred to a new plate. The transferred samples were dried with gentle heat under nitrogen gas (Biotage, Charlotte, NC) followed by reconstitution with 50:50 MeCN:H_2O containing 0.2% acetic acid. Samples were analyzed using a Waters Xevo TQS mass spectrometer paired with a Waters Acquity LC using a 2.1 × 50 mm Waters 1.7 µm C18 column and 0.2% acetic acid in water and 0.2% acetic acid in

MeCN as solvents A and B respectively. The elution of TMSL and TMSL-D7 was achieved with an isocratic gradient held at a 50:50 ratio of solvent A to B. Flow rate was constant at 0.4 mL/min. The transitions used to monitor for methyl metabolite 7α-thiomethylspironolactone (TMSL) and IS TMSL-D7 were 389.223>341.308 and 396>347.05, respectively, and TSL methylation was reported as the peak area ratio (PAR) of TMSL / TMSL-D7.

3.2.3 *Computational structural analysis of TMT1A and TMT1B*

AlphaFold homology models of TMT1A and TMT1B were downloaded from the AlphaFold protein structure database [12] using each enzyme's UniProt accession number—Q9H8H3 and Q6UX53, respectively. The homology model was then uploaded to the Proteins Plus web application curated by the University of Hamburg's Center for Bioinformatics at https://proteins.plus/ for further analysis. Each TMT1 isoform's homology model was then analyzed with DoGSiteScorer, a grid-based method that uses a Difference of Gaussian filter to detect binding pockets based solely on the 3D structure of a protein [15]. The default settings were used. DoGSiteScorer identified a central binding pocket in TMT1A and TMT1B and produced a list of residues that composed each binding pocket. The protein-graphics visualization software, Pymol, was used to render and align the TMT1 homology models. The residues that DoGSiteScorer listed for the central binding pocket of TMT1A and of TMT1B were highlighted in the Pymol-rendered homology models: green if the aligned residues were identical for TMT1A and TMT1B, orange if the aligned residues were homologous, and red if the aligned residues were different in each isoform.

DCMB and captopril were individually docked into the AlphaFold homology model of TMT1A using JAMDA docking software [16]. The docking zone was constrained to TMT1A's central binding pocket identified by DoGSiteScorer. The cofactor SAM was not included in the

docking studies. The small molecules were uploaded to JAMDA as .mol2 files. The .mol2 structural files were geometry optimized by AVOGADRO [17]. Hydrogen atoms and charge states were adjusted for pH 7.4. The only setting that was altered from JAMDA's default settings was the precision level, which was set to high.

Crystal structures of COMT (4XUC, 1.80 Å), INMT (2A14, 1.7 Å), NNMT (7BKG, 2.33 Å), PNMT (2AN3, 2.20 Å), and HNMT (2AOT, 1.9 Å) were downloaded as PDB files from each protein's Uniprot entry. The crystal structures were chosen based on the highest resolution and the presence of a SAH or SAM in the crystal structure. Each crystal structure's PDB file was uploaded to Proteins Plus and the SAM or SAH binding interactions were analyzed with the Proteins Plus web application PoseView, an application that creates two-dimensional diagrams of proteins complexed with small molecules [18]. There are no adjustable settings options for this application. The residues identified by PoseView were highlighted on each methyltransferase's crystal structure using Pymol (Supplementary fig. 3.1 to 3.5). The highlighted residues and the SAM or SAH in each crystal structure were extracted from each whole crystal structure. Then, with Pymol's alignment function, the residue and ligand substructures were all aligned (Supplementary fig. 3.6).

The crystal structure of COMT (4XUC, 1.80 Å) was aligned with TMT1A's homology model. COMT's crystal structure contained a bound SAM. This SAM was extracted into the aligned TMT1A's homology model structure to give an approximation of where SAM would bind. The model of TMT1A with SAM bound was then aligned with the PoseView substructures that were generated from the small molecule methyltransferase crystal structures. TMT1A residues that overlapped with any of the other methyltransferase residues in the PoseView

substructures were identified. TMT1A's homology model was aligned with TMT1B's homology model to identify these residues in TMT1B, as well (Supplementary fig. 3.7).

3.2.4 *Design and construction of TMT1A mutants*

The Q5 Site-Directed Mutagenesis Kit (New England Biolabs, Ipswich, MA, Cat# E0554S) was used to introduce missense mutations in a pCMV6 expression plasmid encoding for wild-type TMT1A-FLAG (WT-TMT1A) (Ref: RC202601; Origene). Six mutant TMT1A expressing pCMV6 expression plasmids were generated: F39L-TMT1A, Y47S-TMT1A, F39L+F43L-TMT1A, F43L+Y47S-TMT1A, F39L+F43L+Y47S-TMT1A, and F199G-TMT1A. The expression plasmids with multiple missense mutations had to be generated in multiple steps by mutating and purifying each expression plasmids sequentially. For example, F39L+F43L-TMT1A was produced by first introducing the F39L missense mutation to the expression plasmid, purifying the mutated plasmid, and then introducing the F43L missense mutation to the F39L-TMT1A expressing plasmid. The only mutant with multiple missense mutations that was not generated this way was the F43L+Y47S-TMT1A mutant, which was produced by introducing an L39F missense mutation to the F39L+F43L+Y47S-TMT1A expressing plasmid, converting TMT1A's codon 39 back from a leucine coding sequence to a phenylalanine coding sequence. Custom forward and reverse non-overlapping mutagenic primers were designed using New England Biolab's NEBaseChanger https://nebasechangerv1.neb.com/. By non-homologous base-pairing, the mutagenic primer incorporates the necessary nucleotide substitutions to generate each missense mutation. The primers utilized for this mutagenesis are listed in supplementary table 3.1.

Each plasmid sequence was verified by whole plasmid sequencing through Eurofins Genomics (Louisville, KY). Eurofins Genomics delivered a sequencing report that included the

nucleotide consensus sequences for each mutated TMT1A-expressing plasmid. Each nucleotide sequence was verified by sequencing to ensure the correct nucleotide substitutions were present and no other mutation was introduced. The consensus sequence for each mutant TMT1A construct was translated and then aligned using Clustal Omega alignment algorithm accessed at https://www.ebi.ac.uk/Tools/msa/clustalo/ [19]. See supplementary figure 3.8 for sequence alignments. After verifying that the correct substitutions were introduced in each mutant TMT1A encoding pCMV6 expression vector, the plasmids were propagated in heat-shocked Stellar cells (Takara, Mountain View CA, Ref: 636763, Lot: 2106487A).

3.2.5 *Overexpression of TMT1A mutants in HeLa cells*

HeLa cells (ATCC, Manassas VA, Ref: CCL-2™) were cultured in EMEM with 10% fetal bovine serum, 0.1% v/v penicillin-streptomycin and seeded into 12-well tissue culture plates at 250K cells/well (n=3). The cells were reverse transfected using Lipofectamine 3000 and P3000 reagent along with different pCMV expression vectors following the manufacturer's protocol. The final concentration of pCMV plasmid expression vector per treatment was 1000 ng/mL, the final concentration of Lipofectamine 3000 reagent was 0.5 µL/mL, and the final concentration of P3000 reagent was 1 µL/mL. Cells were incubated with media containing Lipofectamine reagents and either a TMT1A (Origene, Rockville MD, Ref: RC202601), TMT1B (Origene, Rockville MD, Ref: RC203838), empty control (Origene, Rockville MD, Ref: PS100001), or a mutant TMT1A expression vector for 36 h. The mutant expression vectors were F39L-TMT1A, F39L+F43L-TMT1A, F39L+F43L+Y47S-TMT1A, F43L+Y47S-TMT1A, and F199G-TMT1A. After 36 h, the cell media was removed, the cells washed with warm Dulbecco's Phosphate Buffered Saline (DPBS), and the media replaced with serum-free EMEM containing 125 µM TSL ±20 µM DCMB. Cells were incubated with the TMT substrate TSL and TMT1A inhibitor

DCMB for 24 h before the media was collected and analyzed for methylated metabolites by LC-MS/MS. Cell media (100 µL) was diluted with 100 µL of acetonitrile containing 20 µM TMSL-D7 internal standard (IS) and 1% acetic acid (v/v). The final IS concentration was 10 µM and the final acetic acid concentration was 0.5%. Samples were centrifuged at 16,000 ×g for 15 min. The supernatant was then transferred to a mass spec vial. Samples were analyzed with a Waters Xevo TQS mass spectrometer paired with a Waters ACQUITY LC using a 2.1 × 50-mm Waters CORTECS UPLC 1.6 µm C18 column and 1% acetic acid in water and 1% acetic acid in acetonitrile as solvents A and B, respectively. The elution of TMSL and TMSL-D7 was achieved with an isocratic gradient held at a 50:50 ratio of solvent A to solvent B. Flow rate was constant 0.5 mL/min. The transition states used to monitor for methyl metabolite 7a-thiomethylspironolactone (TMSL) and IS TMSL-D7 were 389.223 > 341.308 and 396.61 > 347.05 , respectively. TSL methylation was reported as the peak area ratio (PAR) of TMSL/TMSL-D7.

Protein overexpression was confirmed by western blot analysis. After incubation with the expression vector for 36 h, cells were washed with 1 mL of cold DPBS. The DPBS was removed, and each treatment was lysed in 150 µL of RIPA buffer containing 1X Halt protease inhibitor cocktail. The lysis was performed by adding 75 µL of lysis buffer to each well followed by shaking the plate at 625 rpm for 5 min with an orbital plate shaker. The volumes of each set of triplicate replicates were pooled and centrifuged at 4°C and 16,000 × g for 15 min. Protein separation by gel-electrophoresis and subsequent western blot analysis were performed on the lysed protein supernatant.

Western blot analysis was conducted with Invitrogen™ NuPAGE™ 4 to 12%, Bis-Tris, 1.0 mm, Mini Protein Gels in the XCell SureLock Mini-Cell Electrophoresis system using

PageRuler Plus Prestained Protein Ladder as a molecular weight marker. Gels were run at room temperature and a constant 200 V. For western blot analysis, proteins were transferred to nitrocellulose membranes using the iBlot™ Gel Transfer Device. Primary antibody incubations were conducted overnight at 4 °C at a 1:500 dilution with rabbit anti-FLAG (Cell Signaling, Danvers MA, Ref: 14793S, Lot: 5) and a 1:1000 dilution of anti-β-actin (Proteintech, Rosemont Il, Ref: 81115-1-RR, Lot: 23002494) primary antibodies. The incubation with the secondary antibody was performed at room temperature for 1 h with IRDye 680RD goat anti-rabbit secondary antibody at a 1:10,000 dilution (LiCor, Lincoln, NE, Ref: 926-68071, Lot: D11102-15). Western blots were visualized using an Odyssey gel scanner, and blot images were analyzed using Image Studio Version 4.0 software.

3.2.6 *Design of TMT1A FLAG or GFP-tagged bacterial expression vectors*

An open reading frame (ORF) for TMT1A-FLAG and another for TMT-GFP were produced using Twist Bioscience's ORF codon optimization tool . The GFP used was TurboGFP [20]. Both tags were on the *C*-terminus. The ORFs were designed for insertion into the pET-21(+) (Supplementary fig. 3.13 and 3.14) bacterial expression vector via ligation cloning using the restriction enzymes BamHI and HindIII. In addition to codon optimization for best translation efficiency in bacteria, two additional features were considered when the TMT1A ORFs were designed.

1. A ribosome binding site (RBS), essential for protein translation, was added immediately upstream of each ORF's start codon. The RBS leader sequence was copied from the pET-22b(+) expression vector. The leader sequence—

5' [BamHI]AATAATTTTGTTTAACTTTAAGAAGGAGATATACATATG 3'

—contained an RBS, highlighted yellow, a start codon, highlighted green, and a NdeI restriction site, red and bolded.

2. We also ensured that the TMT-FLAG and TMT-GFP ORFs did not contain internal restriction sites for BamHI, NdeI, HindIII, or XbaI. We wanted to maintain the option of moving the ORFs to another vector, such as the pCWori expression vector which has been successfully used for the expression of cytochrome P450s, which are also membrane associated, and one we considered as an option to improve the expression of TMT1A. The restriction sites we avoided are common to many expression vectors and could be used for restriction cloning these ORFs into different expression vectors if desired. Plasmid maps and translated protein sequences are included in supplementary figures 3.9 to 3.14.

Designed ORFs were synthesized by Twist Bioscience with relevant restriction sites BamHI and HindIII included on the 5' and 3' ends, respectively. The ORFs were then restriction cloned into a pET-21(+) expression vector.

3.2.7 *Isolation of TMT1A spheroplasts*

Competent cells NiCo21(DE3) (New England Biolabs, Ipswich MA, Ref: C2529H, Lot: 10183698), a modified strain of BL21(DE3) cells, similar to LOBSTR cells that we used for. TMT1 expression, were transformed using heat shock with TMT1A-FLAG or TMT1A-GFP pET-21(+) expression vectors. Transformed *E. coli* cells were cultured in 5 mL culture tubes overnight in an orbital shaker at 250 rpm, 37°C, and in the presence of 100 µg/mL ampicillin. Overnight cultures were added to ampicillin-containing terrific broth (TB) expression media at a ratio of 1:100. Cells grew for an additional 24 h before being harvested. Cells were harvested by centrifuging at 4,500 ×g for 15 min at 4°C. The clear supernatant was decanted, and the wet weight of the pelleted cells was measured. Sonication buffer (2 mL of100 mM KPi, 6 mM

magnesium acetate 20% (w/v) glycerol, 1X Halt Protease Inhibitor Cocktail) was added for every gram of the wet weight of the pelleted cells. Cells were transferred to 50 mL Falcon tubes and sonicated on ice to prevent overheating. The sonication cycle was to sonicate for 20-second sonication at 30% power, followed by a 30-second cooling on ice. After three sonication cycles, the cell homogenate was centrifuged at 10,000 × g for 20 min to pellet cell debris. The supernatant was decanted into ultracentrifuge tubes and centrifuged at 180,000 × g for 70 min. The supernatant was decanted, and the pelleted spheroplasts were resuspended in a minimal volume of TES buffer (50 mM Tris Acetate, 250 mM sucrose, 0.25 mM EDTA, pH 7.6) so that the final protein concentration was between 10-20 mg/mL by the bicinchoninic acid (BCA) method. The spheroplasts containing TMT1A-FLAG or TMT1A-GFP were then aliquoted across 1.5 mL Eppendorf tubes and flash-frozen in an ethanol dry ice bath before being stored long-term at -80°C.

We observed that the TMT1A-GFP expression and spheroplast production succeeded owing to a green fluorescence visible when the spheroplasts were exposed to ultraviolet light supplementary figure 3.15. The presence of TMT1A-FLAG in spheroplasts was confirmed by western blot analysis. Protein separation by gel-electrophoresis, and subsequent western blot analysis were performed as described in **section 3.2.5**. The primary antibody incubation lasted overnight with an anti-FLAG (Cell Signaling, Danvers MA, Ref: 14793S, Lot: 5) antibody.

3.2.8 *In vitro TSL methylation using TMT1A spheroplasts*

To test methyltransferase activity of TMT1A spheroplasts at two different protein concentrations, TMT1A-FLAG and TMT1A-GFP tagged spheroplasts were diluted to 2.14 and 0.54 mg/mL with KPi reaction buffer (50 mM KPi, pH 7.4, 10% glycerol). A fraction of each diluted protein sample was boiled for 10 min. Diluted protein sample (140 µL) was added to 1

mL cluster tubes (Marsh Tubes, FisherSci Cat No. 07-200-318). TSL, dissolved in 9:1 acetonitrile:water, and DCMB, dissolved in KPi reaction buffer, were added to the diluted protein samples. For samples not treated with DCMB, KPi was added instead as a vehicle control. The reaction was initiated with the addition of SAM. The final reaction volume was 150 µL. The final TSL concentration was 200 µM, the final DCMB concentration was 200 µM, and the final SAM concentration was 1 mM. The final spheroplast protein concentration was 2 mg/mL and 0.5 mg/mL. Cluster tubes were vortexed after initiating and incubated at 37°C for 1.5 h in a custom-designed machined aluminum heat block with heat maintained at 37°C by a FisherSci Isotemp heater (Supplementary fig. 3.16). The cluster tubes allowed initiation and quenching steps to be performed with a multichannel pipette and the machined aluminum heat block provided consistent temperature throughout the incubation. This incubation approach was used for all future spheroplasts activity assay work. The reaction was quenched by adding 100 µL of the protein reaction mixture to 100 µL of ice cold acetonitrile containing 20 µM TMSL-D7 internal standard (IS) and 1% acetic acid (v/v). The final IS concentration was 10 µM and the final acetic acid concentration was 0.5%. Samples were centrifuged at 16,000 × g for 15 min to precipitate proteins and salts. The supernatant was then transferred to a mass spec vial.

Samples were analyzed using a Waters Xevo TQS mass spectrometer paired with a Waters ACQUITY LC using a 2.1 × 50-mm Waters CORTECS UPLC 1.6 µm C18 column and 1% acetic acid in water and 1% acetic acid in acetonitrile as solvents A and B, respectively. Elution of TMSL and TMSL-D7 was achieved with an isocratic gradient held at 50:50 ratio of solvent A to solvent B. Flow rate was constant 0.5 mL/min. The transition states used to monitor for methyl metabolite 7α-thiomethylspironolactone (TMSL) and IS TMSL-D7 were 389.223 >

341.308 and 396.61 > 347.05 , respectively. TSL methylation was reported as the peak area ratio (PAR) of TMSL/TMSL-D7.

3.2.9 *In vitro Michaelis-Menten kinetics using TMT1A-FLAG spheroplasts*

To determine protein linearity, TMT1A-FLAG spheroplasts were diluted and incubated with TSL and SAM, similar to what is described in **section 3.2.8**. Final protein concentrations were 0.125, 0.25, 0.5, 1, and 2 mg/mL. The boiled control was performed at 2 mg/mL protein content and was prepped as described in **section 3.2.8**. The final TSL concentration was 100 µM, the final SAM concentration was 1 mM, and the final reaction volume was 150 µM. After the reaction was initiated by SAM addition, cluster tubes (Marsh tubes, FisherSci Cat No. 07-200-318) containing the protein reaction mixtures were vortexed and then incubated for 1 hour at 37°C. Samples were quenched and analyzed by mass spec as described in the procedure in **section 3.2.8**.

To determine time linearity, TMT1A-FLAG spheroplasts were diluted to 0.5 mg/mL and incubated with TSL and SAM similar to the procedure described in **section 3.2.8**. The final TSL concentration was 100 µM, and the final SAM concentration was 1 mM. After the reaction was initiated by SAM, cluster tubes containing the protein reaction mixtures were vortexed and then incubated for different durations. Samples were incubated for 0.25, 0.5, 1, and 2 h at 37°C. The boiled control was incubated for 2 h. As samples were quenched, **section 3.2.8**, they were immediately stored at 4°C until all samples were quenched. Samples were then analyzed by mass spec as described in **section 3.2.8**.

To determine Michaelis-Menten kinetics, TSL was added to a final concentration of 1, 5, 10, 25, 50, and 100 µM. The final TMT-Flag spheroplasts protein concentration was 0.5 mg/mL, and the reaction was initiated by SAM added to a final concentration of 1 mM. A boil control was

included and was incubated with the highest concentration of TSL. After the reaction was initiated by SAM, cluster tubes containing the protein reaction mixtures were vortexed and then incubated for 45 min at 37°C. Samples were quenched and analyzed by mass spec identically to the procedure described in **section 3.2.8**.

3.2.10 *In vitro inhibition kinetics using TMT1A spheroplasts*

For IC_{50} determination, TMT1A-FLAG spheroplasts, diluted to 0.5 mg/mL, were incubated with 50 µM TSL and different concentrations of DCMB. Final DCMB concentrations were 0.001, 0.01, 0.1, 0.5, 1, 10, 50, 100, and 200 µM. The final concentration of SAM was 1 mM. Sample preparation was similar to the procedure described in **section 3.2.8**. After the reaction was initiated by SAM, cluster tubes (Marsh Tubes, FisherSci Cat No. 07-200-318) containing the protein reaction mixtures were vortexed and then incubated for 45 min at 37°C. Samples were quenched and analyzed by mass spec similar to the procedure described in **section 3.2.8**.

For TSL and DCMB single time point inhibition, TMT1A-FLAG spheroplasts, diluted to 0.5 mg/mL, were incubated with different concentrations of TSL and DCMB. Final TSL concentrations were 1, 10, 25, and 50 µM. Final DCMB concentrations were 0, 0.5, 1, 10, and 50 µM. Sample replicates for all combinations of TSL and DCMB concentrations were generated to produce a 4 (TSL) × 5 (DCMB) inhibition matrix. The final concentration of SAM was 1 mM. Sample preparation was similar to the procedure described in **section 3.2.8**. After the reaction was initiated by SAM, cluster tubes containing the protein reaction mixtures were vortexed and then incubated for 45 min at 37°C. Samples were quenched and analyzed by mass spec similar to the procedure described in **section 3.2.8**.

3.2.11 *In vitro inhibition screen using TMT1A spheroplasts*

TMT1A-FLAG spheroplasts were diluted and incubated with TSL and SAM, similar to the procedure described in **section 3.2.8**. The final protein concentration was 0.5 mg/mL. The boiled control was prepped as described in **section 3.2.8**. The diluted proteins were treated with test compounds or DMSO as a vehicle control. Test compounds were: 4-Nitrobenzenethiol (4-NBT), 6-Mercaptopurine (6-MP), Ibuprofen, 2,4-Dichloro-6-methylbenzylamine (DC6MB), Caffeine, 2-amino-1-phenylethanol (2-APE), 1-(2,4-dichlorophenyl)ethylamine (2,4-DCMB), DCMB 2,3-dichloro-α-methylbenzylamine (DCMB), S-methylglutathione (S-Me-GSH), and reduced glutathione (GSH). The final concentration for each test compound was 100 µM. The final TSL concentration was 100 µM, and the final SAM concentration was 1 mM. After the reaction was initiated with SAM, cluster tubes (Marsh Tubes, FisherSci Cat No. 07-200-318) containing the protein reaction mixtures were vortexed and then incubated for 45 min at 37°C. Samples were quenched and analyzed by mass spec as described in **section 3.2.8**.

3.2.12 *Expression and purification of TPMT*

Wildtype TPMT was cloned in *E. coli* using the pET-22b(+) expression plasmid. The pET-22b(+) expression vector adds a pelB signal peptide to the *N* terminus of the inserted ORF and a 6×histidine-tag to the *C*-terminus. The wild-type TPMT ORF was codon-optimized using Twist Bioscience's ORF codon optimization tool. The ORF was synthesized by Twist Bioscience as a single DNA fragment. The ORF was inserted into the plasmid using NcoI and NotI restriction sites general molecular biology techniques. The forward primer for insertion of the TPMT ORF was 5'GCGATGGCCATGGATGGAACCCGTACCTCTCTT 3', and the reverse primer was 5' TCGAGTGCGGCCGCTTTTTCTGTTAACAGATACAGCTTCT 3'.

Expression plasmids were propagated using heat-shocked Stellar cells (Takara, Mountain View, CA). Plasmids, validated by whole plasmid sequencing through Eurofins Genomics (Louisville, KY), were used to transform competent LOBSTR-BL21(DE3) *E. coli* (Kerafast, Winston-Salem, NC) via heat shock. Plasmid maps and translated protein sequences are included in supplementary figures 3.17 and 3.18. Unless otherwise noted, *E. coli* cells were cultured in an orbital shaker at 250 rpm, 37 °C, supplemented with 100 µg/mL ampicillin.

To express recombinant protein in LOBSTR-BL21 (DE3) cells, overnight cultures were added to ampicillin-containing terrific broth (TB) expression media at a ratio of 1:100. The cells were grown for 24 h. Cells were harvested by centrifuging at 4,500 × g for 15 min at 4°C. The resulting cell pellet was stored at -80°C until future processing. Frozen cell pellets were thawed on ice in a 4 °C cold cabinet prior to resuspension in lysis buffer (50 mM KPi pH 7.0, 20% glycerol, 150 mM NaCl, 10 mM CHAPS, EDTA-free 1X Halt Protease Inhibitor Cocktail) supplemented with 100 µg/mL lysozyme (Sigma Aldrich, St. Louis, MO, Ref: L-6876, Lot: 65H7025). The lysate was placed on a rocker at 4 °C until it became extremely viscous, then 100 µg/mL DNA Nuclease I (Sigma Aldrich, St. Louis, MO, Ref: DN25-100MG, Lot: SLCB6648) was added, and the lysate was placed on a rocker at 4 °C until it was no longer viscous. The lysate was then centrifuged at 48,000 × g for 30 min at 4 °C, and the resulting supernatant was retained for subsequent purification steps.

The purification was performed using a vertical column hand-packed with 4 mL of His60 Ni Superflow Resin. The column was equilibrated with lysis buffer. Cell lysate supernatant was added to the column containing nickel resin, and it was recirculated across the column by a peristaltic pump overnight at 0.5 ml/min. The column was washed with 50 column volumes of His60 Ni wash I (50 mM KPi pH 7.0, 20% glycerol, 10 mM CHAPS, 300 mM NaCl, 50 mM

imidazole). The column was then washed with 50 column volumes of His60 Ni wash II (50 mM KPi pH 7.0, 20% glycerol, 10 mM CHAPS, 150 mM NaCl, 50 mM imidazole). The protein was eluted from the column with 2 column volumes of His60 Ni elution buffer (50 mM KPi pH 7.0, 20% glycerol, 1 mM CHAPS, 150 mM NaCl, 250 mM imidazole).

The purified protein was placed in a dialysis cassette with a 10 kDa molecular weight cutoff and immersed in dialysis buffer (50 mM KPi pH 7.0, 20% glycerol). The volume of dialysis buffer was 100× the volume of eluted TPMT. The protein was left in the dialysis buffer at 4°C overnight with gentle agitation with a magnetic stir bar. The next day, the buffer was exchanged for fresh dialysis buffer, and the protein was incubated for another 4 h. This was repeated once more before the protein was transferred from the dialysis cassette to MilliporeSigma Amicon Ultra-15 10K molecule weight cutoff centrifugal filter units. The protein was concentrated, and the final protein concentration was determined by A280 measurement. Purified protein stocks were normalized to 1 mg/mL and stored at -80°C for future use. During the entire purification process, caution was exercised to ensure that the protein was kept at 4°C all the time.

3.2.13 *Purity analysis of TPMT*

All SDS-PAGE Coomassie stained or western blot analysis were conducted with Invitrogen™ NuPAGE™ 4 to 12%, Bis-Tris, 1.0 mm, Mini Protein Gels in the XCell SureLock Mini-Cell Electrophoresis system using PageRuler Plus Prestained Protein Ladder as a molecular weight marker. Gels were run at room temperature, and a constant 200 V. Total protein purity was determined with GelCode™ Blue Stain Reagent, a colloidal Coomassie dye. For western blot analysis, proteins were transferred to nitrocellulose membranes using the iBlot™ Gel Transfer Device. Primary antibody incubations were conducted overnight at 4 °C at a 1:500 dilution with rabbit anti-TPMT (Proteintech, Rosemont Il, Ref: 10682-1-AP, Lot: 00065222). The secondary

incubation was performed at room temperature for 1 h with IRDye 680RD goat anti-rabbit secondary antibody at a 1:10,000 dilution (LiCor, Lincoln, NE, Ref: 926-68071, Lot: D11102-15). Western blots and Coomassie-stained gels were visualized with an Odyssey gel scanner, and blot images were analyzed using Image Studio Version 4.0 software.

To compare the activity of TMT1A and TPMT towards alkyl thiol methylation, TMT1A-FLAG spheroplasts and purified TPMT were incubated with TSL and SAM for 1.5 h. The final protein concentration was 0.5 mg/mL for both TMT1A spheroplasts and TPMT. Final TSL concentration was 200 µM, and the final SAM concentration was 1 mM. The activity assay and LC-MS/MS were performed similar to the procedure that was described in **section 3.2.8**.

3.2.14 *In vitro absorbance assays using recombinant purified TPMT*

To test the thiopurine methyltransferase activity of TPMT, recombinant purified TPMT was diluted to 0.27 mg/mL with KPi reaction buffer (50 mM KPi, pH 7.4, 10% glycerol). A fraction of the diluted protein sample was boiled for 10 min. Diluted protein sample, 95 µL, was deposited in the appropriate wells of a 96-well Corning, black-walled, clear bottom, half area plate (Ref: 07200844). 6-mercaptopurine (6-MP) or 4-nitrobenzenethiol (4-NBT) were added to the appropriate wells containing diluted TPMT. Both 6-MP and 4-NBT were dissolved in DMSO. 4-NBT in DMSO is a beautiful red color at 20 mM. For background “vehicle” control wells, DMSO was added instead. Finally, SAM was added to initiate the reaction. For no SAM control wells, water was added instead of SAM. The final reaction volume was 100 µL, and the final protein centration was 0.25 mg/mL. The final concentration of 6-MP was 100 µM, the final concentration of 4-NBT was 250 µM, and the final concentration of SAM was 1 mM. After initiating the reaction, the 96-well plate was immediately placed in a Tecan Spark Multi-Mode

Microplate Reader, and the samples were scanned from 295 to 550 nm in 1 nm steps for 60 minutes. The plate's temperature was held at 37°C for the duration of this assay.

3.2.15 *Processing TPMT absorbance assay results*

The way the absorbance assay data was processed—discussed below—was based on the analysis method described by Russell *et al.* for a plate-reader-based CO binding assay (see figure 6 in that article) [21]. For each absorbance scan in time, the averaged substrate scan was subtracted from the averaged vehicle control scan. For each scan, the values for each wavelength after subtraction were referred to as Δ(X nm) where X is wavelength. For incubations with 6-MP, the Δ(375 nm) through Δ(400 nm) were averaged. For incubations with 4-NBT, the Δ(525 nm) through Δ(550 nm) were averaged. The average of either of these regions was referred to as the Y-shift. These regions were used to calculate a Y-shift value because each curve was flat in this region. The Y-shift was subtracted from the Δ for each wavelength scanned, this shifted the baseline in each scan close to zero. After the baseline for each scan is moved to zero by subtracting the Y-shift value, each scan can be plotted. These values were referred to as Abs(X nm), where X is wavelength. Finally, to plot absorbance over time, the Abs(X nm) value for each scan was plotted with the scan time as the value on the X-axis.

3.2.16 *Data analysis*

Unless noted otherwise, all experiments were conducted in triplicates and all data is reported as the mean ± standard deviation (S.D.). The ProteinsPlus server was accessed January 2022-December 2023. Statistical significance was determined by a two-tailed unpaired Student's t-test with a threshold P-value of 0.05. A two-tailed Spearman's non-parametric correlation was computed to assess the relationship between two variables with a threshold P value of 0.05. Kinetic parameter K_m (for TSL), K_i (for TSL and SAM), and IC_{50} (for DCMB) values were

calculated using GraphPad Prism, version 9.4.1 for Windows (GraphPad Software, La Jolla, CA). The K_i values were calculated using a partial inhibition model [22] and the following equation which can be pasted directly into prism as a user defined equation under the explicit equation field:

$$Y=Vmax*((X/Km) + (B*X*I)/(Km*Ki))/(1+(I/Ki)+(X/Km)+((X*I)/(Km*Ki)))$$

Where Y is the response, X is substrate concentration, I is inhibitor concentration, Ki is shared and greater than 0, B—or the β, the relative activity of the ESI complex—is shared and greater than 0, Km is constant and equal to Michaelis constant for the substrate, and Vmax is shared and must be greater than 0.

3.3 RESULTS

3.3.1 *Kinetics analysis of TMT1A inhibition by DCMB*

TMT1A is inhibited by DCMB but the activity of its close homolog TMT1B is not affected (Chapter 2, **section 2.3.4**, [1]). By LC-MS/MS analysis, we determined that DCMB inhibits purified N-GST-TMT1A in a concentration-dependent manner. For single time point TSL curves, increasing concentrations of DCMB caused V_{max} to decrease and K_m to increase. This was consistent with a mixed or noncompetitive mechanism of inhibition, but there was still appreciable methylation with DCMB levels 10 to 50× greater than the IC_{50} for DCMB, and because of this, the residual activity at these high concentrations of DCMB could not be fitted to a simple mixed or noncompetitive model. To account for the residual activity at high concentrations of DCMB, the inhibition curves with altered TSL and DCMB levels were fitted to a partial inhibition model (Figure 3.1, [22]). The K_m value was constrained to 40 µM, which we previously determined for TSL metabolized by purified recombinant TMT1A (Figure 2.4, [1]) and no cooperativity was assumed. The resulting K_i from this model fit was 0.9 ±0.5 µM and the

β value was 0.14 ±0.032 (Figure 3.1.A). Interestingly, the single time point SAM curves responded to DCMB similarly to the single time point TSL curves, with increasing concentrations of DCMB causing V_{max} to decrease and K_m to increase, and at DCMB levels 10 to 50× greater than the IC_{50} for DCMB, there was still methyl transfer (Figure 3.1.B). The inhibition curves with altered SAM and DCMB levels were fitted to the same partial inhibition model, but the K_m was constrained to 50 μM, consistent with the value we previously determined (Figure 2.4, [1]). The resulting K_i from this inhibition model fit with respect to SAM was 2.3 ±1.4 μM, and the β value was 0.18 ±0.06.

3.3.2 *Structural analysis of TMT1A and TMT1B*

The structures of TMT1A and TMT1B were analyzed using computational approaches. A central binding pocket was identified within the structure of TMT1A and of TMT1B using DoGSiteScorer, and the volume and location of each enzyme's central binding pocket was similar (1360 $Å^3$ and 1344 $Å^3$, respectively). TMT1A's central binding pocket forms an inverted T-shape (Figure 3.2.A), while the binding pocket in TMT1B had slightly less volume in the lower leftmost quadrant making it appear more spherical (Figure 3.2.B). When the AlphaFold homology models of TMT1A or TMT1B were aligned with the crystal structure of COMT (4XUC, 1.80 Å), SAM was in close proximity to the GXGXG SAM binding region in TMT1A and TMT1B, the SAM ribose was located near each enzyme's conserved acidic residue, Asp-98 (Figure 3.2.C), and the aligned SAM filled the volume of the lower region of TMT1A and TMT1B's central binding pocket (Figure 3.2.D). The binding orientation of SAM is highly conserved, so this alignment is a good approximation of where SAM would bind in TMT1A and TMT1B.

Captopril and DCMB were docked into the AlphaFold homology model of TMT1A using the JAMDA protein ligand docking algorithm [16]. The top ten poses of both the substrate (Figure 3.3.A) and the inhibitor (Figure 3.3.B) were located immediately above the aligned SAM's labile methyl group. Based on these docking results, we identified the middle top region of each enzyme's binding pocket as the substrate binding region (Figure 3.2.D).

DoGSiteScorer generated a list of residues that formed the boundary of each central binding pocket identified for TMT1A and TMT1B. Each binding pocket was composed of 60 residues, 42 identical between TMT1A and TMT1B, 4 homologous, and 13 different (Figure 3.4). Most of the residues that were different between TMT1A and TMT1B were localized to the substrate binding region. Of note, three residues in TMT1A were located along each enzyme's first α-helix—Phe-39, Phe-43, and Tyr-47. This helix defines the top boundary of the substrate binding region. A fourth residue was located in a disordered region paralleling the first α-helix—Phe-199. These four different residues were noteworthy because they surround the area that the top 10 poses of DCMB inhabited when docked into TMT1A (Figure 3.4.A.II). In TMT1A these residues are aromatic, while in TMT1B they are aliphatic (Figure 3.4.A.II and 3.4.B.II). DCMB is aromatic, so it was suspected that it could form π-π stacking interactions with TMT1A's aromatic residues. Because TMT1A is inhibited by DCMB while TMT1B is not, we hypothesized that these four different residues contribute to this binding difference.

Both TMT1A and TMT1B contain nine cysteine residues. Seven of these are conserved, while two are located in different positions along each enzyme's sequence. During our analysis of the TMT1A and TMT1B homology models, cysteine-residue-pairs with thiol sulfurs within 4 Å were considered capable of forming a disulfide bond. (The typical cutoff for disulfide bonds is 3 Å, but because the analysis was performed on homology models, a more permissive cutoff was

used [23]). Only two pairs of cysteine residues met this criterion: Cys-79/Cys-96 and Cys-148/Cys-202 (Figure 3.5).

Dr. Maldonato, in his dissertation work, performed a metal ion screen to determine if purified recombinant TMT1B's activity is enhanced with metal ions like magnesium and nickel. There was no significant effect on enzyme activity [2] with various metals, indicating that it is unlikely that TMT1B utilizes metal ions to facilitate methyl transfer similar to COMT. On the other hand, we identified two cysteine residues in a region near where the substrate thiol is suspected to line up near the labile SAM methyl. Arsenic 3 methyltransferase (AS3MT) has four cysteine residues that are involved in the arsenic methyl transfer reaction [6-10]. TMT1A and TMT1B have two conserved cysteine residues located within 10 Å of the sulfur of the aligned SAM—Cys-148 and Cys-202. The AlphaFold homology models of TMT1A and TMT1B were aligned (Figure 3.6.A) with a crystal structure of *Cyanidioschyzon* AS3MT (6CX6, 2.84 Å,[6]) since no human AS3MT structure has been reported. Interestingly, Cys-148 and Cys-202 of TMT1A and TMT1B are located in the same vicinity as the AS3MT cysteines that are involved in arsenic transfer (Figure 3.6.B). It is possible that these cysteine residues may be involved in TMT1 methyl transfer reactions.

Finally, we wanted to explore how TMT1A and TMT1B bind their cofactor, SAM. Crystal structures of COMT (4XUC, 1.80 Å), INMT (2A14, 1.7 Å), NNMT (7BKG, 2.33 Å), PNMT (2AN3, 2.20 Å), and HNMT (2AOT, 1.9 Å) were downloaded as PDB files from Uniprot entries. Each crystal structure's PDB file was uploaded to ProteinsPlus and the SAM or SAH binding interactions were analyzed with PoseView, an application that creates two-dimensional diagrams of proteins complexed with small molecules [18]. PoseView identified important binding interactions between SAM or SAH and each small molecule methyltransferase (Supplementary

fig. 3.1 to 3.5). The residues identified by PoseView were highlighted on each methyltransferase's crystal structure using the protein structure visualization software, Pymol. The highlighted residues and the SAM or SAH in each crystal structure were extracted and analyzed independent of the entire structure (Supplementary fig. 3.6). Using the alignment function in Pymol, the residue and ligand substructures were all aligned with TMT1A's and TMT1B's homology models and the TMT1A residues that overlapped with the other methyltransferases' residues identified by PoseView were extracted and included in our SAM and SAH binding site analysis (Supplementary fig. 3.7). We identified six conserved binding interactions between the small molecule methyltransferases and SAM/SAH (Figure 3.7). An acidic residue at the end of the second β-strand that interacts with SAM or SAH's ribose hydroxyls is a known binding motif and is shared by all small molecule methyltransferases (Figure 3.7.A, [11]). Other binding motifs identified were: two hydrophobic regions across from each other with the SAM or SAH's adenosyl sandwiched in between (Figure 3.7.B and 3.7.C); an aromatic region adjacent to the adenosyl (Figure 3.7.D); a polar residue that formed a hydrogen bond with SAM or SAH's carboxyl group (Figure 3.7.E); and a polar residue that formed a hydrogen bond with SAM or SAH's adenosyl amine (Figure 3.7.E). TMT1A and TMT1B had residues that aligned well with each binding region we identified. The only region where TMT1A and TMT1B had no residue that could participate in the same binding interaction as the other methyltransferases was the aromatic region (Figure 3.7.D). TMT1A and TMT1B did not have an aromatic residue in this region. There was a final binding interaction that was specific to the *N*-methyltransferase family (INMT/NNMT/PNMT). Each enzyme in the *N*-methyltransferase family had three tyrosine residues that formed hydrogen bonding interactions

with SAM or SAH's carboxyl group. This unique binding interaction we coined the term "tyrosine cage" (Figure 3.7.F).

3.3.3 *Mutagenesis of TMT1A and identification of key residues necessary for inhibition by DCMB*

To test our hypothesis that the aromatic residues F39, F43, and F199 that face into the putative substrate and DCMB binding site contribute to DCMB inhibition of TMT1A, HeLa cells were incubated with pCMV expression vectors encoding FLAG-tagged TMT1A mutants, FLAG-tagged wild type TMT1A (WT-TMT1A), FLAG-tagged wild type TMT1B (WT-TMT1B), or an empty insert to act as a negative control. The mutants included in this analysis were F39L-TMT1A, Y47S-TMT1A, F39L+F43L-TMT1A, F43L+Y47S-TMT1A, F39L+F43L+Y47S-TMT1A, and F199G-TMT1A. Three pCMV vector plasmids—WT-TMT1A, F199G-TMT1A, and F39L+F43L+Y47S-TMT1A—were purified in two separate batches and included as biological replicates to increase confidence.

Protein expression was confirmed by protein normalized anti-FLAG western blotting. An anti-β-actin antibody was included as a co-stain for loading control. FLAG-tagged WT-TMT1A, WT-TMT1B, and all mutant TMT1A were visible at the correct molecular weights (Figure 3.8). No FLAG-tagged protein was visible in the empty control vector-treated cells. Cells expressing FLAG-tagged TMT1A or FLAG-tagged TMT1B, including all mutants, had significantly increased TSL methylation compared with empty vector control-treated cells, determined by LC-MS/MS (Figure 3.9). With the addition of DCMB, only WT-TMT1A, F43L-TMT1A, F39L+F43L-TMT1A, and F199G-TMT1A expressing cells displayed a significant reduction in TSL methylation compared to cells not treated with DCMB. Although F199G-TMT1A activity

was less effected by DCMB than WT-TMT1A. WT-TMT1B and TMT1A mutants that contained the missense F47S mutation were unaffected by the presence of DCMB.

3.3.4 *Expression and purification of TPMT*

To confirm that TSL methylation is unique to TMT1A and TMT1B, we inserted a TPMT open reading frame (ORF) into a pET-22b(+) expression vector and expressed the protein in *E. coli*. The pET-22b(+) expression vector adds a pelB periplasmic translocation sequence to the *N* terminus of the inserted ORF and a 6× histidine-tag to the *C*-terminus. The pelB signal peptide is removed as the protein is translocated to the periplasm [24]. The recombinant protein TPMT-6xHis has a molecular weight of 29.3 kDa. We confirmed the successful purification of TPMT with a visible protein band at ~30 kDa by SDS-PAGE Coomassie stain (Figure 3.10.A). A band at ~30 kDa is also visible on a western blot using an anti-TPMT-antibody (Figure 3.10.B). Two similar molecular weight bands were not detected during SDS-PAGE analysis, which may indicate that the majority of TPMT that was purified had the pelB signal sequence removed during bacterial expression. The recombinant purified TPMT was purified to homogeneity.

3.3.5 *Validation of TPMT activity*

The alkyl thiol methylation activity of purified TPMT was compared with TMT1A. Purified TPMT and TMT1A spheroplasts were protein normalized and incubated with TSL and SAM. Only TMT1A-FLAG spheroplasts methylated TSL (Figure 3.11). 6-mercaptopurine (6-MP) (Figure 3.12), a known substrate of TPMT [25], has an absorption maximum at ~321 nm. We discovered that when 6-MP and SAM were incubated with purified TPMT, 6-MP's absorption maximum decreased with time. This change in absorption was caused by loss of parent substrate through the methylation of 6-MP to form 6-methylmercaptopurine (6-MMP), which does not absorb at 321 nm. We confirmed that purified TPMT was active by monitoring for 6-MP

disappearance over time with a plate reader scanning from 285 nm to 375 nm for 45 min (Figure 3.13.A.I and A.II). During the TPMT activity assay with 6-MP, there was an increase in absorbance between 285 and 295 nm, this absorbance increase was attributed to the formation of 6-MMP (Figure 3.13.A.III). By monitoring absorbance changes at 321 nm and 290 nm, we were able to record 6-MP disappearance and 6-MMP appearance in real time during a TPMT and 6-MP methyl transfer activity assay (Figure 3.13.A).

We discovered that another TPMT substrate, 4-nitrobenzenethiol (4-NBT) (Figure 3.12), has an altered absorption maximum when methylated. 4-NBT absorbs at 411 nm but once methylated absorbs at 350 nm. When 4-NBT and SAM are incubated with purified TPMT, 4-NBT's absorption maximum at 411 nm decreased with time, and 4-nitrobenzenethiomethyl's (4-NBTM) absorption maximum increased at 350 nm (Figure 3.13.B.I, B.II, and B.III).

We performed both 6-MP and 4-NBT absorbance assays with TMT1A-FLAG spheroplasts and were unable to show any change in absorbance for both compounds (data not shown).

3.3.6 *Expression and isolation of TMT1A spheroplasts*

TMT1A-FLAG and TMT1A-GFP were expressed in bacteria. TMT1A is a transmembrane protein and inserts into the inner membrane of *E. coli* during expression. The isolated *E. coli* inner membrane fraction is called spheroplasts [13]. TMT1A-FLAG and TMT1A-GFP containing spheroplasts were isolated from TMT1A expressing *E. coli*. The presence of TMT1A-FLAG in spheroplasts isolated from TMT1A-FLAG expressing bacteria was confirmed by western blot analysis (Figure 3.14.A). The recombinant TMT1A-FLAG has a molecular weight of 31.9 kDa. A band at ~32 kDa was visible on a western blot using an anti-FLAG-antibody (Figure 3.14.A.I). A band at ~55 kDa was also visible but remains unidentified (Figure 3.14.A.II). The presence of TMT1A-GFP in spheroplasts isolated from TMT1A-GFP expressing

bacteria was confirmed by observing a green florescent glow when the spheroplasts were exposed to ultraviolet light (Supplementary fig. 3.15).

3.3.7 *Validation of TMT1A spheroplast Activity*

By LC-MS/MS analysis, isolated TMT1A-FLAG and TMT1A-GFP spheroplasts both methylated TSL and were inhibited by DCMB (Figure 3.14.B). Purified TPMT, normalized to the same protein content as TMT1A-FLAG and TMT1A-GFP spheroplasts, did not methylate TSL (Figure 3.14.B). TMT-FLAG spheroplasts had significantly higher TSL methylation activity than TMT1A-GFP spheroplasts, therefore TMT1A-FLAG spheroplasts were used for all subsequent spheroplast characterization.

TMT1A-FLAG spheroplasts methylated TSL in a time- and protein-dependent fashion (Figure 3.15.A and 3.15.B). We determined the K_m value for TSL by measuring the formation of TSL for TMT1A-FLAG spheroplasts by LC-MS/MS (Figure 3.16). The K_m value for TSL methylation by TMT1A-FLAG spheroplasts was 6.2 ±3.8 μM, lower than the K_m value of 39.4 μM determined for purified recombinant TMT1A (Chapter 2, **section 2.3.6**). DCMB potently inhibits TMT1A-FLAG spheroplasts similar to purified TMT1A. An IC_{50} of 1.0 ±0.2 μM was determined for DCMB and TMT1A-FLAG spheroplasts using TSL as a substrate (Figure 3.17). This value was very similar to the IC_{50} value of 1.2 μM determined for purified TMT1A (Chapter 2, **section 2.3.4**). Finally, consistent with purified TMT1A, DCMB inhibited TMT1A-FLAG spheroplasts in a concentration-dependent manner and exhibited a partial inhibition mechanism with respect to TSL, with a K_i of 0.7 ±0.1 μM and a β value of 0.06 ±0.02 (Figure 3.18). The K_m was constrained to 6 μM, the value determined for TSL and TMT1A spheroplasts.

3.3.8 *Inhibition panel screen using TMT1A spheroplasts*

In the previous section (**section 3.3.7**) we confirmed that TMT1A-FLAG spheroplasts have similar characteristics as purified TMT1A including similar TSL methylation activity and similar inhibition by DCMB. Next, we incubated TMT1A-FLAG spheroplasts with TSL, SAM, and various test compounds to confirm that spheroplasts can be used to screen compounds for TMT1A inhibition and for SAR analysis of DCMB inhibition. The test compounds used in this screen were: 4-Nitrobenzenethiol (4-NBT), 6-Mercaptopurine (6-MP), Ibuprofen, 2,4-Dichloro-6-methylbenzylamine (DC6MB), Caffeine, 2-amino-1-phenylethanol (2-APE), 1-(2,4-dichlorophenyl)ethylamine (2,4-DCMB), DCMB 2,3-dichloro-α-methylbenzylamine (DCMB), S-methylglutathione (S-Me-GSH), and reduced glutathione (GSH). The final concentration of each test compound was 100 µM. Of the compounds tested, 4-NBT, 6-MP, DC-6-MB, 2,4-DCMB, and DCMB significantly inhibited TMT1A-FLAG (Figure 3.19).

3.4 DISCUSSION

The key finding in this research is that we identified the binding site residue that is responsible for DCMB mediated inhibition of TMT1A (Figure 3.9). We also confirmed that the other human thiol *S*-methyltransferase, TPMT, does not methylate alkyl thiols. Similarly, the TMT1 family members do not methylate thiols conjugated to ring systems with electron withdrawing properties (Figure 3.11). We also developed a bacterial expression method to produce large quantities of TMT1A by isolating TMT1A-containing spheroplasts. These TMT1A spheroplasts were suitable for biochemical characterization and were used to conduct a SAR analysis of DCMB congeners as potential inhibitors of TMT1A (Figure 3.14 and 3.19). Finally, using computational approaches including docking and protein structural alignment, we identified key

residues in TMT1A and TMT1B that participate in binding SAM (Figure 3.7 and Supplementary fig. 3.7).

Glauser *et al.* determined that microsomal alkyl thiol methyltransferase (TMT) is inhibited by DCMB, a compound that was originally designed to be an inhibitor of phenylethanolamine N-methyltransferase (PNMT). DCMB exhibited mixed type inhibition of TMT with a K_i value, of 1.1 μM towards SAM, and 0.29 μM towards β-mercaptoethanol [3]. In close agreement with literature findings for TMT, DCMB inhibited recombinant purified *N*-GST-TMT1A in a concentration dependent manner and exhibited a mechanism of partial inhibition with respect to both TSL and SAM. The K_i values were 0.9 and 2.3 μM, respectively (Figure 3.1). Partial inhibition is a specialized case of mixed inhibition, but the enzyme-inhibitor-substrate complex is not considered completely inactive. Glauser *et al.* did not include DCMB concentrations greater than 1 μM in their kinetic analysis, so they would not have observed residual activity at high concentrations of DCMB, which would explain why they reported the mechanism as mixed. We repeated the inhibition assay with TMT1A spheroplasts; and similar to our previous results, DCMB exhibited a partial mechanism of inhibition and a K_i value of 0.7 ±0.1 μM (Figure 3.18). The partial inhibition model fit the spheroplast inhibition data much better than the purified TMT1A inhibition data, the K_m values for the two protein sources was also slightly different TMT1A spheroplasts methylated TSL with a K_m Michaelis constant of 6.2 μM compared to 39.4 μM for purified TMT1A (Figure 3.16 and Chapter 2, **section 2.3.6**). Purified TMT1A is reconstituted in DMPG liposomes while TMT1A spheroplasts are composed of TMT1A embedded in bacterial membrane. TMT1A is sensitive to its lipid environment, it is possible the difference in purified and spheroplast lipid composition could affect protein activity and explain the differences between the two protein sources. Another factor that could have contributed to

these differences is that the TSL activity assay for purified recombinant TMT1A required TSL to be dried onto the reaction plate to accommodate the small volumes necessary to preserve purified enzyme. Drying the TSL on the plate could have influenced the accuracy of the concentration of TSL that the enzyme was exposed to during an incubation. Despite these differences, the mechanism of DCMB inhibition of TMT1A is clearly not competitive and cannot be modeled by a simple mixed inhibition model, more kinetic work is necessary to develop an improved understanding of how DCMB is inhibiting TMT1A.

The crystal structures of several small molecule methyltransferases were examined to identify important binding interactions with SAM and/or SAH. Small molecule methyltransferases are class I methyltransferases and have a highly conserved SAM binding region consisting of a GXGXG sequence and an acidic residue at the end of their second β-strand (Chapter 1, **section 1.1**, [11]). The aligned crystal structures each had their conserved acidic residue, at a position nearly identical relative to SAM or SAH, that formed a hydrogen bond with one of the hydroxyl groups on the ribose of SAM/SAH (Figure 3.7.A). We identified several other conserved binding interactions between these small molecule methyltransferases and SAM or SAH. Each methyltransferase had hydrophobic residues on opposite sides of the SAM or SAH adenosyl (Figure 3.7.B and 3.7.C), and an aromatic residue adjacent to the adenosyl (Figure 3.7.D). They also each had a polar residue that formed a hydrogen bond with the carboxylic acid of SAM or SAH and another polar residue that formed a hydrogen bond with the adenosyl amine (Figure 3.7.E). AlphaFold homology models of TMT1A and TMT1B were aligned with the crystal structures of the small molecule methyltransferase, and several TMT1A and TMT1B residues were in approximately similar positions to participate in the conserved binding interactions with SAM or SAH (Figure 3.7 and Supplementary fig. 3.7).

It was established from previous mutagenesis work that Asp-98 is important for TMT1B activity [2]. Both TMT1A and TMT1B Asp-98 aligned perfectly with the other small molecule methyltransferase acidic residues. Other TMT1 residues that were identified to be important for SAM or SAH binding where Glu-128, which was in the correct position to form a hydrogen bond with the SAM or SAH adenosyl amine, and Thr-144, which was positioned to form a hydrogen bond with the SAM or SAH carboxylic acid (Figure 3.7.E and Supplementary fig. 3.7). These binding interactions are in close agreement with the SAR analysis published by Borchardt *et al.*; decarboxylation of SAH or conversion of the adenosyl amine to a methyl prevents SAH from binding to microsomal TMT [26]. Future work should explore if these interactions are important for SAH and SAM binding in TMT1A and TMT1B.

Using AlphaFold homology models of TMT1A and TMT1B for small molecule docking analysis, we identified a site directly above the SAM binding region where either a substrate or DCMB could potentially bind (Figure 3.2 and 3.3). This site is mostly conserved between TMT1A and TMT1B, with important distinct features. There are four residues that appear to point into this substrate binding site that are not conserved between TMT1A and TMT1B. At residue positions 39, 43, 47, and 199, in TMT1A, these residues are aromatic—F39, F43, Y47, and F199—while in TMT1B these residues are aliphatic—L39, L43, S47, G199 (Figure 3.4). We hypothesized that DCMB can reside in TMT1A's substrate binding region by forming π-π stacking interactions with the aromatic residues of TMT1A while no similar interactions are possible in TMT1B due to the aliphatic nature of these residues. To test this, we generated TMT1A mutants by introducing missense mutations at the 39, 43, 47, or 199 residue positions to convert TMT1A's aromatic residues to the corresponding TMT1B aliphatic residues (Figure 3.8). We then compared each mutant's methyltransferase activity in the presence of DCMB, with

WT-TMT1A activity and discovered that each mutant TMT1A with a Y47S mutation had methyltransferase activity consistent with WT-TMT1B and conferred resistance to DCMB (Figure 3.9). These results highlighted the importance of Tyr-47 as a critical residue for DCMB binding and inhibition of TMT1A.

TMT1A and TMT1B homology models were aligned with a crystal structure of SAM-bound COMT, and two cysteine residues, Cys-148 and Cys-202 were identified in the substrate binding region of TMT1A and TMT1B near bound SAM. The closest cysteine residue to the aligned SAM, Cys-148, is 7.5 Å away from the SAM sulfur and 6 Å apart from the SAM methyl Figure 3.6.B and 3.6.C). Some small molecule methyltransferases like AS3MT require cysteine residues in their active sites to catalyze methyl transfer. AS3MT transfers a methyl group to arsenic by first binding arsenic to one of its cysteine thiols that are near SAM, before the SAM methyl is transferred to arsenic [6-10]. In a previous study, microsomal TMT was incubated with a thiol alkylating agent and then dialyzed and analyzed for activity, the enzyme's activity was completely lost, which suggests that cysteine thiols are important for TMT activity [26]. Methyl transfer occurs when the substrate's nucleophilic methyl acceptor atom is positioned linear with the methyl carbon and sulfonium atoms of SAM and is approximately 3 and 4 Å away, respectively [27, 28]. For a detailed analysis of the methyl transfer reaction, see Liscombe *et al.* and Abdelraheem *et al.* [27, 28]. A typical disulfide bond is about 2 Å [23], so during methyl transfer reactions catalyzed by TMT1A and TMT1B, the substrate thiol is potentially close enough for Cys-148 to participate in the methyl transfer reaction. It seems that Cys-202 and Cys-148 thiols are also close enough to form an intramolecular disulfide bond with each other which could influence how Cys-148 interacts with substrate thiols. Future studies reacting TMT1A and

TMT1B with a thiol alkylating agent will be necessary to determine if the catalytic reaction requires free cysteine-thiols for activity.

One major setback we faced while studying TMT1A and TMT1B was the difficulty to produce large quantities of pure enzymes for biochemical analysis. These enzymes are membrane associated and difficult to efficiently solubilize from membranes. Spheroplasts are the inner membrane of gram-negative bacteria like *E. coli*. When TMT1A or TMT1B are expressed in bacteria, they are imbedded in the bacterial inner membrane. During conventional lysis of TMT1A or TMT1B, most of the protein would remain in the bacterial membrane but when preparing spheroplasts which are mostly bacterial inner membrane, most of the expressed protein will be in the isolated spheroplasts.

After confirming that TMT1A spheroplasts methylated substrates similar to purified TMT1A, they were used to screen DCMB congeners for TMT1A inhibition (Figure 3.19). Four DCMB-like compounds were screened, as well as ibuprofen, a commonly prescribed small aromatic molecule, 4-NBT, and 6-MP because they are substrates of TPMT, and caffeine, because it chemically resembles 6-MP. We also included methyl glutathione and reduced glutathione to determine the effect of endogenous thiols on TMT1A activity. Interestingly, 4-NBT significantly inhibited TMT1A and caused a 90% decrease in activity. 4-NBT is not a substrate of TMT1A, but it is a small neutral aromatic compound which could explain why it inhibits TMT1A. 6-MP also significantly inhibited TMT1A, but it only caused a 20% decrease in activity. Of the four DCMB analogs that were screened, only the phenylethanol analog 2-APE did not inhibit TMT1A, consistent with the SAR analysis of DCMB and microsomal TMT by Glauser *et al.*, which demonstrated that phenylethanol DCMB analogs do not inhibit microsomal TMT [3]. This supports our hypothesis, that TMT1A accounts for the majority of microsomal TMT activity.

Historically, prior to the discovery of TMT1A and TMT1B, alkyl thiol methyltransferase activity was attributed to an unknown microsomal enzyme and thiopurine activity was attributed to cytosolic TPMT, there was no substrate overlap reported for these two enzymes except for thiophenol compounds which seemed to be methylated by both enzymes [29, 30]. TPMT was expressed and purified to function as a negative control for alkyl thiol methyltransferase activity (Figure 3.10). Purified TPMT did not methylate TSL but methylated both 6-MP and 4-NBT. To our knowledge, 4-NBT is not a known substrate of TPMT, but along with 6-MP it has thiol groups conjugated to an electron withdrawing ring systems which could be an important feature for small molecules to be preferred substrates of TPMT.

A phenomenon unique to thiols that are conjugated to electron withdrawing ring systems is that their absorbance changes when alkylated [31]. We developed a TPMT activity assay using either 6-MP or 4-NBT absorbance changes to report on methyltransferase activity and serve in the future as a rapid method to screen for TPMT inhibitors. When 4-NBT is methylated, its absorbance maximum shifts form 411 nm to 350 nm. During a 4-NBT and TPMT activity assay, both parent disappearance and product appearance were monitored in real time using a plate reader and scanning for changes in absorbance at 350 and 411 nm (Figure 3.13). We are confident that electron withdrawing aromatic thiol compounds are exclusively substrates of TPMT. There was no change in 6-MP or 4-NBT absorbance when these compounds were incubated with SAM and TMT1A spheroplasts. The ability to monitor parent disappearance and product formation simultaneously presents an opportunity to study the kinetics of thiol methyl transfer reactions. Absorbance based assays are also significantly cheaper, and have the potential for high throughput, than assays that rely on mass spectrometry for separation and quantification.

Eventually, we hope to identify a specific substrate for TMT1A and TMT1B that changes absorbance with methylation like 6-MP and 4-NBT.

3.5 CONCLUSION

The structure and function of TMT1A and TMT1B have been analyzed through the use of homology models, docking analysis, site directed mutagenesis, enzyme kinetics, and SAR inhibitor analysis. The SAM and substrate binding sites have been putatively located in TMT1A and TMT1B and key SAM-binding residues were identified including Asp-98, Glu-128, and Thr-144. TMT1A is inhibited by DCMB, while TMT1B is not, due to single residue difference between TMT1A and TMT1B at codon 47. Finally, SAR analysis of DCMB concluded that TMT1A is inhibited by neutral or positive aromatic small molecules. The methods developed during this study will be invaluable for continued biochemical analysis of TMT1A and TMT1B and the eventual development of specific probe inhibitors for these enzymes.

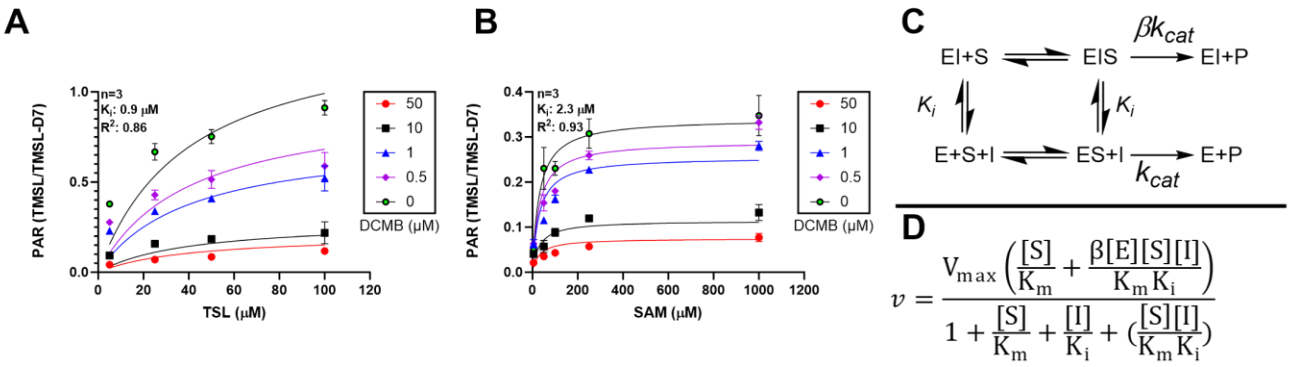

$$v = \frac{V_{max}\left(\frac{[S]}{K_m} + \frac{\beta[E][S][I]}{K_m K_i}\right)}{1 + \frac{[S]}{K_m} + \frac{[I]}{K_i} + \left(\frac{[S][I]}{K_m K_i}\right)}$$

Figure 3.1. Inhibition of purified N-GST-TMT1A by DCMB

TSL methylation by N-GST-TMT1A at various concentrations of TSL (A) or SAM (B) in the presence of increasing concentrations of DCMB. Partial inhibition reaction scheme (C). The equation for partial inhibition (D). Data (n = 3) are reported as the mean ± S.D.

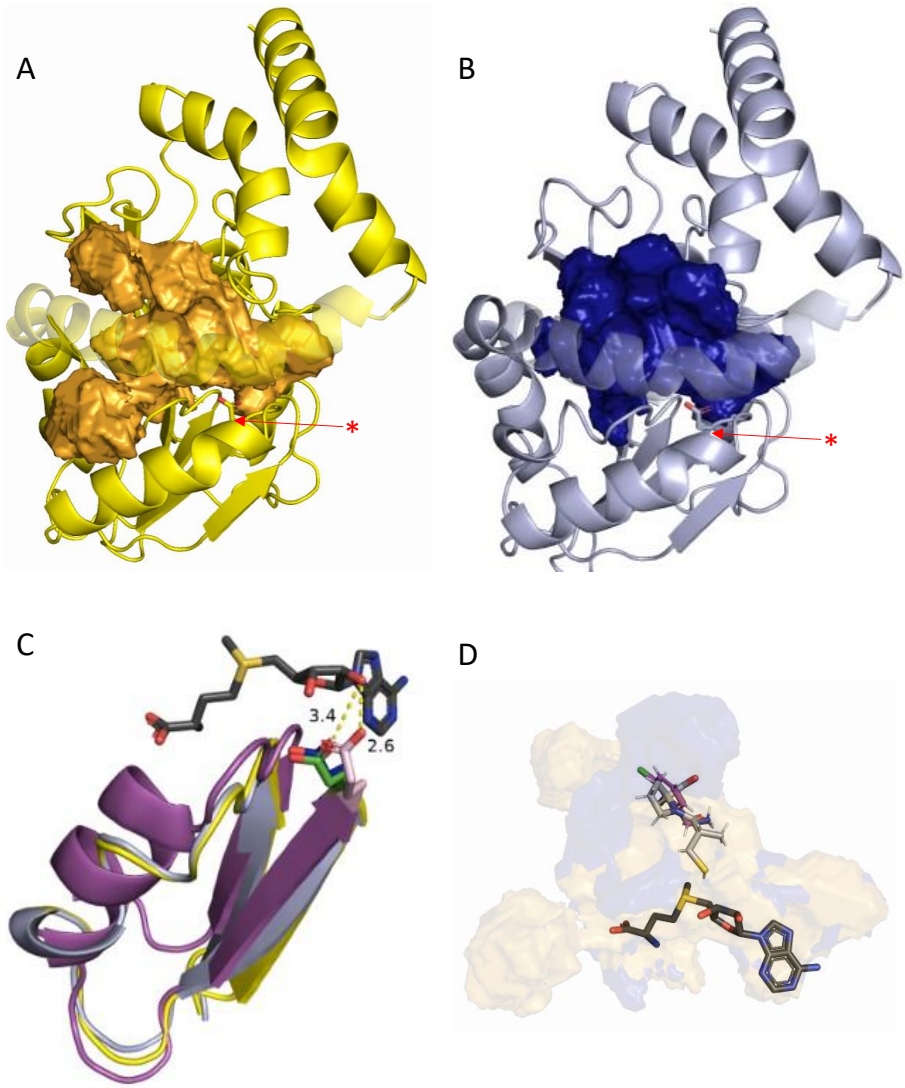

Figure 3.2. Active site analysis of TMT1A and TMT1B

AlphaFold homology model of TMT1A (A) and TMT1B (B) with the volume of their central binding pockets rendered as a solid infill. The asterisk (*) identifies the conserved acidic residues to orient the reader. SAM, bound to the aligned first and second β-strands of TMT1A (yellow), TMT1B (light blue), and COMT (purple) (C). Each methyltransferase's conserved acidic residue sidechain is visible with the distance (Å) measured to the nearest ribose hydroxyl—TMT1A (green), TMT1B (blue), and COMT (pink). The TMT1A and TMT1B central binding pockets overlayed with DCMB (magenta) and captopril (grey), from TMT1A docking, bound in the substrate binding site immediately above SAM (black) (D).

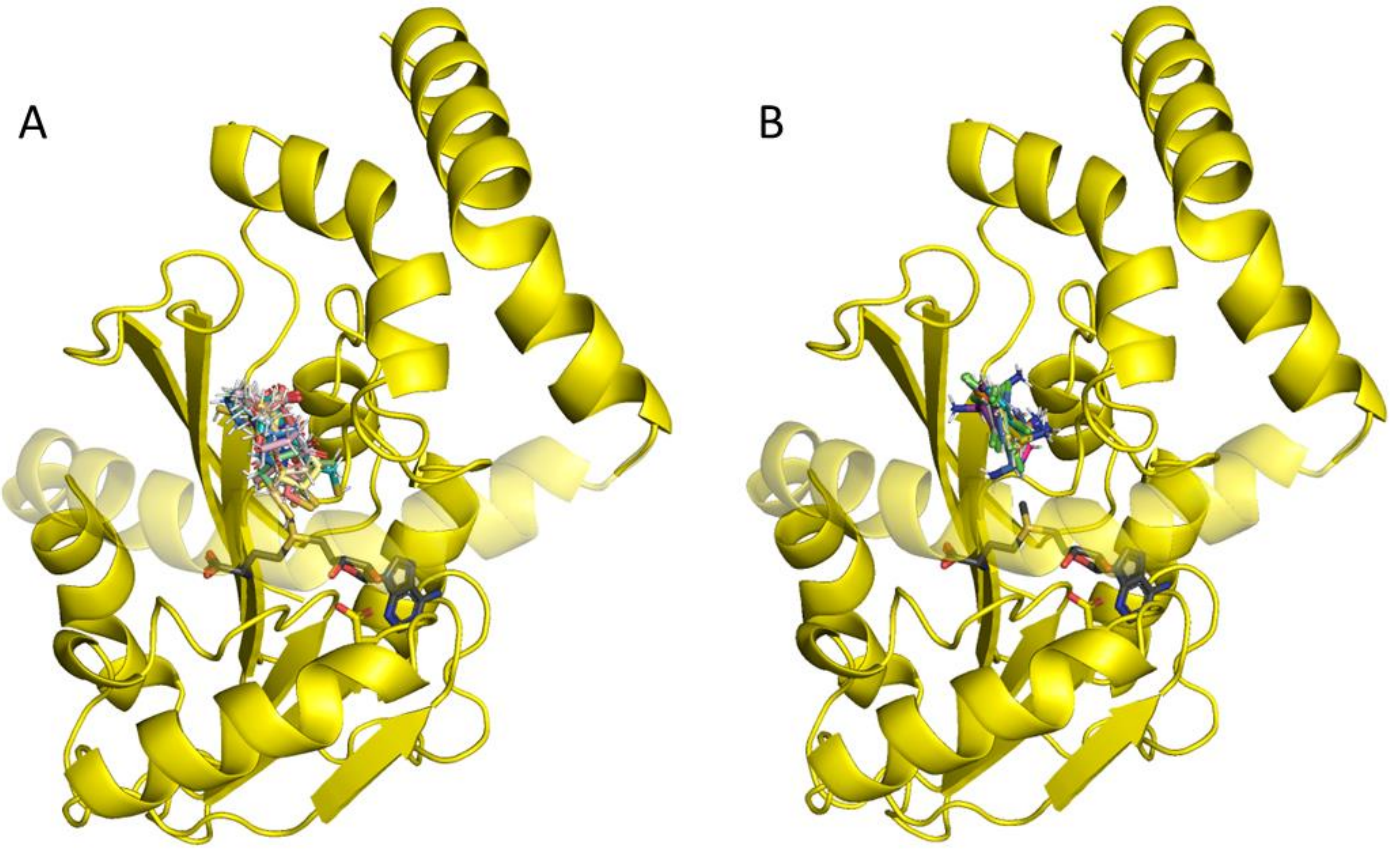

Figure 3.3. Captopril and DCMB docked into TMT1A homology model

AlphaFold homology models of TMT1A with the top ten poses of docked captopril (A) and docked DCMB (B). SAM (black) is aligned from the crystal structure of COMT (**section 3.2.2**)

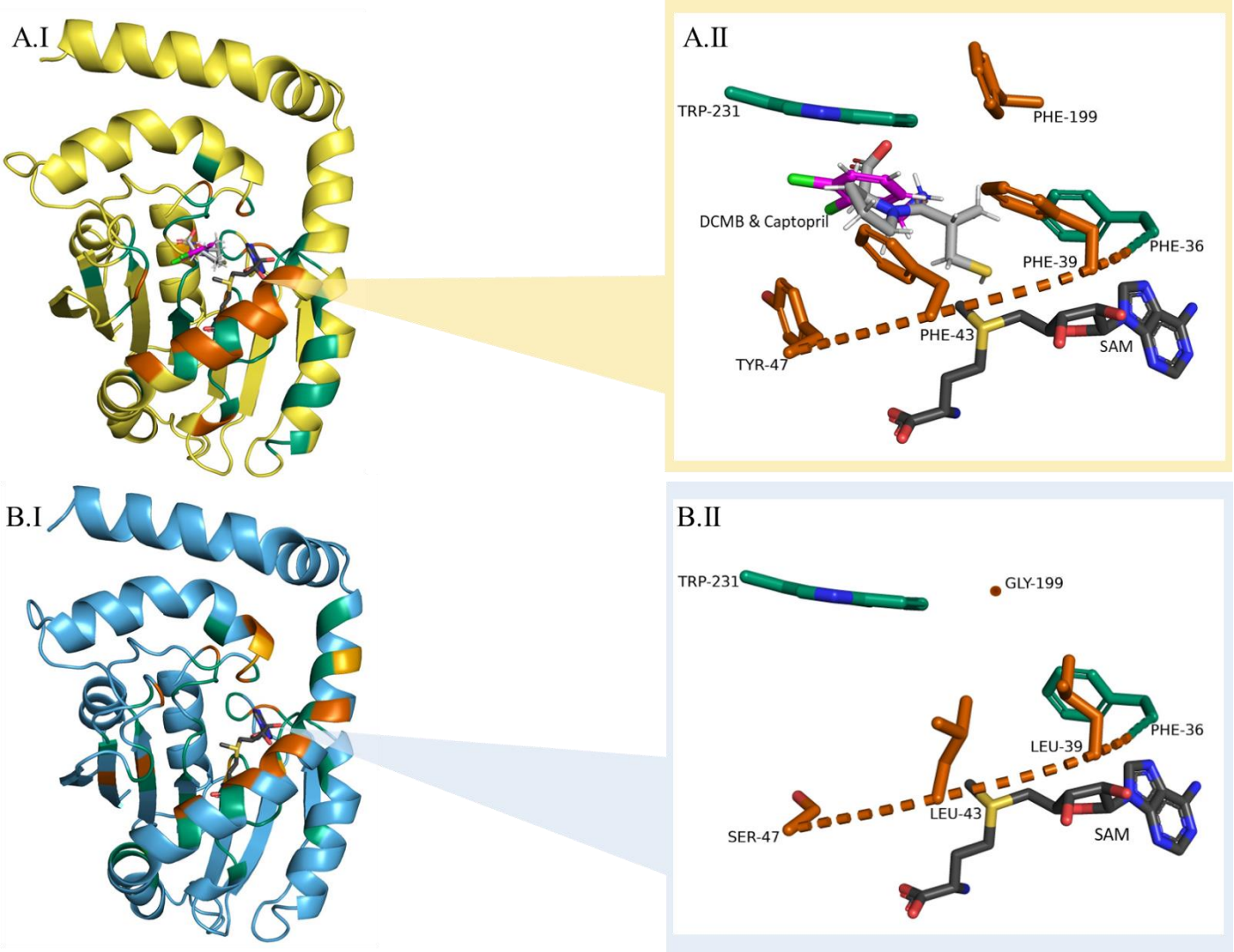

Figure 3.4. Substrate binding sites of TMT1A and TMT1B compared

AlphaFold homology models of TMT1A (A) and TMT1B (B) with residues that make up each enzyme's central binding pocket highlighted (I) green if identical between both enzymes, yellow-orange if homologous, and red-orange if different. SAM (black) and the residues identified as different in the substrate binding region are labeled and shown in proximity to DCMB (magenta) and captopril (grey) docked into TMT1A (A.II) or alone in the same orientation for TMT1B (B.II).

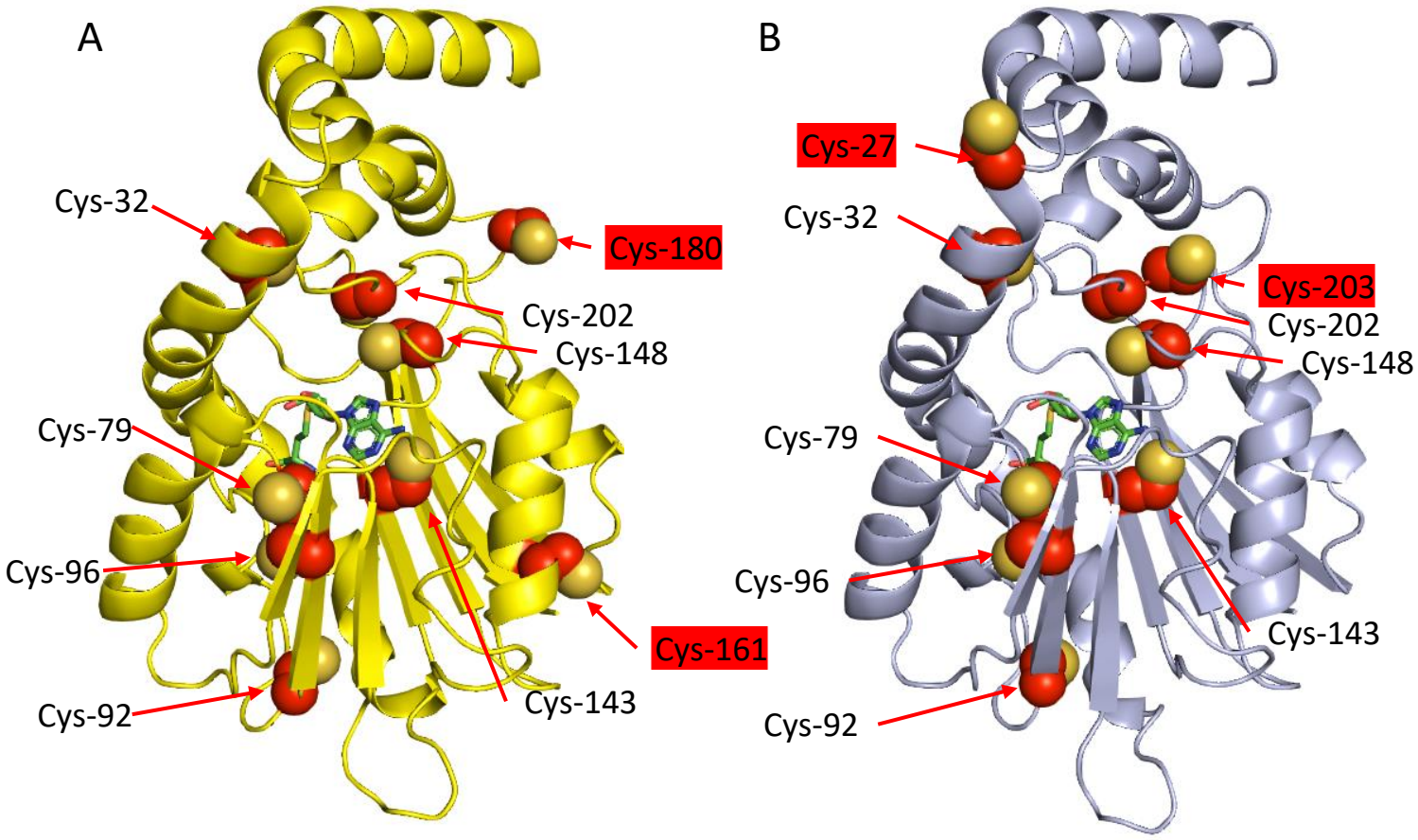

Figure 3.5. TMT1A and TMT1B cysteine residues, labeled

AlphaFold homology models of TMT1A (A) and TMT1B (B) with SAM (green) aligned in SAM binding site and cysteine residues labeled and rendered as yellow and red spheres. The cysteine residues with red labels are not conserved between TMT1A and TMT1B.

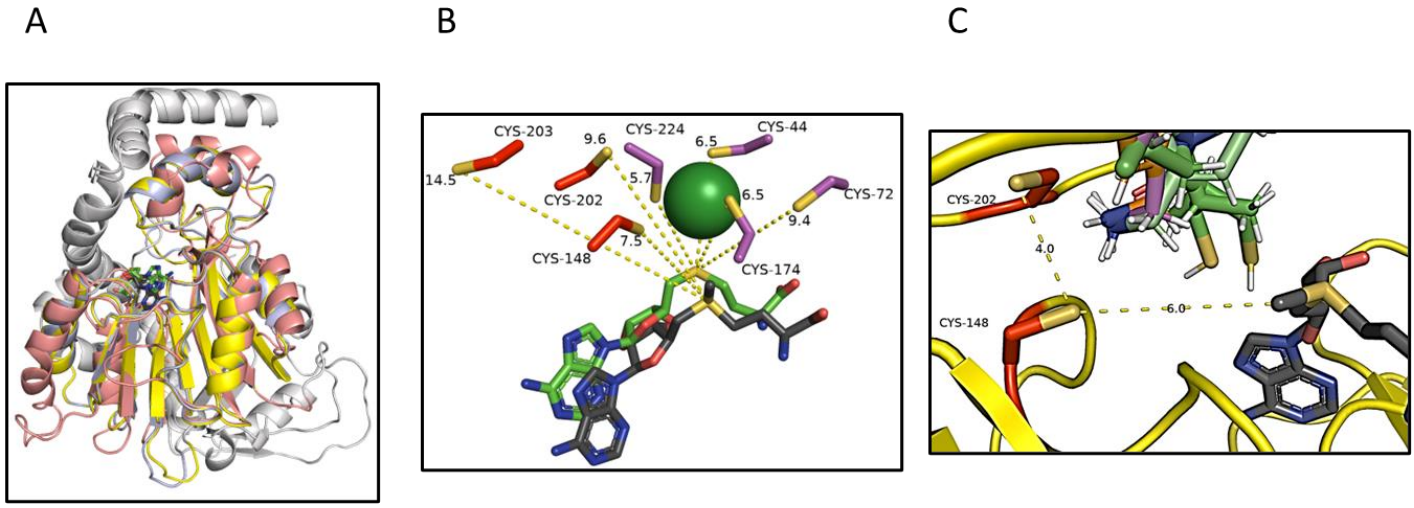

Figure 3.6. Cysteine residues in TMT1A and TMT1B compared with those in AS3MT

The crystal structure of *Cyanidioschyzon* AS3MT (6CX6, 2.84 Å, pink) aligned with TMT1A (yellow) and TMT1B (light blue) (A). The *N*- and *C*- termini are not structurally homologous so for clarity these regions are colored white. Residues from the aligned TMT1A and B (red) and AS3MT (purple) (B). Arsenic from the AS3MT crystal structure is rendered as a green sphere. SAH from the AS3MT crystal structure is green and the align SAM from the TMT1 homology models is black. Distances from each cysteine's thiol sulfur and SAM or SAH's sulfur are given in angstroms. The first and second docked pose of captopril (green) in TMT1A (yellow) with Cys-148 and Cys-202 side chains shown (red) relative to aligned SAM (black) (C). The distance between Cys-148 and the aligned SAM methyl is in angstroms as is the distance measured between Cys-202 and Cys-148.

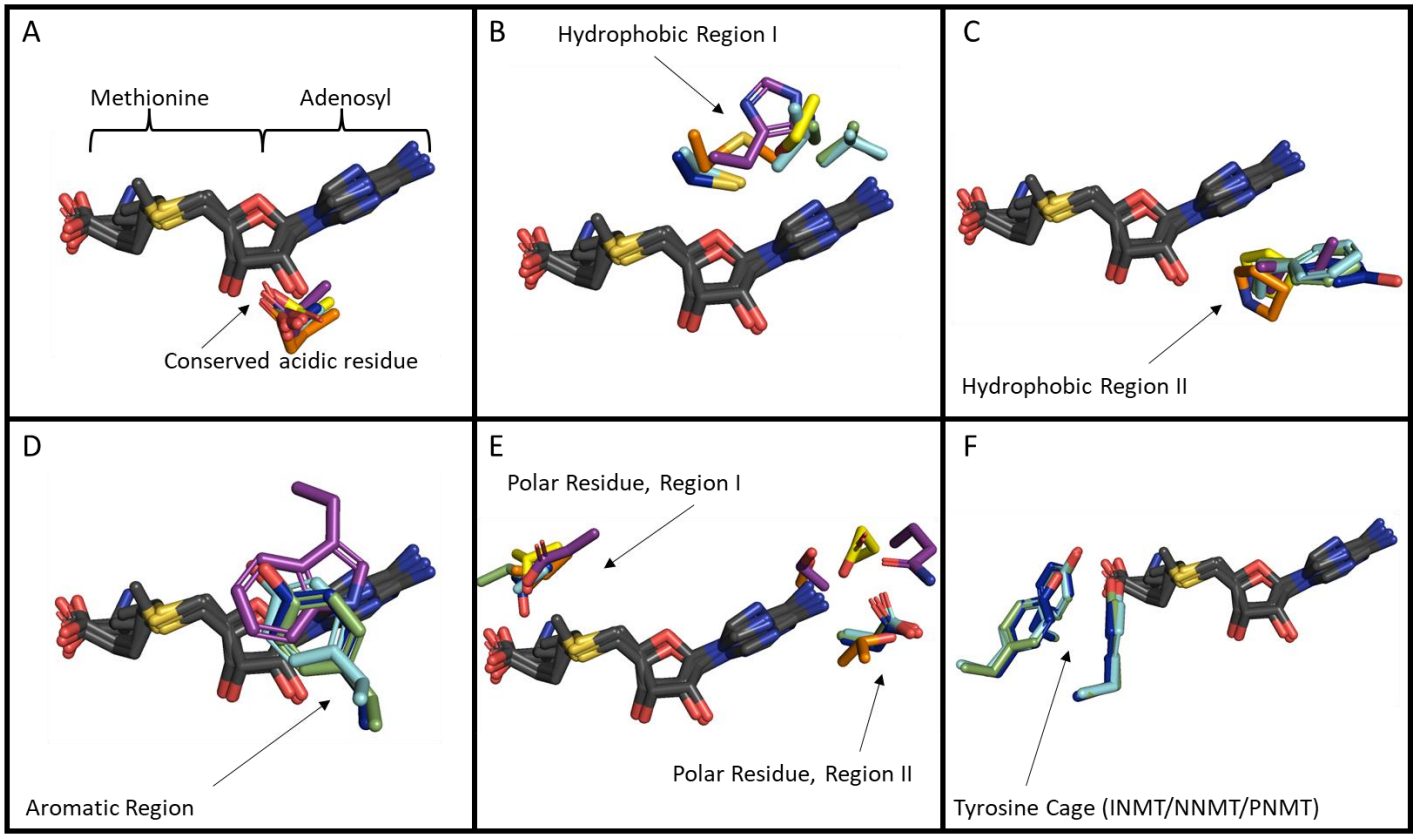

Figure 3.7. SAM binding interactions identified from small molecule methyltransferase crystal structures

SAH or SAM (black) from aligned crystal structures and residues specific to: the conserved acidic residue binding interaction (A), hydrophobic region I (B), hydrophobic region II (C), aromatic region (D), polar regions I and II (E), and the tyrosine cage binding interaction with SAM or SAH (F). Residues are color coded by the crystal structure or homology model they are from: COMT (purple), HNMT (orange), INMT (green), PNMT (cyan), NNMT (dark blue), and TMT1A (yellow).

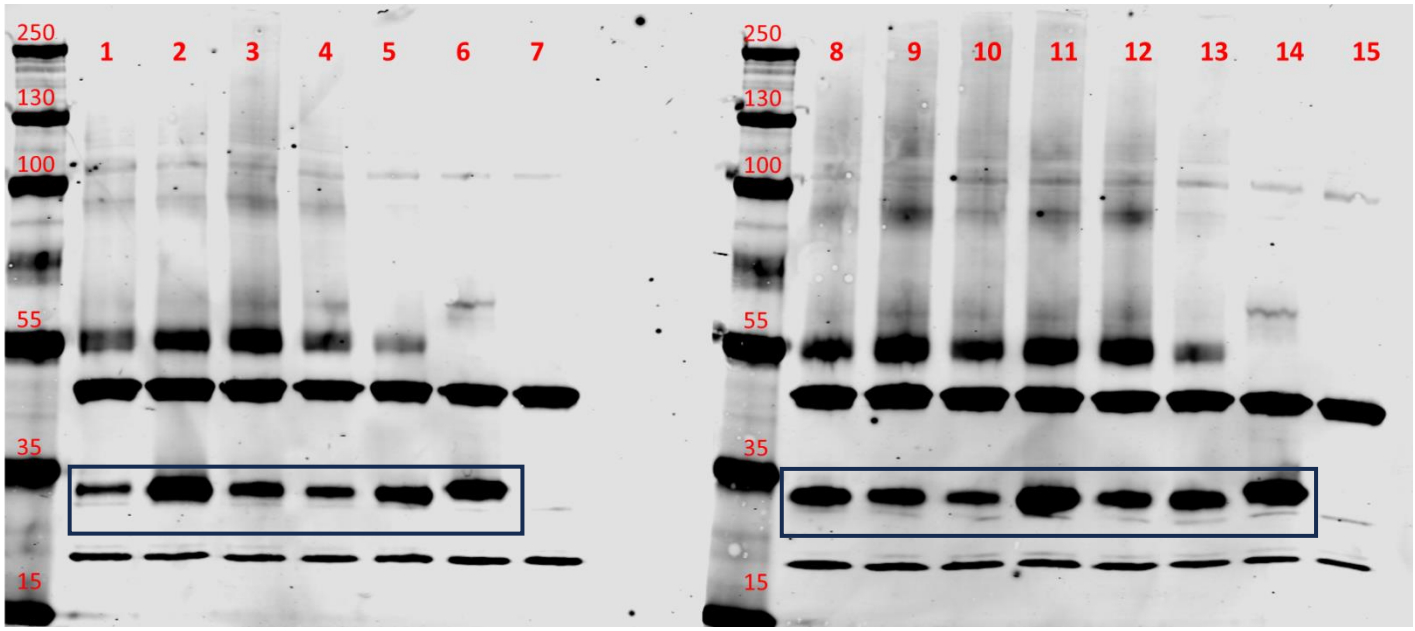

Figure 3.8. Western blot analysis of overexpressed TMT1A, TMT1B, and TMT1A mutants

Overexpression of WT-TMT1A, WT-TMT1B or mutant-TMT1A in HeLa cells. Anti-flag and anti-β-actin western blots verify the overexpression of flag tagged proteins. Lanes are protein lysate from F43L-TMT1A (1), F39L+F43L+Y47S-TMT1A (2), F199G-TMT1A (3), F39L+F43L-TMT1A (4), WT-TMT1A (5), WT-TMT1B (6), empty control vector (7), F39L+F43L+Y47S-TMT1A (8), Y47S-TMT1A (9), WT-TMT1A (10), F43L+Y47S-TMT1A (11), F199G-TMT1A (12), WT-TMT1A (13), WT-TMT1B (14), and empty control vector (15). The box indicates the TMT1 bands of interest. β-actin is the strong band near 42 kDa.

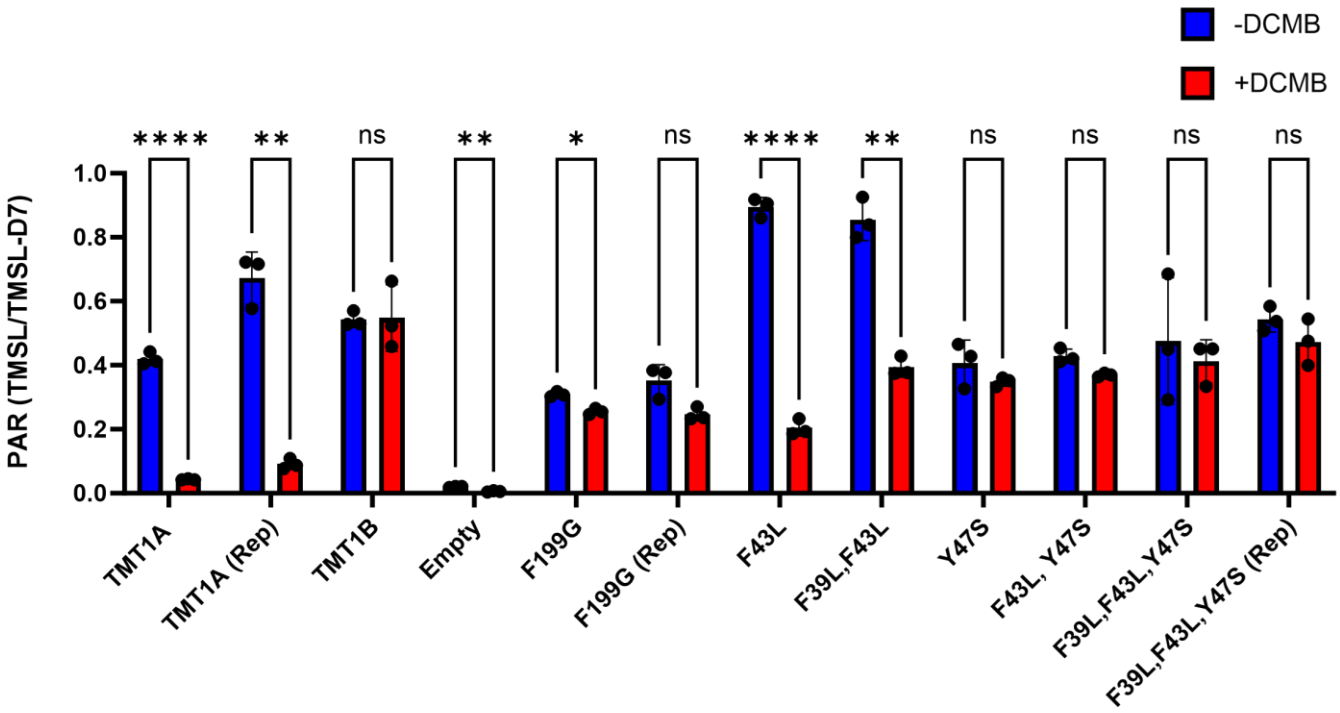

Figure 3.9. Methylation of TSL by Mutant TMT1A expressed in HeLa cells

Formation of TMSL in HeLa cells overexpressing WT-TMT1A, mutant-TMT1A, or WT-TMT1B after a 24-hour incubation with TSL ±DCMB. All data (n = 3) are presented as the mean ± S.D. Significance was determined using a two-tailed t test. ****P < 0.0001; ***P < 0.001; **P < 0.01.

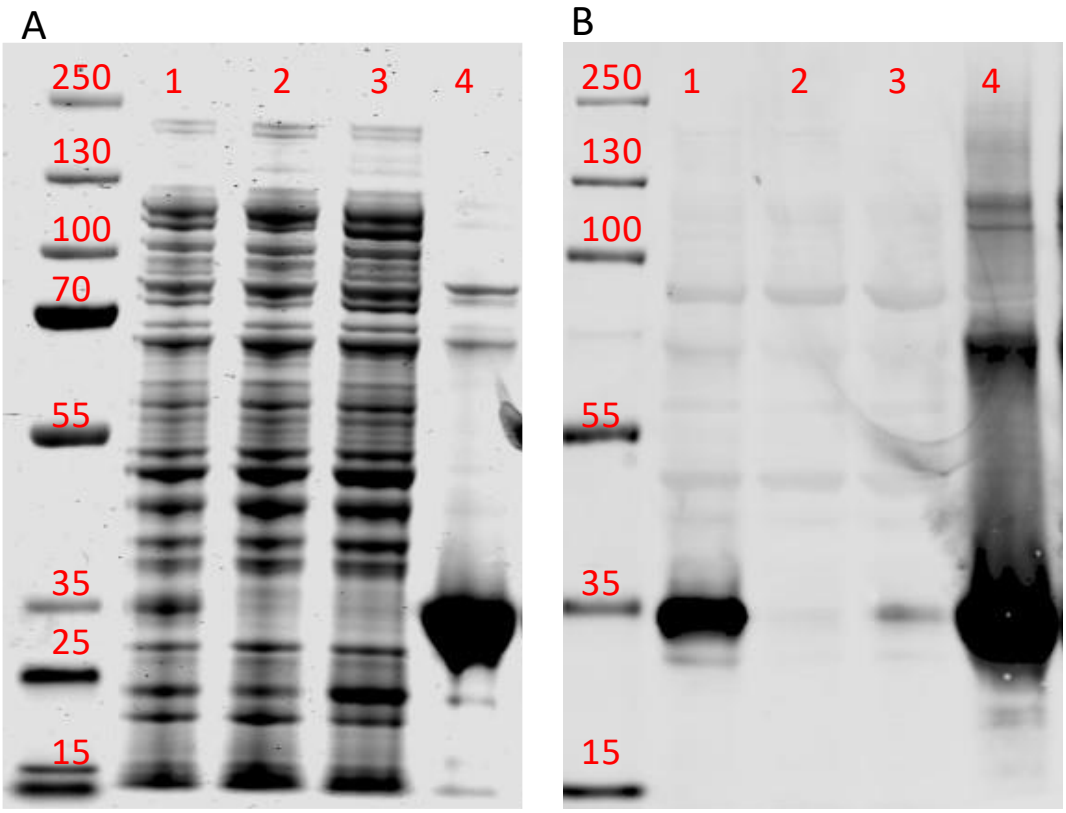

Figure 3.10. SDS-PAGE analysis of purified TPMT

SDS-PAGE Coomassie stain (A) and anti-TPMT western blot (B) of TPMT expressing bacterial lysate (lane 1), TPMT purification wash 1 (lane 2), wash 2 (lane 3), and recombinant purified TPMT eluent (lane 4).

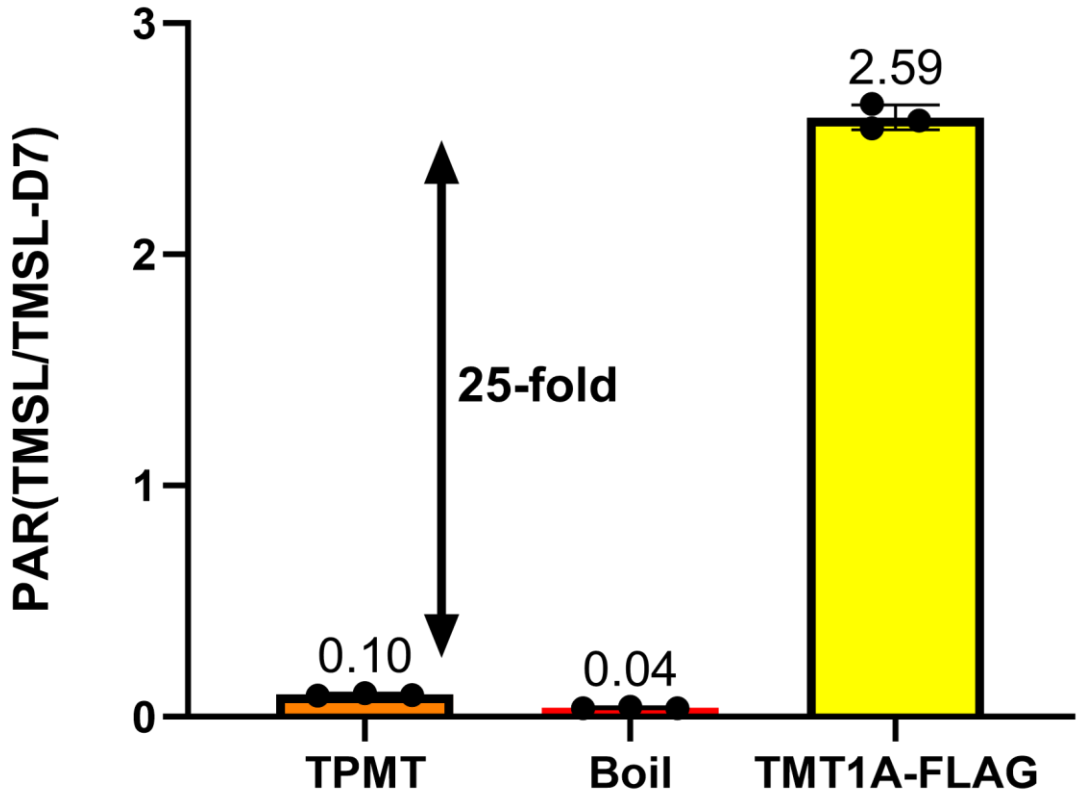

Figure 3.11. TMT activity of TPMT compared with TMT1A

Methylation of TSL by TPMT and TMT1A-Flag spheroplasts. Both proteins normalized to 0.5 mg/mL. Data demonstrate that there is a 25-fold difference in alkyl thiol methylation activity between TPMT and TMT1A. Data (n = 3) are presented as the mean (labeled) ± S.D.

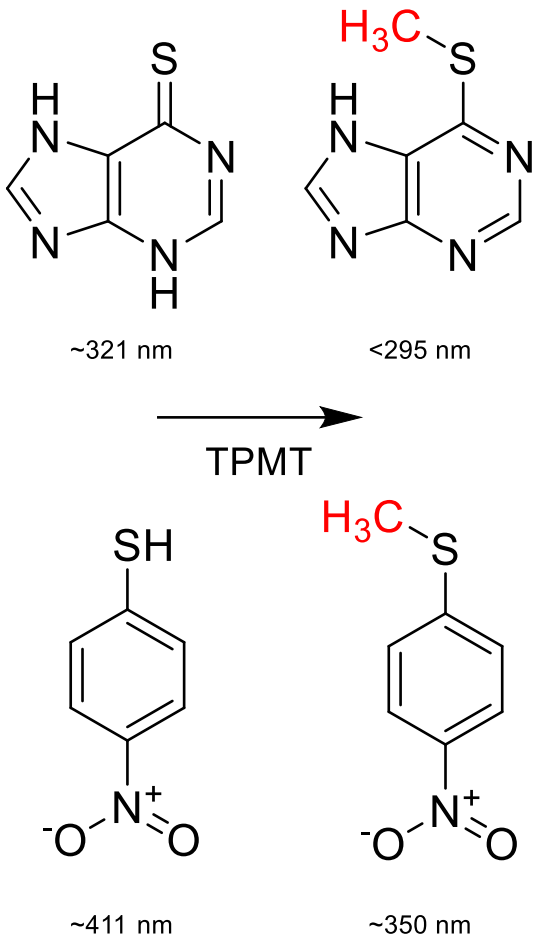

Figure 3.12. TPMT substrates

6-mercaptopurine (top) and 4-nitrobenzenethiol (bottom) and absorbance maxima before and after methylation.

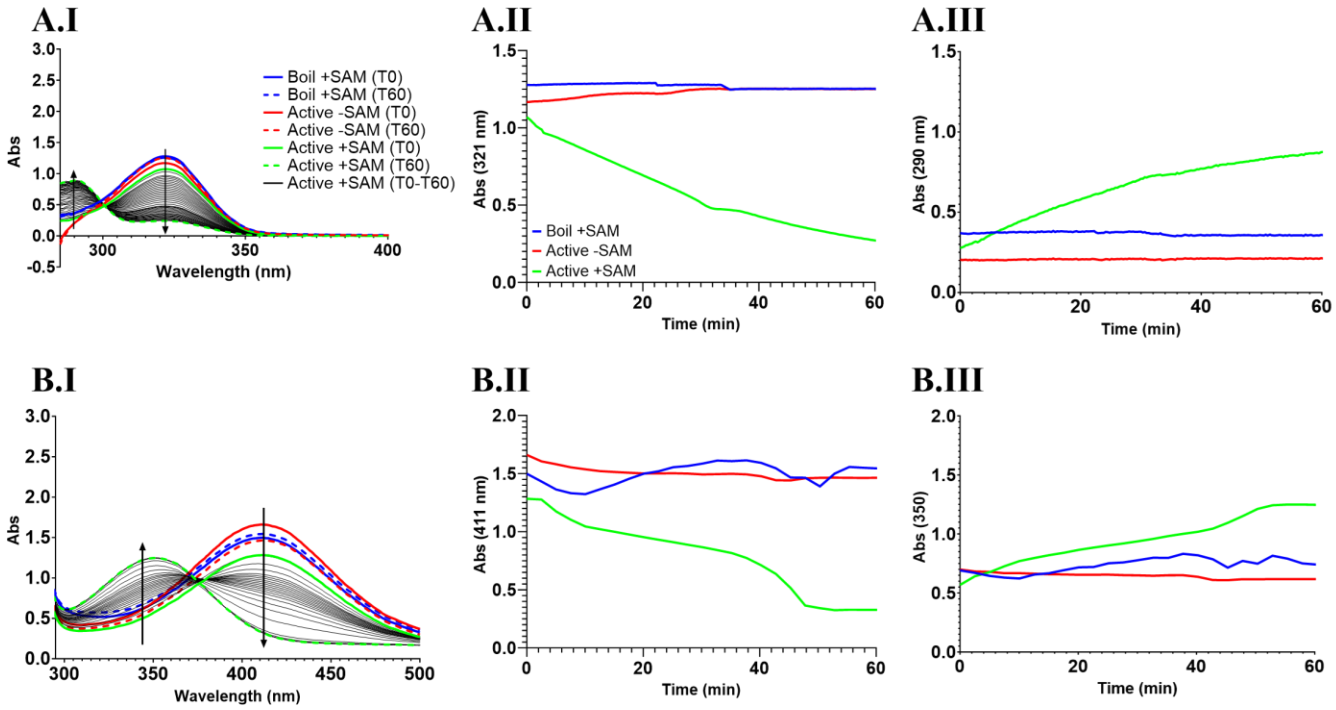

Figure 3.13. TPMT absorbance based activity assay.

Methylation of 6-MP (A) and 4-NBT (B) by purified recombinant TPMT. Absorbance scan during 6-MP or 4-NBT activity assay, every fifth scan is shown from T0-T60 (I). Plots showing the real time disappearance of parent (II) and appearance of methyl metabolite (III) during 6-MP or 4-NBT activity assay.

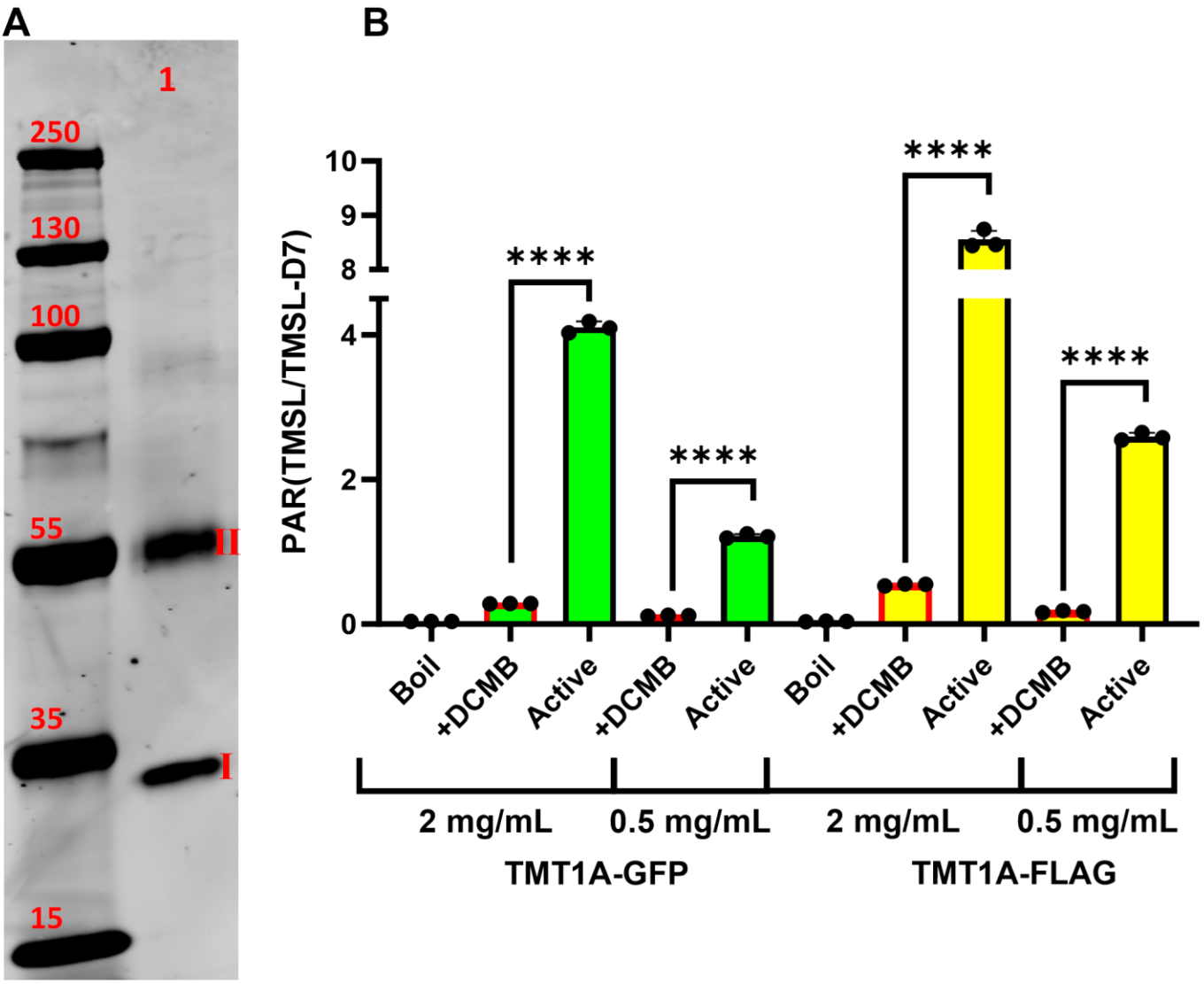

Figure 3.14. Western blot analysis of TMT1A spheroplasts and TSL activity assay

Anti-FLAG western blot verifies the isolation of TMT1A-FLAG spheroplasts (A). The band at I is FLAG tagged TMT1A and the band at II is currently unknown. Methylation of TSL by 2 mg/mL or 0.5 mg/mL TMT1A-FLAG and TMT1A-GFP ±DCMB (B). All data (n = 3) are presented as the mean ± S.D. Significance was determined using a two-tailed t-test. ****P < 0.0001; ***P < 0.001; **P < 0.01.

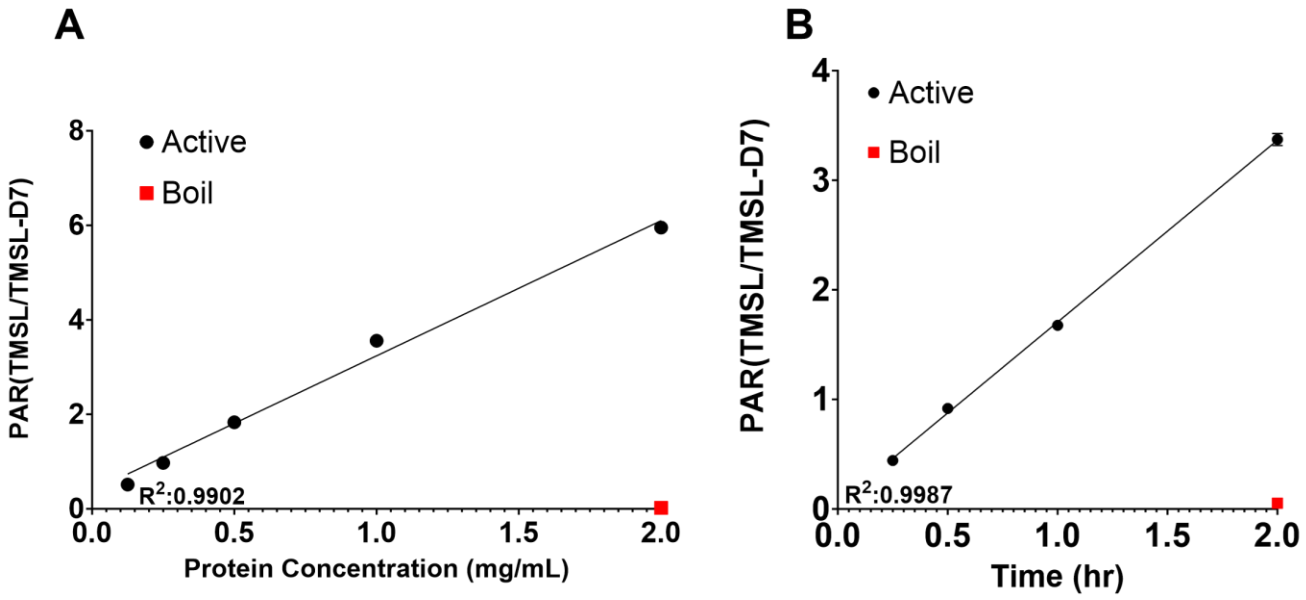

Figure 3.15. Protein and time linearity of TMT1A catalyzed methylation of TSL

The methylation of TSL by various concentrations of TMT1A-FLAG spheroplasts (A) and the methylation of TSL by a fixed concentration of 0.5 mg/mL TMT1A-FLAG spheroplasts over different incubation times (B). All data (n = 3) are presented as the mean ± S.D.

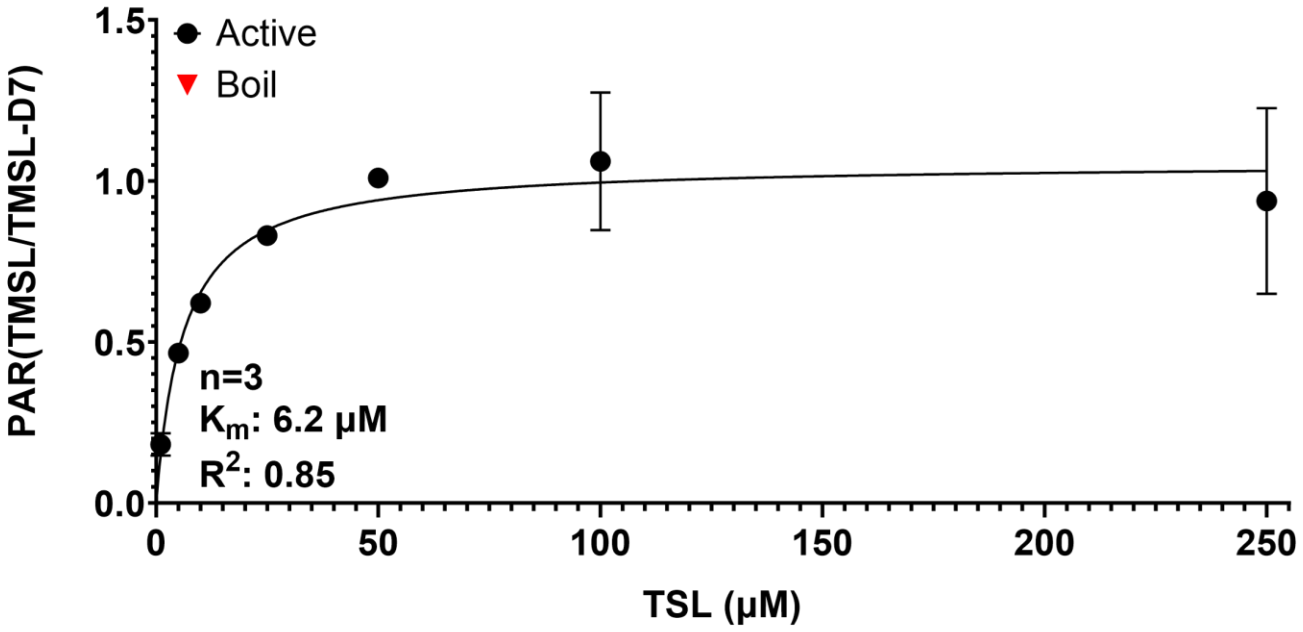

Figure 3.16. TSL methylation by TMT1A-FLAG spheroplasts at various concentrations of TSL

All data (n = 3) are presented as the mean ± S.D.

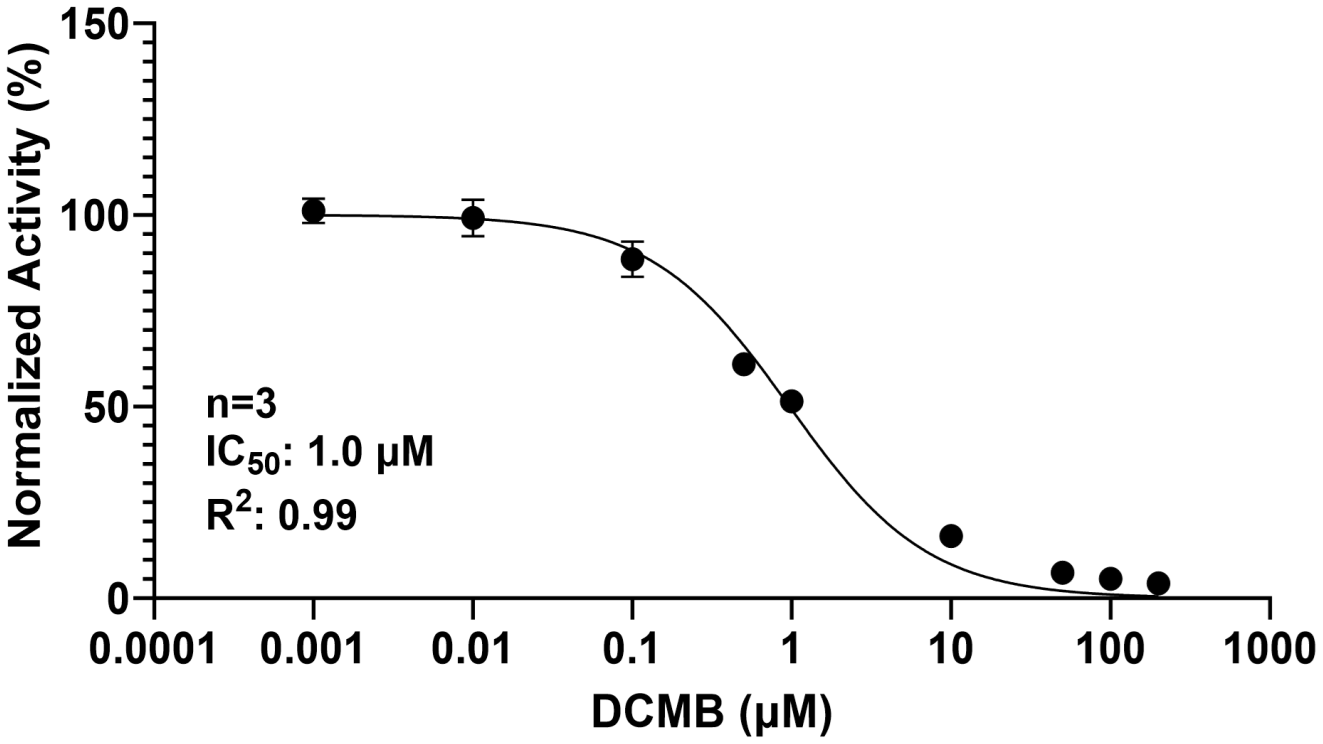

Figure 3.17. IC_{50} for the inhibition of TMT1A-FLAG spheroplasts

This was determined by single time point activity assays with increasing concentrations of DCMB using TSL as the substrate. All data (n = 3) are presented as the mean ± S.D.

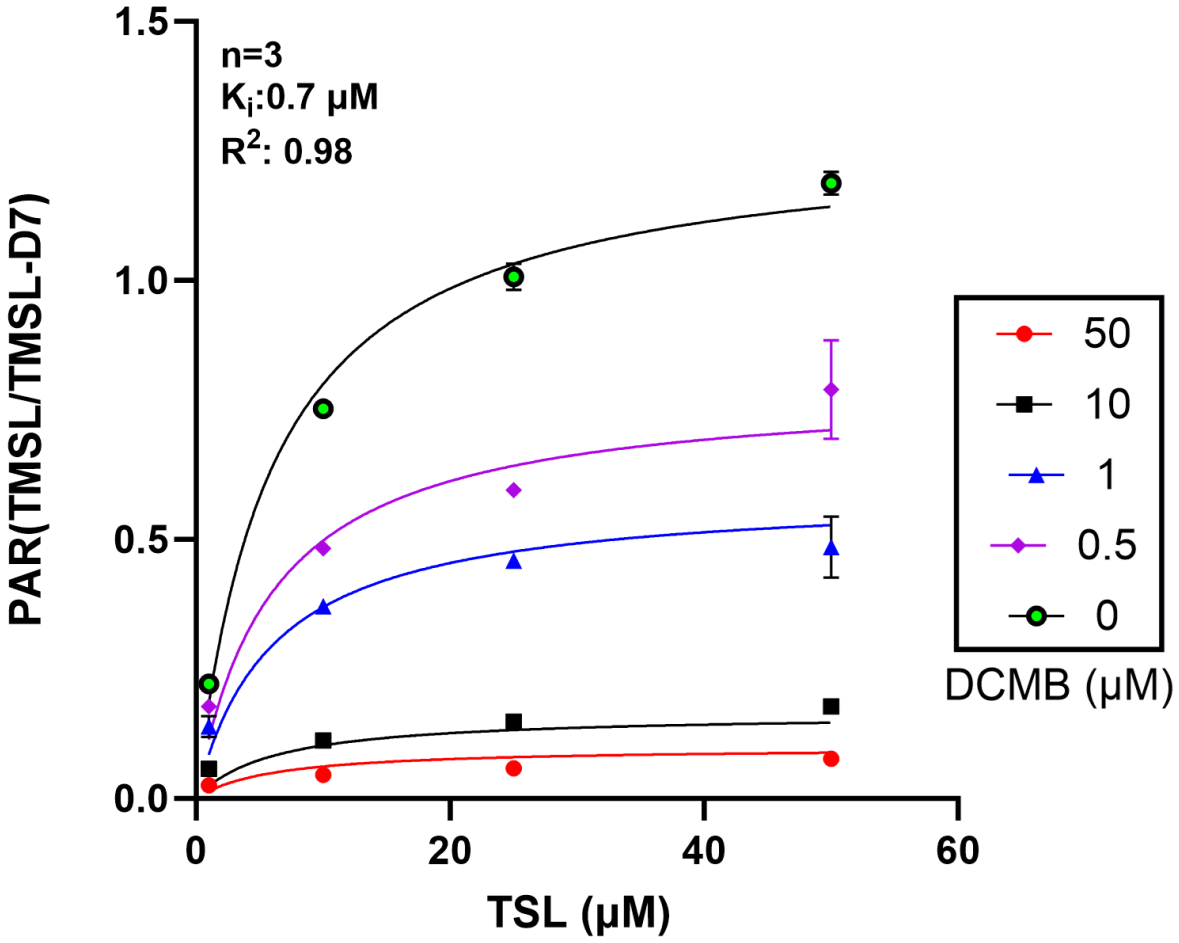

Figure 3.18. Inhibition of TMT1A spheroplasts by DCMB

TSL methylation by TMT1A-FLAG spheroplasts at various concentrations of TSL in the presence of increasing concentrations of DCMB. Data (n = 3) are reported as the mean ± S.D.

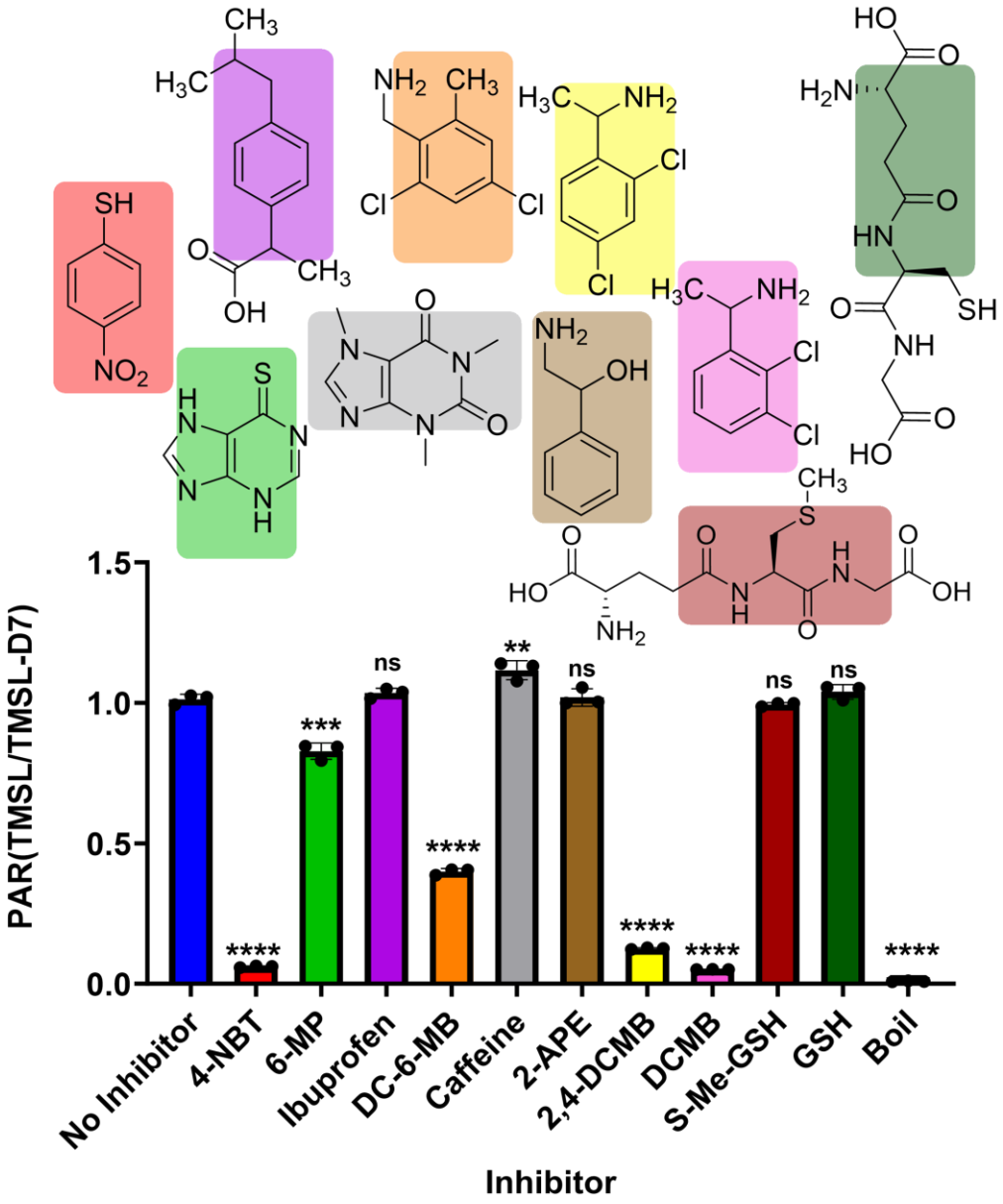

Figure 3.19. TSL methylation by TMT1A-FLAG spheroplasts in the presence of different test inhibitors

Inhibitor structures are color coded to match the bar in the chart that they are associated with. Data (n = 3) are reported as the mean ± S.D. Significance was determined using a two-tailed *t* test comparing inhibitor treated samples with the sample containing no inhibitor. ****$P < 0.0001$; ***$P < 0.001$; **$P < 0.01$.

3.6 REFERENCES

1. Russell, D.A., et al., *METTL7A (TMT1A) and METTL7B (TMT1B) Are Responsible for Alkyl.* Drug Metab Dispos, 2023. **51**(8): p. 1024-1034.

2. Maldonato, B.J., D.A. Russell, and R.A. Totah, *Human METTL7B is an alkyl thiol methyltransferase that metabolizes hydrogen sulfide and captopril.* Sci Rep, 2021. **11**(1): p. 4857.

3. Glauser, T.A., et al., *Human liver microsomal thiol methyltransferase: inhibition by arylalkylamines.* Xenobiotica, 1993. **23**(6): p. 657-69.

4. Jeffery, D.R. and J.A. Roth, *Kinetic reaction mechanism for magnesium binding to membrane-bound and soluble catechol O-methyltransferase.* Biochemistry, 1987. **26**(10): p. 2955-2958.

5. Abdelraheem, E., et al., *Methyltransferases: Functions and Applications.* ChemBioChem, 2022. **23**(18): p. e202200212.

6. Packianathan, C., P. Kandavelu, and B.P. Rosen, *The Structure of an As(III) S-Adenosylmethionine Methyltransferase with 3-Coordinately Bound As(III) Depicts the First Step in Catalysis.* Biochemistry, 2018. **57**(28): p. 4083-4092.

7. Hayakawa, T., et al., *A new metabolic pathway of arsenite: arsenic-glutathione complexes are substrates for human arsenic methyltransferase Cyt19.* Arch Toxicol, 2005. **79**(4): p. 183-91.

8. Song, X., et al., *New insights into the mechanism of arsenite methylation with the recombinant human arsenic (+3) methyltransferase (hAS3MT).* Biochimie, 2010. **92**(10): p. 1397-406.

9. Song, X., et al., *Functional and structural evaluation of cysteine residues in the human arsenic (+3 oxidation state) methyltransferase (hAS3MT).* Biochimie, 2011. **93**(2): p. 369-75.

10. Song, X., et al., *Structure-function roles of four cysteine residues in the human arsenic (+3 oxidation state) methyltransferase (hAS3MT) by site-directed mutagenesis.* Chem Biol Interact, 2009. **179**(2-3): p. 321-8.

11. Schubert, H.L., R.M. Blumenthal, and X. Cheng, *Many paths to methyltransfer: a chronicle of convergence.* Trends in Biochemical Sciences, 2003. **28**(6): p. 329-335.

12. Jumper, J., et al., *Highly accurate protein structure prediction with AlphaFold.* Nature, 2021. **596**(7873): p. 583-589.

13. Jenkins, C.M., I. Pikuleva, and M.R. Waterman, *Expression of eukaryotic cytochromes P450 in E. coli.* Methods Mol Biol, 1998. **107**: p. 181-93.

14. Agusti, G., et al., *A safe and practical method for the preparation of 7α-thioether and thioester derivatives of spironolactone.* Steroids, 2013. **78**(1): p. 102-7.

15. Volkamer, A., et al., *DoGSiteScorer: a web server for automatic binding site prediction, analysis and druggability assessment.* Bioinformatics, 2012. **28**(15): p. 2074-2075.

16. Flachsenberg, F., et al., *A Consistent Scheme for Gradient-Based Optimization of Protein.* J Chem Inf Model, 2020. **60**(12): p. 6502-6522.

17. Hanwell, M.D., et al., *Avogadro: an advanced semantic chemical editor, visualization, and analysis platform.* J Cheminform, 2012. **4**(1): p. 17.

18. Stierand, K. and M. Rarey, *Drawing the PDB: Protein-Ligand Complexes in Two Dimensions.* ACS Med Chem Lett, 2010. **1**(9): p. 540-5.

19. Sievers, F., et al., *Fast, scalable generation of high-quality protein multiple sequence alignments using Clustal Omega.* Mol Syst Biol, 2011. **7**: p. 539.

20. Evdokimov, A.G., et al., *Structural basis for the fast maturation of Arthropoda green fluorescent protein.* EMBO Rep, 2006. **7**(10): p. 1006-12.

21. Russell, D.A. and M.A. Cerny, *High-throughput cytochrome P450 loss and metabolic intermediate complex assays to aid in designing out of CYP3A inactivation.* Methods Enzymol, 2023. **690**: p. 341-368.

22. Masson, P. and A.R. Mukhametgalieva, *Partial Reversible Inhibition of Enzymes and Its Metabolic and Pharmaco-Toxicological Implications.* Int J Mol Sci, 2023. **24**(16).

23. Sun, M.A., et al., *Prediction of reversible disulfide based on features from local structural signatures.* BMC Genomics, 2017. **18**(1): p. 279.

24. Sockolosky, J.T. and F.C. Szoka, *Periplasmic production via the pET expression system of soluble, bioactive human growth hormone.* Protein Expr Purif, 2013. **87**(2): p. 129-35.

25. Yates, C.R., et al., *Molecular diagnosis of thiopurine S-methyltransferase deficiency: genetic basis for azathioprine and mercaptopurine intolerance.* Ann Intern Med, 1997. **126**(8): p. 608-14.

26. Borchardt, R.T. and C.F. Cheng, *Purification and characterization of rat liver microsomal thiol methyltransferase.* Biochim Biophys Acta, 1978. **522**(2): p. 340-53.

27. Abdelraheem, E., et al., *Methyltransferases: Functions and Applications.* Chembiochem, 2022. **23**(18): p. e202200212.

28. Liscombe, D.K., G.V. Louie, and J.P. Noel, *Architectures, mechanisms and molecular evolution of natural product methyltransferases.* Nat Prod Rep, 2012. **29**(10): p. 1238-50.

29. Weisiger, R.A. and W.B. Jakoby, *Thiol S-methyltransferase from rat liver.* Arch Biochem Biophys, 1979. **196**(2): p. 631-7.

30. Woodson, L.C., et al., *Thiopurine methyltransferase. Aromatic thiol substrates and inhibition by benzoic acid derivatives.* Molecular Pharmacology, 1983. **24**(3): p. 471-478.

31. ELLMAN, G.L., *Tissue sulfhydryl groups.* Arch Biochem Biophys, 1959. **82**(1): p. 70-7.

Chapter 4. **Development of a Homogenous Label Adductomics Method to Identify Sulfmethylation of Human Serum Albumin**

4.1 INTRODUCTION

TMT1A and TMT1B are well conserved, they share 75% homology with each other. They also each share greater than 70% sequence identity with many of other mammalian isoforms (Figure 1.11 and 1.12). In this research project, TMT1A and TMT1B have been discussed so far in the context of their roles in drug metabolism, but humans and the rest of Mammalia did not evolve under the selective pressure of modern medicine. The high sequence similarity of TMT1 across mammals indicates that these enzymes have a conserved endogenous function beyond drug metabolism. Our lab became interested in hydrogen sulfide (H_2S) as an endogenous substrate of TMT1A and TMT1B after Dr. Benjamin Maldonato demonstrated that recombinant purified TMT1B can methylate H_2S [1]. Preliminary data from my work also suggests that TMT1A can also methylate H_2S [2]. The methylation of H_2S, an endogenous gasotransmitter by TMT1A and TMT1B, could be an important yet unstudied component of gaseous sulfide signaling.

A major mechanism in which H_2S signals is through a process that involves sulfhydration of cysteines. Sulfhydration involves H_2S forming a covalent bond with a protein cysteine residue resulting in changes to the structure and function of the modified protein [3]. Sulfhydration regulates a wide variety of protein functions. Mustafa *et al.* demonstrated that up to 25% of many liver proteins, including actin, tubulin, and glyceraldehyde-3-phosphate dehydrogenase (GAPDH), are sulfhydrated under physiological conditions [4, 5]. In the cardiovascular system, *S*-sulfhydration has been reported on several enzymes or receptors, including protein tyrosine phosphatase 1B, mitogen-activated extracellular signal-regulated kinase 1, and ATP synthase

subunit α. Sulfhydration induces transcription factors (such as specific protein-1 and NF-κB and interferon regulatory factor-1), and activates ion channels (including the voltage-activated Ca^{2+} channels and ATP-sensitive K+ channels), which all play a crucial role in lung biology and function [6].

Mechanistically, sulfhydration occurs through a nucleophilic attack of H_2S on an oxidized cysteine thiol. Methyl sulfide (MeSH), the methyl metabolite of H_2S, is a stronger nucleophile than H_2S because of the inductive effect of the methyl group and should theoretically react with protein cysteines at rates similar to or even better than H_2S. Similar to H_2S, MeSH also circulates in plasma and RBC. Blom *et al.* identified a reduction-labile pool of MeSH bound to blood proteins suggesting that there is a sizable portion of blood proteins that are adducted by MeSH. Zeigler *et al.* developed a method to measure H2S and MeSH in blood and plasma and measured significantly higher MeSH levels in the plasma of postpartum women compared to levels during gestation, but only when women with hypertension or preeclampsia were not included in the analysis[7]. Lower MeSH levels in women with pathological pregnancies may indicate that this metabolite is important in the biochemical etiology of hypertension or preeclampsia. In addition, low mass resolution evidence of MeSH adducted to Cys-34 of human serum albumin (HSA) has been published previously [7-9]. We hypothesize that circulating endogenous MeSH can adduct protein cysteine thiols, in a mechanism similar to sulfhydration that we have coined sulfmethylation. However, to date, this endogenous protein mass modification has not been unequivocally confirmed due to limitations to the current analytical methods to measure sulfmethylated protein cysteine thiols.

Sulfhydration has historically been studied using an affinity capture technique, allowing sulfhydrated and non-sulfhydrated proteins to be separated and analyzed independently. Free

cysteine thiols and sulfhydrated cysteine thiols will both react with alkylating agents such as maleimide. The alkylating agent is conjugated to an affinity capture tag such as biotin. The free thiol and sulfhydryl population of proteins can be separated from other proteins through affinity capture. The sulfhydryl proteins can then be separated from the free thiol population by releasing them from the affinity tag following reduction (Figure 4.1 step 3). Unfortunately, this analytical method cannot be applied to sulfmethylated proteins because they are chemically indistinguishable from protein inter and intramolecular disulfides. To identify a sulfmethylated protein, two conditions need to be met. First, the sulfmethylated peptide in the protein needs to be amenable to digestion by non-reducing proteolysis, and second, the free peptide needs to be abundant enough to be measured on a high-resolution mass spectrometer. Adding to the complexity of accurately identifying a sulfmethylated peptide, the sulfmethyl modification is nearly identical in mass to another potential protein cysteine modification, methyl sulfinate (Figure 4.2).

To overcome the challenges in detecting a sulfmethyl modification, we combined a directed proteomics approach with an isotope-based quantitative strategy that is tailored to both identify and quantify MeSH modifications. Briefly, this technique utilized ^{13}C-S-methyl methanthiosulfonate (^{13}C-MMTS) to cap free cysteine thiols. Free cysteine thiols that are labeled by ^{13}C-MMTS are chemically identical to sulfmethylated cysteine thiols. We assumed that proteins with endogenously sulfmethylated cysteines will also have a population with free cysteines. Once ^{13}C-MMTS is added to a protein homogenate, the free thiol population and the sulfmethylated populations of single proteins would become chemically identical but no information is lost as the free thiol population could be distinguished by the heavy isotope label.

This labeling approach allows us to confidently identify and quantify endogenously sulfmethylated proteins.

In this chapter, for the first time, we demonstrate that sulfmethylation is chemically possible under physiological conditions, and we cover the development of a novel labeling technique that allows for the confident identification and quantification of endogenous sulfmethylated proteins using conventional LC-MS bottom-up proteomic analysis of labeled protein homogenate. We used human plasma to develop this methodology because it contains a high amount of human serum albumin, a protein that is reportedly sulfmethylated [9-13]. The techniques developed in our lab, and reported in this chapter, will allow future researchers to probe the relationship between TMT1-mediated H_2S methylation and gaseous sulfide signaling, identify proteins that carry this post translational modification, and investigate the role of cysteine sulfmethylation in physiology and pathophysiology.

4.2 Materials and Methods

4.2.1 *Materials*

^{13}C-methyl methanethiosulfonate, ammonium bicarbonate, methyl methanethiosulfonate, sodium hydrosulfide, sodium methyl sulfide (also known as sodium thiomethoxide), and phosphate buffered saline were obtained from Sigma Aldrich (St. Louis, MO). Chloroform, formic acid (Optima grade), hydrogen peroxide, methanol, reduced glutathione, and water (Optima grade) were obtained from Fisher Scientific (Hampton, NH). MS grade trypsin was purchased from Thermo Fisher Scientific (Waltham, MA). The human blood plasma was obtained from Bloodworks Northwest.

4.2.2 *Non-reducing digestion and proteomic analysis of human plasma treated with gaseous sulfides*

Single donor human plasma was combined 1:1 with phosphate-buffered saline (PBS) pH 7.4. A 70 µL volume of diluted plasma was combined with reduced glutathione, sodium hydrosulfide (H_2S donor), sodium thiomethoxide (MeSH donor), or a combination of sodium hydrosulfide and sodium thiomethoxide. The sulfide donors were dissolved in PBS within 5 min of adding to plasma. Each sulfide-treated sample was made in duplicate. Half of the samples, were treated with hydrogen peroxide (H_2O_2) diluted in PBS and the other half were treated with PBS. The final concentration of each sulfide was 100 µM. The samples had a final H_2O_2 content of 0.1% and the final total volume was 100 µL. Samples were then incubated in a shaking bath (300 rpm, 37°C) for 1 h.

Solution (A) made up of methanol:chloroform:water, 5:1:4, was prepared and then stirred vigorously to emulsify the immiscible components. After the 1 h incubation, 1 mL of solution A was transferred to the plasma samples. During this pipetting step, solution (A) was stirred with a magnetic stir bar to keep components emulsified. The plasma samples diluted with solution A, were then centrifuged for 5 min at 16,000 × g and 4°C. During centrifugation the protein in the samples precipitated and formed a disc that floated on the chloroform layer that formed between the water and methanol layer (Supplementary fig. 4.1). The solvent layers were aspirated by gently aspirating the top layer and then flicking the protein disc to the side wall of the tube to aspirate the bottom layer. After the water and methanol layers were aspirated, 0.5 mL of methanol was added to each tube. The methanol was gently rocked over the protein disc to wash it. The methanol wash was then aspirated, and the protein pellets were left to dry for 30 min by laying the tubes on their sides with the caps open at room temp.

After the pellets air dried, 65 µL of ammonium bicarbonate (ABC, 50 mM) was added to dissolve the pellet followed by 35 µL of trypsin (diluted in ABC to 1 µg/µL, MS grade, Thermo Fisher Scientific, Waltham MA, Ref: 90058, Lot: YE376315) added to each sample. This gave a rough mass ratio trypsin to plasma protein of 1:40. The samples were then digested for 16 h at 37°C, shaking at 300 rpm.

After 16 h, 30 µL of each sample was diluted into 70 µL of optima-grade water containing 0.1% formic acid. Finally, the samples were centrifuged for 15 min at 16,000 × g and 4°C. The supernatant was transferred to mass spec vials and analyzed by LC-MS analysis.

An Orbitrap Ascend Tribrid Mass Spectrometer coupled to an ACQUITY UPLC system was used for proteomic analysis, and 1 µL of each sample was injected into the column (1.0 ×150-mm Acquity UPLC BEH 1.7 µm C8 ;Waters, Milford, MA). A gradient (0.1 mL/min) with mobile phase A consisting of 0.1% formic acid in water and mobile phase B consisting of 0.1% formic acid in acetonitrile was used for peptide separation. The stepwise gradient used was: 0 to 2 min, 99% A. From 2 to 5 min the gradient shifted from 99% A to 88% A. From 5 min to 45 min the gradient shifted from 88% A to 50% A. The column was then washed with 100% B from 47 min to 52 min and finally equilibrated to starting conditions 99% A and 1 % B from 52 min to 60 min. Relevant peptides eluted between minute 26 and minute 36, during which mobile phase A was between 70% and 60%. Mass spec instrument tune settings were set for conventional data-dependent acquisition (DDA) for peptides. See supplementary table 4.1 for mass spectrometer instrument settings.

4.2.3 *Determining the lower limit of detection of naturally occurring sulfmethylated Cys-34*

Single donor human plasma was combined 1:1 with PBS pH 7.4. A 70 µL volume of diluted plasma was combined with 1 µL of sulfmethylating agent methyl methanethiosulfonate (MMTS)

or 1 µL of carbon-13 labeled MMTS (^{13}C-MMTS). PBS was added to increase the volume to 100 µL. Diluted plasma containing either MMTS or ^{13}C-MMTS was then incubated for 1 h at 37°C, shaking at 300 rpm. After 1 h, the plasma samples were prepped for digestion similar to the method described above in **section 4.2.2**. Plasma samples were then digested for 16 h. After 16 h, 90 µL of plasma digests were diluted into 210 µL of optima-grade water containing 0.1% formic acid. The samples were centrifuged for 15 min at 16,000 × g and 4°C. The MMTS labeled plasma sample and the ^{13}C-MMTS labeled plasma sample supernatant were combined to make 1:1000, 1:100, 1:10, and 1:1 (MMTS:^{13}C-MMTS) samples. Samples were then transferred to mass spec vials and analyzed by LC-MS analysis. MMTS labeled plasma digest, ^{13}C-MMTS labeled plasma digest, and the 1:1000, 1:100, 1:10, and 1:1 (MMTS:^{13}C-MMTS) samples were analyzed using the LC-MS method as described in **section 4.2.**

4.2.4 *Data Analysis*

Raw mass spec files containing relevant chromatographic and spectral data from the LC-MS analysis of the samples were analyzed with Byonic, a comprehensive peptide and protein search software, to identify HSA peptides, both free and modified. There were two parameter files used. One parameter file was set to identify HSA peptides with predefined modifications. See supplementary figure 4.2 for the full list of modifications. The second parameter file used a wildcard search function to identify HSA peptides with any mass modification from 0 to +308 Da on a cysteine residue. 308 was chosen as the maximum mass increase to search for because it is two Da above the expected mass increase from glutathionylation. The first parameter file was used to identify known peptide modifications while the wildcard search parameters were used as an unbiased screen to identify mass modifications. Once Byonic assigned peptide identities to the spectra in our raw mass spec files, the spectral ID files (MZID) generated using the first

parameter search were then used to build a spectral library in the MacCoss lab's Skyline, a peptide chromatography and analysis software suite (skyline.ms) [14, 15]. Peptides were then integrated with Skyline. For each treatment or experiment, Byonic analysis identified, with high confidence, over 90% of the peptides that make up HSA. The peptide that contains HSA's Cys-34 was the most abundant cysteine-containing peptide identified (Figure 4.3). Only peptides with Byonic identifications that scored greater than 150 were accepted and analyzed and only modified peptides with delta mod scores greater than 150 were accepted and analyzed.

4.3 RESULTS

4.3.1 *Methyl sulfide modifies cysteines under physiologically relevant reaction conditions.*

Human serum albumin, the most abundant protein in blood plasma, has a single free cysteine thiol that can react with circulating sulfides—Cys-34 [9]. Glutathione, an H_2S donor, or a MeSH donor were incubated with human plasma in the presence or absence of the oxidizing agent H_2O_2. The plasma proteins were then digested under non-reducing conditions and analyzed by conventional high-mass resolution LC-MS bottom-up proteomics techniques. The data analysis workflow was described in detail in the data analysis **section 4.2.4.** Briefly, raw mass spec files containing relevant chromatographic and spectral data from the LC-MS analysis of the samples were analyzed with Byonic, a comprehensive peptide and protein search software, to identify HSA peptides, both free and modified. The spectra files from the identified peptides were then used to build spectral libraries in The MacCoss lab's Skyline, a peptide chromatography and analysis software suite [15]. Peptides were then integrated with Skyline [14]. For each treatment, Byonic analysis identified, with high confidence, over 90% of the peptides that make up HSA. The peptide that contains HSA's Cys-34 was the most abundant cysteine-containing peptide identified (Figure 4.3).

Byonic's "wildcard" search identifies peptides with a defined range of modification on a user-defined residue. The wildcard search was set to identify peptides modified by a mass between 0 and +308 Da on a cysteine residue. Several modified Cys-34 peptides were identified in the untreated (control) plasma sample, including carboxymethylated, cysteinylated, di-oxidized, and tri-oxidized Cys-34 (Figure 4.2 & Figure 4.4). When plasma was incubated with the MeSH donor, sulfmethylated Cys-34 adducts were identified using the wildcard search as a +45.9877 Da mass increase (Figure 4.4.B & Supplementary fig. 4.3). This modification was observed in samples treated with a MeSH donor with and without H_2O_2 but not in control samples. The most prevalent modification in samples treated with H_2O_2 was di-oxidation (Figure 4.4.D). The prevalence of cysteinylated Cys-34 also increased under oxidizing conditions. The carboxymethyl adducted Cys-34 containing peptide was identified in the control samples, but it diminished in prevalence following the addition of sulfides, and it disappeared entirely in samples treated with H_2O_2. Cys-34 modified by sulfur dioxide was identified in low abundance, compared to other modifications, in the sample treated with both the H_2S donor and H_2O_2 (Supplementary fig. 4.4). Glutathionylated Cys-34 was identified in very low abundance in the sample treated with glutathione and H_2O_2 (Supplementary fig. 4.4). See supplementary figure 4.5 for chromatograms for the modified peptides discussed in this section. The experiment reported in this section was performed multiple times, and the results were consistent across the days that this experiment was performed.

4.3.2 *Development of a labeling method to confidently identify and quantify sulfmethylated HSA Cys-34*

To improve confidence that a peptide identified as a sulfmethylated peptide, following proteomic analysis, is indeed sulfmethylated and not mislabeled by peptide identification

software, we developed a novel labeling technique we call “homogenous label adductomics”. This technique assumes that for most adducts, the unmodified population is larger than the modified population. The unmodified and modified populations can then be homogenized by labeling the unmodified population with a label identical to the modified population. The information is maintained because the unmodified population’s label will contain a heavy isotope to differentiate it from the endogenous label. The ratio of a peptide’s precursor isotopes can then be used to determine the abundance of the modified population relative to the unmodified population (Figure 4.5). In practice, we assumed HSA has a large population of free thiol Cys-34 and a small population of sulfmethylated Cys-34. The free thiol and sulfmethylated populations were homogenized by incubating human plasma with the isotopically stable labeled sulfmethylating agent ^{13}C-MMTS.

The sulfmethylated Cys-34 containing peptide was identified with high confidence in samples treated with ^{13}C-MMTS. Whether the plasma samples were labeled with ^{13}C-MMTS or MMTS, the retention times for both sulfmethylated peptides at Cys-34 were identical (data not shown). MMTS and ^{13}C-MMTS plasma digests were combined in different ratios to identify a lower limit of detection of the sulfmethylated Cys-34 containing peptide. The monoisotopic (M) precursor ion for the sulfmethylated Cys-34 containing peptide was decreased in the ^{13}C-MMTS treated sample and at an expected level relative to the M+1 and M+2 ions in the sample treated with MMTS (Supplementary fig. 4.6). The M, M+1, and M+2 precursor ions can be clearly resolved by the Thermo Fisher Scientific Ascend (Figure 4.6.A). The ratio of M and M+1 or M and M+2 increased with the percent of MMTS labeled plasma digest added to ^{13}C-MMTS labeled plasma digest (Figure 4.6.B). A small but detectable signal from the M precursor ion in the ^{13}C-MMTS only labeled plasma was observed (Figure 4.6.A). We considered this the baseline signal for the

M precursor for ^{13}C-MMTS labeled plasma because with no MMTS added to the samples, there was no signal at all for any precursor of the sulfmethylated Cys-34 containing peptide. The sample containing 0.1% MMTS had a larger M precursor signal than the ^{13}C-MMTS baseline. From this study's results, the limit of detection is assumed to be at least 0.1% modified Cys-34 per unmodified Cys-34, but to identify a true limit of detection for this method, multiple replicates of ^{13}C-MMTS labeled plasma would need to be analyzed to determine the variation in the M precursor signal.

4.4 DISCUSSION

Here, we establish that under physiologically relevant reaction conditions—pH 7.4, 37°C, and physiologically relevant low micromolar MeSH, human serum albumin can be sulfmethylated by MeSH. Furthermore, we developed a labeling technique we call "homogenous label adductomics" that allows for the high-confidence identification of sulfmethylated HSA.

Plasma was chosen as the ideal matrix for these assays because the most abundant plasma protein, HSA, contains a free thiol cysteine that is prone to small molecule modifications *in vivo* [16]. HSA contains 35 cysteine residues, 34 of which are involved in 17 intramolecular disulfide bonds that stabilize the tertiary structure of HSA, leaving one (Cys-34) unpaired thiol that accounts for 80% of plasma's free thiol [17, 18]. Several authors have published low-mass-resolution evidence of sulfmethylated Cys-34 following non-reducing tryptic digestion and bottom-up proteomic analysis, but they did not confirm with a peptide standard that the modification in question was indeed sulfmethylation or any other modification with similar molecular weight [9-13].

The homogenous label adductomics technique developed here allows high-confidence identification of small molecule adducts like the Cys-34-sulfmethyl adduct by labeling

unmodified protein residues with the heavy stable isotopes of the modification of interest. The technique is powerful for proteomics applications: a protein modified by a ^{13}C isotope label will behave the same as a protein modified by the same endogenous label. The artificially modified proteins will be digested with the same efficiency as endogenously modified proteins, and the heavy labeled and naturally modified peptides liberated during digestion should have the same retention time and, ionize and fragment, in an identical fashion during proteomic analysis.

We applied the homogenous label adductomics technique to identify naturally occurring sulfmethylated Cys-34 in human donor plasma by incubating plasma with ^{13}C-MMTS, a sulfmethylating agent, prior to non-reducing proteomic analysis. To test this assay, we diluted different quantities of MMTS-labeled plasma digest into ^{13}C-MMTS plasma digest and analyzed the digested plasma samples with LC-MS bottom-up proteomics. Cys-34 was the only HSA residue that was sulfmethylated by MMTS. Byonic, the peptide and protein search software used to assign peptides and mass modifications to LC-MS precursor and fragmentation spectra, identified the Cys-34 containing HSA peptide in the ^{13}C-MMTS labeled plasma digest with a mass increase consistent with sulfmethylation and an isotopic distribution that is consistent with a peptide containing a ^{13}C-enriched modification—the monoisotopic, M, precursor mass was nearly undetectable (Figure 4.6.A and Supplementary fig. 4.6). A positively skewed isotopic distribution is a powerful secondary confirmation that the modified peptide has been correctly identified. As the percentage of MMTS-labeled plasma digest was increased relative to ^{13}C-MMTS labeled plasma, the M precursor ion increased proportionately, confirming that homogenized label adductomics can be used to identify endogenously modified residues and compare their abundance with the abundance of the same unmodified residue (Figure 4.6.B).

We demonstrate that it is chemically possible for MeSH to adduct Cys-34 in absence of hydrogen peroxide, while it is necessary for sulfhydration to occur. However, we could not detect sulfmethylation on Cys-34 of HSA in the individual single donor plasma we used for these proteomics assays. We did observe a small signal from the M precursor ion in the ^{13}C-MMTS only labeled plasma (Figure 4.6.A); but this signal can be attributed to the ^{13}C-MMTS label because no signal exists for any sulfmethylated peptide precursors without the addition of MMTS or exogenous methyl sulfide. Either the sulfmethylated modification does not occur on Cys-34 in this plasma sample, or the sulfmethylated species falls below the limit of detection of this method. More work is necessary to define the limit of detection. Once it is confirmed, several different donor plasma samples can be screened for sulfmethylation to confirm or negate the existence of endogenously sulfmethylated Cys-34.

We predicted that since MeSH is a better nucleophile than H_2S and it circulates at similar concentrations, it should theoretically be better at adducting cysteine thiols. We incubated plasma with an H_2S or MeSH donor under identical reaction conditions. Only the sulfmethyl adduct was observed in MeSH-donor-treated samples, and no sulfhydrated Cys-34 was identified in any of the treatments. Sulfhydration require an oxidized cysteine thiol to proceed, so we expected the oxidizing agent H_2O_2 to increase the prevalence of sulfhydrated Cys-34 [3, 19]. The prevalence of sulfmethylated Cys-34 was not altered by cotreatment with H_2O_2 compared to plasma treated with the MeSH donor alone (Figure 4.4.B). H_2O_2-treated plasma, in the presence of H_2S or MeSH, contained increased levels of di-oxidized Cys-34 (Figure 4.4.D), which cannot react with MeSH. For Cys-34 to be sulfmethylated in samples not treated with H_2O_2, a certain level of endogenous population of oxidation state 0 or -1 on the Cys-34 sulfur must exist to react with MeSH (Figure 4.7) [3, 19]. It is possible that MeSH reacted with Cys-34 disulfide bonded

to a peptide, protein, or a circulating thiol-metabolite. MeSH could also have reacted with cys-34 oxidized to sulfenic acid, or even with nitrosylated (Cys-S-NO) Cys-34 [3]. Human plasma treated with MeSH-donor alone or cotreated with MeSH-donor and H_2O_2 both had the same level of sulfmethylated Cys-34. This suggests that the endogenous population of Cys-34 that MeSH must have reacted with was unaffected by H_2O_2. Sulfinic acid and nitrosylated cysteine thiols can be further oxidized by H_2O_2, while disulfides cannot. Therefore, it is most likely that MeSH is reacting with an endogenous disulfide bond, releasing a free thiol in samples treated with or without H_2O_2 [19]. More work is necessary to understand what conditions promote sulfmethylation.

Other Cys-34 modifications were identified while analyzing the digested plasma samples treated with sulfide donors and/or H_2O_2, the modifications included di-oxidation, tri-oxidation, carboxymethylation, and cysteinylation (Figure 4.4). Each Cys-34 modification identified has been previously reported, however, the carboxymethyl modification was unexpected as it normally occurs on residues with primary amine R groups that have reacted with endogenous glyoxal [10, 20]. As expected, the sulfinate and sulfonate Cys-34 modifications were more prevalent in samples treated with H_2O_2, with sulfinic Cys-34 being the predominant modification in H_2O_2-treated samples (Figure 4.4.D and 4.4.E). Cysteinylated Cys-34 was present in untreated plasma, however, its levels decreased in plasma samples treated with sulfides, and increased in samples treated with H_2O_2 (Figure 4.4.F).

Cysteine is reported to be the most abundant thiol bound to HSA's Cys-34 [21]. Increased cysteinylation is associated with various diseases, including heart failure, kidney disease, and diabetes [22-24]. Bocedi *et al.* report cysteine, compared to other circulating small molecule thiols, is the most efficient at reducing mono-oxidized (sulfenic acid) Cys-34 [17]. Free thiol

cysteine in the plasma likely reacted with Cys-34 when it was oxidized by H_2O_2; this could explain why cysteinylation increased in the presence of H_2O_2. It is possible that the decrease in cysteinylation when plasma samples were incubated with sulfides was caused by the exogenous sulfides reducing cysteinylated Cys-34 through a di-sulfide exchange. The plasma concentration of cysteine is between 200 and 300 µM. The concentration of MeSH in plasma is below 50 µM. Future work should explore the rank order reducing power of MeSH and cysteine. Also, it will be important to determine if MeSH can react with cysteinylated Cys-34 and, if so, which sulfur is the preferred electrophile if MeSH is the acting nucleophile.

Homogenous label adductomics was applied in this work to confidently identify sulfmethylated cysteine residues but its utility can extend to other protein modifications. If efficient cysteinylation of free thiol cysteine residues is possible without disrupting endogenous modifications, the homogenous label adductomics technique can be applied to identify and quantify cysteinylated-Cys residues. Cysteine is chemically similar to many of the small molecule thiols in plasma. If the homogenous label adductomics technique can be applied to cysteinylation, it will work for many other small molecule disulfide modifications.

4.5 CONCLUSION

In previous chapters, we presented the characterization of TMT1A and TMT1B, the thiol methyltransferases responsible for the methylation of exogenous alkyl thiols. In this chapter, we discussed the development of a proteomics technique and workflow to identify and study sulfmethylation, a protein mass modification caused by MeSH, a putative endogenous metabolite of TMT1A and TMT1B. Through the homogenous label adductomics method, which utilized MMTS labeling, that we developed in this work; we can identify and quantify sulfmethylated cysteine residues at least as low as 0.1% of their respective free thiols but more work is

necessary to calculate an accurate limit of detection. This method was developed using plasma because of plasma's well characterized HSA protein modifications; however, the method will be more powerful when it is applied to a complex protein homogenate from, for example, heart tissue to observe many modified proteins at once. In future work, we will use this homogenous label adductomics MMTS labeling method to survey several donor plasma samples for sulfmethylated Cys-34. Additionally, we aim to identify other sulfmethylated proteins in heart tissue. Finally, we hope to expand the homogenized label adductomics method to other protein modifications such as cysteinylation. The methods developed and discussed in this chapter will help improve our understanding of H_2S and MeSH mediated cysteine adduction and the importance of these adducts in physiology and pathophysiology.

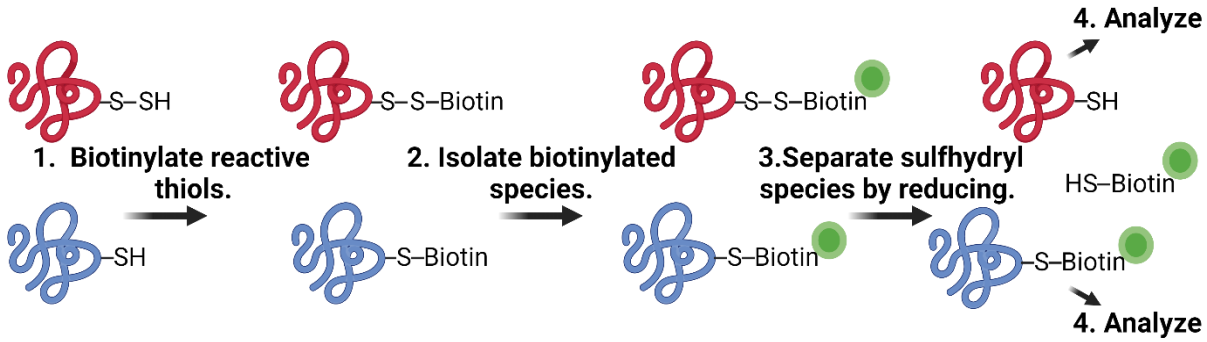

Figure 4.1. General scheme for isolating and analyzing sulfhydrated proteins

Adduct	Structure	Mass Addition	+3 Precursor M/Z
No Adduct		00.0000	811.7594
Sulfhydration		31.9720	822.4167
Sulfmethylation	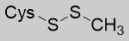	45.9877	827.0886
Methyl Sulfinate	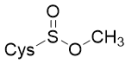	46.0054	827.0945
Sulfenic Acid		47.9669	827.7484
Sulfinic Acid		31.9898	822.4226
Sulfonic Acid		47.9847	827.7544
Sulfur Dioxide	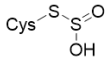	63.9619	833.0800
Carboxymethyl	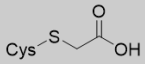	58.0055	831.0945
Cysteinylation	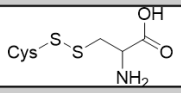	119.0041	851.4274
Glutathionylation		305.0681	913.4488

Figure 4.2. Small molecule cysteine protein adductions for the HSA peptide that contains Cys-34

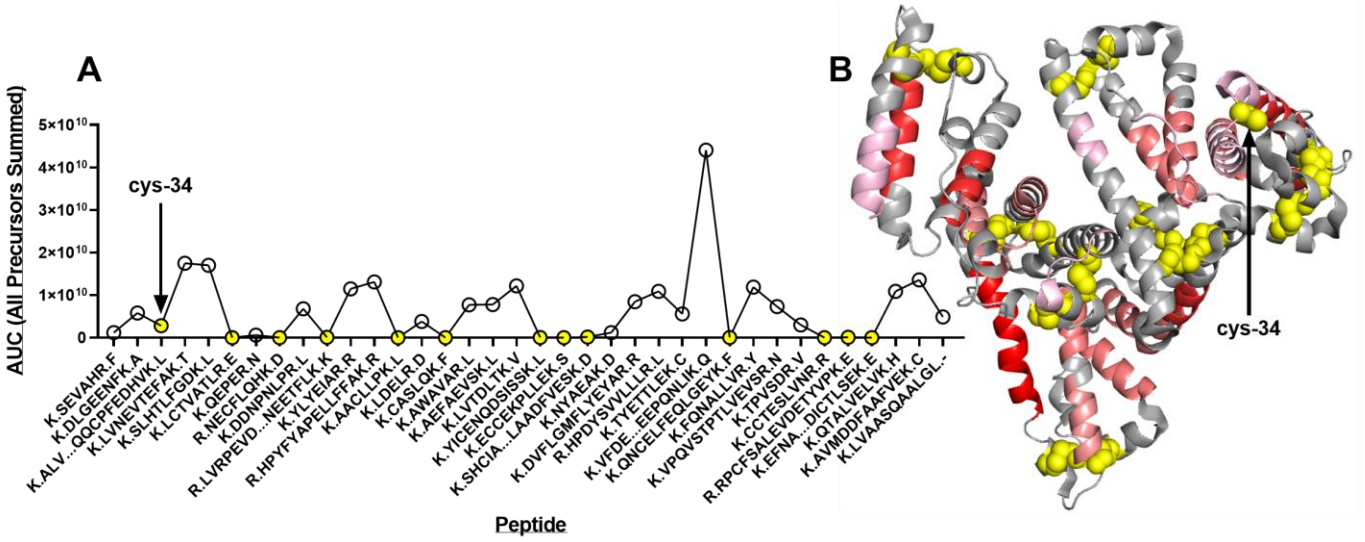

Figure 4.3. Precursor abundance of cysteine containing peptides identified by proteomic analysis

AUC of all precursors for each HSA peptide identified in untreated (control), digested human plasma (A). HSA crystal structure 1H9Z [25] with peptides highlighted based on precursor abundance (B). Grey—least abundant. Bright red—most abundant. Cysteine side chains are rendered as bright yellow spheres.

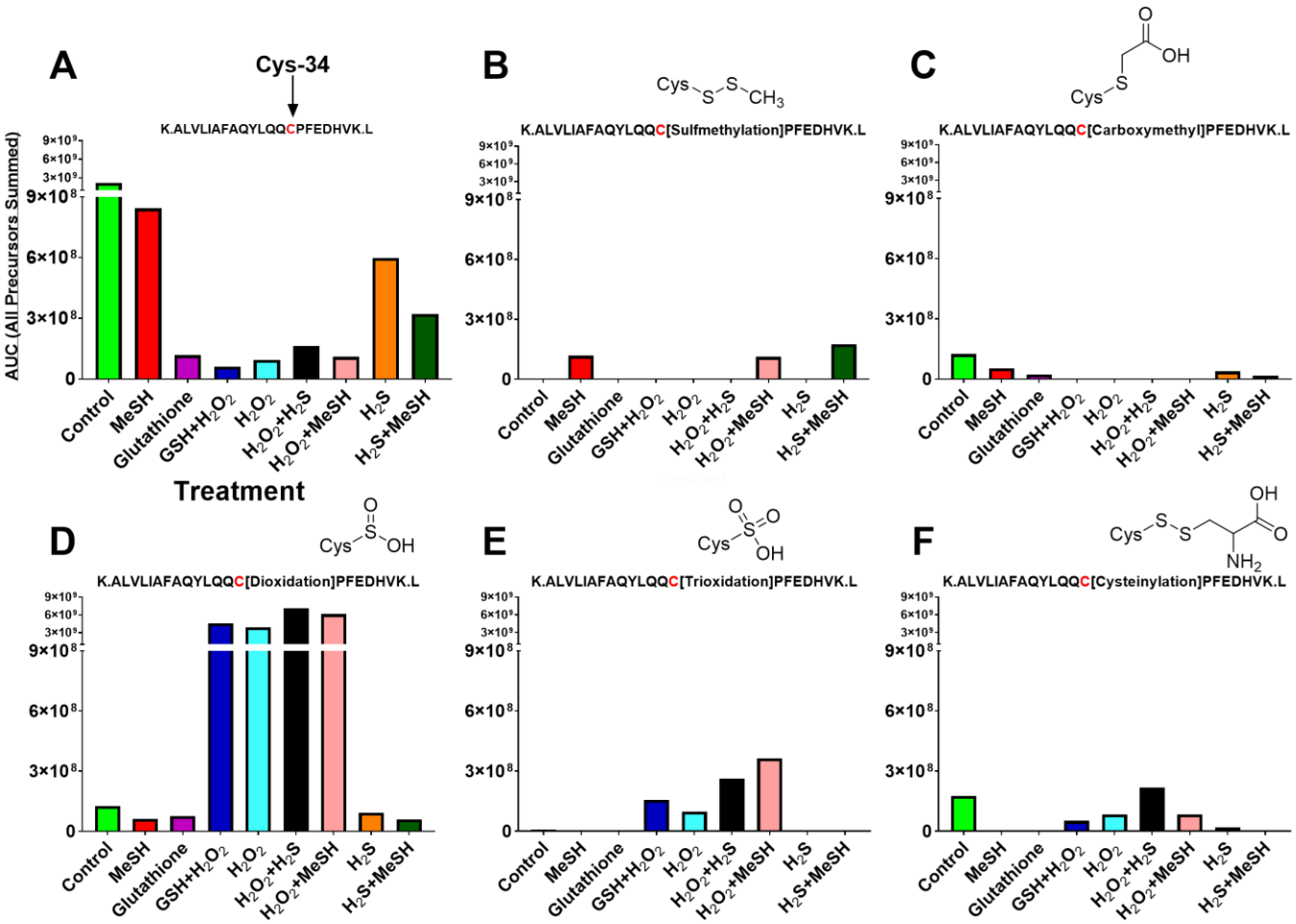

Figure 4.4. Cys-34 peptide modifications identified by proteomic analysis

AUC of all precursors for each modified HSA Cys-34 peptide identified in untreated (control), and sulfide treated samples ±H_2O_2. Panes are as follows: native, no modification (A), sulfmethylated (B), carboxymethylated (C), di-oxidized (D), tri-oxidized (E), and cysteinylated (F) Cys-34.

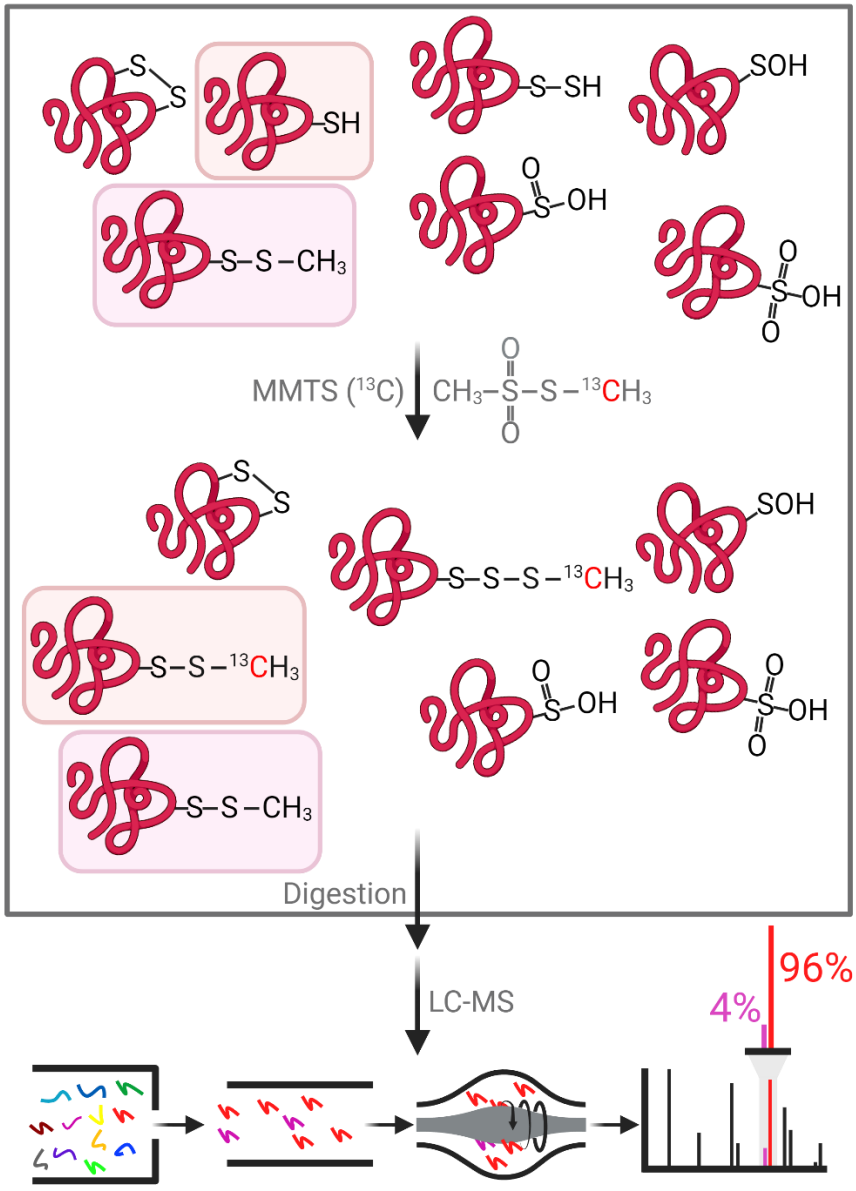

Figure 4.5. General workflow for homogenous label adductomics

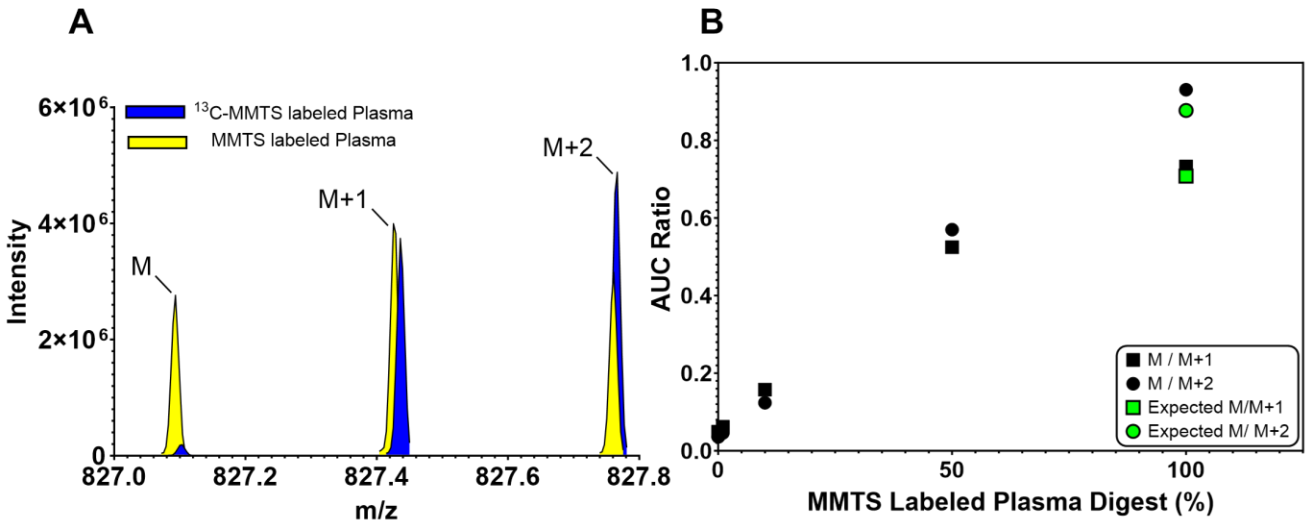

Figure 4.6. Mass spectrum of Cys-34 peptide precursor ions and ratio of precursor masses correlated with ratio of MMTS labeled and ^{13}C-MMTS labeled plasma

Mass spectrum of M, M+1, and M+2 peptide precursor ions identified as HSA's sulfmethylated Cys-34 containing peptide. From the proteomic analysis of ^{13}C-MMTS treated plasma and MMTS treated plasma. The ^{13}C-MMTS spectrum is shifted by 0.01 m/z to allow each mass peak to be observed (A). MMTS labeled plasma digest was combined with ^{13}C-MMTS labeled plasma, digested and analyzed, and the ratio of the M and M+1 or M+2 precursor ions assigned to HSA's sulfmethylated Cys-34 containing peptide are plotted by percent MMTS labeled plasma added to ^{13}C-MMTS labeled plasma (B).

Compound	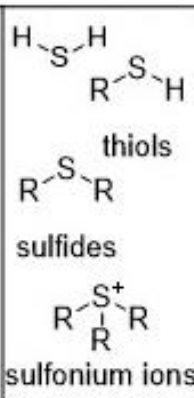	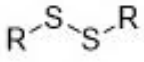	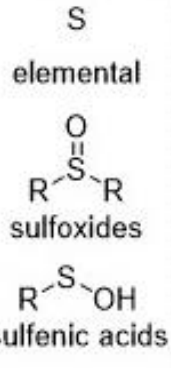	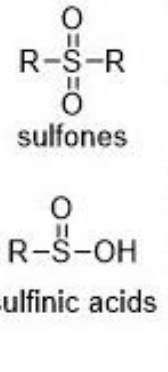	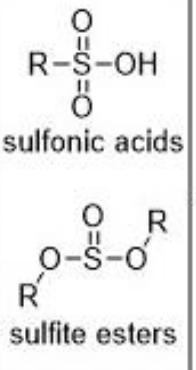	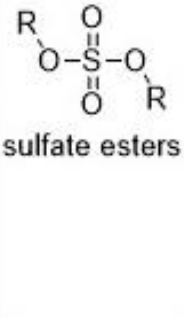
Oxidation State	**-2**	**-1**	**0**	**+2**	**+4**	**+6**

Figure 4.7. Sulfur oxidation states in some relevant organic compounds

.

4.6 REFERENCES

1. Maldonato, B.J., *METTL7 Alkyl Thiol Methyltransferases: Implications in Drug Metabolism and Human Health,* in *Medicinal Chemistry*. 2020, University of Washington: Seattle. p. 238.

2. Maldonato, B.J., D.A. Russell, and R.A. Totah, *Human METTL7B is an alkyl thiol methyltransferase that metabolizes hydrogen sulfide and captopril.* Sci Rep, 2021. **11**(1): p. 4857.

3. Zhang, D., et al., *H2S-Induced Sulfhydration: Biological Function and Detection Methodology.* Front Pharmacol, 2017. **8**: p. 608.

4. Mustafa, A.K., et al., *H2S signals through protein S-sulfhydration.* Sci Signal, 2009. **2**(96): p. ra72.

5. Mustafa, A.K., et al., *Hydrogen sulfide as endothelium-derived hyperpolarizing factor sulfhydrates potassium channels.* Circ Res, 2011. **109**(11): p. 1259-68.

6. Meng, G., et al., *Protein S-sulfhydration by hydrogen sulfide in cardiovascular system.* Br J Pharmacol, 2018. **175**(8): p. 1146-1156.

7. Zeigler, M.B., et al., *Plasma hydrogen sulfide, nitric oxide, and thiocyanate levels are lower during pregnancy compared to postpartum in a cohort of women from the Pacific northwest of the United States.* Life Sci, 2023. **322**: p. 121625.

8. Blom, H.J., et al., *Transamination of methionine in humans.* Clin Sci (Lond), 1989. **76**(1): p. 43-9.

9. Funk, W.E., et al., *Human Serum Albumin Cys34 Adducts in Newborn Dried Blood Spots: Associations With Air Pollution Exposure During Pregnancy.* Front Public Health, 2021. **9**: p. 730369.

10. Carlsson, H., S.M. Rappaport, and M. Törnqvist, *Protein Adductomics: Methodologies for Untargeted Screening of Adducts to Serum Albumin and Hemoglobin in Human Blood Samples.* High Throughput, 2019. **8**(1).

11. Grigoryan, H., et al., *Adductomic signatures of benzene exposure provide insights into cancer induction.* Carcinogenesis, 2018. **39**(5): p. 661-668.

12. Lu, S.S., et al., *Profiling the Serum Albumin Cys34 Adductome of Solid Fuel Users in Xuanwei and Fuyuan, China.* Environ Sci Technol, 2017. **51**(1): p. 46-57.

13. Yano, Y., et al., *Untargeted adductomics of Cys34 modifications to human serum albumin in newborn dried blood spots.* Anal Bioanal Chem, 2019. **411**(11): p. 2351-2362.

14. MacLean, B., et al., *Skyline: an open source document editor for creating and analyzing targeted proteomics experiments.* Bioinformatics, 2010. **26**(7): p. 966-8.

15. Pino, L.K., et al., *The Skyline ecosystem: Informatics for quantitative mass spectrometry proteomics.* Mass Spectrom Rev, 2020. **39**(3): p. 229-244.

16. Turell, L., R. Radi, and B. Alvarez, *The thiol pool in human plasma: the central contribution of albumin to redox processes.* Free Radic Biol Med, 2013. **65**: p. 244-253.

17. Bocedi, A., et al., *Thiol disulfide exchange reactions in human serum albumin: the apparent paradox of the redox transitions of Cys.* FEBS J, 2018. **285**(17): p. 3225-3237.

18. M, H., E. Azzazy, and R.H. Christenson, *All About Albumin: Biochemistry, Genetics, and Medical Applications. Theodore Peters, Jr. San Diego, CA: Academic Press, 1996, 432 pp, $85.00. ISBN 0-12-552110-3.* Clinical Chemistry, 1997. **43**(10): p. 2014a-2015.

19. Turell, L., et al., *Sulfenic acid--a key intermediate in albumin thiol oxidation.* J Chromatogr B Analyt Technol Biomed Life Sci, 2009. **877**(28): p. 3384-92.

20. Anguizola, J., et al., *Review: Glycation of human serum albumin.* Clin Chim Acta, 2013. **425**: p. 64-76.

21. Mansoor, M.A., A.M. Svardal, and P.M. Ueland, *Determination of the in vivo redox status of cysteine, cysteinylglycine, homocysteine, and glutathione in human plasma.* Anal Biochem, 1992. **200**(2): p. 218-29.

22. Brioschi, M., et al., *S-Thiolation Targets Albumin in Heart Failure.* Antioxidants (Basel), 2020. **9**(8).

23. Figueroa, S.M., et al., *Oxidized Albumin as a Mediator of Kidney Disease.* Antioxidants (Basel), 2021. **10**(3).

24. Imafuku, T., et al., *Cysteinylated Albumin as a Potential Biomarker for the Progression of Kidney Disease in Patients With Type 2 Diabetes.* Diabetes Care, 2021. **44**(6): p. e115-e117.

25. Petitpas, I., et al., *Crystal structure analysis of warfarin binding to human serum albumin: anatomy of drug site I.* J Biol Chem, 2001. **276**(25): p. 22804-9.

Chapter 5. **Conclusion and Future Directions**

5.1 CONCLUSION

The main goal of this dissertation project was to biochemically characterize the enzyme thiol methyltransferase 1A (TMT1A, formally METTL7A), and to identify key features that are important for its activity. This work builds on the discovery that thiol methyltransferase 1B (TMT1B), an enzyme homologous to TMT1A and in the same family, is an alkyl thiol methyltransferase (TMT, [1]). Active TMT1A was overexpressed in *E. coli* and purified. The purified enzyme was biochemically similar to TMT1B, in that it required the lipid DMPG for activity, and preferentially methylated alkyl thiols. Interestingly, TMT1A was inhibited by DCMB, while purified TMT1B was not. Overexpression and knockdown of *TMT1A* and *TMT1B* in immortalized human cancer cells confirmed that TMT1A and TMT1B are both alkyl thiol methyltransferases but only TMT1A is inhibited by DCMB.

A panel of individual donor human liver microsomes was screened using 7α-thiospironolactone (TSL) methylation to report TMT activity. The protein levels of TMT1A and TMT1B in each donor microsomal sample were measured using quantitative proteomic analysis. TMT activity correlated well with the sum of TMT1A and TMT1B protein levels. Microsomal TMT activity was almost completely inhibited by DCMB, consistent with what has been reported previously. Because TMT1A is inhibited by DCMB while TMT1B is not, we concluded that TMT1A must be responsible for the majority of TMT activity in human liver.

TMT1A and TMT1B have similar amino acid sequences, it was surprising that one would be potently inhibited by a small molecule such as DCMB while the other is not at all affected. AlphaFold homology models were examined to understand the differences in structure and activity of TMT1A and TMT1B. A conserved substrate binding site was identified in each

homology model. This site contains four residues that are distinct between TMT1A and TMT1B. The different residues are aromatic in the TMT1A substrate binding site but are aliphatic in the TMT1B. Through site directed mutagenesis, a single aromatic residue, Tyr-47, was identified to be vital for DCMB inhibition of TMT1A. When Tyr-47 was mutated to the corresponding Ser residue at position 47 in TMT1B, (Tyr47Ser) TMT1A was no longer inhibited by DCMB.

A bacterial expression system was developed to produce large quantities of TMT1A by isolating TMT1A spheroplasts. The isolated spheroplasts were suitable for biochemical characterization and were used to conduct a structure activity relationship (SAR) analysis of DCMB congeners as potential inhibitors of TMT1A. Consistent with the SAR analysis conducted by Glauser *et al.*, we determined that TMT1A is inhibited by neutral to positively charged small aromatic molecules [2].

The other thiol methyltransferase, thiopurine methyltransferase (TPMT), was also expressed in bacteria and purified. Purified TPMT methylated both 6-mercaptopurine (6-MP) and 4-nitrobenzenethiol (4-NBT), but it did not methylate the alkyl thiol TSL. TMT1A spheroplasts did not methylate 6-MP or 4-NBT, which is consistent with what has been reported in the literature for microsomal and erythrocyte TMT [3, 4].

Hydrogen sulfide (H_2S) was identified as a putative substrate of TMT1A. A metabolite of H_2S, methylsulfide (MeSH), can potentially adduct cysteine thiols. A homogenous label adductomics technique was developed which allowed for the confident identification and quantification of MeSH adducted cysteine residues relative to their respective free thiols. Using this adductomics technique, MeSH adducted human serum albumin was confidently identified in plasma that had been incubated with physiologically relevant levels of the MeSH donor sodium methyl sulfide but no endogenous sulfmethylation was detected in untreated plasma. This

confirmed that MeSH adduction of protein thiols is chemically possible at physiological conditions, but endogenous Cys-34 sulfmethylation either does not occur or is below the limit of detection of our assay.

5.2 Future Directions

The focus of thiol methyltransferase research so far has been geared towards drug metabolism but TMT1A and TMT1B are clearly important for endogenous signaling. Future work should aim to identify how these enzymes are involved in cellular signaling, especially as it pertains to cancer. The endogenous gasotransmitter hydrogen sulfide is a potential endogenous substrate for TMT1A and TMT1B, but it is difficult to study because it is a gas with a very short half-life. A specific inhibitor for TMT1B would be a useful tool to study the relationship between these enzymes and endogenous small molecule metabolism. We identified key differences between TMT1A and TMT1B that will help researchers design an inhibitor that is specific for TMT1B. We also developed a methodology to screen potential inhibitors using TMT1 spheroplasts.

The mutagenesis work that we discussed clearly demonstrates that Tyr-47 is important for DCMB to inhibit TMT1A, but to improve confidence and explore this relationship further, the same mutagenesis experiment should be attempted using the plasmid designed for TMT1A spheroplasts. Mutant TMT1A expressed in bacteria and isolated as spheroplasts would be amendable to biochemical characterization. Furthermore, a more nuanced understanding of TMT1A and TMT1B inhibition could be achieved by also generating TMT1B spheroplast mutants with the TMT1B residues being mutated to the TMT1A residues at the same sequence position. S47Y-TMT1B should be the first mutant tested for inhibition in the presence of DCMB. The cysteine residues discussed in Chapter 3 should be studied as well. To start, the cysteine alkylation experiment performed by Borchardt *et al.* should be repeated with recombinant

TMT1A and TMT1B to determine if cysteine alkylation affects TMT1 activity. An improved understanding of these enzymes' structure and function will help with the development of a specific inhibitor for TMT1B.

Finally, we demonstrated that MeSH can adduct protein cysteine thiols and were able to identify and quantify MeSH adducted proteins but no endogenous MeSH adducted protein was observed in the single donor plasma that was used for method development in Chapter 4 despite being reported in the literature. Several single donor plasma samples should be screened to improve the chances of observing endogenous sulfmethylation if it is variable among subjects. Cysteinylated human serum albumin appears to be related to oxidation in plasma. The homogenous label adductomics technique could be applied to identify and quantify cysteinylated proteins. If heavy labeled cysteine could be activated to efficiently label free cysteine thiols, then the homogenous label adductomics technique could be applied to identify and quantify cysteinylated proteins. This could be another useful application of this proteomics technique.

5.3 REFERENCES

1. Maldonato, B.J., D.A. Russell, and R.A. Totah, *Human METTL7B is an alkyl thiol methyltransferase that metabolizes hydrogen sulfide and captopril.* Sci Rep, 2021. **11**(1): p. 4857.

2. Glauser, T.A., et al., *Human liver microsomal thiol methyltransferase: inhibition by arylalkylamines.* Xenobiotica, 1993. **23**(6): p. 657-69.

3. Keith, R.A., et al., *Human erythrocyte membrane thiol methyltransferase. S-methylation of captopril, N-acetylcysteine, and 7 alpha-thio-spirolactone.* Drug Metabolism and Disposition, 1984. **12**(6): p. 717-724.

4. Weisiger, R.A. and W.B. Jakoby, *Thiol S-methyltransferase.* Methods Enzymol, 1981. **77**: p. 257-62.

APPENDIX: CHAPTER 1

Supplementary Table 1.1 The distribution of TMT by specific activity

The distribution of TMT by specific activity [1-3] (left side of table). The RNA expression of TMT1A and TMT1B [4](right side of table).

Tissue Distribution of TMT					
	(Based on Specific activity)			(RNA Expression, From Tissue Atlas)	
	Jakoby (1980)	**Pacifici (1991)**	**Drummer (1983)**	**TMT1A**	**TMT1B**
1	Cecal Mucosa	Liver	Liver	Liver	Liver
2	Colonic Mucosa	Adrenal Gland	Heart	Thyroid Gland	Epididymis
3	Liver	Kidney	Spleen	Adipose Tissue	Heart
4	Lung	Lung	Lung	Kidney	Duodenum
5	Kidney	Intestine	Kidney	Pancreas	Small intestine
6	Jejunal mucosa		Erythrocyte	Fallopian Tube	Kidney
7	Ileal mucosa			Stomach	Colon

Supplementary Table 1.2 A list of *METTL* genes with known function, top tissue, and cellular distribution.

The gene's protein name, function, and cellular distribution are from protein reports curated by the universal protein database at www.uniprot.org. Top tissue by RNA expression is from tissue atlas [4].

The METTLs					
METTL	**Name**	**Function?**	**Specificity**	**Top Tissue**	**Cellular Distribution**
METTL1	**tRNA (guanine-N(7)-)-methyltransferase**	YES	RNA	Pancreas	Nucleoplasm
METTL2A	**tRNA N(3)-methylcytidine methyltransferase**	YES	RNA	Skeletal Muscle	NA
METTL2B	**tRNA N(3)-methylcytidine methyltransferase**	YES	RNA	Skeletal Muscle	NA
METTL3	**N6-adenosine-methyltransferase catalytic subunit**	YES	RNA	Tonsil	Cytosol and Nucleus
METTL4	**N(6)-adenine-specific methyltransferase**	YES	RNA	Adrenal Gland	Cytosol and Mitochondrial Matrix
METTL5	**rRNA N6-adenosine-methyltransferase**	YES	RNA	Stomach/Liver	Nucleus
METTL6	**tRNA N(3)-methylcytidine methyltransferase**	YES	RNA	Everywhere	Localized to vesicles
METTL7A	**Thiol methyltransferase family 1A**	NO	Alkyl Thiols	Liver	MembraneER/Lipid Droplets
METTL7B	**Thiol methyltransferase family 1B**	YES	Alkyl Thiols	Liver	MembraneER/Lipid Droplets
METTL8	**mRNA N(3)-methylcytidine methyltransferase**	YES	RNA	Esophagus	Cytoplasm/Nucleus
METTL9	**Protein-L-histidine N-pros-methyltransferase**	YES	Protein	Everywhere	MembraneER/Mitochondria
METTL10	**EEF1A lysine methyltransferase 2**	YES	Protein	Everywhere	Cytosol/Nucleus
METTL11A	**N-terminal Xaa-Pro-Lys N-methyltransferase 1**	YES	Protein	Everywhere	Nucleus
METTL11B	**N-terminal Xaa-Pro-Lys N-methyltransferase 2**	YES	Protein	Heart Muscle	Nucleus
METTL12	**Citrate synthase-lysine N-methyltransferase**	YES	Protein	Skeletal Muscle	Mitochondrial
METTL13	**eEF1A lysine and N-terminal methyltransferase**	YES	Protein	Epididymis	Cytosol/Mitochondria/Nucleus
METTL14	**N6-adenosine-methyltransferase non-catalytic subunit**	YES	RNA	Bone Marrow	Nucleus
METTL15	**12S rRNA N4-methylcytidine (m4C) methyltransferase**	YES	RNA	Tongue	Mitochondrial
METTL16	**RNA N6-adenosine-methyltransferase**	YES	RNA	Ovary	Cytosol/Nucleus
METTL17	**Methyltransferase-like protein 17, mitochondrial**	NO	NA	Adrenal Gland	Mitochondrial
METTL18	**Histidine protein methyltransferase 1 homolog**	YES	Protein	Parathyroid gland	Cytosol/Nucleus
METTL19	**Probable tRNA (uracil-O(2)-)-methyltransferase**	NO	NA	Skin	Cytosol
METTL20	**Electron transfer flavoprotein beta subunit lysine mTase**	YES	Protein	Liver	Cytosol
METTL21A	**Protein N-lysine methyltransferase**	YES	Protein	White matter	Cytosol
METTL21B	**EEF1A lysine methyltransferase 3**	YES	Protein	Pancreas	Cytosol
METTL21C	**Protein-lysine methyltransferase**	YES	Protein	Epididymis	Nucleus
METTL22	**Methyltransferase-like protein 22**	YES	Protein	Skeletal Muscle	Nucleus
METTL23	**Probable methyltransferase-like protein 23**	NO	NA	Testes/Liver	Membrane Bound
METTL24	**Probable methyltransferase-like protein 24**	NO	NA	Smooth muscle	Secreted
METTL25	**Probable methyltransferase-like protein 25**	NO	NA	White matter	Unknown
METTL25B	**Methyltransferase-like protein 25B**	NO	NA	Skeletal muscle	Membrane Bound
METTL26	**Methyltransferase-like 26**	NO	NA	Cerebral cortex	Golgi Apparatus
METTL27	**Methyltransferase-like protein 27**	NO	NA	Pancreas	Cytosol/Mitochondria

1. Drummer, O.H., P. Miach, and B. Jarrott, *S-methylation of captopril: Demonstration of captopril thiol methyltransferase activity in human erythrocytes and enzyme distribution in rat tissues.* Biochemical Pharmacology, 1983. **32**(10): p. 1557-1562.

2. Weisiger, R.A., & Jakoby, W.B, *S-Methylation: Thiol S-Methyltransferase*, in *Enzymatic Basis of Detoxication Volume 2*, W.B. Jakoby, Editor. 1980, Academic Press: New York, NY. p. 131-140.

3. Pacifici, G.M., et al., *Thiol methyltransferase in humans: development and tissue distribution.* Dev Pharmacol Ther, 1991. **17**(1-2): p. 8-15.

4. Uhlén, M., et al., *Proteomics. Tissue-based map of the human proteome.* Science, 2015. **347**(6220): p. 1260419.

.

APPENDIX: CHAPTER 2

Supplementary Table 2.1 Table showing sex of individual liver donors.

Liver ID	Sex	Age
HL-102	Male	21
HL-111	Male	28
HL-112	Male	28
Hl-114	Male	19
HL-136	Male	39
HL-141	Male	99
HL-154	Male	26
HL-161	Male	53
HL-163	Male	55
HL-105	Female	21
HL-108	Female	42
HL-115	Female	52
HL-131	Female	62
HL-132	Female	50
HL-135	Female	45
HL-152	Female	64
HL-159	Female	53
HL-164	Female	50
HL-165	Female	61

Supplementary Table 2.2 Table showing transitions for heavy labeled and unlabeled surrogate peptides for METTL7A (TMT1A) and METTL7B (TMT1B).

Peptide list	parent ions	fragmentations
sp|Q9H8H3|MET7A_HUMAN.VTC[CAM]IDPNPNFEK.+2y9.light	717.34	1073.53
sp|Q9H8H3|MET7A_HUMAN.VTC[CAM]IDPNPNFEK.+2y8.light	717.34	960.44
sp|Q9H8H3|MET7A_HUMAN.VTC[CAM]IDPNPNFEK.+2y7.light	717.34	845.42
sp|Q9H8H3|MET7A_HUMAN.VTC[CAM]IDPNPNFEK.+2y5.light	717.34	634.32
sp|Q9H8H3|MET7A_HUMAN.VTC[CAM]IDPNPNFEK.+2y9.heavy	721.35	1081.54
sp|Q9H8H3|MET7A_HUMAN.VTC[CAM]IDPNPNFEK.+2y8.heavy	721.35	968.46
sp|Q9H8H3|MET7A_HUMAN.VTC[CAM]IDPNPNFEK.+2y7.heavy	721.35	853.43
sp|Q9H8H3|MET7A_HUMAN.VTC[CAM]IDPNPNFEK.+2y5.heavy	721.35	642.33
MET7A.FYPPGC[CAM]R.+2y5.light	448.71	586.28
MET7A.FYPPGC[CAM]R.+2y4.light	448.71	489.22
MET7A.FYPPGC[CAM]R.+2y5+2.light	448.71	293.64
MET7A.FYPPGC[CAM]R.+2y4+2.light	448.71	245.12
MET7A.FYPPGC[CAM]R.+2y5.heavy	453.71	596.28
MET7A.FYPPGC[CAM]R.+2y4.heavy	453.71	499.23
MET7A.FYPPGC[CAM]R.+2y5+2.heavy	453.71	298.65
MET7A.FYPPGC[CAM]R.+2y4+2.heavy	453.71	250.12
sp|Q6UX53|MET7B_HUMAN.VTC[CAM]LDPNPHFEK.+3y7.light	486.23	868.43
sp|Q6UX53|MET7B_HUMAN.VTC[CAM]LDPNPHFEK.+3y11+2.light	486.23	679.31
sp|Q6UX53|MET7B_HUMAN.VTC[CAM]LDPNPHFEK.+3y10+2.light	486.23	628.79
sp|Q6UX53|MET7B_HUMAN.VTC[CAM]LDPNPHFEK.+3y7+2.light	486.23	434.72
sp|Q6UX53|MET7B_HUMAN.VTC[CAM]LDPNPHFEK.+3y7.heavy	488.91	876.45
sp|Q6UX53|MET7B_HUMAN.VTC[CAM]LDPNPHFEK.+3y11+2.heavy	488.91	683.32
sp|Q6UX53|MET7B_HUMAN.VTC[CAM]LDPNPHFEK.+3y10+2.heavy	488.91	632.8
sp|Q6UX53|MET7B_HUMAN.VTC[CAM]LDPNPHFEK.+3y7+2.heavy	488.91	438.73
MET7B.ELFSQIK.+2y6.light	432.74	735.44
MET7B.ELFSQIK.+2y5.light	432.74	622.36
MET7B.ELFSQIK.+2y4.light	432.74	475.29
MET7B.ELFSQIK.+2y6+2.light	432.74	368.22
MET7B.ELFSQIK.+2y6.heavy	436.75	743.45
MET7B.ELFSQIK.+2y5.heavy	436.75	630.37
MET7B.ELFSQIK.+2y4.heavy	436.75	483.3
MET7B.ELFSQIK.+2y6+2.heavy	436.75	372.23

```
      #       1         10         20         30         40         50         60
METTL7A       MELTIFILRL AIYILTFPLY LLNFLGLWSW ICKKWFPYFL VRFTVIYNEQ MASKKRELFS
              M++ + +L+L  + +LT PL+ L+  LG W   +CK +FPY +    T   N + M SKKRELFS
METTL7B       MDILVPLLQL LVLLLTLPLH LMALLGCWQP LCKSYFPYLM AVLTPKSNRK MESKKRELFS
      #       61        70         80         90         100        110        120
METTL7A       NLQEFAGPSG KLSLLEVGCG TGANFKFYPP GCRVTCIDPN PNFEKFLIKS IAENRHLQFE
               ++   G SG K++LLE+GCG TGANF+FYPP GCRVTC+DPN P+FEKFL KS +AENRHLQ+E
METTL7B       QIKGLTGASG KVALLELGCG TGANFQFYPP GCRVTCLDPN PHFEKFLTKS MAENRHLQYE
      #       121       130        140        150        160        170        180
METTL7A       RFVVAAGENM HQVADGSVDV VVCTLVLCSV KNQERILREV CRVLRPGGAF YFMEHVAAEC
              RFVVA GE+M  Q+ADGS+DV VVCTLVLCSV ++  ++L+EV  RVLRPGG   +F EHVA
METTL7B       RFVVAPGEDM RQLADGSMDV VVCTLVLCSV QSPRKVLQEV RRVLRPGGVL FFWEHVAEPY
      #       181       190        200        210        220        230        240
METTL7A       STWNYFWQQV LDPAWHLLFD GCNLTRESWK ALERASFSKL KLQHIQAPLS WELVRPHIYG
               +W + WQQV  +P W  + D GC LTRE+WK  LE A FS++ +++    PL  W  V PHI G
METTL7B       GSWAFMWQQV FEPTWKHIGD GCCLTRETWK DLENAQFSEI QMERQPPPLK WLPVGPHIMG
      #          244
METTL7A       YAVK
               AVK
METTL7B       KAVK
```

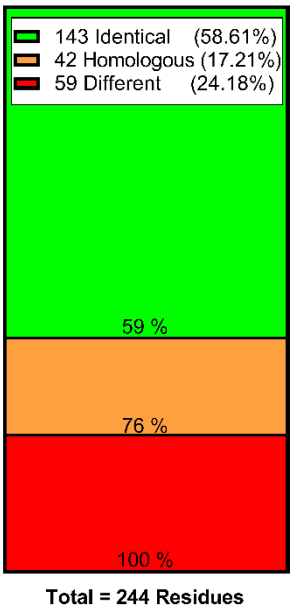

Supplementary Figure 2.1 Basic local alignment results for METTL7A (TMT1A) compared with METTL7B (TMT1B).

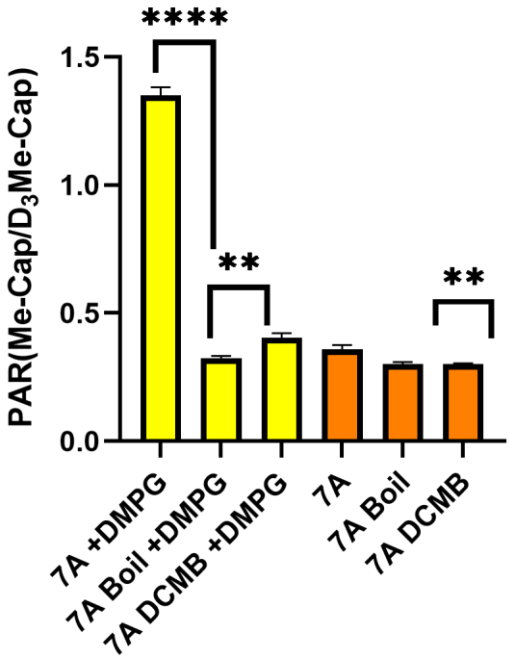

Supplementary Figure 2.2 Activity assay monitoring the formation of S-methyl captopril ±DMPG by recombinant purified *N*-GST-METTL7A (*N*-GST-TMT1A). All data (n=3) are presented as the mean ±S.D.

For this captopril methylation assay, samples were incubated for 45 min ±DMPG, the final DCMB concentration was 100 µM, and all other parameters and analysis techniques were performed similar to the captopril assay that is described in **section 2.2.4**.

A

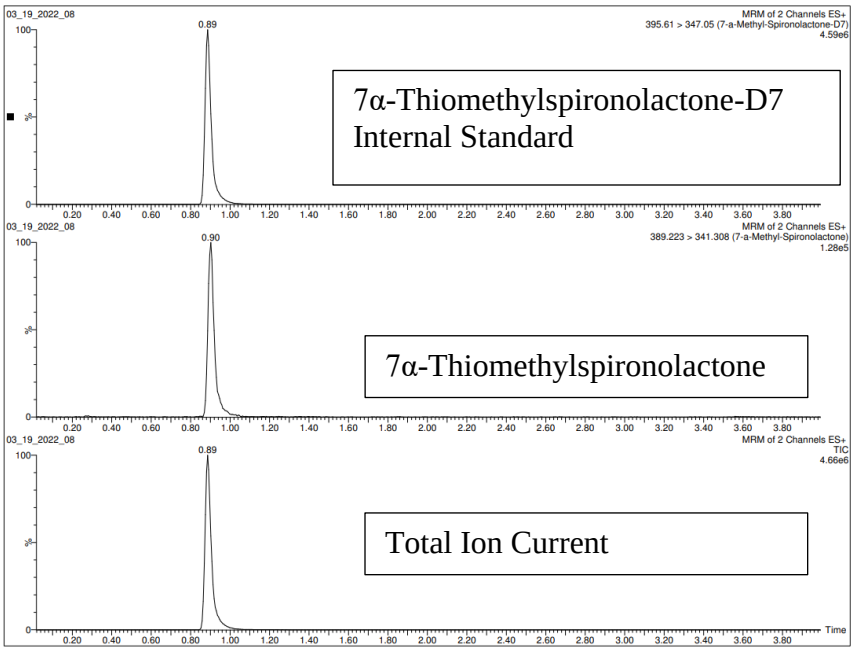

B

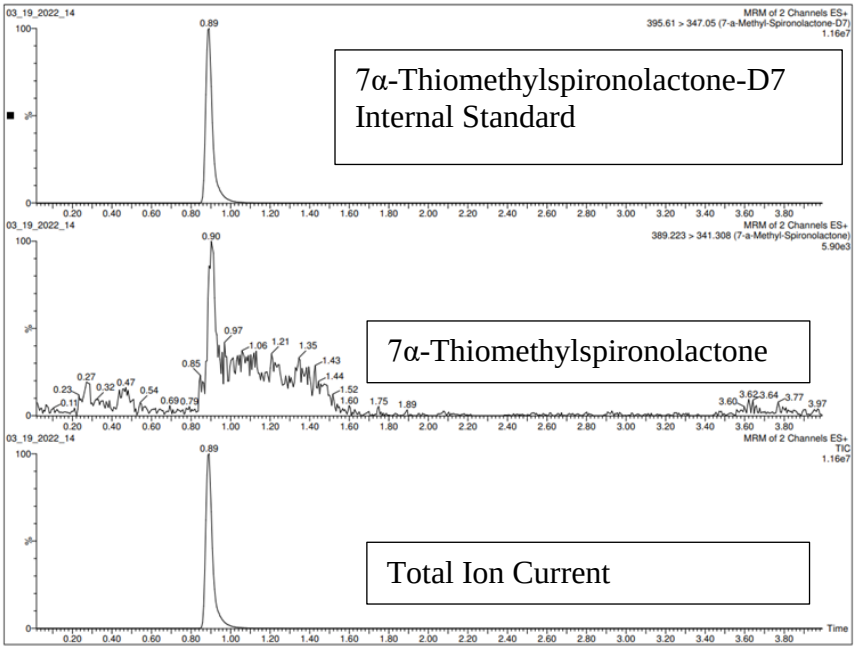

Supplementary Figure 2.3 Representative chromatogram traces from a TSL methylation activity assay with recombinant purified active (A) and boiled (B) *N*-GST-METTL7A (*N*-GST-TMT1A).

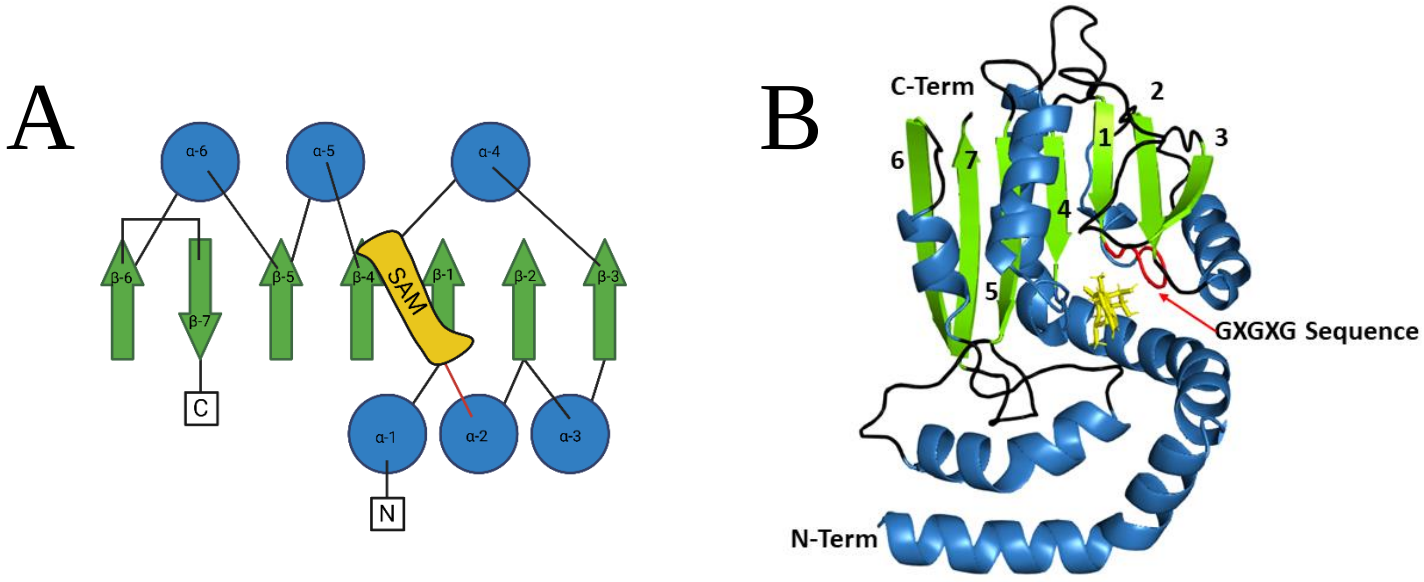

Supplementary Figure 2.4 Cartoon representation of class I methyltransferases (A) as described by Schubert *et al.*, 2003. Alpha helices (blue) are labeled α-1 through α-6 beta sheets (green) are labeled β-1 through β-7. The SAM binding site is marked in yellow, and the GXGXG sequence location is marked by a red line. An AlphaFold produced homology model of METTL7A (TMT1A) (B) with beta sheets numbered in order along protein sequence and colored green. Alpha helices are colored blue, the GXGXG sequence is colored red, and SAM (yellow) is oriented in the SAM binding domain. The order and number of alpha helices and beta sheets along the AlphaFold-produced homology model is identical to what was described by Schubert *et al.*, 2003.

The homology model for METTL7A was downloaded from The AlphaFold Protein Structure Database https://alphafold.ebi.ac.uk/files/AF-Q9H8H3-F1-model_v2.pdb. The homology model was colored using PyMOL Molecular Graphics System. Pymol renders secondary structures, which allowed us to distinguish segments as alpha helices or beta sheets. SAM was docked into the METTL7A homology model with The University of Hamburg's Center for Bioinformatics protein-ligand docking software, JAMDA.

A

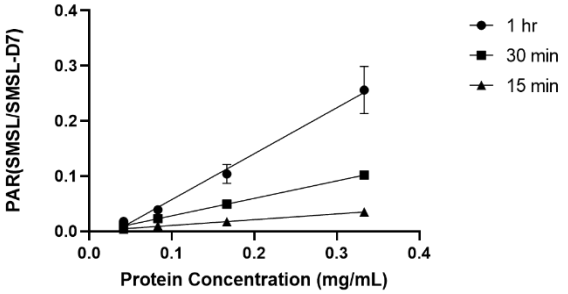

	1 hr	30 min	15 min
R squared	0.9647	0.9954	0.9928

B

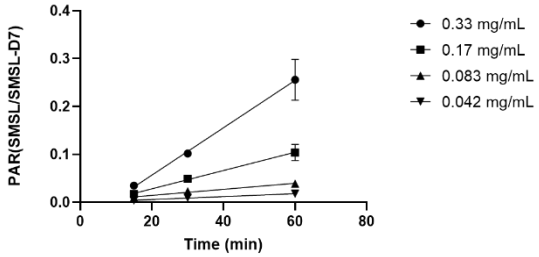

	0.33 mg/mL	0.17 mg/mL	0.083 mg/mL	0.042 mg/mL
R squared	0.9637	0.9613	0.9816	0.9477

Supplementary Figure 2.5 The methylation of TSL at various concentrations of purified recombinant *N*-GST-METTL7A (*N*-GST-TMT1A) over the course of a 1 hr, 30 min, or 15 min incubation plotted with respect to protein concentration (A) or time increments (B).

Purified recombinant METTL7A was diluted to 0.125. 0.25, 0.5, and 1 mg/mL and then further diluted the purified protein into reaction buffer containing DMPG as described in **section 2.2.4**. TSL was deposited onto a 96-well plate as previously described, and the diluted protein was then added to the appropriate wells. The final protein concentrations were 0.042, 0.083, 0.17, and 0.33 mg/mL. The final TSL concentration was 100 µL. SAM was added in staggered time increments to induce the reaction. The final SAM concentration was 100 µM. The final incubation times for the various protein concentrations were 1 h, 30 min, and 15 min. The reaction was quenched, and the samples were analyzed by LC-MS/MS as was described in **section 2.2.4**.

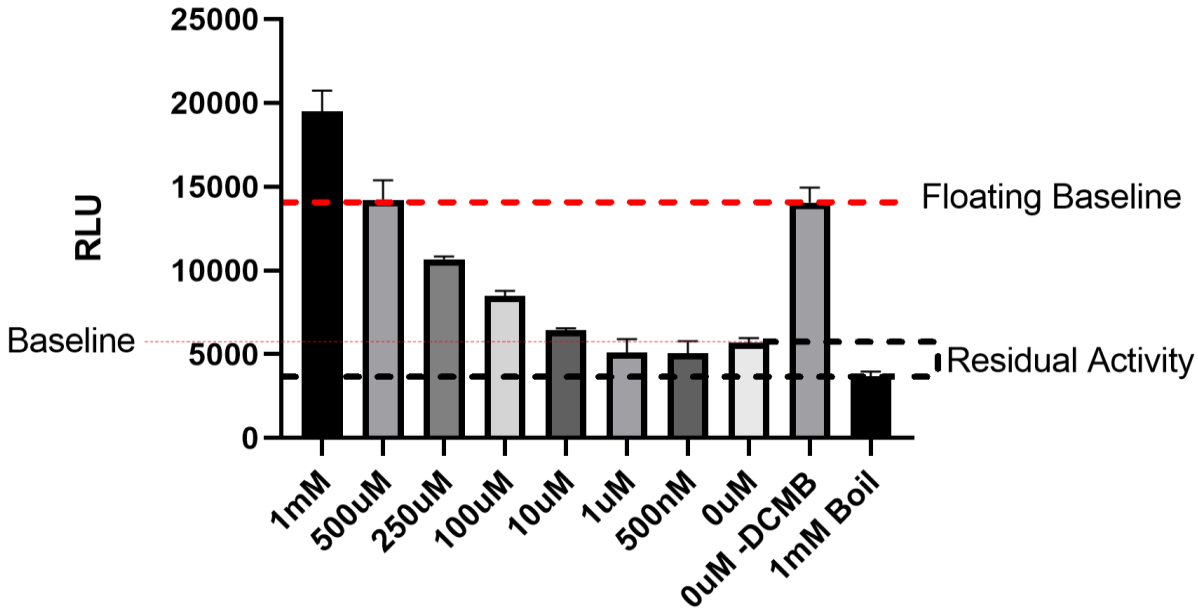

Supplementary Figure 2.6 The relative luminescence unit response from purified recombinant METTL7A incubated with various concentrations of 4-chlorothiophenol. The reaction was quenched by the addition of DCMB to a final concentration of 100 µM and all treatments were analyzed using Promega's MTaseGlo Assay. For one set of replicates, no substrate was included in the incubation and no DCMB was added to quench the reaction prior to adding the MTaseGlo development reagents. The difference between the response from this set of replicates and a set also incubated without substrate but with the addition of DCMB represents the activity that can be attributed to the methylation of a compound present in the MTaseGlo development reagents by METTL7A. There is still a response above boil in no-substrate treated replicates, but this response is low enough to identify the methylation of substrates during the activity assay.

Purified recombinant METTL7A was incubated with various concentrations of 4-chlorothiophenol for 30 minutes. The final concentration of SAM was 100 µM. All reaction conditions and analyses using the MTaseGlo Assay were identical to what was described in the substrate screening methods section. For one set of replicates, no substrate was included in the incubation and no DCMB was added to quench the reaction prior to adding the MTaseGlo development reagents.

A. METTL7B siRNA Sequence:
5’ CCUUCAUGUGGCAGCAAGUdTdT 3’ / 5’
ACUUGCUGCCACAUGAAGGdTdT 3’

B. METTL7A mRNA coding region sequence:

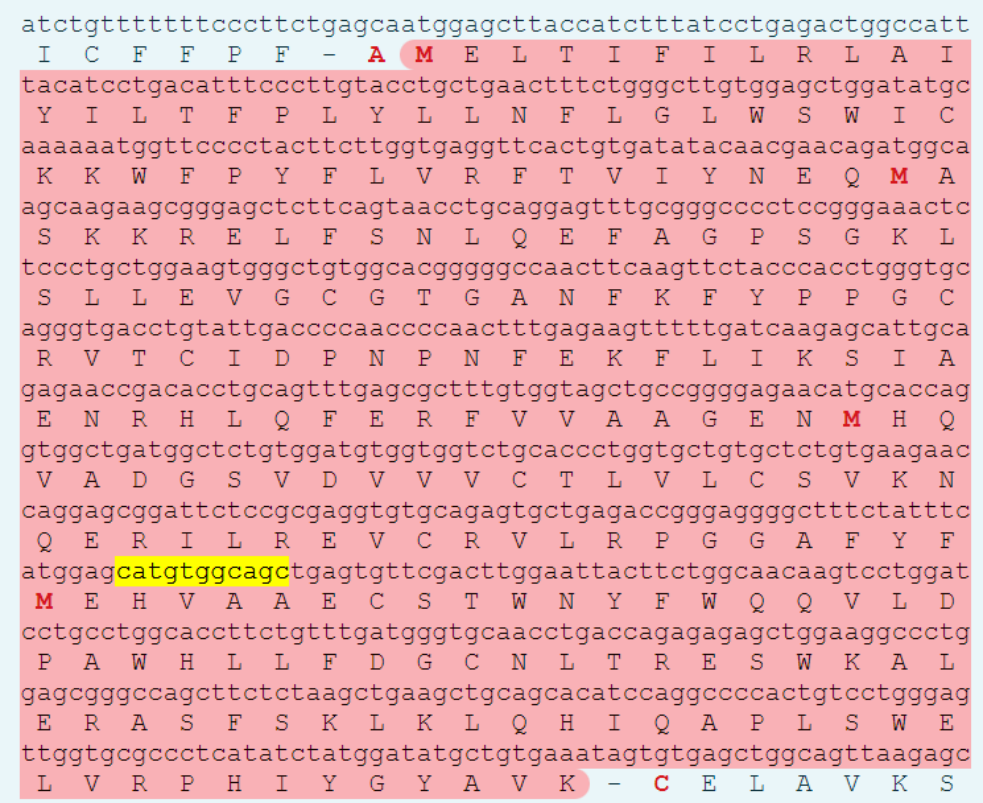

Supplementary Figure 2.7 METTL7B (TMT1B) siRNA sequence with region complementary to METTL7A (TMT1A) coding region of NCBI Reference Sequence: NM_014033.4 highlighted (A). METTL7A (TMT1A) coding region of NCBI Reference Sequence: NM_014033.4 with region complementary to METTL7B (TMT1B) siRNA sequence highlighted (B).

APPENDIX: CHAPTER 3

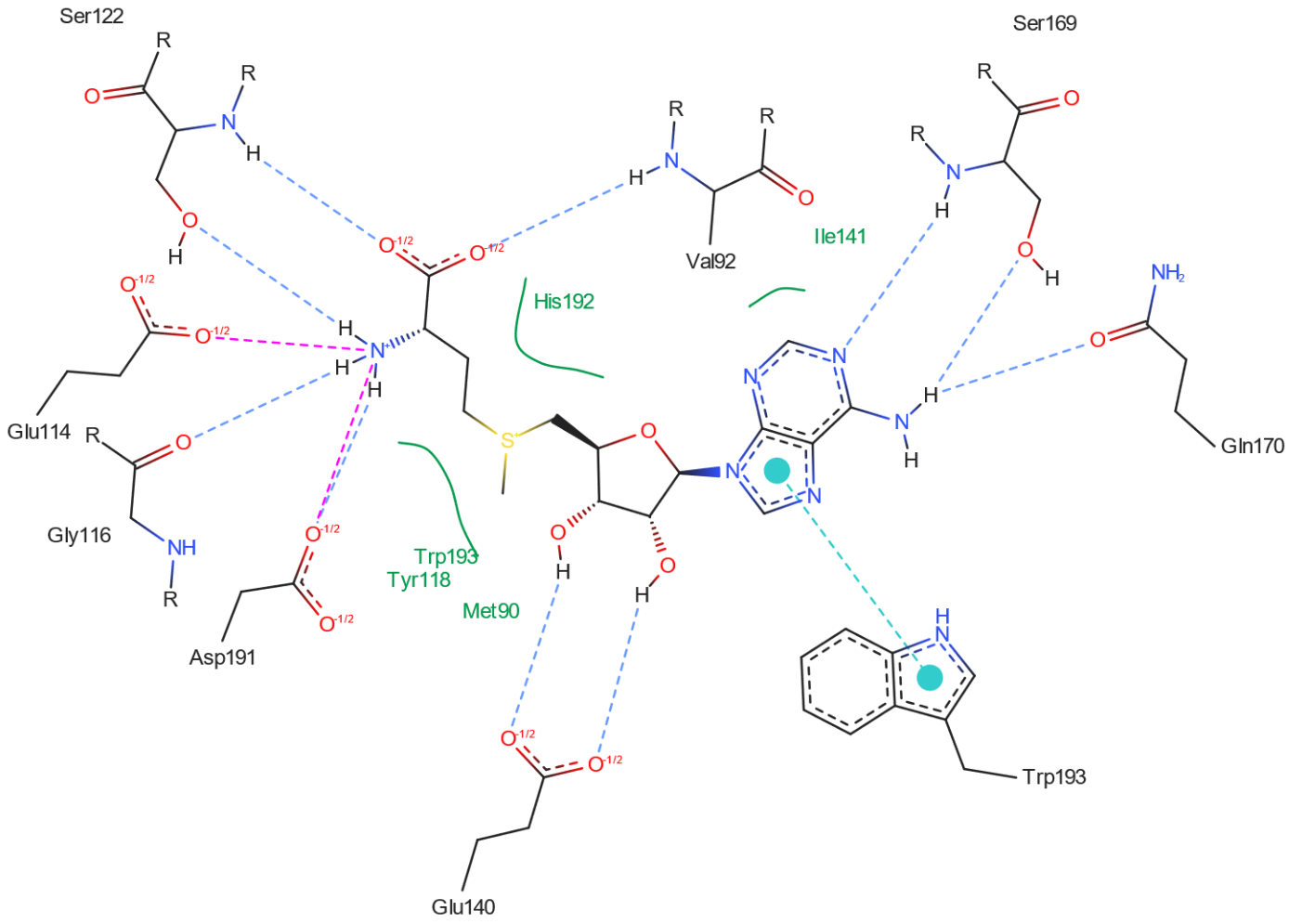

Supplementary Figure 3.1. PoseView results for 4XUC_COMT_SAM (crystal structure ID_methyltransferase_bound small molecule).

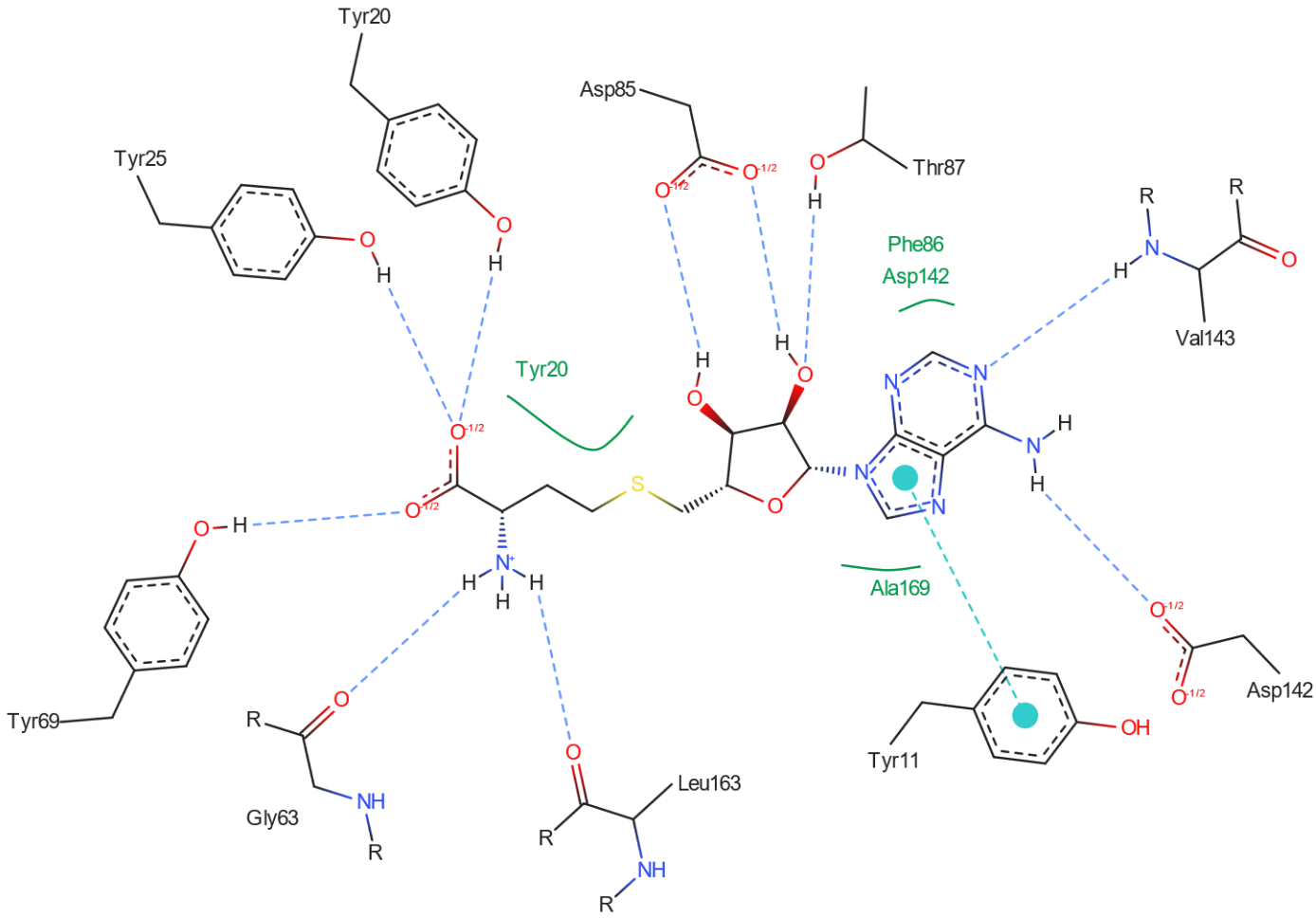

Supplementary Figure 3.2. PoseView results for 2A14_INMT_SAH (crystal structure ID_methyltransferase_bound small molecule).

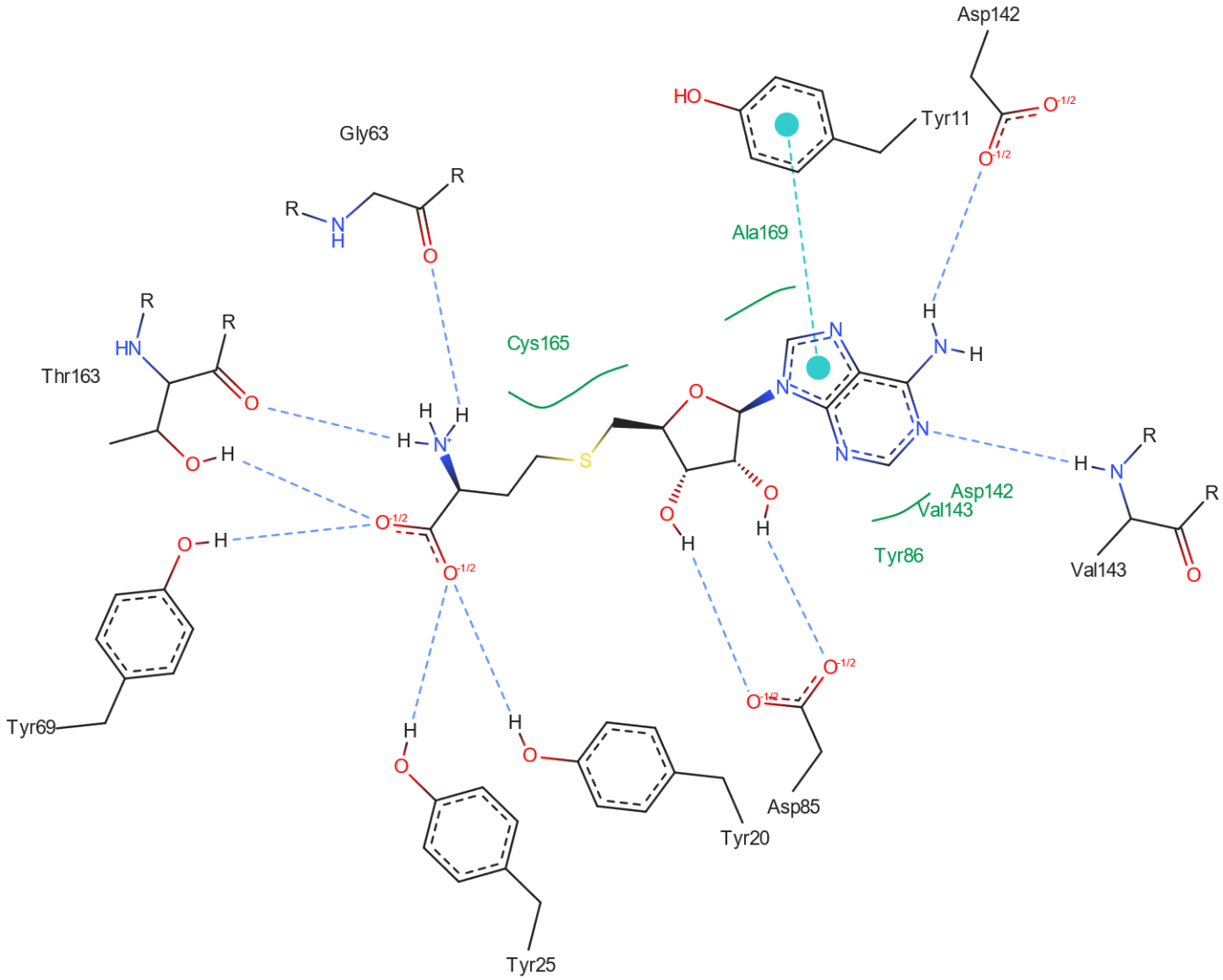

Supplementary Figure 3.3. PoseView results for 7BKG_NNMT_SAH (crystal structure ID_methyltransferase_bound small molecule).

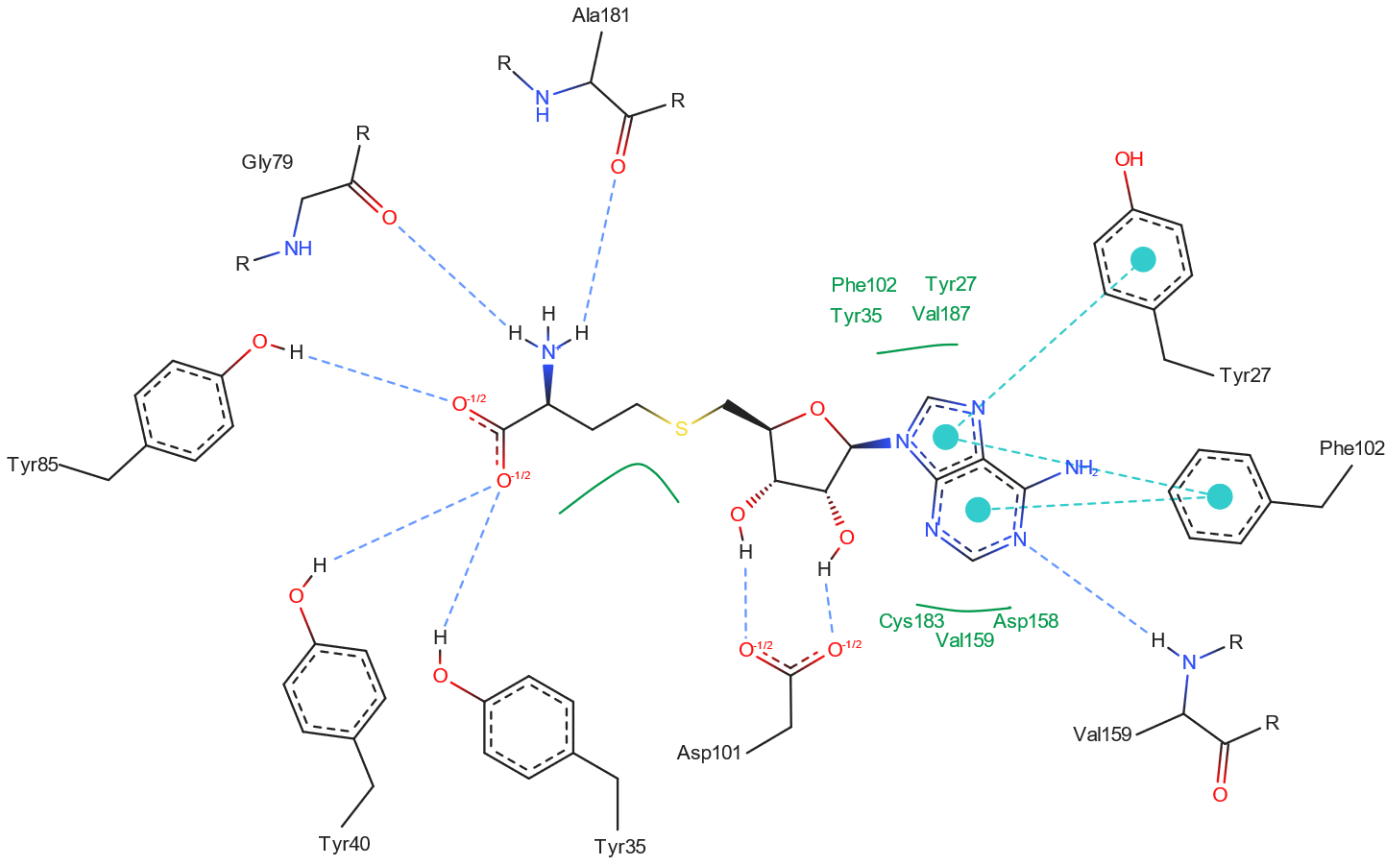

Supplementary Figure 3.4. PoseView results for 2AN3_PNMT_SAH (crystal structure ID_methyltransferase_bound small molecule).

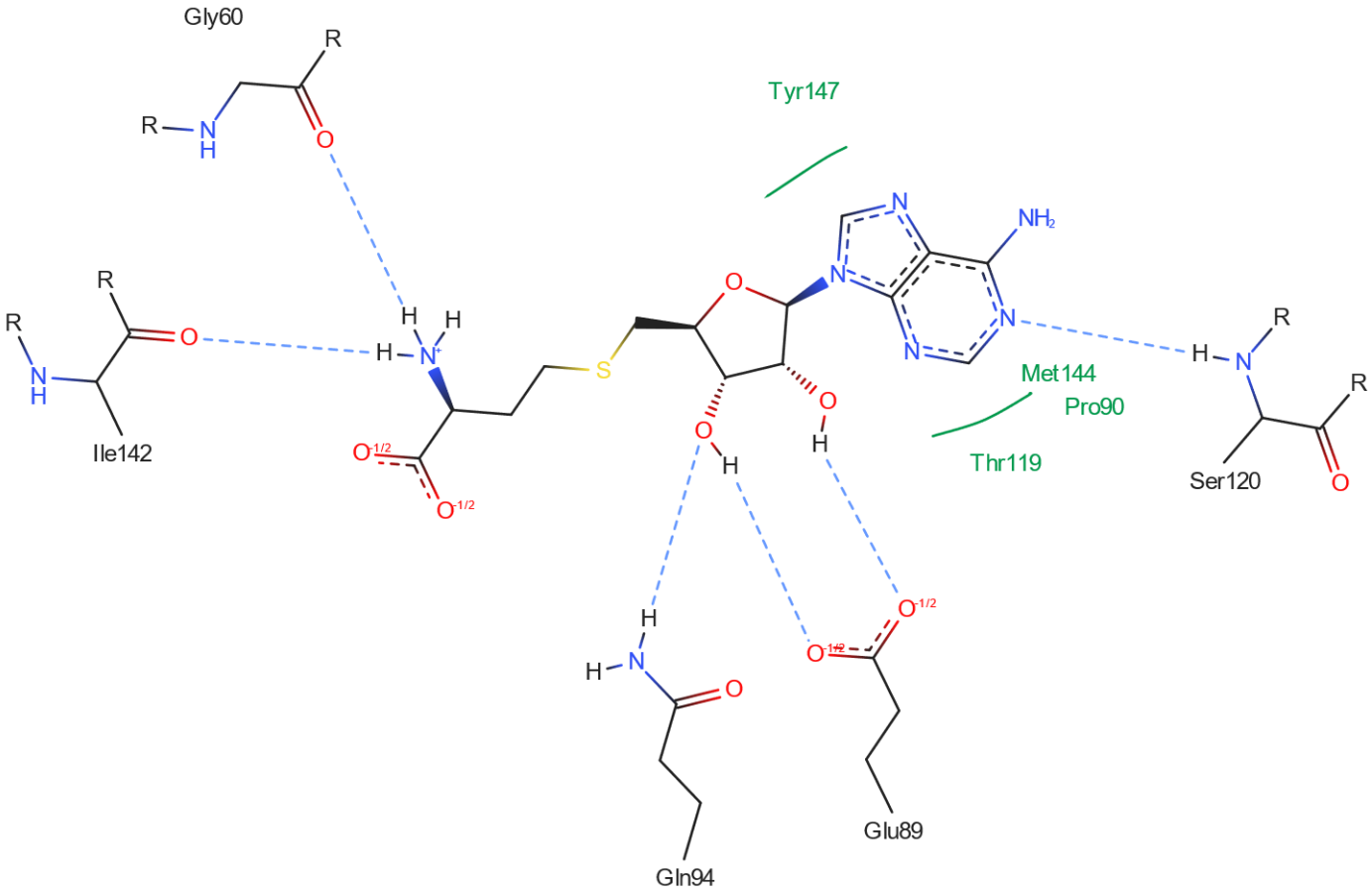

Supplementary Figure 3.5. PoseView results for 2AOT_HNMT_SAH (crystal structure ID_methyltransferase_bound small molecule).

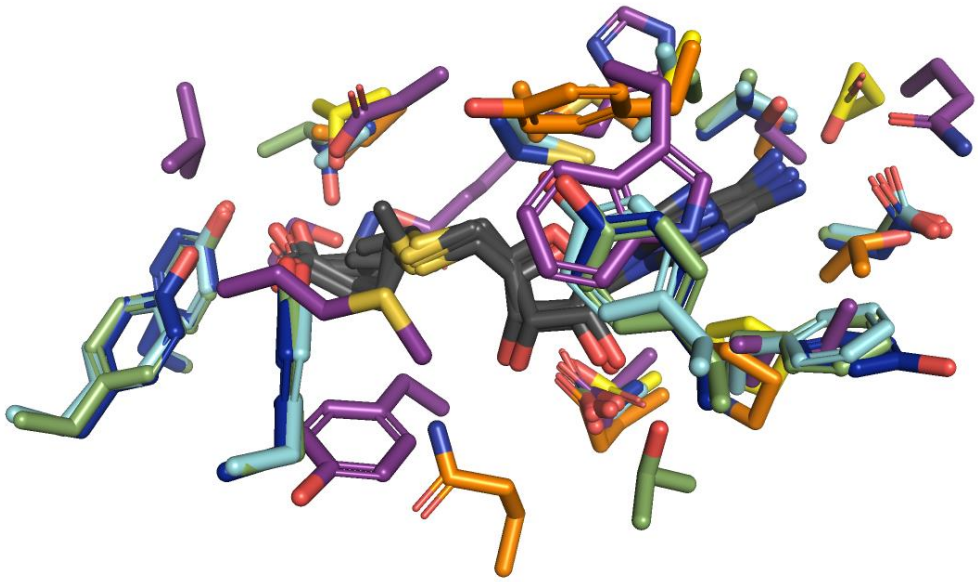

Supplementary Figure 3.6. Residues, from small molecule methyltransferases, that were identified by PoseView that form binding interactions with SAM or SAH. Also the residues from TMT1A that could participate in the SAM or SAH binding interactions described in **section 3.3.2**. Residues are color coded by the crystal structure or homology model they are from: COMT (purple), HNMT (orange), INMT (green), PNMT (cyan), NNMT (dark blue), and TMT1A (yellow).

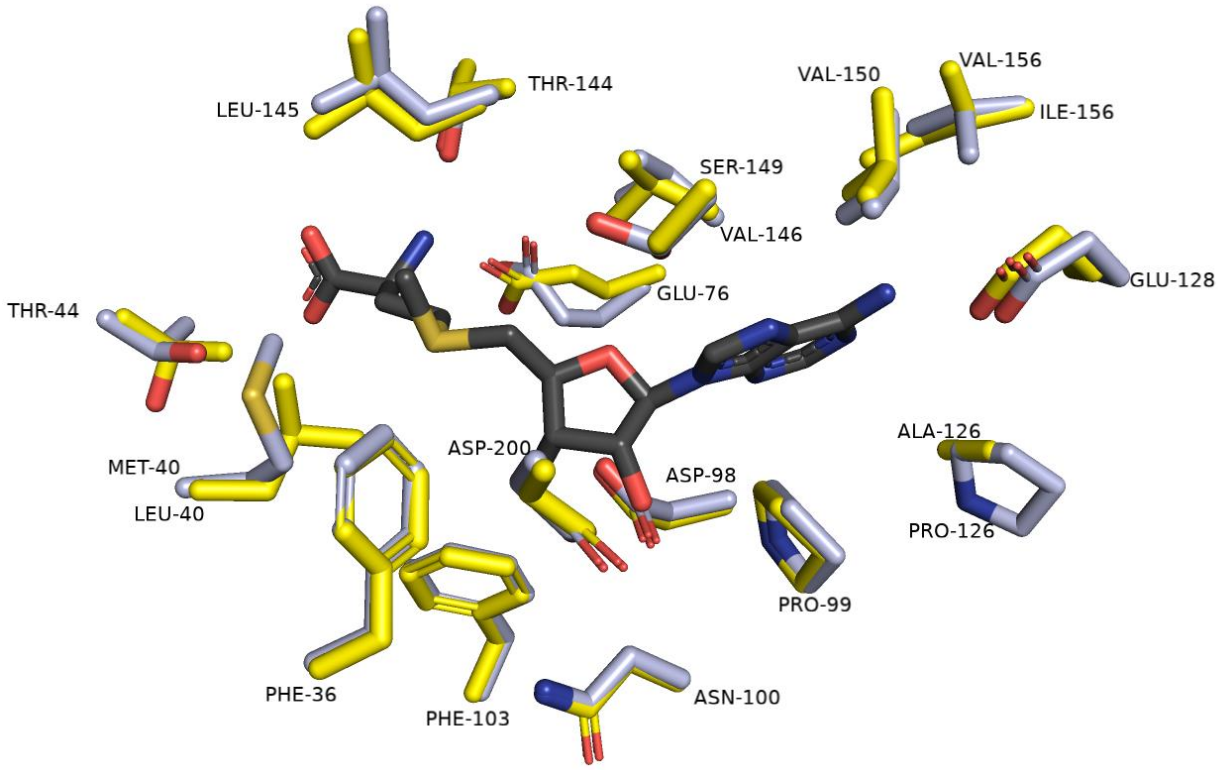

Supplementary Figure 3.7. TMT1A (yellow) and TMT1B (light blue) residues that are potentially involved in SAM or SAH binding interactions. Residues are labeled once if conserved and twice with both residue names if not.

Supplementary Table 3.1 Table of primers utilized to incorporate missense mutations.

The input plasmid is the plasmid that received the missense mutation, and the output plasmid is the plasmid that resulted from the mutagenesis.

Input Plasmid	Forward Primer 5'- 3'	Reverse Primer 5'- 3'	Output Plasmid
WT	GTTCCCCTACctgTTGGTGAGGT	CATTTTTTGCATATCCAGCTC	F39L
F39L	GTTGGTGAGGctgACTGTGATATAC	AGGTAGGGGAACCATTTTTTG	F39L+F43L
F39L+F43L	GACTGTGATAagcAACGAACAGATGG	AGCCTCACCAACAGGTAG	F39L+F43L+Y47S
F39L+F43L+Y47S	GTTCCCCTACttcTTGGTGAGGC	CATTTTTTGCATATCCAGC	F43L+Y47S
WT	CACTGTGATAagcAACGAACAGATG	AACCTCACCAAGAAGTAG	Y47S
WT	GCACCTTCTGggcGATGGGTGCAACC	CAGGCAGGATCCAGGACT	F199G

```
F43L        MELTIFILRLAIYILTFPLYLLNFLGLWSWICKKWFPYFLVRLTVIYNEQMASKKRELFS    60
F199G_A     MELTIFILRLAIYILTFPLYLLNFLGLWSWICKKWFPYFLVRFTVIYNEQMASKKRELFS    60
F199G_B     MELTIFILRLAIYILTFPLYLLNFLGLWSWICKKWFPYFLVRFTVIYNEQMASKKRELFS    60
WT          MELTIFILRLAIYILTFPLYLLNFLGLWSWICKKWFPYFLVRFTVIYNEQMASKKRELFS    60
Y47S        MELTIFILRLAIYILTFPLYLLNFLGLWSWICKKWFPYFLVRFTVISNEQMASKKRELFS    60
F39L,F43L   MELTIFILRLAIYILTFPLYLLNFLGLWSWICKKWFPYLLVRLTVIYNEQMASKKRELFS    60
Triple_A    MELTIFILRLAIYILTFPLYLLNFLGLWSWICKKWFPYLLVRLTVISNEQMASKKRELFS    60
Triple_B    MELTIFILRLAIYILTFPLYLLNFLGLWSWICKKWFPYLLVRLTVISNEQMASKKRELFS    60
F43L,Y47S   MELTIFILRLAIYILTFPLYLLNFLGLWSWICKKWFPYFLVRLTVISNEQMASKKRELFS    60
            ************************************!***!*** ************

F43L        NLQEFAGPSGKLSLLEVGCGTGANFKFYPPGCRVTCIDPNPNFEKFLIKSIAENRHLQFE    120
F199G_A     NLQEFAGPSGKLSLLEVGCGTGANFKFYPPGCRVTCIDPNPNFEKFLIKSIAENRHLQFE    120
F199G_B     NLQEFAGPSGKLSLLEVGCGTGANFKFYPPGCRVTCIDPNPNFEKFLIKSIAENRHLQFE    120
WT          NLQEFAGPSGKLSLLEVGCGTGANFKFYPPGCRVTCIDPNPNFEKFLIKSIAENRHLQFE    120
Y47S        NLQEFAGPSGKLSLLEVGCGTGANFKFYPPGCRVTCIDPNPNFEKFLIKSIAENRHLQFE    120
F39L,F43L   NLQEFAGPSGKLSLLEVGCGTGANFKFYPPGCRVTCIDPNPNFEKFLIKSIAENRHLQFE    120
Triple_A    NLQEFAGPSGKLSLLEVGCGTGANFKFYPPGCRVTCIDPNPNFEKFLIKSIAENRHLQFE    120
Triple_B    NLQEFAGPSGKLSLLEVGCGTGANFKFYPPGCRVTCIDPNPNFEKFLIKSIAENRHLQFE    120
F43L,Y47S   NLQEFAGPSGKLSLLEVGCGTGANFKFYPPGCRVTCIDPNPNFEKFLIKSIAENRHLQFE    120
            ************************************************************

F43L        RFVVAAGENMHQVADGSVDVVVCTLVLCSVKNQERILREVCRVLRPGGAFYFMEHVAAEC    180
F199G_A     RFVVAAGENMHQVADGSVDVVVCTLVLCSVKNQERILREVCRVLRPGGAFYFMEHVAAEC    180
F199G_B     RFVVAAGENMHQVADGSVDVVVCTLVLCSVKNQERILREVCRVLRPGGAFYFMEHVAAEC    180
WT          RFVVAAGENMHQVADGSVDVVVCTLVLCSVKNQERILREVCRVLRPGGAFYFMEHVAAEC    180
Y47S        RFVVAAGENMHQVADGSVDVVVCTLVLCSVKNQERILREVCRVLRPGGAFYFMEHVAAEC    180
F39L,F43L   RFVVAAGENMHQVADGSVDVVVCTLVLCSVKNQERILREVCRVLRPGGAFYFMEHVAAEC    180
Triple_A    RFVVAAGENMHQVADGSVDVVVCTLVLCSVKNQERILREVCRVLRPGGAFYFMEHVAAEC    180
Triple_B    RFVVAAGENMHQVADGSVDVVVCTLVLCSVKNQERILREVCRVLRPGGAFYFMEHVAAEC    180
F43L,Y47S   RFVVAAGENMHQVADGSVDVVVCTLVLCSVKNQERILREVCRVLRPGGAFYFMEHVAAEC    180
            ************************************************************

F43L        STWNYFWQQVLDPAWHLLFDGCNLTRESWKALERASFSKLKLQHIQAPLSWELVRPHIYG    240
F199G_A     STWNYFWQQVLDPAWHLLGDGCNLTRESWKALERASFSKLKLQHIQAPLSWELVRPHIYG    240
F199G_B     STWNYFWQQVLDPAWHLLGDGCNLTRESWKALERASFSKLKLQHIQAPLSWELVRPHIYG    240
WT          STWNYFWQQVLDPAWHLLFDGCNLTRESWKALERASFSKLKLQHIQAPLSWELVRPHIYG    240
Y47S        STWNYFWQQVLDPAWHLLFDGCNLTRESWKALERASFSKLKLQHIQAPLSWELVRPHIYG    240
F39L,F43L   STWNYFWQQVLDPAWHLLFDGCNLTRESWKALERASFSKLKLQHIQAPLSWELVRPHIYG    240
Triple_A    STWNYFWQQVLDPAWHLLFDGCNLTRESWKALERASFSKLKLQHIQAPLSWELVRPHIYG    240
Triple_B    STWNYFWQQVLDPAWHLLFDGCNLTRESWKALERASFSKLKLQHIQAPLSWELVRPHIYG    240
F43L,Y47S   STWNYFWQQVLDPAWHLLFDGCNLTRESWKALERASFSKLKLQHIQAPLSWELVRPHIYG    240
            ******************!*****************************************

F43L        YAVK 244
F199G_A     YAVK 244
F199G_B     YAVK 244
WT          YAVK 244
Y47S        YAVK 244
F39L,F43L   YAVK 244
Triple_A    YAVK 244
Triple_B    YAVK 244
F43L,Y47S   YAVK 244
            ****
```

Supplementary Figure 3.8 Aligned TMT1A, translated from Eurofins Genomics whole plasmid sequencing results of mutated TMT1A encoding pCMV6 expression vectors. The sequence for wildtype TMT1A is highlighted yellow, and the mutated residues are highlighted green—leucine, magenta—serine, or cyan—glycine. The * symbol means no difference was identified, and an ! means a single-point mutation was detected.

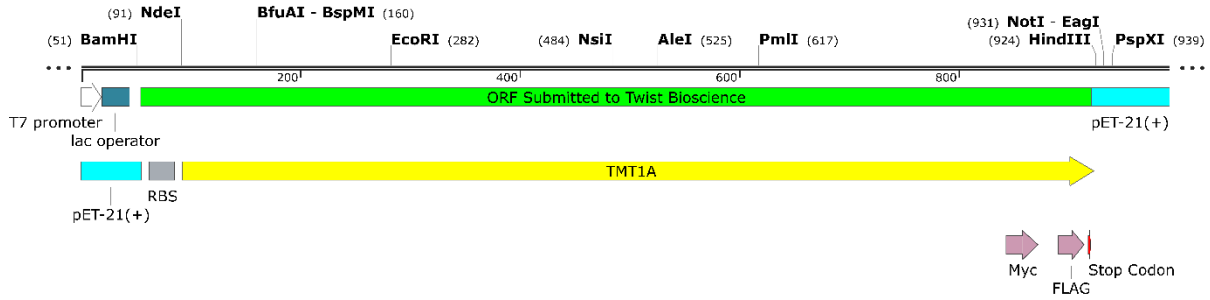

Supplementary Figure 3.9 pET-21(+)-TMT1A-FLAG construct. ORF segment and relevant features.

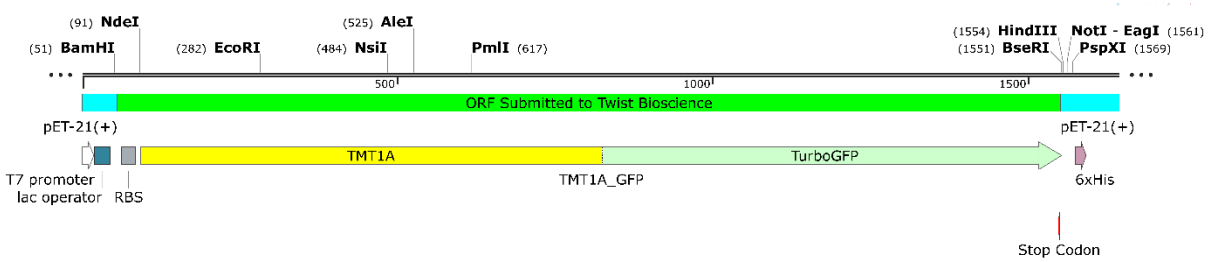

Supplementary Figure 3.10 pET-21(+)-TMT1A-GFP construct. ORF segment and relevant features.

N-MELTIFILRLAIYILTFPLYLLNFLGLWSWICKKWFPYFLVRFTVIYNEQMASKKRELFSNL
QEFAGPSGKLSLLEVGCGTGANFKFYPPGCRVTCIDPNPNFEKFLIKSIAENRHLQFERFVVAA
GENMHQVADGSVDVVVCTLVLCSVKNQERILREVCRVLRPGGAFYFMEHVAAECSTWNYFWQQV
LDPAWHLLFDGCNLTRESWKALERASFSKLKLQHIQAPLSWELVRPHIYGYAVKTRTRPLEQKL
ISEEDLAANDILDYKDDDDKV**-C

Supplementary Figure 3.11 TMT1A-FLAG Translated Sequence. Estimated molecular weight 31.9 kDa, calculated with Expasy Molecular Weight Calculator, accessed at https://web.expasy.org/compute_pi/.

N-MELTIFILRLAIYILTFPLYLLNFLGLWSWICKKWFPYFLVRFTVIYNEQMASKKRELFSNL
QEFAGPSGKLSLLEVGCGTGANFKFYPPGCRVTCIDPNPNFEKFLIKSIAENRHLQFERFVVAA
GENMHQVADGSVDVVVCTLVLCSVKNQERILREVCRVLRPGGAFYFMEHVAAECSTWNYFWQQV
LDPAWHLLFDGCNLTRESWKALERASFSKLKLQHIQAPLSWELVRPHIYGYAVKTRTRPLEMES
DESGLPAMEIECRITGTLNGVEFELVGGGEGTPEQGRMTNKMKSTKGALTFSPYLLSHVMGYGF
YHFGTYPSGYENPFLHAINNGGYTNTRIEKYEDGGVLHVSFSYRYEAGRVIGDFKVMGTGFPED
SVIFTDKIIRSNATVEHLHPMGDNDLDGSFTRTFSLRDGGYYSSVVDSHMHFKSAIHPSILQNG
GPMFAFRRVEEDHSNTELGIVEYQHAFKTPDADAGEERV**-C

Supplementary Figure 3.12 TMT1A-GFP Translated Sequence. Estimated molecular weight 55.1 kDa, calculated with Expasy Molecular Weight Calculator, accessed at https://web.expasy.org/compute_pi/.

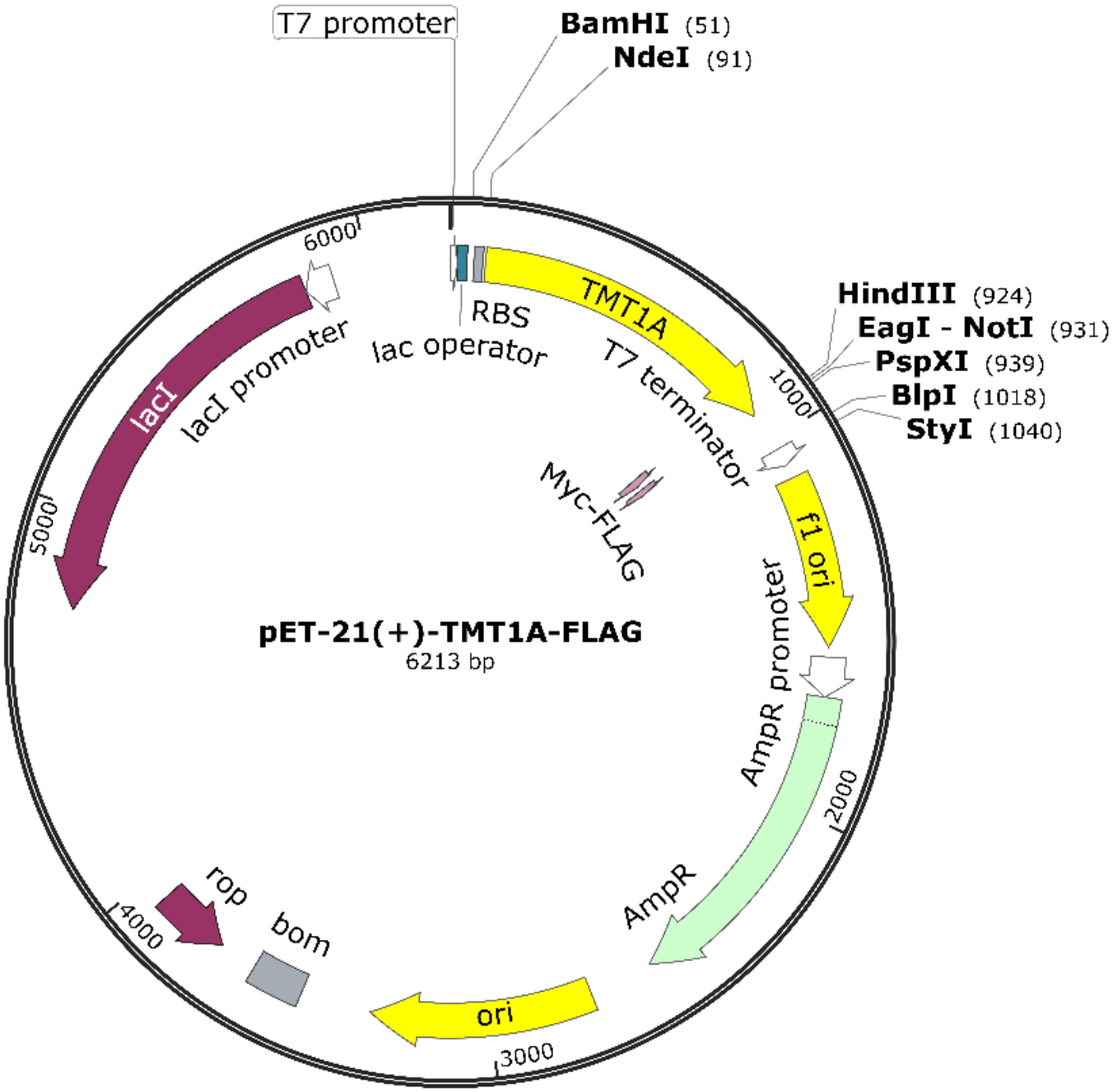

Supplementary Figure 3.13 pET-21(+)-TMT1A-FLAG plasmid map.

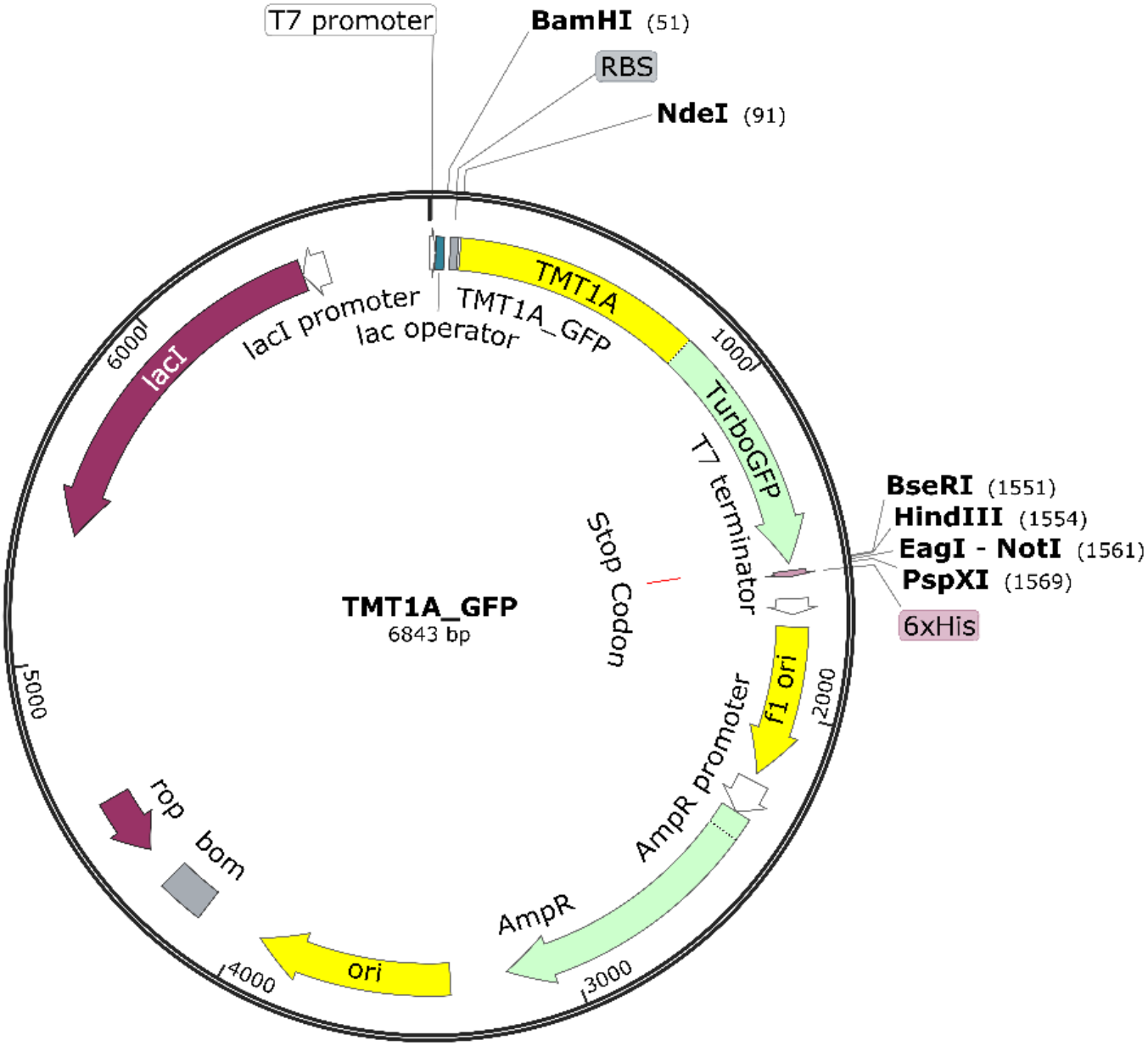

Supplementary Figure 3.14 pET-21(+)-TMT1A-GFP plasmid map.

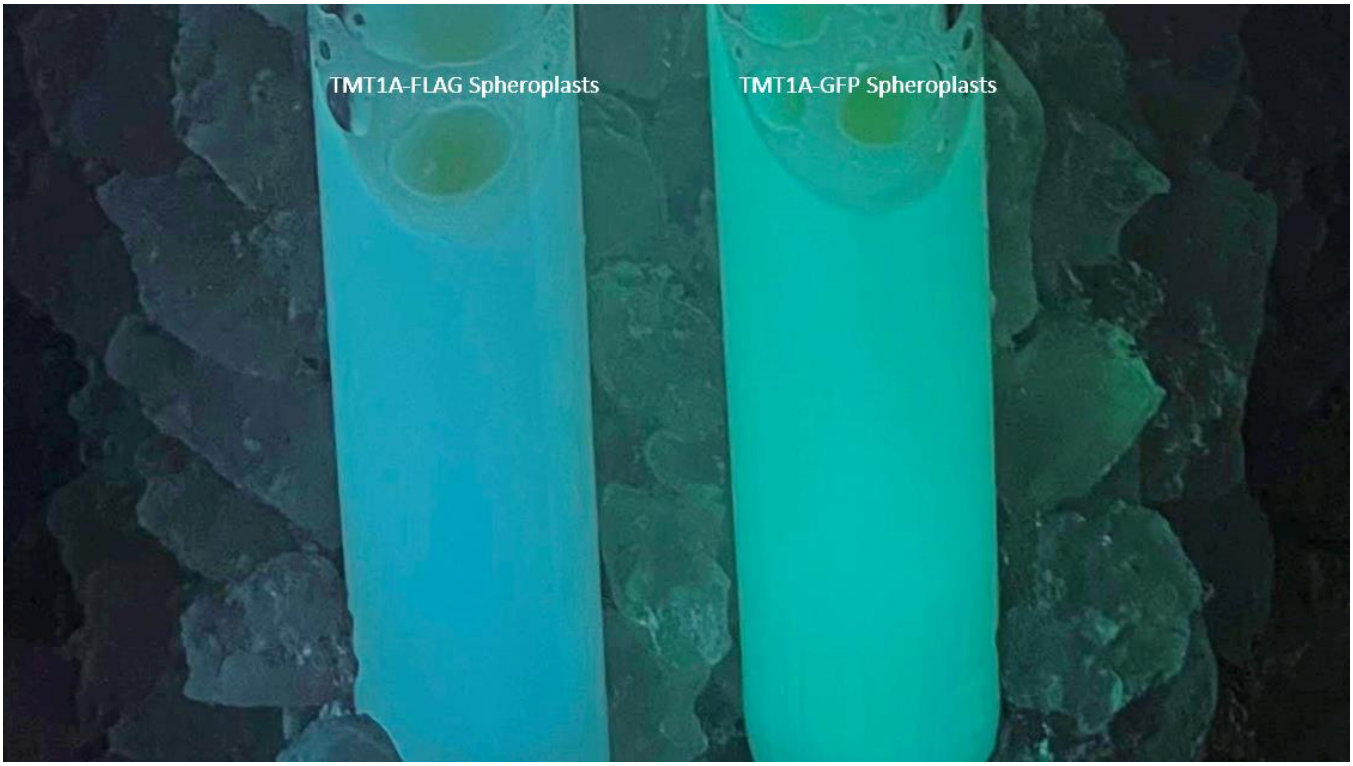

Supplementary Figure 3.15. TMT1A-FLAG (Left) and TMT1A-GFP (Right) exposed to ultraviolet light.

Supplementary Figure 3.16. Machined aluminum plate for cluster tubes (Marsh Tubes, FisherSci Cat No. 07-200-318) in isotemp system.

Supplementary Figure 3.17. pET-22b(+)-TPMT plasmid map.

N-MKYLLPTAAAGLLLLAAQPAMAMDGTRTSLDIEEYSDTEVQKNQVLTLEEWQDKWVNGKTAF
HQEQGHQLLKKHLDTFLKGKSGLRVFFPLCGKAVEMKWFADRGHSVVGVEISELGIQEFFTEQN
LSYSEEPITEIPGTKVFKSSSGNISLYCCSIFDLPRTNIGKFDMIWDRGALVAINPGDRKCYAD
TMFSLLGKKFQYLLCVLSYDPTKHPGPPFYVPHAEIERLFGKICNIRCLEKVDAFEERHKSWGI
DCLFEKLYLLTEKAAALEHHHHHH*-**C**

Supplementary Figure 3.18. pelB-TPMT-6×His Translated Sequence. The pelB sequence is underlined. Estimated molecular weight 31.7 kDa with pelB and 29.3 kDa without pelB, calculated with Expasy Molecular Weight Calculator, accessed at https://web.expasy.org/compute_pi/.

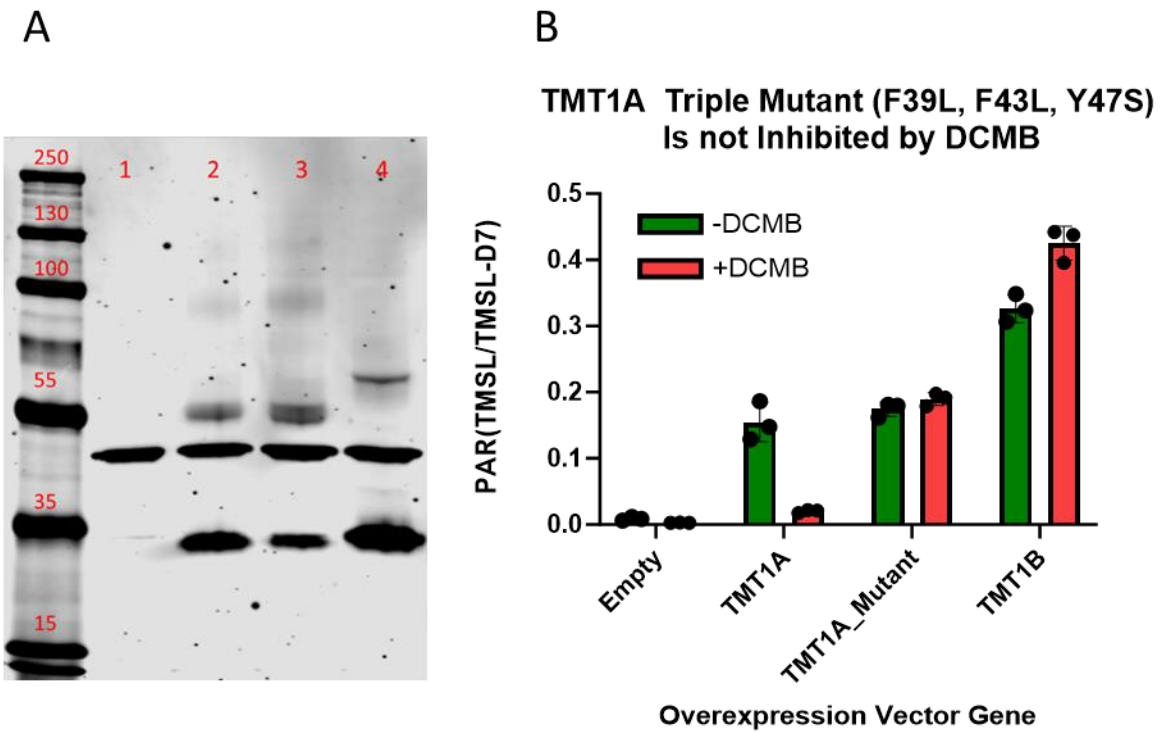

Supplementary Figure 3.19. Overexpression of F39L+F43L+Y47S-TMT1A, WT-TMT1A or WT-TMT1B in HeLa cells. Anti-flag and anti-B-actin western blots verify the overexpression of flag tagged proteins (A). Lanes are protein lysate from empty control vector (1), F39L+F43L+Y47S-TMT1A (2), WT-TMT1A (3), and WT-TMT1B (4). Formation of TMSL in HeLa cells overexpressing F39L+F43L+Y47S-TMT1A, WT-TMT1A, or WT-TMT1B after a 24-hour incubation with TSL ±DCMB. All data (n = 3) are presented as the mean ±S.D.

APPENDIX: CHAPTER 4

Supplementary Table 4.1 Thermo Ascend tune settings.

Method Summary
Method Settings
Application Mode: Peptide
Method Duration (min): 60

Global Parameters
Ion Source
Ion Source Type: H-ESI
Spray Voltage: Static
Positive Ion (V): 3500
Negative Ion (V): 2500
Gas Mode: Static
Sheath Gas (Arb): 12
Aux Gas (Arb): 2
Sweep Gas (Arb): 2.8
Ion Transfer Tube Temp (°C): 275
Vaporizer Temp (°C): 30
APPI Lamp: Not in Use
Use Ion Source Settings from Tune: False
FAIMS Mode: Not Installed
MS Global Settings
Infusion Mode: Liquid Chromatography
Expected LC Peak Width (s): 30
Advanced Peak Determination: True
Default Charge State: 2
Enable Xcalibur AcquireX Ab method modifications: False
Internal Mass Calibration: Off
Experiment #1 [MS]
Start Time (min): 0
End Time (min): 60
Cycle Time (sec): 2
Master Scan:
MS OT
Detector Type: Orbitrap
Orbitrap Resolution: 120000
Mass Range: Normal
Use Quadrupole Isolation: True
Scan Range (m/z): 300-2000
RF Lens (%): 60
AGC Target: Custom
Normalized AGC Target (%): 100
Mass Tolerance: ppm
Low: 10
High: 10
Exclude Isotopes: True
Perform dependent scan on single charge state per precursor only: False
Exclude Within Cycle: True
Data Dependent
Data Dependent Mode: Cycle Time
Time between Master Scans (sec): 2
Scan Event Type 1:
Sort by Charge
Precursor Priority: Highest Charge State
Scan:
ddMS² IT HCD
Isolation Mode: Quadrupole
Isolation Window (m/z): 2
Isolation Offset: Off
Activation Type: HCD
Collision Energy Mode: Fixed
HCD Collision Energy Type: Normalized
HCD Collision Energy (%): 30
Detector Type: Ion Trap
Ion Trap Scan Rate: Rapid
Mass Range: Normal

Scan Range Mode: Auto
AGC Target: Standard
Maximum Injection Time Mode: Auto
Microscans: 1
Data Type: Centroid
Scan Description:
Data Dependent
Data Dependent Mode: Number of Scans
Number of Dependent Scans: 1
Scan Event Type 1:
Scan:
ddMS² IT CID
MSⁿ Level: 2
Isolation Mode: Quadrupole
Isolation Window (m/z): 2
Isolation Offset: Off

Maximum Injection Time Mode: Custom
Maximum Injection Time (ms): 251
Microscans: 1
Data Type: Profile
Polarity: Positive
Source Fragmentation: Disabled
Scan Description:
Filters:
MIPS
Monoisotopic Peak Determination: Peptide
Intensity
Filter Type: Intensity Threshold
Intensity Threshold: 5.0e4
Dynamic Exclusion
Exclude after n times: 1
Exclusion duration (s): 8

Activation Type: CID
Collision Energy Mode: Fixed
CID Collision Energy (%): 35
CID Activation Time (ms): 10
Activation Q: 0.25
Multistage Activation: False
Detector Type: Ion Trap
Ion Trap Scan Rate: Rapid
Mass Range: Normal
Scan Range Mode: Auto
AGC Target: Standard
Maximum Injection Time Mode: Auto
Microscans: 1
Data Type: Centroid
Scan Description: NA

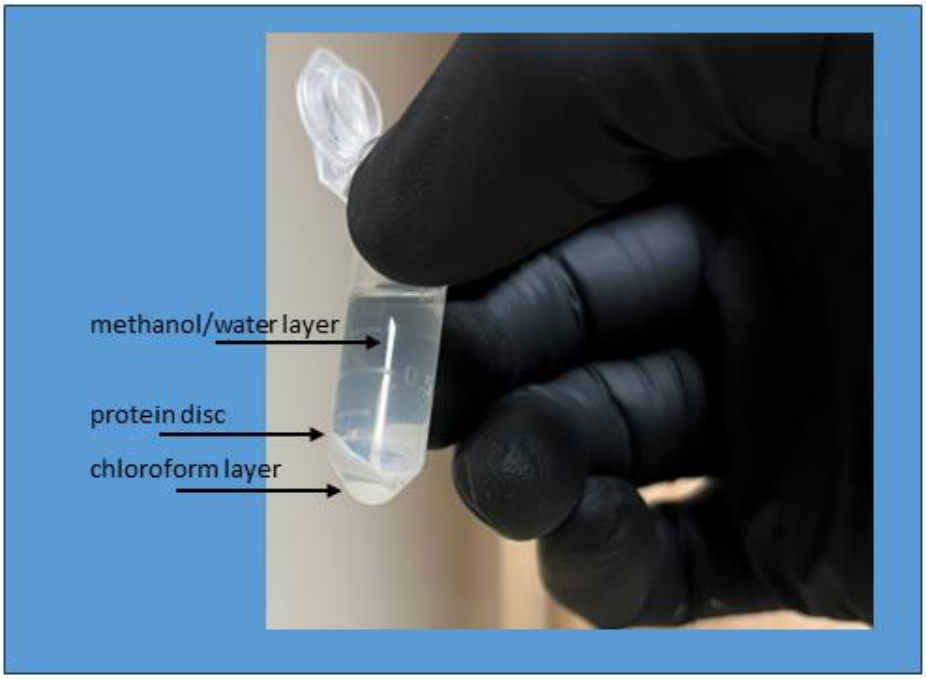

Supplementary Figure 4.1 Representative image of protein that has been precipitated using the 5:1:4 precipitation technique.

Oxidation / +15.994915 @ C, M | common1
Deamidated / +0.984016 @ N | common1
Deamidated / +0.984016 @ Q | common1
Gln->pyro-Glu / -17.026549 @ NTerm Q | rare1
Glu->pyro-Glu / -18.010565 @ NTerm E | rare1
Acetyl / +42.010565 @ Protein NTerm | rare1
Dioxidation / +31.989829 @ C | common1
Methylthio / +45.987721 @ C | common1
Sulfide / +31.972071 @ C | common1
SulfurDioxide / +63.961900 @ C | common1
Trioxidation / +47.984744 @ C | common1
Hex / +162.052824 @ K | rare1
Cysteinyl / +119.004099 @ C | common1
Glutathione / +305.068156 @ C | common1

Supplementary Figure 4.2 List of modifications used in Byonic parameter file.

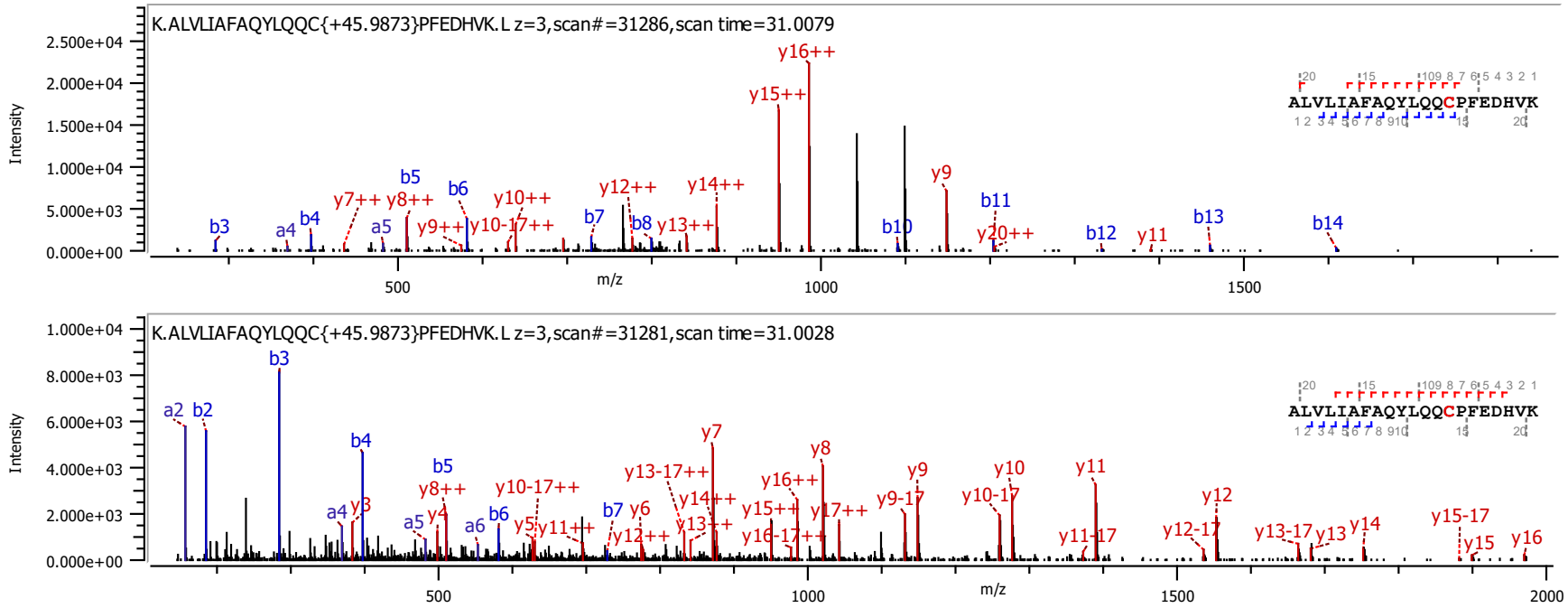

Supplementary Figure 4.3 Representative MS2 fragmentation spectra for Cys-34 containing +3 precursor—fragmented with CID (top) or HCD (bottom). These spectra match what would be expected for the Cys-34 containing peptide with a +45.9873 Da mass shift.

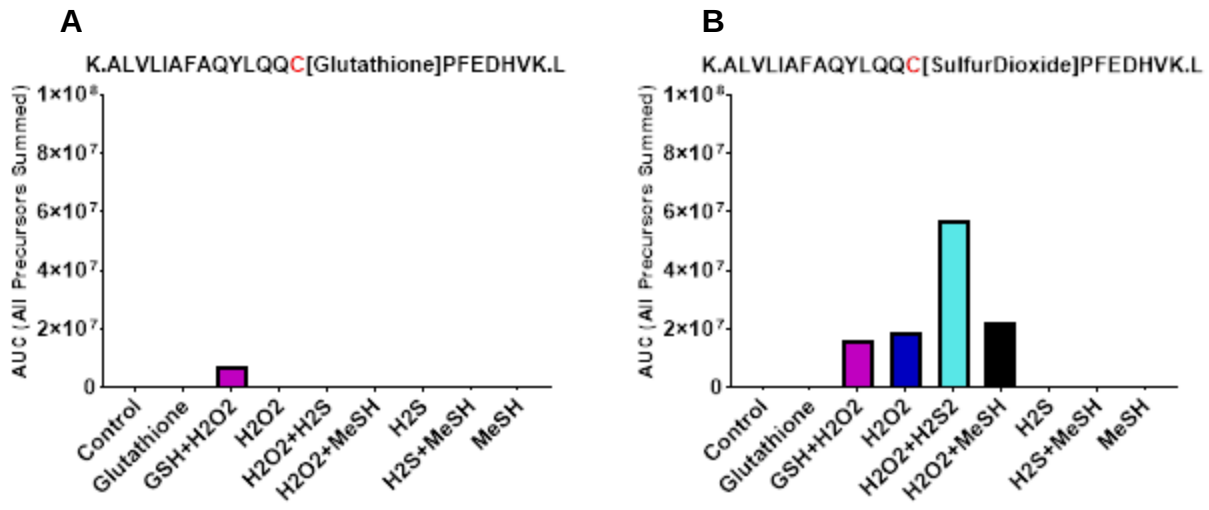

Supplementary Figure 4.4 AUC of all precursors for glutathione (A) and sulfur dioxide (B) modified HSA Cys-34 containing peptide identified in untreated (control), and sulfide treated samples $\pm H_2O_2$.

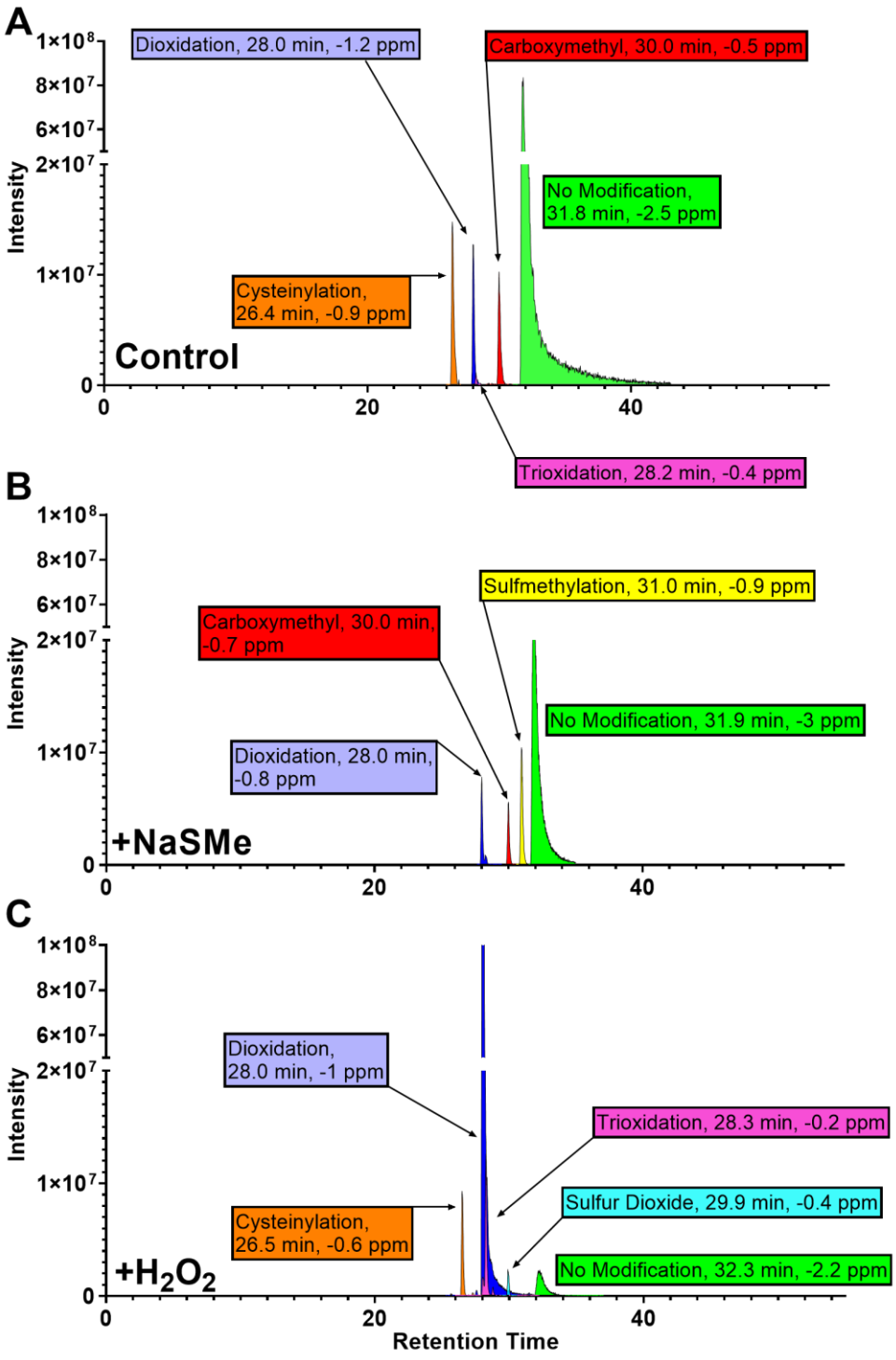

Supplementary Figure 4.5 chromatograms for the modified peptides discussed in **section 4.3.1** from plasma samples; untreated (control) (A), MeSH donor treated (B), and H_2O_2 treated (C).

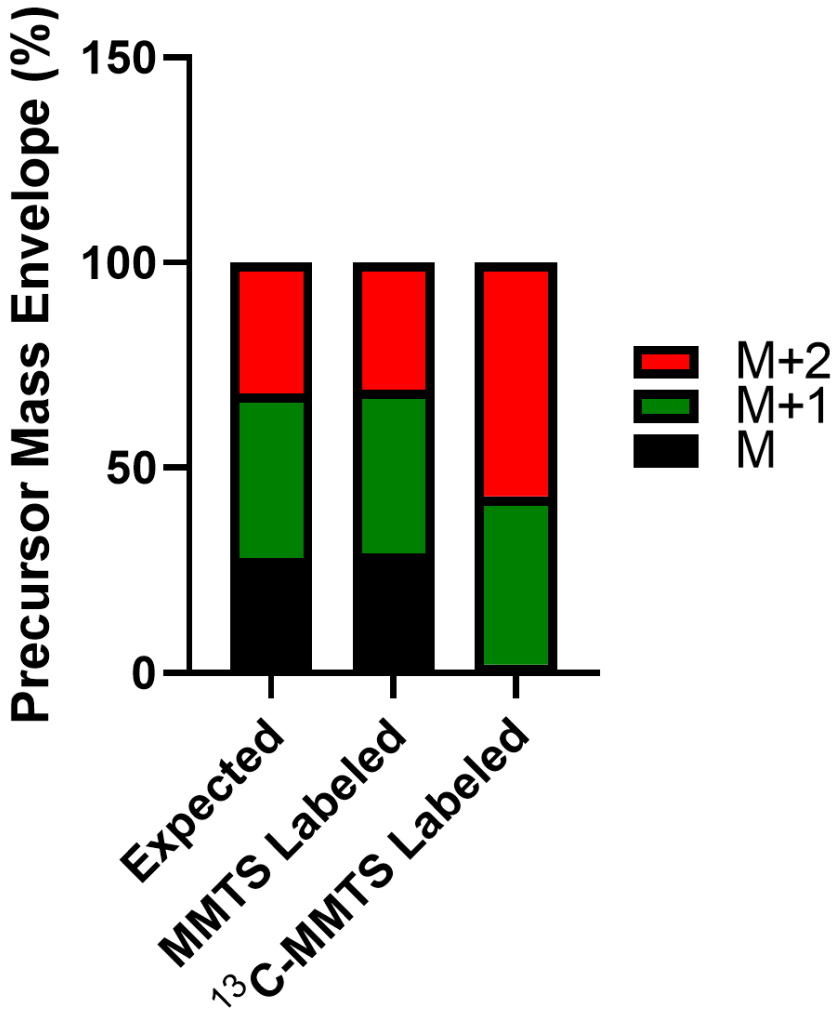

Supplementary Figure 4.6 The percent composition of the +3 sulfmethylated Cys-34 peptide ion's mass envelope. Envelope consists of M, M+1, and M+2 isotopes. When plasma digest is labeled with ^{13}C-MMTS, the resulting sulfmethylated Cys-34 containing peptide has little M precursor ion when labeled with MMTS, the isotope distribution matches expectation. The expected isotope distribution was calculated with Skyline [1].

1. Pino, L.K., et al., *The Skyline ecosystem: Informatics for quantitative mass spectrometry proteomics.* Mass Spectrom Rev, 2020. **39**(3): p. 229-244.